ON-LINE APPENDICES TO

Thermal Radiation Heat Transfer

7th Edition, Taylor and Francis, 2021
John R. Howell, M. Pinar Mengüç,
Kyle Daun, and Robert Siegel

A: Wide-Band Models
B: Derivation of Geometric Mean Beam Length Relations
C: Exponential Kernel Approximation
D: Curtis-Godson Approximation
E: The YIX Method
F: Graphs for CO_2, H_2O and CO Emittance
G: Radiative Transfer in Porous and Dispersed Media
H: Benchmark Solutions for Verification of Radiation Solutions
I: Integration and Numerical Solution Methods
J: Radiation Cooling
K: Radiation from Flames
L: Commercial Codes
M: References to Reviews and Historical Papers
N: Short Biographies and a History of Thermal Radiation
O: Timeline of Important Events in Radiation
P: Additional Homework Problems
Q: Proposed One-Semester Syllabus

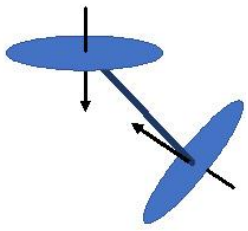

A. WIDE-BAND MODELS

A.1 WIDE-BAND MODELS AND CORRELATIONS

Edwards and Menard (1964) modeled a band of rotation lines that are reordered in wave number, so they form an array with exponentially decreasing line intensities moving away from the band center and covering the entire band. This is the *exponential wide-band* model. Edwards and co-workers [Edwards (1960,1962,1965), Edwards and Menard (1964a,b), Edwards and Sun (1964), Edwards et al. (1965), Edwards and Nelson (1962), Edwards and Balakrishnan (1973), Weiner (1966), Hines and Edwards (1968)] assembled a large body of data on the important radiating gases at typical engineering conditions. By comparing their band-correlation relations with data over large ranges of pressure and temperature, they determined empirically how the physical variables are related to the effective bandwidth $\tilde{A}_l(T)$, to an effective bandwidth parameter $\omega(T)$, and to a modified pressure-broadening parameter $B(T, P_e)$, where P_e is the effective broadening pressure. The μ was expressed in the form of a modified variable $u = X\alpha/\omega$, that is in terms of the mass path length $X = \rho S$ of the absorbing gas component and a quantity $\alpha(T)$ that will be determined. Available correlations are summarized in Table A.1.

The newer and more accurate models based on k-distributions (Chapter 9 of the text) have largely superseded the exponential wide-band models, especially for combustion gases; however, some gases such as SO_2 and HCl do not have the line-by-line data available for computing k-distributions, so the correlations presented here may still be useful.

TABLE A.1
Available Band Absorptance Correlations for Isothermal Media

Gas	Bands	Reference	Comments	Type of Correlation
CO_2	2.0, 2.7, 4.3, 9.4, 10.4, and 15 μm	Table 9.3 [Marin and Buckius (1998b)]	Wide band $300 < T < 1390$ K $0.1 < X < 23{,}000$ g/m^2	*c-k* wide-band distribution
	WSGG (all)	Table 9.7 [Denison and Webb (1995)]	$400 < T < 2500$ K 3×10^{-5} to 600 m^2/mol	Spectral line WSGG
	2.0, 2.7, 4.3, 9.4, 10.4, and 15 μm	[Domoto (1974)]	$300 < T < 1390$ K $0.1 < X < 23{,}000$ g/m^2	*k*-distribution (wide band)
	2.7,4.3, and 15 μm	[Chu and Greif (1978)]	$T \approx 300$ K $0.1 < X < 23{,}000$ g/m^2	Nonrigid rotator spectroscopic wide band
	2.7 μm	[Lin and Greif (1974)]	$T \approx 300$ K $0.081 < pS < 1300$ atm ◺cm	Rigid rotator spectroscopic wide band
	2.0, 2.7, 4.3, and 15 μm	Table 9.2 [Edwards (1976); Edwards and Menard (1964b); Edwards and Balakrishnan (1973); Edwards et al. (1967)]	$300 < T < 1390$ K $0.1 < X < 23{,}000$ g/m^2	Exponential wide band
	9.4 and 10.4 μm	Table 9.2 [Edwards (1976); Edwards and Menard (1964); Edwards and Balakrishnan (1973); Edwards et al. (1967)]	$300 < T < 1390$ K $0.1 < X < 23{,}000$ g/m^2	Exponential wide band
	2.0, 2.7, 4.3, 9.4, 10.4, and 15 μm	[Edwards (1960)]	$300 < T < 1390$ K $0.1 < X < 23{,}000$ g/m^2	Equivalent bandwidth
H_2O	1.38, 1.87, 2.7, and 6.3 μm, rotational	Table 9.4 [Marin and Buckius (1998a)]	$300 < T < 2900$ K (except rotational band, $300 < T < 1900$ K) $10^{-5} < pS < 10^4$ atm ◺m	*c-k* (wide-band) distribution
	WSGG (all)	Table 9.5 [Denison and Webb (1993)]	$400 < T < 2500$ K 3×10^{-5} to 60 m^2/mol	Spectral line WSGG
	1.38, 1.87, 2.7, and 6.3 μm, rotational	[Kamiuto and Tokita (1994)]	$300 < T < 3000$ K $0.1 < pS < 1000$ bar ◺cm	Modified exponential wide band
	2.7 μm	[Lin and Greif (1974)]	$T = 300$ K $3.3 < pS < 2800$ atm ◺cm	Rigid rotator spectroscopic wide band
	2.7 and 6.3 μm	[Weiner (1966)]	$300 < T < 2100$ K $1 < X < 21000$ g/m^2	Equivalent line
	1.38, 1.87, 2.7, and 6.3 μm	Table 9.2 [Edwards (1976); Edwards et al. (1965); Edwards and Balakrishnan (1973); Edwards et al. (1967)]]	$300 < T < 2250$ K $1 < X < 38{,}000$ g/m^2	Exponential wide band
	Rotational band ($\kappa > 10$ μm)	[Charalampopoulos and Felske (1983)]	$500 < T < 2400$ K $1.5 < pS < 30$ atm ◺cm	Exponential wide band
	[a] Varies with band.			

TABLE A.1 (CONTINUED)
Available Band Absorptance Correlations for Isothermal Media

Gas	Bands	Reference	Comments	Type of Correlation
CO	WSGG (all bands)	Solovjov and Webb (1998)]	$300 < T < 2500$ K	Spectral line WSGG
	2.35 and 4.67 μm	Table 9.2 [Edwards (1976); Edwards and Menard (1964b); Edwards and Balakrishnan (1973)]	$300 < T < 1500$ K (2.35) $300 < T < 1800$ K (4.67) $19 < X < 650$ g/m^2	Exponential wide band
	4.7 μm	[Hsieh and Greif (1972); Hashemi et al. (1976); Chu and Greif (1978)]	$300 < T < 1800$ K $19 < X < 650$ g/m^2	Rigid and nonrigid rotator spectroscopic wide-band model
CH_4	1.71, 2.37, 3.31, and 7.66 μm	Table 9.2 [Edwards (1976); Edwards and Menard (1964b); Edwards and Balakrishnan (1973)]	$300 < T < 1000$ K[a] $19 < X < 650$ g/m^2	Exponential wide band
HCl		[Stull and Plass (1960a)]	1000–3400 cm^{-1}	Spectral emittance
SO_2	4.00, 4.34, 5.33, 7.35, 8.68, and 19.27 μm	[Kunitomo et al. (1981)]	$300 < T < 2000$ K $0.06 < pS < 180$ atm ⇦cm	Statistical narrow band and exponential wide band
	4.00, 4.34, 7.35, 8.68, and 19.27 μm	[Chan and Tien (1971)]	$500 < T < 3500$°R $0.002 < pS < 2$ atm ⇦ft	Elsasser narrow band and exponential wide band
H_2		[Aroeste and Benton (1956)]	Not correlated-presented in terms of spectral and total emittance	
Atmospheric gases—N_2, O_2, CO_2, O_3, H_2O, CH_3, and nitrogen oxides		[Goody and Yung (1989)]	Discussion of literature up to 1960	
Air	All important contributing bands	[Bond et al (1965)]	The citation [Bond et al. (1965)] provides references up to 1965 for data to calculate band absorptance	
NH_3	3.0, 10.5, 2.9, and 6.15 μm	[Tien (1973)]	$T < 300$ K $2 < X < 312$ g/m^2	Exponential wide band
NO	5.35 μm	[Hashemi et al. (1976); Chu and Greif (1978)]	$T < 300$ K $0.845 < pS < 12.56$ atm·cm	Rigid and nonrigid rotator spectroscopic wide-band model
N_2O	4.5 μm	[Chu and Greif (1978)]	$T < 303$ K $0.0186 < pS < 76.4$ atm·cm	Nonrigid rotator spectroscopic wide-band model
CCl_4 (liquid)	All important	[Novotny et al. (1974)]		Two-parameter Elsasser and statistical narrow band

[a] Varies with band.

TABLE A.1 (CONTINUED)
Available Band Absorptance Correlations for Isothermal Media

Gas	Bands	Reference	Comments	Type of Correlation
H_2, N_2, O_2, CH_4, CO, Ar (liquids only)	All important far-infrared bands in 40 to 500 μm region; for H_2, 16.7 to 500 μm	[Jones (1970)]	T near normal boiling point at 1 atm, S = 1.27 and 2.54 cm, plus 3.25 cm for H_2	Data for absorption coefficient versus wave number
C_2H_2	Wave number, (cm^{-1}) 3287; 1328, 729	[Brosmer and Tien (1985)]	Discussion of literature; measurements from T = *290* to 600 K	Exponential wide band
C_2H_4	Four in infrared	[Tuntomo et al. (1989)]	Measurements and correlation	Statistical narrow band, wide band

[a] Varies with band.

A brief description of the exponential wide band correlation is given here for the four gases in Table A.2. Information for NO and SO_2 is in Edwards and Balakrishnan (1973) [see also Edwards (1976)]. The correlation is in terms of three quantities: α, the integrated band intensity; B, the line-width parameter; and ω, the bandwidth parameter. The desired total band absorption $\bar{A}$ is found from the following correlations (the band subscript l on $\bar{A}$ has been dropped for convenience):

$$\text{For } B<1: \quad \left.\begin{aligned} \bar{A} &= \omega u & 0 \le u \le B \\ \bar{A} &= \omega(2\sqrt{Bu} - B) & B \le u \le \frac{1}{B} \\ \bar{A} &= \omega[\ln(Bu) + 2 - B] & \frac{1}{B} \le u \le \infty \end{aligned}\right\} \tag{A.1a}$$

$$\text{For } B \ge 1: \quad \left.\begin{aligned} \bar{A} &= \omega u & 0 \le u \le 1 \\ \bar{A} &= \omega(\ln u + 1) & 1 \le u \le \infty \end{aligned}\right\} \tag{A.1b}$$

The B is π times the ratio of mean line width to spacing, i.e., the parameter β adjusted for broadening effects, including pressure broadening: $B = ßP_e$, where $P_e = [P/P_0 + (p/P_0)(b-1)]^n$, P is the total pressure (atm) of radiating and nonradiating gas, P_0 =1 atm, and p is the partial pressure of the radiating gas ($p_e \to 1$ as $p_e \to 0$ and $P \to P_0$). The b and n are in Table A.2 for each gas band. The $u = X\alpha/\omega$, where X is the mass path length of the radiating gas. The ω is found from $\omega = \omega_0 (T/T_0)^{1/2}$, where ω_0 is in Table A.2 and T_0 = 100 K. The table also gives the quantities necessary to obtain α and β from the following:

$$\alpha(T) = \alpha_0 \frac{1 - \exp\left(-\sum_{k=1}^{m} u_k \delta_k\right)}{1 - \exp\left(-\sum_{k=1}^{m} u_{0,k} \delta_k\right)} \left[\frac{\Psi(T)}{\Psi(T_0)}\right] \tag{A.2a}$$

$$\beta(T) = \beta_0 \left(\frac{T_0}{T} \right)^{1/2} \frac{\Phi(T)}{\Phi(T_0)} \tag{A.2b}$$

where

$$\Psi(T) = \frac{\prod_{k=1}^{m} \sum_{\upsilon_k=\upsilon_{0,k}}^{\infty} \left\{ \left(\upsilon_k + g_k + |\delta_k| - 1 \right)! / \left[\left(g_k - 1 \right)! \upsilon_k ! \right] \right\} e^{-u_k \upsilon_k}}{\prod_{k=1}^{m} \sum_{\upsilon_k=0}^{\infty} \left\{ \left(\upsilon_k + g_k - 1 \right)! / \left[\left(g_k - 1 \right)! \upsilon_k ! \right] \right\} e^{-u_k \upsilon_k}} \tag{A.2c}$$

$$\Phi(T) = \frac{\left[\prod_{k=1}^{m} \sum_{\upsilon_k=\upsilon_{0,k}}^{\infty} \left(\left\{ \left(\upsilon_k + g_k + |\delta_k| - 1 \right)! / \left[\left(g_k - 1 \right)! \upsilon_k ! \right] \right\} e^{-u_k \upsilon_k} \right)^{1/2} \right]^2}{\prod_{k=1}^{m} \sum_{\upsilon_k=\upsilon_{0,k}}^{\infty} \left\{ \left(\upsilon_k + g_k + |\delta_k| - 1 \right)! / \left[\left(g_k - 1 \right)! \upsilon_k ! \right] \right\} e^{-u_k \upsilon_k}} \tag{A.2d}$$

in which

$$u_k = \frac{hc\eta_k}{kT}, \qquad u_{0,k} = \frac{hc\eta_k}{kT_0}$$

and $\upsilon_{0,k} = 0$ if δ_k is positive or zero and is $|\delta_k|$ if δ_k is negative. Some illustrative numerical examples are in Edwards (1976) and Example A.1.

TABLE A.2
Exponential Wide-Band Parameters

				Pressure Parameters (T_o = 100 K)				
Gas $m, \eta\,(cm^{-1}), g$	Band (μm)	Band Center η (cm^{-1})	$\delta_1 \ldots . \delta_m$	b	n	α_o(cm^{-1}/g·m^{-2})	β_o	ω_0 (cm^{-1})
CO_2	15	667	0, 1, 0	1.3	0.7	19.0	0.06157	12.7
m = 3, η = 1351, g_1 = l	10.4	960	−1, 0, 1	1.3	0.8	2.47 x 10^{-9}	0.04017	13.4
η = 667, g_1 = 2	9.4	1060	0, −2, l[b]	1.3	0.8	2.48 x 10^{-9}[b]	0.11888[b]	10.1
η = 2396, g_3 = l	4.3	2410[a]	0, 0, 1	1.3	0.8	110.0	0.24723	11.2
	2.7	3660	1, 0, 1	1.3	0.65	4.0	0.13341	23.5
	2.0	5200	2, 0, 1	1.3	0.65	0.066	0.39305	34.5
CH_4	7.66	1310	0, 0, 0, 1	1.3	0.8	28.0	0.08698	21.0
m = 4, η_1 = 2914, g_1 = 1	3.31	3020	0, 0, 1, 0	1.3	0.8	46.0	0.06973	56.0
η_2 =1526, g_2 = 2	2.37	4220	1, 0, 0, 1	1.3	0.8	2.9	0.35429	60.0
η_3 =3020, g_3 = 3	1.71	5861	1, 1, 0, 1	1.3	0.8	0.42	0.68598	45.0
η_4 = 1306, g_4 = 3								
H_2O	rotational[d]	140	0, 0, 0	8.6(T_0/T)$^{1/2}$ + 0.5	1	44205	0.14311	69.3
m = 3, η_1 = 3652, g_1 = l	6.3	1600	0, 1, 0	8.6(T_0/T)$^{1/2}$ + 0.5	1	41.2	0.09427	56.4

$\eta_1 = 1595$, $g_2 = 1$	2.7	3760[a]	0, 2, 0	$8.6(T_0/T)^{1/2} + 0.5$	1	0.19	0.13219	60.0
$\eta_3 = 3756$, $g_3 = 1$			1, 0, 0			2.30		
			0, 0, 1			22.40		
	1.87	5350	0, 1, 1	$8.6(T_0/T)^{1/2} + 0.5$	1	3.0	0.08169	43.1
	1.38	7250	1, 0, 1	$8.6(T_0/T)^{1/2} + 0.5$	1	2.5	0.11628	32.0
CO	4.7	2143	1	1.1	0.8	20.9	0.07506	25.5
$m = 1$, $\eta_1 = 2143$, $g_1 = 1$	2.35	4260	2	1.0	0.8	0.14	0.16758	20.0

Sources: Edwards, D. K.: Molecular Gas Band Radiation, in T. F. Irvine, Jr., and J. P. Hartnett (eds.), *Advances in Heat Transfer*, vol. 12, pp. 115–193, Academic Press, New York, 1976; Edwards, D. K., and Balakrishnan, A.: Thermal Radiation by Combustion Gases, *IJHMT*, vol. 16, no. 1, pp. 25–40, 1973.

[a] Upper band limit.

[b] Use values for the 10.4-μm band instead of those for the 9.4-μm band.

[c] See notes in Edwards and Balakrishnan (1973).

[d] For the H_2O rotational band, $\alpha(T) = \alpha_0 \exp[-9.0(T_0/T)^{1/2}], \beta(T_0/T)^{1/2}, \omega_0(T/T_0)^{1/2}$ $a(T)$; if the calculated lower band limit is negative, use $\eta = 0$ for the lower limit (the band width then equals the calculated upper limit); further details are in Modak (1979).

Greif and coworkers [Hsieh and Greif (1972), Lin and Greif (1973, 1974), Hashemi et al. (1976), Chu and Greif (1978)] developed wide-band correlations from basic spectroscopic theory, finding good agreement with experimental measurements in many cases. With this approach, no arbitrary constants are introduced, and recourse to experimental data is not needed to evaluate the constants.

Tien and Lowder (1966) devised the continuous correlation

$$\frac{\bar{A}_1}{\omega} = \ln\left[uf(B)\frac{u+2}{u+2f(B)}+1\right] \tag{A.3}$$

where ω is the bandwidth parameter and $f(B) = 2.94[1 - \exp(-2.60B)]$. This does not satisfy the square-root limit in Equation 9.30 [Cess and Tiwari (1972)], and has been found to be in error for very small values of B. Other correlations have been constructed by Cess and Tiwari:

$$\frac{\bar{A}_1}{\omega} = 2\ln\left[1+\frac{u}{2+u^{1/2}(1+1/B)^{1/2}}\right] \tag{A.4}$$

and Goody and Belton (1967):

$$\frac{\bar{A}_1}{\omega} = 2\ln\left[1+\frac{\sqrt{B}u}{(u+4B)^{1/2}}\right] \tag{A.5}$$

A more complicated expression that covers all ranges is given by Morizumi (1979) who also summarizes some of the other correlations. Tiwari (1976) compares the results of using various narrow-band models in developing the exponential wide-band model. In addition, the correlations outlined above are compared and analyzed for regions of accurate use.

To determine the effect of the band models on the final radiative transfer results, several band models were applied to two problems [Tiwari (1977)] involving radiative transfer in gases with internal heat sources and heat transfer. In most instances good agreement was obtained by using the various models, but it is necessary to examine the reference to appreciate the detailed comparisons. A model to apply the exponential wide-band properties in a multidimensional geometry is in Modest (1983).

EXAMPLE A.1 Find the effective bandwidth $\bar{A}$ of the 9.4-μm band for pure CO_2 at 1 atm and 500K for a path length S of 0.364 m.

To obtain $\bar{A}$ from the relations in Equation A.1, the values of u and B must be determined so the correct relation can be selected. To find $u = X\alpha/\omega$, the values of all three quantities on the right need to be determined using data from Table A.2 and the corresponding relations, and to determine $B = \beta P_e$, values of β and P_e must be found.

To find α, the values of $\Psi(T)$ and $\Psi(T_0)$ must be found using Equation A.2c. For the 9.4 μm band, values from Table A.2 (noting the footnote for this band) are $\alpha_0 = 2.48 \times 10^{-9}$ m^2/g · cm, $\delta_1 = -1$, $\delta_2 = 0$, $\delta_3 = -1$, giving $\upsilon_{0,1} = 1$, $\upsilon_{0,2} = \upsilon_{0,3} = 0$· Also $g_1 = 1$, $g_2 = 2$, $g_3 = 1$, and $\eta_1 = 1351$cm ^{1}, $\eta_2 = 667$cm $^{-1}$, and $\eta_3 = 2396$ cm $^{-1}$. Using $h = 6.626 \times 10^{-34}$ J · s, $k = 1.381 \times 10^{-23}$ J/K, and $c = 2.998 \times 10^{10}$ cm/s gives $\mu_1 = 3.887$, $\mu_2 = 1.919$, and $\mu_3 = 6.893$. The μ_0 values are a factor of 5 larger, respectively. Substituting into Equation A.33*c*) gives $\Psi(T) = 0.0415$ and $\Psi(T_0) = 7.266 \times 10^{-9}$. Substituting further into Equation A.1*a* gives $\alpha(T) = 0.01341$ m^2/g · cm.

To find a value for β, values of $\Phi(T)$ and $\Phi(T_0)$ must now be determined. Substituting into Equation (A.2*d*) results in $\Phi(T)$=4.479 and $\Phi(T_0) = 1.0237$, and from Equation (A.2*b*), $\beta(T) = 0.04017(100/500)^{1/2}$ (4.479/1.024) = 0.079.

The value of ω is obtained from $\omega = \omega_0(T/T_0)^{1/2}$ using ω_0 from Table A.2 to give $\omega = 10.1(500/100)^{1/2} = 22.58$cm^{-1}.

The mass path length X is defined as ρS, and the value of ρ is found from the ideal gas law as $\rho = PM/RT$= 1 atm x 44 (kg/kg · mol)/[0.08206(atm · m^3/kg · mol · K) × 500K] = 1.072kg/m^3 = 1.072 × 10^{3}g/m^3. Thus, X= 1.07 × 10^{3}g/m^3 × 0.364m = 390.3 g/m^2, and $u = X\alpha/\omega$ = 389.5 (g/m^2) × 0.01346 (m^2/g · cm)/22.58 (cm^{-1}) = 0.232.

Now the value of $P_e = [P/P_0 + (p/P_0)(b - 1)]^n$ is found for pure CO_2 at 1 atm using b and n from Table A.2 to give P_e, = $(1.3)^{0.8}$= 1.234, so $B = ßP_e$ = 0.0970. Examining the relation for $\bar{A}$ (Equations A.1) shows that for B< 1 and for u between B = 0.0970 and B^{-1} = 10.309, which is the case here,

$$\bar{A} = \omega[2(Bu)^{1/2} - B] = 22.58[2(0.0970 \times 0.232)^{1/2} - 0.0970] = 4.58 \text{ cm}^{-1}$$

This compares reasonably well with the experimental value for these conditions of 5.9 cm^{-1} from Edwards (1960). The predictions from other correlations for this band at these conditions are $\bar{A}_{CT}$ = 2.81 (Equation A.4), $\bar{A}_{GB}$ = 3.97 (Equation A.5), and $\bar{A}_{TL}$ = 4.49 (Equation A.3).

Additional complexities are introduced when a gas mixture is considered. For example, the partial pressure p of an absorbing gas in a multi-component system varies with T and P, the populations of the energy states vary with T, and the overlapping of spectral lines changes with P. It is thus very complex to formulate analytically the dependence of $\bar{A}_l$ on T, p, and P for a real gas mixture. Useful results must depend heavily on experiment while theory is used as a guide. Some calculations for mixtures are in Edwards and Balakrishnan (1973). If two gases are present that both absorb energy, their band absorptivities may overlap in some spectral regions. In this case, Hottel and Sarofim (1967) show that, for two gases a and b in an overlapping band of width $\Delta\eta$,

$$\bar{A}_{a+b} = \Delta\eta\left[1-\left(1-\frac{\bar{A}_a}{\Delta\eta}\right)\left(1-\frac{\bar{A}_b}{\Delta\eta}\right)\right] = \bar{A}_a + \bar{A}_b - \frac{\bar{A}_a\bar{A}_b}{\Delta\eta} \tag{A.6}$$

thus, the simple sum of the two $\bar{A}$ is reduced by the quantity $\bar{A}_a\bar{A}_b/\Delta\eta$ (see also Equations 9.64 and 9.65 of the text). Restriction is to wave number intervals over which both A_a and $\bar{A}_a$ and $\bar{A}_b$, are applicable average values and in which there is no correlation between the positions of the individual spectral lines of gases *a* and *b*.

HOMEWORK (Solutions are in the Homework Solution Manual for Chapter 9.)

A.1 For a line-width parameter of B = 0.2, prepare a plot comparing various band correlation functions of effective bandwidth to actual bandwidth, $\frac{\bar{A}_\ell}{\omega}$, as a function of the parameter u containing mass path length, for $0.01 \le u \le 100$. Compare the correlation functions of Edwards and Menard (Equation A.1), Tien and Lowder (Equation A.3), Cess and Tiwari (Equation A.4), and Goody and Belton (Equation (A.5).

A.2 Find the effective bandwidth $\bar{A}$ of the 9.4 μm band of CO_2 at a partial pressure of 0.4 atm in a mixture with nitrogen at a total pressure of 1 atm. The gas temperature is 500 K, and the path length S is 0.364 m. Compare with the result in Example A.1.

Answer: 2.09 cm^{-1}.

A.3 For pure CO gas at 1 atm pressure, determine the effective bandwidth for the 4.67 μm spectral band at T = 600 K for a path length of S = 0.5 m.

Answer: 207.3 cm^{-1}.

A.4 From Figure 9.5 of the text, estimate the effective bandwidth for the 2.7 μm CO_2 band at 830 K, 10 atm, and a path length of 38.8 cm. Compare this with the result computed from the correlations in Table A.2.

Answer: 414 cm^{-1}.

REFERENCES:

Aroeste, H. and Benton, W.C.: Emissivity of Hydrogen Atoms at High Temperatures, *J. Appl. Phys.*, vol. 27, pp. 117–121, 1956.

Bond, J. W., Jr., Watson, K. M., and Welch, J. A. Jr.: *Atomic Theory of Gas Dynamics*, Addison-Wesley, Reading, MA, 1965.

Brosmer, M. A., and Tien, C. L.: Thermal Radiation Properties of Acetylene, *JHT*, vol. 107, pp. 943–948, 1985.

Charalampopoulos, T. T., and Felske, J. D.: Total Band Absorptance, Emissivity, and Absorptivity of the Pure Rotational Band of Water Vapor, *JQSRT*, vol. 30, no. 1, pp. 89–96, 1983.

Cess, R. D., and Tiwari, S. N.: Infrared Radiative Energy Transfer in Gases, in T. F. Irvine, Jr., and J. P. Hartnett (eds.), *Advances in Heat Transfer*, vol. 8, pp. 229–283, Academic Press, New York, 1972

Chan, S. H., and Tien, C. L.: Infrared Radiation Properties of Sulfur Dioxide, *JHT*, vol. 93, no. 2, pp. 172–178, 1971.

Chu, K. H., and Greif, R.: Theoretical Determination of Band Absorption for Nonrigid Rotation with Applications to CO, NO, N_2O and CO_2, *JHT*, vol. 100, pp. 230–234, 1978.

Denison, M. K., and Webb, B. W.: A Spectral Line-Based Weighted-Sum-of-Gray-Gases Model for Arbitrary RTE Solvers, *JHT*, vol. 115, no. 4, pp. 1004–1012, 1993.

Denison, M. K., and Webb, B. W.: The Spectral-Line Weighted-Sum-of-Gray-Gases Model for H_2O/CO_2 Mixtures, *JHT*, vol. 117, pp. 788–798, 1995.

Domoto, G. A.: Frequency Integration for Radiative Transfer Problems Involving Homogeneous Non-Gray Gases: The Inverse Transmission Function, *JQSRT*, vol. 14, pp. 935–942, 1974.

Edwards, D. K.: Absorption of Infrared Bands of Carbon Dioxide Gas at Elevated Pressures and Temperatures, *JOSA*, vol. 50, no. 6, pp. 617–626, 1960.

Edwards, D. K.: Radiant Interchange in a Nongray Enclosure Containing an Isothermal Carbon Dioxide–Nitrogen Gas Mixture, *JHT*, vol. 84, no. 1, pp. 1–11, 1962.

Edwards, D. K.: Absorption of Radiation by Carbon Monoxide Gas According to the Exponential Wide-Band Model, *Appl. Opt.*, vol. 4, no. 10, pp. 1352–1353, 1965.

Edwards, D. K.: Molecular Gas Band Radiation, in T. F. Irvine, Jr., and J. P. Hartnett (eds.), *Advances in Heat Transfer*, vol. 12, pp. 115–193, Academic Press, New York, 1976.

Edwards, D. K., and Menard, W. A.: Comparison of Models for Correlation of Total Band Absorption, *Appl. Opt.*, vol. 3, no. 5, pp. 621–625, 1964a.

Edwards, D. K., and Menard, W. A.: Correlations for Absorption by Methane and Carbon Dioxide Gases, *Appl. Opt.*, vol. 3, no. 7, pp. 847–852, 1964b.

Edwards, D. K., and Nelson, K. E.: Rapid Calculation of Radiant Energy Transfer between Nongray Walls and Isothermal H_2O or CO_2 Gas, *JHT*, vol. 84, no. 4, pp. 273–278, 1962.

Edwards, D. K., and Sun, W.: Correlations for Absorption by the 9.4- and 10.4- CO_2 Bands, *Appl. Opt.*, vol. 3, no. 12, pp. 1501–1502, 1964.

Edwards, D. K., Flornes, B. J., Glassen, L. K., and Sun, W.: Correlation of Absorption by Water Vapor at Temperatures from 300 K to 1100 K, *Appl. Opt.*, vol. 4, no. 6, pp. 715–721, 1965.

Edwards, D. K., Glassen, L. K., Hauser, W. C., and Tuchscher, J. S.: Radiation Heat Transfer in Nonisothermal Nongray Gases, *JHT*, vol. 89, no. 3, pp. 219–229, 1967.

Edwards, D. K., and Balakrishnan, A.: Thermal Radiation by Combustion Gases, *IJHMT*, vol. 16, no. 1, pp. 25–40, 1973.

Felske, J. D., and Tien, C. L.: A Theoretical Closed-Form Expression for the Total Band Absorptance of Infrared–Radiating Gases, *IJHMT*, vol. 17, pp. 155–158, 1974

Goody, R. M., and Belton, M. J. S.: Radiative Relaxation Times for Mars (Discussion of Martian Atmospheric Dynamics), *Planet. Space Sci.*, vol. 15, no. 2, pp. 247–256, 1967.

Hashemi, A., Hsieh, T. C., and Greif R.: Theoretical Determination of Band Absorption with Specific Application to Carbon Monoxide and Nitric Oxide, *JHT*, vol. 98, pp. 432–437, 1976.

Hines, W. S., and Edwards, D. K.: Infrared Absorptivities of Mixtures of Carbon Dioxide and Water Vapor, *Chem. Eng. Prog. Symp. Ser.*, vol. 64, no. 82, pp. 173–180, 1968.

Hottel, H. C, and Sarofim, A. F.: *Radiative Transfer*, McGraw–Hill, New York, 1967.

Hsieh, T. C, and Greif, R.: Theoretical Determination of the Absorption Coefficient and the Total Band Absorptance Including a Specific Application to Carbon Monoxide, *IJHMT*, vol. 15, pp. 1477–1487, 1972.

Jones, M. C.: Far Infrared Absorption in Liquefied Gases, NBS Technical Note 390, National Bureau of Standards, Boulder, CO, 1970.

Kamiuto, K., and Tokita, Y.: Wideband Spectral Models for the Absorption Coefficient of Water Vapor, *JTHT*, vol. 8, no. 4, pp. 808–810, 1994.

Kunitomo, T., Masuzaki, H., Ueoka, S., and Osumi, M.: Experimental Studies of the Properties of Sulfur Dioxide, *JQSRT*, vol. 25, pp. 345–349, 1981.

Lin, J. C., and Greif, R.: Total Band Absorptance of Carbon Dioxide and Water Vapor Including Effects of Overlapping, *IJHMT*, vol. 17, pp. 793–795, 1974.

Marin, O., and Buckius, R.: A Simplified Wide Band Model of the Cumulative Distribution Function for Water Vapor, *IJHMT*, vol. 41, pp. 2877–2892, 1998a.

Marin, O., and Buckius, R.: A Simplified Wide Band Model of the Cumulative Distribution Function for Carbon Dioxide, *IJHMT*, vol. 41, pp. 3881–3897, 1998b.

Modest, M. F.: Evaluation of Spectrally–Integrated Radiative Fluxes of Molecular Gases in Multi-dimensional Media, *IJHMT*, vol. 26, no. 10, pp. 1533–1546, 1983.

Morizumi, S. J.: Comparison of Analytical Model with Approximate Models for Total Band Absorption and Its Derivative, *JQSRT*, vol. 22, no. 5, pp. 467–474, 1979.

Novotny, J. L., Negrelli, D. E., and Van der Driessche, T.: Total Band Absorption Models for Absorbing-Emitting Liquids: CCl_4, *JHT*, vol. 96, pp. 27–31, 1974.

Solovjov, V. P., and Webb, B. W.: Radiative Transfer Model Parameters for Carbon Monoxide at High Temperature, in J. S. Lee (ed.), *Heat Transfer*—1998, *Proc. 11th Int. Heat Transfer Conf*, KyongJu, Korea, vol. 7, pp. 445–450, Taylor & Francis, New York, 1998.

Stull, V. R., and Plass, G. N.: Emissivity of Dispersed Carbon Particles, *JOSA*, vol. 50, no. 2, pp. 121–129, 1960.

Tien, C. L.: Band and Total Emissivity of Ammonia, *IJHMT*, vol. 16, pp. 856–857, 1973.

Tien, C. L., and Lowder, J. E.: A Correlation for Total Band Absorptance of Radiating Gases, *IJHMT*, vol. 9, no. 7, pp. 698–701, 1966.

Tiwari, S. N.: Band Models and Correlations for Infrared Radiation, in *Radiative Transfer and Thermal Control*, vol. 49 of *Progress in Astronautics and Aeronautics Series*, pp. 155–182, AIAA, 1976.

Tiwari, S. N.: Applications of Infrared Band Model Correlations to Nongray Radiation, *IJHMT*, vol. 20, no. 7, pp. 741–751, 1977.

Tuntomo, A., Park, S. H., and Tien, C. L.: Infrared Radiation Properties of Ethylene, *Exp. Heat Transfer*, vol. 2,

pp. 91–103, 1989.
Weiner, M. M.: Radiant Heat Transfer in Non-isothermal Gases, Ph.D. thesis, University of California at Los Angeles, 1966.

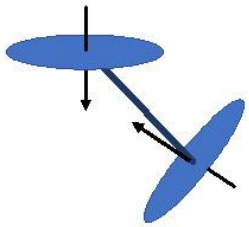

B: DERIVATION OF GEOMETRIC MEAN BEAM LENGTH RELATIONS

The Geometric Mean Beam Lengths depend on both geometry and wavelength through the definitions

$$A_j F_{j-k} \bar{t}_{\lambda,j-k} = \int_{A_k} \int_{A_j} \frac{e^{-\kappa_\lambda S} \cos\theta_k \cos\theta_j}{\pi S^2} dA_j \; dA_k \tag{B.1}$$

$$A_j F_{j-k} \bar{\alpha}_{\lambda,j-k} = A_j F_{j-k} \left(1 - \bar{t}_{\lambda,j-k}\right) \tag{B.2}$$

The double integral in Equation B.1 must be evaluated for various orientations of surfaces A_j and A_k; the result will depend on k_λ. Derivations for some specific geometries are now considered.

B.1 HEMISPHERE TO DIFFERENTIAL AREA AT CENTER OF ITS BASE

Let A_j be the surface of a hemisphere of radius R, and dA_k be a differential area at the center of the base (Figure B.1). Then Equation B.1 becomes, since $S=R$ and $\theta_i = 0$,

$$A_j dF_{j-dk} \bar{t}_{\lambda,j-dk} = dA_k \int_{A_j} \frac{e^{-\kappa_\lambda R} \cos\theta_k \cos(0)}{\pi R^2} dA_j$$

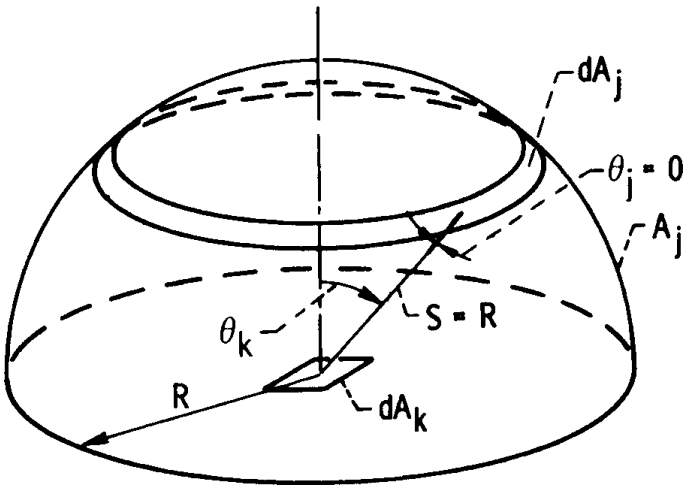

FIGURE B.1 Hemisphere filled with isothermal medium.

The convenient dA_j is a ring element $dA_j = 2\pi R^2 \sin\theta_k \, d\theta_k$, and the factors involving R can be taken out of the integral. This gives

$$A_j dF_{j-dk} \bar{t}_{\lambda,j-dk} = dA_k \int_{A_j} \frac{e^{-\kappa_\lambda R} 2\pi R^2}{\pi R^2} \int_{\theta_k=0}^{\pi/2} \cos\theta_k \sin\theta_k \; d\theta_k = dA_k e^{-\kappa_\lambda R}$$

With $A_j \, dF_{j-dk} = dA_k \; F_{dk-j}$ and $F_{dk-j} = 1,$, this reduces to

$$\bar{t}_{\lambda,j-dk} = e^{-\kappa_\lambda R} \tag{B.3}$$

This especially simple relation is used later in the concept of mean beam length where radiation from an actual volume of a medium is replaced by that from an equivalent hemisphere.

B.2 TOP OF RIGHT CIRCULAR CYLINDER TO CENTER OF ITS BASE

This geometry is in Figure B.2. Since $\theta_j = \theta_k = \theta$, the integral in Equation B.1 becomes, for the top of the cylinder A_j radiating to the element dA_k at the center of its base,

$$A_j dF_{j-dk} \bar{t}_{\lambda,j-dk} = dA_k \int_{A_j} \frac{e^{-\kappa_\lambda S} \cos^2\theta}{\pi S^2} dA_j \tag{B.4}$$

Since $\xi^2 = S^2 - h^2, dA_j = 2\pi\xi\, d\xi = 2\pi S\, dS.$ Then, using $\cos\theta = h/S$,

$$A_j\, dF_{j-dk} \bar{t}_{\lambda,j-dk} = dA_k\, 2h^2 \int_h^{\sqrt{R^2+h^2}} \frac{e^{-\kappa_\lambda S}}{S^3} dS \tag{B.5}$$

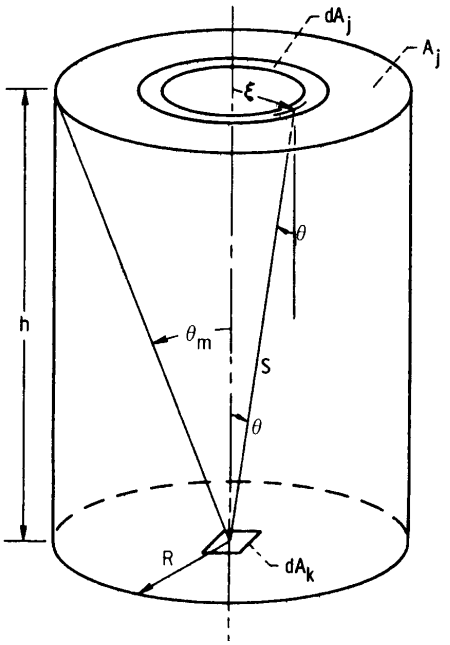

FIGURE B.2 Geometry for exchange from top of gas-filled cylinder to center of its base.

Now let $\kappa_\lambda S = \tau_\lambda$ to obtain

$$A_j\, dF_{j-dk} \bar{t}_{\lambda,j-dk} = dA_k\, 2h^2 \kappa_\lambda^2 \int_{\tau_\lambda=\kappa_\lambda h}^{\kappa_\lambda\sqrt{R^2+h^2}} \frac{e^{-\tau_\lambda}}{\tau_\lambda^3} d\tau_\lambda \tag{B.6}$$

This integral can be expressed in terms of the exponential integral function defined in Appendix D of the text, by writing

$$\int_{\tau_\lambda=\kappa_\lambda h}^{\kappa_\lambda\sqrt{R^2+h^2}} \frac{e^{-\tau_\lambda}}{\tau_\lambda^3} d\tau_\lambda = \int_{\tau_\lambda=\infty}^{\kappa_\lambda\sqrt{R^2+h^2}} \frac{e^{-\tau_\lambda}}{\tau_\lambda^3} d\tau_\lambda - \int_{\tau_\lambda=\infty}^{a_\lambda h} \frac{e^{-\tau_\lambda}}{\tau_\lambda^3} d\tau_\lambda \tag{B.7}$$

Letting $\tau_\lambda = \left(\kappa_\lambda \sqrt{R^2+h^2}\right)\Big/\mu$ and $\kappa_\lambda h/\mu$, respectively, in the two integrals gives

$$-\frac{1}{\left(\kappa_\lambda \sqrt{R^2+h^2}\right)^2}\int_0^1 \mu e^{-\kappa_\lambda \sqrt{R^2+h^2}/\mu} d\mu + \frac{1}{\left(\kappa_\lambda h\right)^2}\int_0^1 \mu e^{-\kappa_\lambda h/\mu} d\mu$$

The integral in Equation B.6 is then written in terms of the exponential integral function as

$$\int_{\tau_\lambda=\kappa_\lambda h}^{\kappa_\lambda\sqrt{R^2+h^2}} \frac{e^{-\tau_\lambda}}{\tau_\lambda^3} d\tau_\lambda = \frac{1}{\left(\kappa_\lambda h\right)^2} E_3\left(\kappa_\lambda h\right) - \frac{1}{\left[\kappa_\lambda h\sqrt{(R/h)^2+1}\right]^2} E_3\left[\kappa_\lambda h\sqrt{\left(\frac{R}{h}\right)^2+1}\right] \qquad \text{(B.8)}$$

so, it can be readily evaluated for various values of the parameters *R/h* and $\kappa_\lambda h$.

B.3 SIDE OF CYLINDER TO CENTER OF ITS BASE

Let dA_j be a ring around the wall of a cylinder as in Figure B.3, and note that $dA_j = 2\pi R dz$, $\cos\theta_k = z/S$, $\cos\theta_j = R/S$, and $z\,dz = S dS$. Then Equation B.1 is written for the side of the cylinder to dA_k as

$$A_j dF_{j-dk}\,\overline{\tau}_{\lambda,j-dk} = 2dA_k R^2 \int_R^{\sqrt{R^2+h^2}} \frac{e^{-a_\lambda S}}{S^3} dS \qquad \text{(B.9)}$$

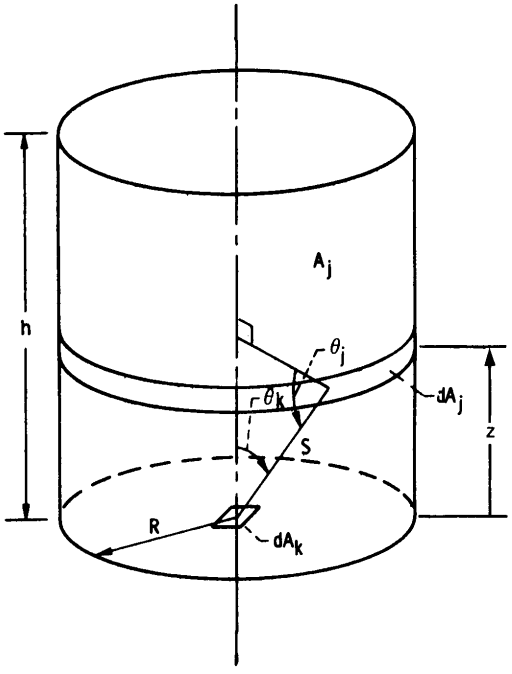

FIGURE B.3 Geometry for exchange from side of gas-filled cylinder to center of its base.

This is of the same form as Equation B.5, and gives the result

$$A_j dF_{j-dk}\bar{t}_{\lambda,j-dk}$$

$$= 2dA_k\left(\frac{R}{h}\right)^2(\kappa_\lambda h)^2\left\{\frac{1}{\left[\kappa_\lambda h\left(R/h\right)^2\right]}E_3\left[\kappa_\lambda h\left(\frac{R}{h}\right)\right]-\frac{1}{\left[\kappa_\lambda h\sqrt{(R/h)^2+1}\right]^2}E_3\left[\kappa_\lambda h\sqrt{\left(\frac{R}{h}\right)^2+1}\right]\right\} \tag{B.10}$$

As for Equation B.8, this is readily evaluated for various values of R/h and $\kappa_\lambda h$.

B.4 ENTIRE SPHERE TO ANY AREA ON ITS SURFACE OR TO ITS ENTIRE SURFACE

From Figure B.4, since $\theta_k = \theta_j$ let them be simply θ; then $S = 2R\cos\theta$. Starting with Equation B.4, $dA_j \cos\theta/S^2$ is the solid angle by which dA_j is viewed from dA_k. The intersection of the solid angle with a unit hemisphere shows that this equals $2\pi \sin\theta\, d\theta$. Then

$$A_j\, dF_{j-dk}\bar{t}_{\lambda,j-dk} = dA_k\int_{\theta=0}^{\pi/2}e^{-\kappa_\lambda S}\,2\cos\theta\sin\theta d\theta = \frac{2dA_k}{4R^2}\int_{S=0}^{2R}e^{-\kappa_\lambda S}SdS$$

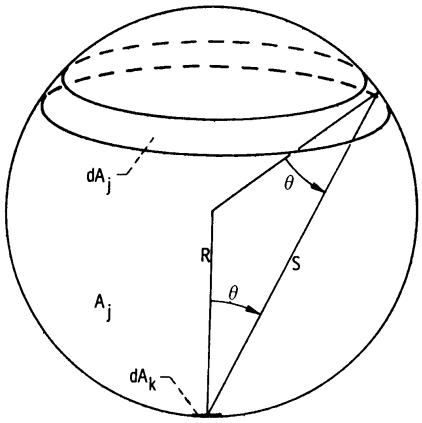

FIGURE B.4 Geometry for exchange from surface of gas-filled sphere to itself.

Integrating gives

$$A_j\, dF_{j-dk}\bar{t}_{\lambda,j-dk} = \frac{2dA_k}{(2a_\lambda R)^2}\left[1-\left(2\kappa_\lambda R+1\right)e^{-2\kappa_\lambda R}\right] \tag{B.11}$$

which has a single parameter $2\kappa_\lambda R$, the sphere optical diameter.

Equation B.11 is integrated over any finite area A_k to give $\bar{t}_\lambda$ from the entire sphere to A_k as $A_j F_{j-k}\bar{t}_{\lambda,j-k} = \left[2A_k/\left(2\kappa_\lambda R\right)^2\right]\left[1-\left(2\kappa_\lambda R+1\right)e^{-2\kappa_\lambda R}\right]$. Since $F_{j-k} = A_k/A_j$, from Equation 4.17,

$$\bar{t}_{\lambda,j-k} = \frac{2}{(2\kappa_\lambda R)^2}\left[1-\left(2\kappa_\lambda R+1\right)e^{-2\kappa_\lambda R}\right] \tag{B.12}$$

which also applies for the entire sphere to its entire surface.

B.5 INFINITE PLATE TO ANY AREA ON PARALLEL PLATE

In Figure B.5 consider on one plate an element dA_k, and on the other plate a concentric ring element dA_j centered about the normal to dA_k. The geometry is like that in Figure B.2 for a ring on the top of a cylinder to the center of its base. Then, from Equation B.6,

$$A_j\, dF_{j-dk}\, \bar{t}_{\lambda,\, j-dk} = dA_k\, 2(\kappa_\lambda D)^2 \int_{\tau_\lambda=\kappa_\lambda D}^{\infty} \frac{e^{-\tau_\lambda}}{\tau_\lambda^3}\, d\tau_\lambda$$

where $\kappa_\lambda D$ is the optical spacing between the plates. By using the procedure leading to Equation B.8, the integral is transformed to $E_3(\kappa_\lambda D)/(\kappa_\lambda D)^2$. Then integrating over any finite area A_k as in Figure B.5 gives $A_j F_{j-k}\, \bar{t}_{\lambda,\, j-k} = A_k\, 2E_3(\kappa_\lambda D)$. With $A_j F_{j-k} = A_k F_{k-j}$ and $F_{k-j} = 1$, this reduces to

$$\bar{t}_{\lambda,\, j-k} = 2E_3(\kappa_\lambda D) \tag{B.13}$$

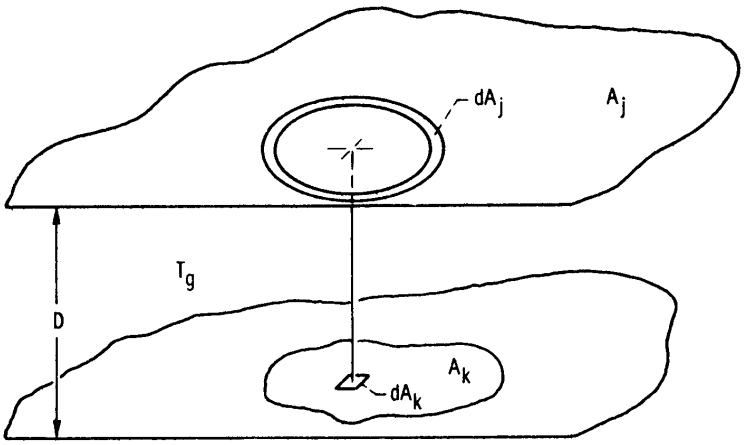

FIGURE B.5 Isothermal layer of medium between infinite parallel plates.

B.6 RECTANGLE TO A DIRECTLY OPPOSED PARALLEL RECTANGLE

Consider, as in Figure B.6, the exchange from a rectangle to an area element on a directly opposed parallel rectangle. The upper rectangle is divided into a circular region and a series of partial rings of small width. The contribution from the circle of radius R to $A_j dF_{j-dk}\, \bar{t}_{\lambda,\, j-dk}$ can be found from Equations B.6 and B.8, for the top of a cylinder to the center of its base. For the nth partial ring, let f_n be the fraction it occupies of a full circular ring. Then, by use of Equation B.4, the contribution of all the partial rings to $A_j dF_{j-dk}\, \bar{t}_{\lambda,\, j-dk}$ is approximated by

$$dA_k \sum_m f_n \frac{e^{-\kappa_\lambda S_n}}{\pi S_n^2} \left(\frac{D}{S_n}\right)^2 2\pi R_n \Delta R_n = dA_k\, 2D^2 \sum_n f_n \frac{e^{-\kappa_\lambda S_n}}{\left(D^2 + R_n^2\right)} R_n \Delta R_n$$

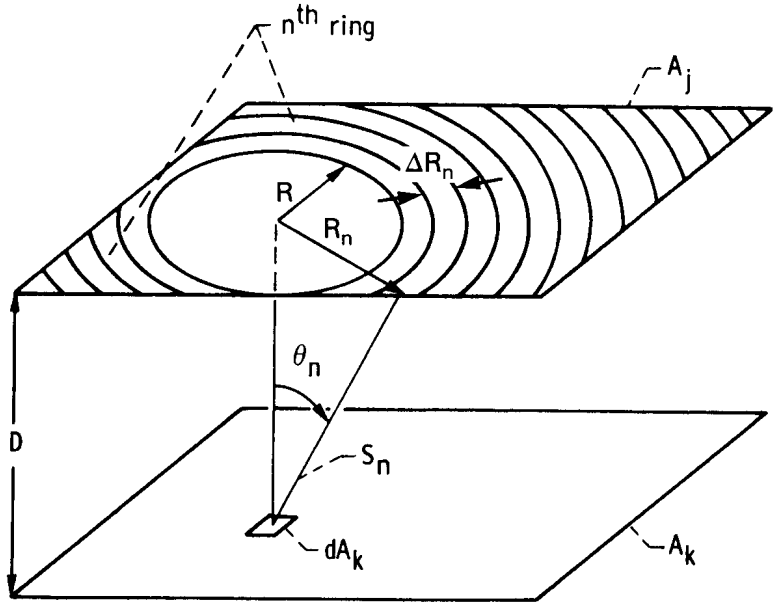

FIGURE B.6 Geometry for exchange between two directly opposed parallel rectangles with intervening translucent medium.

This evaluation of $A_j dF_{j-dk}\bar{t}_{\lambda,j-dk}$ is carried out for several area patches on A_k. This is usually enough, so the integration over A_k can be performed as indicated by Equation B.1 to yield

$$A_j F_{j-k}\bar{t}_{\lambda,j-k} = \int_{A_k} A_j dF_{j-dk}\bar{t}_{\lambda,j-dk}$$

EXAMPLE B.1 A nongray, absorbing-emitting plane layer with κ_λ as in Figure B.7 is 1.2 cm thick and is on top of an opaque diffuse-gray infinite plate. The plate temperature has been raised suddenly, so the layer is still at its initial uniform temperature. What is the net heat flux being lost from the plate-layer system? Neglect heat conduction effects in the layer and neglect any reflections at the upper boundary of the layer.

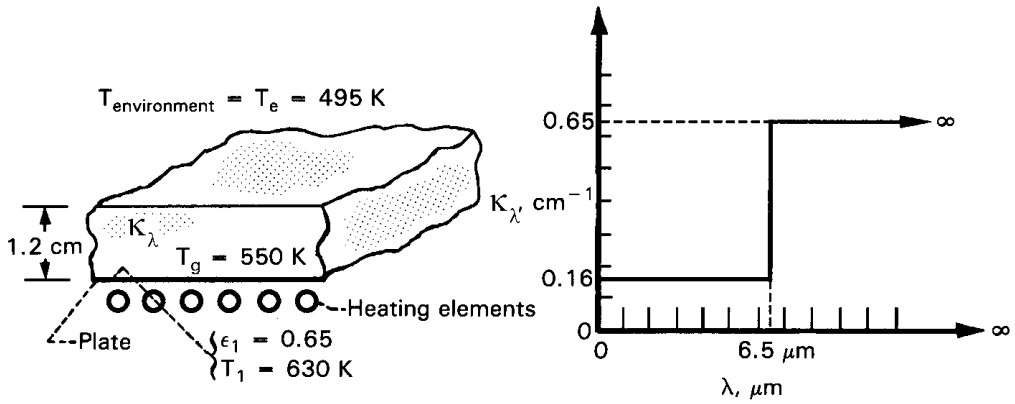

FIGURE B.7 Plane layer of nongray absorbing-emitting material.

The uniform environment above the layer acts as a black enclosure at T_e. Equation 11.77 of the text can be applied directly by integrating in two spectral bands and using $\varepsilon_{\lambda 2} = 1$. The geometric-mean transmittance factors are obtained from Equation B.13 as

$\bar{t}_{\lambda,1} = 2E_3(0.16\times1.2) = 0.7142, \quad 0 \le \lambda \le 6.5\mu\text{m}; \; \bar{t}_{\lambda,2} = 2E_3(0.65\times1.2)$
$= 0.2974, \quad 6.5\mu\text{m} \le \lambda \le \infty$. This yields

$$q = -q_2 = \varepsilon_1 \bar{t}_{\lambda,1}(\sigma T_1^4 F_{0\to6.5T_1} - \sigma T_e^4 F_{0\to6.5T_e})$$
$$+ (1-\bar{t}_{\lambda,1})[1+(1-\varepsilon_1)\bar{t}_{\lambda,1}](\sigma T_g^4 F_{0\to6.5T_g} - \sigma T_e^4 F_{0\to6.5T_e})$$
$$+ \varepsilon_1 \bar{t}_{\lambda,2}[\sigma T_1^4(1-F_{0\to6.5T_1}) - \sigma T_e^4(1-F_{0\to6.5T_e})$$
$$+ (1-\bar{t}_{\lambda,2})[1+(1-\epsilon_1)\bar{t}_{\lambda,2}][\sigma T_g^4(1-F_{0\to6.5T_g}) - \sigma T_e^4(1-F_{0\to6.5T_e})]$$

Inserting the values $F_{0\to6.5\times630} = 0.4978$, $F_{0\to6.5\times550} = 0.3985$ and $F_{0\to6.5\times495} = 0.3220$ yields q = 2954 W/m^2.

B.7 GEOMETRIC-MEAN BEAM LENGTH FOR SPECTRAL BAND ENCLOSURE EQUATIONS

For use in the spectral band enclosure Equation 11.77 in the text, the absorption integral in Equation 11.82 must be evaluated between pairs of enclosure surfaces for the wavelength bands involved. When more than a few bands absorb appreciably, the enclosure solution requires considerable computational effort. A simplification was developed by Dunkle (1964) by assuming that the integrated band absorption $\bar{\alpha}_l(S)$ is a *linear function* of path length. This has some physical basis, as it holds exactly for a band of weak nonoverlapping lines (Equation 9.19 in the text). Also, it is the form of some of the effective bandwidths in the exponential wide band correlations of on-line Appendix A (Equation A.1). As shown in Dunkle by means of a few examples, reasonable values for the energy exchange are obtained using this approximation. Hence, let $\bar{A}_l$ in Equation 11.83 have the linear form from Equation 9.30 (note that the bandwidth $\Delta\lambda_l = \omega$ in Equation 9.30)

$$\alpha_l(S) = \frac{\bar{A}_l(S)}{\Delta\lambda_l} = \frac{\bar{A}_l(S)}{\omega} = \frac{\bar{A}_l(S)}{m\delta} = \frac{S_c}{\delta}S \tag{B.14}$$

where S_c and δ are the line intensity and the spacing of the individual weak spectral lines, as in Chapter 9 of the text.

Now define a mean path length $\bar{S}_{k-j}$ called the *geometric-mean beam length*, such that α_l evaluated from Equation B.14 by using $S = \bar{S}_{k-j}$ will equal $\bar{\alpha}_{l,k-j}$ from the integral in Equation 11.81 of the text. After substituting $\bar{\alpha}_{l,k-j} = (S_c/\delta)\bar{S}_{k-j}$ and $\alpha_l = (S_c/\delta)S$ into Equation 11.81, the relation for $\bar{S}_{k-j}$ is

$$\bar{S}_{k-j} = \bar{S}_{j-k} = \frac{1}{A_k F_{k-j}} \int_{A_j}\int_{A_k} \frac{\cos\theta_j \cos\theta_k}{\pi S} dA_k dA_j \tag{B.15}$$

which depends only on geometry. This integral is also obtained in Equation B.1 when $\kappa_\lambda S$ is small (optically thin limit). In Dunkle, S_{k-j} values are tabulated for parallel equal rectangles, for rectangles at right angles, and for a differential sphere and a rectangle. Analytical relations for rectangles are in Equations B.16*a*,*b*. For directly opposed parallel equal rectangles with sides of length *a* and *b* and spaced a distance *c* apart,

$$\frac{\bar{S}_{k-j}A_kF_{k-j}}{abc}=\frac{4}{\pi}\left\{\tan^{-1}\frac{\eta\beta}{\xi}+\frac{1}{\eta}\ln\left[\frac{\beta+\xi}{\sqrt{1+\eta^2}(\beta+\sqrt{1+\beta^2}}\right]+\frac{1}{\beta}\ln\left[\frac{\eta+\xi}{\sqrt{1+\beta^2}(\eta+\sqrt{1+\eta^2})}\right]\right.$$
$$\left.+\frac{1}{\eta\beta}\left[\sqrt{1+\eta^2}+\sqrt{1+\beta^2}-1-\xi\right]\right\} \qquad \text{(B.16}a\text{)}$$

where $\eta = a/c$, $\beta = b/c$ and $\xi=\sqrt{1+\eta^2+\beta^2}$. The F_{k-j} can be obtained from Factor 4 in Appendix C of the text. For rectangles *ab* and *bc* at right angles with a common edge *b*,

$$\frac{\bar{S}_{k-j}A_kF_{k-j}}{abc}=\frac{1}{\pi}\left\{\frac{\gamma}{\alpha}\ln\frac{(1+\sqrt{1+\gamma^2})\sqrt{\alpha^2+\gamma^2}}{\gamma(1+\sqrt{1+\alpha^2+\gamma^2}}+\frac{\alpha}{\gamma}\ln\frac{(1+\sqrt{1+\alpha^2})\sqrt{\alpha^2+\gamma^2}}{\alpha(1+\sqrt{1+\alpha^2+\gamma^2})}\right.$$
$$+\frac{1}{3\gamma\alpha}[(1+\gamma^2)^{3/2}+(1+\alpha^2)^{3/2}+(\alpha^2+\gamma^2)^{3/2}-(1+\alpha^2+\gamma^2)^{3/2}]$$
$$+\frac{\alpha}{\gamma}[\sqrt{1+\alpha^2+\gamma^2}-\sqrt{\alpha^2+\gamma^2}-\sqrt{1+\alpha^2}]$$
$$\left.+\frac{\gamma}{\alpha}[\sqrt{1+\alpha^2+\gamma^2}-\sqrt{\alpha^2+\gamma^2}-\sqrt{1+\gamma^2}]+\frac{2}{3}\left[\frac{\gamma^2}{\alpha}+\frac{\alpha^2}{\gamma}-\frac{1}{2\gamma\alpha}\right]\right\} \qquad \text{(B.16}b\text{)}$$

where $\alpha = a/b$ and $\gamma = c/b$. The F_{k-j} is obtained from Factor 8 in Appendix C of the text. Results for equal opposed parallel rectangles are in Figure B.8, and values for equal parallel rectangles and for rectangles at right angles are in Tables B.1 and B.2. Other $\bar{S}_{k-j}$ values are referenced by Hottel and Sarofim (1967). In Anderson and Hadvig (1989), values are obtained for a medium in the space between two infinitely long coaxial cylinders.

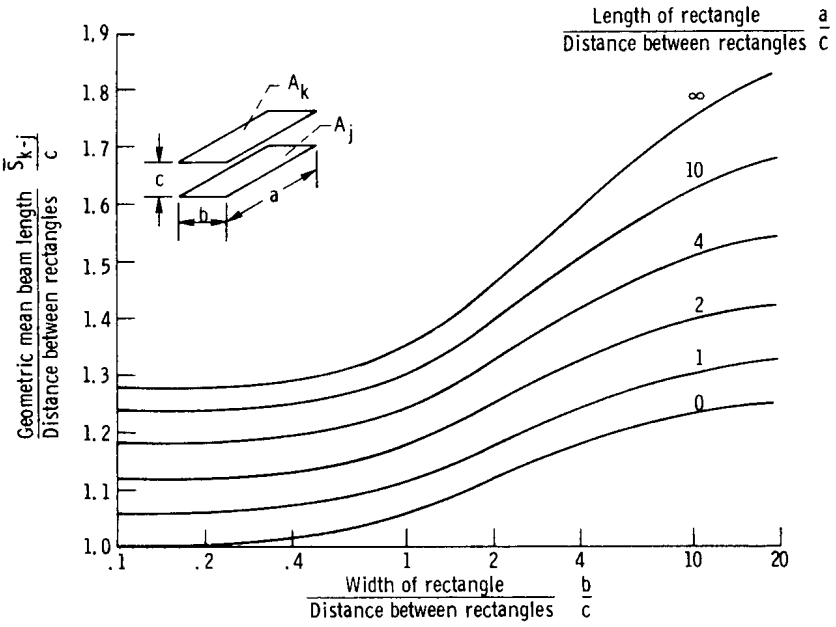

FIGURE B.8 Geometric mean beam lengths for equal parallel rectangles [Dunkle (1964)].

B. Geometric Mean Beam Lengths

For a medium at uniform conditions, the geometric-mean beam length can be used in the effective-bandwidth correlations in on-line Appendix A to obtain $\bar{A}_l(\bar{S})$. Using $\Delta\lambda_l$ obtained in the next paragraph yields $\bar{\alpha}_l\left(\bar{S}\right) = \bar{A}_l\left(S\right)/\Delta\lambda_l$ from Equation 11.83 of the text and $\bar{t}_l$ from $1-\bar{\alpha}_l$. Then Equations 11.78 and 11.79 of the text can be solved for $q_{l,k}$ for each wavelength band *l*. The total energies at each surface *k* are found from a summation over all bands

$$q_k = \sum_{\substack{absorbing\\bands}} q_{l,k}\Delta\lambda_l + \sum_{\substack{nonabsorbing\\bands}} q_{l,k}\Delta\lambda_l \tag{B.17}$$

The wavelength span $\Delta\lambda_l$ of each band is needed to carry out the solution. This span can increase with path length. Edwards and coworkers [Edwards and Nelson (1962), Edwards (1962), Edwards et al. (1967)] give recommended spans for CO_2 and H_2O vapor; these values, in wave number units, are in Table A.3 for the parallel-plate geometry. For other geometries, Edwards and Nelson give methods for choosing approximate spans for CO_2 and H_2O bands. Briefly, the method is to use approximate band spans based on the longest important mass path length in the geometry being studied. The limits of Table B.3 are probably adequate for problems involving CO_2 and H_2O vapor.

If all surface temperatures are specified in a problem, the results from Equation B.17 complete the solution. If q_k is specified for *n* surfaces and T_k for the remaining *N*–*n* surfaces, then the *n* unknown surface temperatures are guessed, the equations are solved for all *q*, and then the calculated q_k are compared to the specified values. If they do not agree, new values of T_k for the *n* surfaces are assumed and the calculation is repeated until the given and calculated q_k agree for all A_k with specified q_k. Equation 11.76, expressed as a sum over the wavelength bands, gives the required energy input to the medium for the specified T_g.

TABLE B.1 Geometric mean beam-length ratios and configuration factors for parallel equal rectangles [Dunkle (1964)]

		c/b										
		0	0.1	0.2	0.4	0.6	1.0	2.0	4.0	6.0	10.0	20.0
a/c												
0	$\bar{S}_{k-j}/c$	1.000	1.001	1.003	1.012	1.025	1.055	1.116	1.178	1.205	1.230	1.251
	F_{k-j}											
0.1	$\bar{S}_{k-j}/c$	1.001	1.002	1.004	1.013	1.026	1.056	1.117	1.179	1.207	1.233	1.254
	F_{k-j}		0.00316	0.00626	0.01207	0.01715	0.02492	0.03514	0.04210	0.04463	0.04671	0.04829
0.2	$\bar{S}_{k-j}/c$	1.003	1.004	1.006	1.015	1.028	1.058	1.120	1.182	1.210	1.235	1.256
	F_{k-j}		0.00626	0.01240	0.02391	0.03398	0.04941	0.06971	0.08353	0.08859	0.09271	0.09586
0.4	$\bar{S}_{k-j}/c$	1.012	1.013	1.015	1.024	1.037	1.067	1.129	1.192	1.220	1.245	1.267
	F_{k-j}		0.01207	0.02391	0.04614	0.06560	0.09554	0.13513	0.16219	0.17209	0.18021	0.18638
0.6	$\bar{S}_{k-j}/c$	1.025	1.026	1.028	1.037	1.050	1.080	1.143	1.206	1.235	1.261	1.282
	F_{k-j}		0.01715	0.03398	0.06560	0.09336	0.13627	0.19341	0.23271	0.24712	0.25896	0.26795
1.0	$\bar{S}_{k-j}/c$	1.055	1.056	1.058	1.067	1.080	1.110	1.175	1.242	1.272	1.300	1.324
	F_{k-j}		0.02492	0.04941	0.09554	0.13627	0.19982	0.28588	0.34596	0.36813	0.38638	0.40026
2.0	$\bar{S}_{k-j}/c$	1.116	1.117	1.120	1.129	1.143	1.175	1.246	1.323	1.359	1.393	1.421
	F_{k-j}		0.03514	0.06971	0.13513	0.19341	0.28588	0.41525	0.50899	0.54421	0.57338	0.59563
4.0	$\bar{S}_{k-j}/c$	1.178	1.179	1.182	1.192	1.206	1.242	1.323	1.416	1.461	1.505	1.543
	F_{k-j}		0.04210	0.08353	0.16219	0.23271	0.34596	0.50899	0.63204	0.67954	0.71933	0.74990
6.0	$\bar{S}_{k-j}/c$	1.205	1.207	1.210	1.220	1.235	1.272	1.359	1.461	1.513	1.564	1.609
	F_{k-j}		0.04463	0.08859	0.17209	0.24712	0.36813	0.54421	0.67954	0.73258	0.77741	0.81204

10.0	$\bar{S}_{k-j}/c$	1.230	1.233	1.235	1.245	1.261	1.300	1.393	1.505	1.564	1.624	1.680
	F_{k-j}		0.04671	0.09271	0.18021	0.25896	0.38638	0.57338	0.71933	0.77741	0.82699	0.86563
20.0	$\bar{S}_{k-j}/c$	1.251	1.254	1.256	1.267	1.282	1.324	1.421	1.543	1.609	1.680	1.748
	F_{k-j}		0.04829	0.09586	0.18638	0.26795	0.40026	0.59563	0.74990	0.81204	0.86563	0.90785
	$\bar{S}_{k-j}/c$	1.272	1.274	1.277	1.289	1.306	1.349	1.452	1.584	1.660	1.745	1.832
	F_{k-j}		0.04988	0.09902	0.19258	0.27698	0.41421	0.61803	0.78078	0.84713	0.90499	0.95125

TABLE B.2 Configuration factors and mean beam-length functions for rectangles at right angles [Dunkle (1964)]

		c/b											
a/b		0.05	0.10	0.20	0.4	0.6	1.0	2.0	4.0	6.0	10.0	20.0	∞
0.02	A_kF_{k-j}/b^2	0.007982	0.008875	0.009323	0.009545	0.009589	0.009628	0.009648	0.009653	0.009655	0.009655	0.009655	0.009655
	$A_kF_{k-j}\bar{S}_{k-j}/abc$	0.17840	0.12903	0.08298	0.04995	0.03587	0.02291	0.01263	0.006364	0.004288	0.002594	0.001305	
0.05	A_kF_{k-j}/b^2	0.014269	0.018601	0.02117	0.02243	0.02279	0.02304	0.02316	0.02320	0.02321	0.02321	0.02321	0.02321
	$A_kF_{k-j}\bar{S}_{k-j}/abc$	0.21146	0.18756	0.13834	0.08953	0.06627	0.04372	0.02364	0.01234	0.008342	0.005059	0.002549	
0.10	A_kF_{k-j}/b^2		0.02819	0.03622	0.04086	0.04229	0.04325	0.04376	0.04390	0.04393	0.04394	0.04394	0.04395
	$A_kF_{k-j}\bar{S}_{k-j}/abc$		0.20379	0.17742	0.12737	0.09795	0.06659	0.03676	0.01944	0.013184	0.008018	0.004049	
0.20	A_kF_{k-j}/b^2			0.05421	0.06859	0.07377	0.07744	0.07942	0.07999	0.08010	0.08015	0.08018	0.08018
	$A_kF_{k-j}\bar{S}_{k-j}/abc$			0.18854	0.15900	0.13028	0.09337	0.05356	0.02890	0.01972	0.012047	0.006103	
0.40	A_kF_{k-j}/b^2				0.10013	0.11524	0.12770	0.13514	0.13736	0.13779	0.13801	0.13811	0.13814
	$A_kF_{k-j}\bar{S}_{k-j}/abc$				0.16255	0.14686	0.11517	0.07088	0.03903	0.02666	0.01697	0.008642	
0.60	A_kF_{k-j}/b^2					0.13888	0.16138	0.17657	0.18143	0.18239	0.18289	0.18311	0.18318
	$A_kF_{k-j}\bar{S}_{k-j}/abc$					0.14164	0.11940	0.07830	0.04467	0.03109	0.02025	0.010366	

B. Geometric Mean Beam Lengths

1.0	$A_k F_{k-j}/b^2$	0.20004	0.23285	0.24522	0.24783	0.24921	0.24980	0.25000
	$A_k F_{k-j} \bar{S}_{k-j} / abc$	0.11121	0.08137	0.04935	0.03502	0.02196	0.01175	
2.0	$A_k F_{k-j}/b^2$		0.29860	0.33462	0.34386	0.34916	0.35142	0.35222
	$A_k F_{k-j} \bar{S}_{k-j} / abc$		0.07086	0.04924	0.03670	0.02401	0.01325	
4.0	$A_k F_{k-j}/b^2$			0.40544	0.43104	0.44840	0.45708	0.46020
	$A_k F_{k-j} \bar{S}_{k-j} / abc$			0.04051	0.03284	0.02320	0.01300	
6.0	$A_k F_{k-j}/b^2$				0.46932	0.49986	0.51744	0.52368
	$A_k F_{k-j} \bar{S}_{k-j} / abc$				0.02832	0.02132	0.01272	
10.0	$A_k F_{k-j}/b^2$					0.5502	0.5876	0.6053
	$A_k F_{k-j} \bar{S}_{k-j} / abc$					0.01759	0.01146	
20.0	$A_k F_{k-j}/b^2$						0.6608	0.7156
	$A_k F_{k-j} \bar{S}_{k-j} / abc$						0.008975	

TABLE B.3 Approximate band limits for parallel-plate geometry [Edwards and Nelson (1962), Edwards (1962), Edwards et al. (1967)]

Gas	Band center λ, μm	Band center η, cm^{-1}	Band limits η, cm^{-1}[a] Lower	Upper
CO_2	15	667	$667 - (\bar{A}_{15}/1.78)$	$667 + (\bar{A}_{15}/1.78)$
	10.4	960	849	1013
	9.4	1060	1013	1141
	4.3	2350	$2350 - (\bar{A}_{4.3}/1.78)$	2430
	2.7	3715	$3715 - (\bar{A}_{2.7}/1.76)$	3750
H_2O	6.3	1600	$1600 - (\bar{A}_{6.3}/1.6)$	$1600 + (\bar{A}_{6.3}/1.6)$
	2.7	3750	$3750 - (\bar{A}_{2.7}/1.4)$	$3750 + (\bar{A}_{2.7}/1.4)$
	1.87	5350	4620	6200
	1.38	7250	6200	8100

[a] $\bar{A}$ is found for various bands as in Example A.1. Terms such as $\bar{A}_{15}/1.78$ are $\bar{A}/2(1-\tau_g)$ from Equation 17 and Tables 1 and 2 of Edwards and Nelson (1962).

EXAMPLE B.2 Two black parallel plates are D = 1 m apart. The plates are of width W = 1 m and have infinite length normal to the cross section shown. Between the plates is carbon dioxide gas at $p_{CO_2} = 1$ atm and T_g = 1000 K. If plate 1 is at 2000 K and plate 2 is at 500 K, find the energy flux that must be supplied to plate 2 to maintain its temperature. The surroundings are at T_e << 500 K.

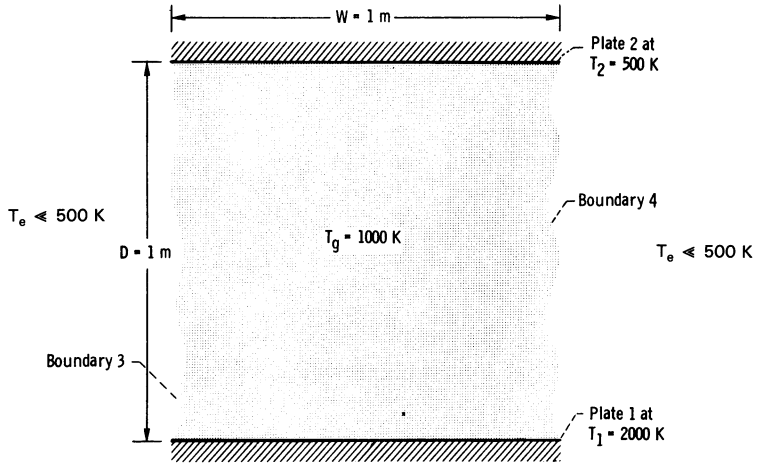

The geometry is a four-boundary enclosure formed by two plates and two open planes. The open areas are perfectly absorbing (nonreflecting) and radiate no significant energy as the surrounding temperature is low. The energy flux added to surface 2 is found by using the enclosure Equation 11.78 of the text where k = 2 and N = 4. All surfaces are black, $\varepsilon_{\lambda,j}$ = 1, so Equation 11.78 reduces to

$$\sum_{j=1}^{4} \delta_{2j} q_{\lambda,j} = \sum_{j=1}^{4} [(\delta_{2j} - F_{2-j}\bar{\tau}_{\lambda,2-j})E_{\lambda b,j} - F_{2-j}\bar{\alpha}_{\lambda,2-j}E_{\lambda b,g}] \tag{B.18}$$

The self-view factor $F_{2-2} = 0$ and $E_{\lambda b,3} = E_{\lambda b,4} \approx 0$, so this becomes

$$q_{\lambda,2} = -F_{2-1}\bar{t}_{\lambda,2-1}E_{\lambda b,1} + E_{\lambda b,2} - (F_{2-1}\bar{\alpha}_{\lambda,2-1} + F_{2-3}\bar{\alpha}_{\lambda,2-3} + F_{2-4}\bar{\alpha}_{\lambda,2-4})E_{\lambda b,g} \tag{B.19}$$

To simplify the example, it is carried out by considering the entire wavelength region as a single spectral band. To obtain the total energy supplied to plate 2, integrate over all wavelengths to obtain

$$q_2 = -F_{2-1}\int_0^\infty \bar{t}_{\lambda,2-1}E_{\lambda b,1}d\lambda + \sigma T_2^4$$

$$-\int_0^\infty (F_{2-1}\bar{\alpha}_{\lambda,2-1} + F_{2-3}\bar{\alpha}_{\lambda,2-3} + F_{2-4}\bar{\alpha}_{\lambda,2-4})E_{\lambda b,g}d\lambda$$

By use of the definitions of total transmission and absorption factors,

$$\bar{t}_{2-1}\sigma T_1^4 = \int_0^\infty \bar{t}_{\lambda,2-1}E_{\lambda b,1}d\lambda \qquad \bar{\alpha}_{2-1}\sigma T_g^4 = \int_0^\infty \bar{\alpha}_{\lambda,2-1}E_{\lambda b,g}d\lambda$$

and so forth, q_2 becomes

$$q_2 = \sigma T_2^4 - F_{2-1}\bar{t}_{2-1}\sigma T_1^4 - (F_{2-1}\bar{\alpha}_{2-1} + F_{2-3}\bar{\alpha}_{2-3} + F_{2-4}\bar{\alpha}_{2-4})\sigma T_g^4 \tag{B.20}$$

To determine $\bar{t}$ and $\bar{\alpha}$, the geometric-mean beam length is used. For opposing rectangles (Figure B.8 of this Appendix) at an abscissa of 1.0 and on the curve for a length-to-spacing ratio of ∞, the $\bar{S}_{2-1}/D = 1.34$, so $\bar{S}_{2-1} = 1.34$ m. To determine $\bar{\alpha}_{2-1}$, which determines the emission of the gas, use the emittance chart in Figure 9.18 or the Alberti et al. (2018) at EXCEL spreadsheet at ***https://doi.org/10.1016/j.jqsrt.2018.08.008*** at a pressure of 1 atm, L_e = 1.34 m and T_g = 1000 K. This gives $\bar{\alpha}_{2-1} = 0.22$. When obtaining $\bar{\tau}_{2-1}$, note from Equation B.20 that the radiation in the $\bar{\tau}_{2-1}$ term is $E_{\lambda b,1}$ and is coming from wall 1. Therefore, it has a spectral distribution different from that of the gas radiation. To account for this nongray effect, Equation 10.121 is used with ε^+ evaluated at $p_{CO_2}\bar{S}_{2-1}(T_1/T_g) = 1.34(2000/1000) = 2.68\ atm\cdot m$ and T_1 = 2000 K. Then, using Figure 9.18 (extrapolated) or the spread sheet results in $\bar{\tau}_{2-1} \approx 1 - 0.2(\frac{1}{2})^{0.5} = 0.86$.

From Factor 3 in Appendix C of the text, the F_{2-1} is given by $F_{2-1} = [(D^2 + W^2)^{1/2} - D]/W = \sqrt{2} - 1 = 0.414$. Then $F_{2-3} = F_{2-4} = \frac{1}{2}(1 - 0.414) = 0.293$. The $\bar{\alpha}_{2-3} = \bar{\alpha}_{2-4}$, and they remain to be found. For adjoint planes, as in the geometry for Table B.2, the following expression from Equation 12 of Dunkle (1964) can be used, obtained for the present case where $b \to \infty$, $a = 1$, and $c = 1$:

$\bar{S}_{2-3} = 2\ln\sqrt{2}/(\pi F_{2-3}) = 2\times 0.347/(\pi\times 0.293) = 0.753\ m.$ Using Figure 9.18 $p\bar{S} = 0.753 \text{atm}\cdot\text{m}$ and T_g = 1000 K gives $\bar{\alpha}_{2-3} = \bar{\alpha}_{2-4} = 0.19$. Then the desired result is

$$q_2 = \sigma T_2^4 - 0.414(0.86)\sigma T_1^4 - (0.414\times 0.22 + 2\times 0.293\times 0.19)\sigma T_g^4$$

$$= 5.6704\times 10^{-12}(500^4 - 0.36\times 2000^4 - 0.20\times 1000^4)$$

$$= -33.4\ W/cm^2$$

Note that the largest contribution to q_2 is by energy leaving surface 1 that reaches and is absorbed by surface 2. Emission from the gas to surface 2, and emission from surface 2, are small.

An alternative approach for this example is to note that the term involving T_g in Equation B.20 is the flux received by surface 2 as a result of emission by the entire gas. This can be calculated from Equation 11.115 using the mean beam length. Then $q_2 = \sigma T_2^4 - F_{2-1}\bar{\tau}_{2-1}\sigma T_1^4 - \varepsilon_g \sigma T_g^4$. For this symmetric geometry the average flux from the gas to one side of the enclosure is the same as that to the entire enclosure boundary. Consequently, the mean beam length can be obtained from Equation 11.111 as $L_e = 0.9(4)V/A = 0.9(4)(1\text{ m})^2/4\text{ m} = 0.9$ m. Then, from Figure 9.18 at T_g = 1000 K and $p_{CO_2}L_e = 0.9\ \text{atm}\cdot\text{m}$, the ε_g = 0.20. This gives the same q_2 as previously calculated.

HOMEWORK (Solutions are included in the Solution Manual under Chapter 11)

B.1 Two opposed parallel rectangles are separated by 0.5 m. The rectangles are of size 1.2 x 1.8 m. The space between the rectangles is filled with H_2O vapor at P = 1 atm and T = 1200 K. Assume for this calculation that only the 2.7-μm spectral band of H_2O participates in radiative absorption and emission by the gas and use the data of Table A.2 of on-line Appendix A to compute ε_g. Rectangle 1 has T_1 = 1460 K, ε_1 = 1.0. Rectangle 2 has T_2 = 515 K, ε_2 = 0.6. Assume that the surroundings are at low temperature. Compute the total energy being added to each plate, using the method of Section 10.6.4 of the text.

B.2 A rectangular enclosure that is very long normal to the cross section shown has diffuse-gray walls at conditions shown below and encloses a uniform gray gas at T_g = 1500 K. The gas has an absorption coefficient of 0.25 m^{-1}. Find the average net radiative flux at each surface, and the energy necessary to maintain the gas at 1500 K.

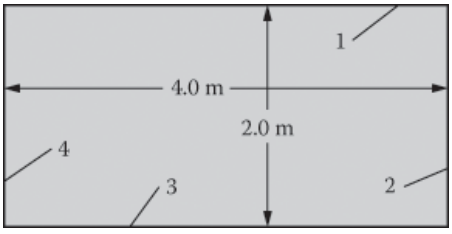

Surface	ε	T_w(K)
1	1.0	2000
2	0.5	1500
3	0.1	1000
4	0	500

Answer: $q_1 = 607$ kW/m^2; $q_2 = -75.1$ kW/m^2; $q_3 = -39.3$ kW/m^2;
energy added = 2,121 kW/m.

REFERENCES

Anderson, K. M., and Hadvig, S.: Geometric Mean Beam Lengths for a Space between Two Coaxial Cylinders, *JHT*, vol. 111, no. 3, pp. 811–813, 1989.

Dunkle, R. V.: Geometric Mean Beam Lengths for Radiant Heat-Transfer Calculations, *JHT*, vol. 86, no. 1, pp. 75–80, 1964.

Edwards, D. K.: Radiant Interchange in a Nongray Enclosure Containing an Isothermal Carbon Dioxide–Nitrogen Gas Mixture, *JHT*, vol. 84, no. 1, pp. 1–11, 1962.

Edwards, D. K., and Nelson, K. E.: Rapid Calculation of Radiant Energy Transfer between Nongray Walls and Isothermal H_2O or CO_2 Gas, *JHT*, vol. 84, no. 4, pp. 273–278, 1962.

Edwards, D. K., Glassen, L. K., Hauser, W. C., and Tuchscher, J. S.: Radiation Heat Transfer in Nonisothermal Nongray Gases, *JHT*, vol. 89, no. 3, pp. 219–229, 1967.

Hottel, H. C, and Sarofim, A. F.: *Radiative Transfer*, McGraw–Hill, New York, 1967.

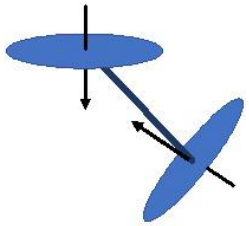

C: EXPONENTIAL KERNEL APPROXIMATION

The solution for a gray medium in radiative equilibrium without internal heat sources between diffuse-gray walls was derived in Section 12.4.5 of the text in terms of the functions ψ_b and ϕ_b, that have been evaluated numerically and are in Table 12.2 and Figure 12.4 of the text. An approximate solution for ψ_b and ϕ_b is found here by using an approximation for the exponential integrals in the radiative flux equation. The ψ_b and ϕ_b are for black walls, so that $J_1 = \sigma T_{w1}^4$ and $J_2 = \sigma T_{w2}^4$ Without convection, conduction, or internal heat sources, the radiative flux q_r is independent of position and is equal to the flux q transferred between the walls. Then, with the dimensionless forms in Equation 12.71 of the text, Equation 12.63 relating the flux and temperature distribution becomes

$$\psi_b = 2E_3(\tau) + 2\int_{\tau^*=0}^{\tau} \phi_b(\tau^*)E_2(\tau-\tau^*)d\tau^* - 2\int_{\tau^*=\tau}^{\tau_D} \phi_b(\tau^*)E_2(\tau^*-\tau)d\tau^* \qquad (C.1)$$

From Appendix D of the text, the E_2 and E_3 are closely approximated by the exponential functions $E_2(\tau) \cong \frac{3}{4}\exp\left(-\frac{3}{2}\tau\right)$ $E_3(\tau) \cong \frac{1}{2}\exp\left(-\frac{3}{2}\tau\right)$. These approximations are inserted into Equation C.1 to yield

$$\psi_b = e^{-3\tau/2} + \frac{3}{2}e^{-3\tau/2}\int_{\tau^*=0}^{\tau} \phi_b(\tau^*)e^{-3\tau^*/2}d\kappa^* - \frac{3}{2}e^{3\tau/2}\int_{\tau^*=\tau}^{\tau_D} \phi_b(\tau^*)e^{-3\tau^*/2}d\tau* \qquad (C.2)$$

To solve for ψ_b and ϕ_b, Equation C.2 is differentiated twice with respect to τ, and, to satisfy the heat flux being constant across the distance between the walls, $d\psi_b/d\tau = 0$. This yields

$$0 = e^{-3\tau/2} + \frac{4}{3}\frac{d\phi_b}{d\tau} + \frac{3}{2}e^{-3\tau/2}\int_{\tau^*=0}^{\tau} \phi_b(\tau^*)e^{3\tau^*/2}d\tau^* - \frac{3}{2}e^{3\tau/2}\int_{\tau^*=\tau}^{\tau_D} \phi_b(\tau^*)e^{-3\tau^*/2}d\tau^* \qquad (C.3)$$

Equation C.3 is subtracted from Equation C.2 to give $\psi_b = -(4/3)(d\phi_b/d\tau)$. Since ψ_b, is a constant, this is integrated to yield

$$\phi_b = -\frac{3}{4}\psi_b\tau + C \qquad (C.4)$$

where C is an integration constant. The ψ_b, and C are found by substituting Equation C.4 back into the integral Equation C.2 to obtain

$$\psi_b = e^{-3\tau/2} + \frac{3}{2}e^{-3\tau/2}\int_{\tau^*=0}^{\tau}\left(-\frac{3}{4}\psi_b\tau^* + C\right)e^{3\tau^*/2}d\tau^* - \frac{3}{2}e^{3\tau/2}\int_{\tau^*=\tau}^{\tau_D}\left(-\frac{3}{4}\psi_b\tau^* + C\right)e^{-3\tau^*/2}d\tau^*$$

The integrations are carried out, and after simplification this becomes

$$0 = e^{-3\tau/2}\left(1 - \frac{1}{2}\psi_b - C\right) + e^{3(\tau-\tau_D)/2}\left(-\frac{3}{4}\psi_b\tau_D - \frac{1}{2}\psi_b + C\right)$$

Thus, there are two simultaneous equations for ψ_b and C:

$$1-\frac{1}{2}\psi_b - C = 0 \text{ and } -\frac{3}{4}\psi_b\tau_D - \frac{1}{2}\psi_b + C = 0$$

The solution yields

$$\psi_b = \frac{1}{\frac{3}{4}\tau_D + 1} \tag{C.5a}$$

and $C = 1 - \psi_b/2$. These are substituted into Equation C.4 to give

$$\phi_b(\tau) = \frac{1}{\frac{3}{4}\tau_D + 1}\left[\frac{3}{4}(\tau_D - \tau) + \frac{1}{2}\right] \tag{C.5b}$$

Table C.1 compares Equation C.5*a* with the analytical results from Table 12.2 of the text; agreement is within about 3% for all τ_D.

TABLE C.1
Comparison of Dimensionless Radiative Flux in a One-Dimensional Slab by the Exponential Kernel Approximation with Exact Solution

	Dimensionless Radiative Flux, $\Psi_b(\tau_D)$	
τ_D	Equation C.5*a*	Text Table 11.2
0.2	0.8696	0.8491
0.4	0.7692	0.7458
0.6	0.6897	0.6672
1	0.5714	0.5532
1.5	0.4706	0.4572
2	0.4000	0.3900
3	0.3077	0.3016

The use of the approximate kernel for nongray media and for situations without radiative equilibrium is discussed in Gilles et al. (1969).

REFERENCE:

Gilles, S. E., Cogley, A. C., and Vincenti, W. G.: A Substitute-Kernel Approximation for Radiative Transfer in a Non-Grey Gas near Equilibrium, with Application to Radiative Acoustics, *IJHMT*, vol. 12, pp. 445–458, 1969.

C. Exponential Kernel Approximation

HOMEWORK

C.1 Consider a gray absorbing medium with isotropic scattering between parallel diffuse gray plates at temperatures T_1 and T_2, and spaced D apart. Heat conduction is negligible. Show that the exponential kernel approximation yields the same result for radiative heat transfer as obtained by the diffusion solution with jump boundary conditions. The medium has extinction coefficient β.

C.2 A gray gas is contained between infinite parallel plates. The plates both have emissivity $\varepsilon = 0.30$. Plate 1 is held at temperature $T_1 = 1150$ K, and plate 2 is at $T_2 = 525$ K. The medium between the plates is nonscattering and has a uniform absorption coefficient of $\kappa = 0.75$ m^{-1}. Heat conduction in the gas is neglected. The plane layer geometry is shown below.

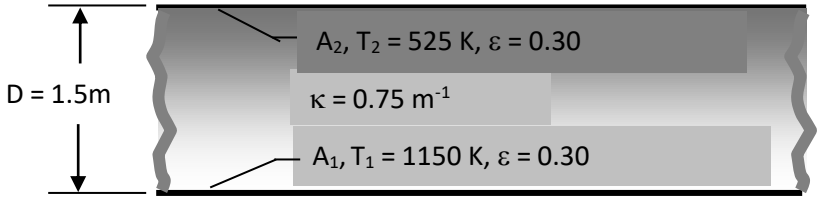

Predict the net radiative heat flux transferred between the surfaces (W/m^2) and plot the temperature profile $[T^4(\kappa) - T_2^4] / (T_1^4 - T_2^4)$ in the gas, where $\tau = \kappa x$. Solve the problem using the exponential kernel approximation. Compare the results with those of Homework Problems 13.4, 13.5 and 13.6.

(SOLUTIONS TO APPENDIX C PROBLEMS ARE IN THE SOLUTION MANUAL AT THE END OF CHAPTER 13 SOLUTIONS)

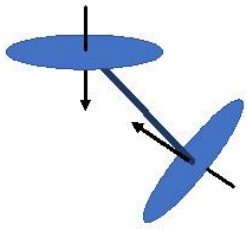

D: CURTIS-GODSON APPROXIMATION

For nonuniform gases a useful method for some radiation analyses is the Curtis-Godson approximation [Edwards and Weiner (1966), Krakow et al. (1966), Simmons (1966, 1968), Goody and Yung (1989)]. The transmittance of a given path through a nonisothermal gas is related to the transmittance through an equivalent isothermal gas. Then the solution is obtained by using isothermal-gas methods. The relation between the nonisothermal and the isothermal gas is found by assigning an equivalent amount of isothermal absorbing material to act in place of the nonisothermal gas. The amount is based on a scaling temperature and a mean density or pressure obtained in the analysis. These mean quantities are found by having the transmittance of the uniform gas be equal to the transmittance of the nonuniform gas in the weak and strong absorption limits.

Goody and Yung , Krakow et al., and Simmons discuss the Curtis-Godson method for attenuation in a narrow vibration-rotation band. Comparisons with exact numerical results were obtained. Weiner and Edwards (1968) applied the method for steep temperature gradients in gases with overlapping band structures. Comparison of the analysis with experimental data was excellent. The Curtis-Godson technique is useful when the gas temperature distribution is specified. If the gas temperature distribution is not known, an iterative procedure would be needed; this is not very practical.

In this development, spectral variations are in terms of wave number, as is common for band correlations. For a nonuniform gas the absorption coefficient κ_η is variable along the path. An effective bandwidth $\bar{A}_t(S)$ is defined, analogous to Equation 9.26 of the text but using an integrated absorption coefficient:

$$\begin{aligned}\bar{A}_t(S) &= \int_{\substack{\text{absorption}\\ \text{bandwidth}}} \left\{1-\exp\left[-\int_0^S \kappa_\eta(S^*)dS^*\right]\right\} d\eta \\ &= \Delta\eta_l - \int_l \left\{\exp\left[-\int_0^S \kappa_\eta(S^*)dS^*\right]\right\} d\eta\end{aligned} \tag{D.1}$$

Similarly, for a path length from S^* to S, the effective bandwidth is

$$\bar{A}_t(S-S^*) = \int_{\substack{\text{absorption}\\ \text{bandwidth}}} \left\{1-\exp\left[-\int_{S^{**}=S^*}^S \kappa_\eta(S^{**})dS^{**}\right]\right\} d\eta \tag{D.2}$$

The integrated equation of transfer for intensity at S by radiation (without scattering) traveling from 0 to S is, from Equation 11.15 of the text,

$$\begin{aligned}I_\eta(S) &= I_\eta(0)\exp\left[-\int_{S^*=0}^S \kappa_\eta(S^*)dS^*\right] + \int_{S^*=0}^S \kappa_\eta(S^*)I_{\eta b}(S^*)\exp\left[-\int_{S^{**}=S^*}^S \kappa_\eta(S^{**})dS^{**}\right]dS^* \\ &= I_\eta(0)\exp\left[-\int_{S^*=0}^S \kappa_\eta(S^*)dS^*\right] - \int_{S^*=0}^S I_{\eta,b}(S^*)\frac{\partial}{\partial S^*}\left\{1-\exp\left[-\int_{S^{**}=S^*}^S \kappa_\eta(S^{**})dS^{**}\right]\right\}dS^*\end{aligned} \tag{D.3}$$

Equation D. 3 is integrated over the bandwidth $\Delta\eta_l$, of the lth band, and the order of integration is changed on the last term. The $I_\eta(S)$, $I_\eta(\eta,0)$, and $I_{\eta b}(S)$ are approximated by average values within the band to yield

$$\begin{aligned} I_l(S)\Delta\eta_l &= I_l(0)\int_l \left\{\exp\left[-\int_{S^*=0}^{S}\kappa_\eta(S^*)\,dS^*\right]\right\}d\eta \\ &= -\int_{S^*=0}^{S} I_{l,\mathrm{b}}(S^*)\frac{\partial}{\partial S^*}\int_l\left\{1-\exp\left[-\int_{S^{**}=S^*}^{S}\kappa_\eta(S^{**})\,dS^{**}\right]\right\}d\eta\,dS^* \end{aligned} \tag{D.4}$$

Equations D.1 and D.2 are substituted into Equation D.4 to obtain the radiative transfer equation in terms of the $\bar{A}_l$.

$$I_l(S)\Delta\eta_l = I_l(0)\left[\Delta\eta_l - \bar{A}_l(S)\right] - \int_{S^*=0}^{S} I_{l,b}(S^*)\frac{\partial\bar{A}_l(S-S^*)}{\partial S^*}dS^* \tag{D.5}$$

An alternative form is found by integrating Equation D.5 by parts to obtain

$$I_l(S)\Delta\eta_l = I_l(0)\left[\Delta\eta_l - \bar{A}_l(S)\right] + I_{l,\mathrm{b}}(0)\bar{A}_l(S) + \int_{S^*=0}^{S}\bar{A}_l(S-S^*)\frac{dI_{l,\mathrm{b}}(S^*)}{dS^*}dS^* \tag{D.6}$$

Equations D.5 and D.6 are nearly exact forms of the integrated RTE in terms of the band properties. The only approximation is that the intensity in each term does not vary significantly across the wave number span of the band. For a uniform gas, Equation D.6 gives (since $dI_{l,\mathrm{b}}/dS = 0$)

$$I_{l,\mathrm{u}}(S)\Delta\eta_l = I_l(0)\left[\Delta\eta_l - \bar{A}_{l,\mathrm{u}}(S)\right] + I_{l,\mathrm{b,u}}(0)\bar{A}_{l,\mathrm{u}}(S) \tag{D.7}$$

where the u subscript denotes a uniform gas.

To compute $I_l(S)$ or $I_{l,u}(S)$ from Equations D.5, D.6, or D.7, expressions are needed for the effective bandwidth $\bar{A}_l$ for nonuniform and uniform gases. From Equations 9.16 and 9.20 of the text, the limiting cases of $\bar{A}_l$ for bands of independent weak or Lorentz strong absorption lines in a uniform gas have the forms

$$\bar{A}_{l,\mathrm{u}}(S) = C_{1,l}\rho S_{\mathrm{u}} \tag{D.8a}$$

$$\bar{A}_{l,\mathrm{u}}(S) = C_{2,l}\rho_{\mathrm{u}}S_{\mathrm{u}}^{1/2} \tag{D.8b}$$

where $C_{l,,1}$ and $C_{2,l}$ are coefficients of proportionality for the lth band, and S_c and γ_c for the lines have been taken as proportional to gas density. For the nonuniform gas the effective bandwidth depends on the variation of properties along the path. The effective bandwidths are obtained by using Equations D.8a and D.8b locally along the path. This gives, for a band of weak lines,

$$\bar{A}_l(S) = C_{1,l}\int_{S^*=0}^{S}\rho(S^*)\,dS^* \qquad \text{(weak)} \tag{D.9a}$$

Similarly, for a band of strong lines, after first squaring Equation D.8b, $\bar{A}_l^2(S) = C_{2,l}^2 \int_{S^*=0}^{S} \rho^2(S^*)\, dS^*$, so that

$$\bar{A}_l(S) = C_{2,l}\left[\int_0^S \rho^2(S^*)\, dS^*\right]^{1/2} \qquad \text{(strong)} \tag{D.9b}$$

It is assumed that the $C_{1,l}$ and $C_{2,l}$ do not vary along the path.

In the Curtis-Godson method the nonuniform gas is replaced by an effective amount of uniform gas such that the correct intensity is obtained at the weak and strong absorption limits. To have the uniform intensity equal the nonuniform intensity, equate Equations D.7 and D.6 and simplify to obtain

$$\left[I_{l,\mathrm{b,u}}(T_\mathrm{u}) - I_l(0)\right]\bar{A}_{l,\mathrm{u}}(S) = \left[I_{l,\mathrm{b}}(0) - I_l(0)\right]\bar{A}_l(S) + \int_{S^*=0}^{S} \bar{A}_l(S - S^*)\frac{dI_{l,\mathrm{b}}(S^*)}{dS^*}\, dS^* \tag{D.10}$$

To have Equation D.10 valid at the weak absorption limit, substitute $\bar{A}_{l,u}$ from Equation D.8a and $\bar{A}_l$ from Equation D.9a to obtain the following after canceling the $C_{1,l}$.

$$\begin{aligned}&\left[I_{l,\mathrm{b,u}}(T_\mathrm{u}) - I_l(0)\right]\rho_\mathrm{u} S_\mathrm{u} \\ &= \left[I_{l,\mathrm{b}}(0) - I_l(0)\right]\int_{S^*=0}^{S} \rho(S^*)dS^* + \int_{S^*=0}^{S}\left[\int_{S^{**}=S^*}^{S} \rho(S^{**})dS^{**}\right]\frac{dI_{l,\mathrm{b}}(S^*)}{dS^*}\, dS^*\end{aligned} \tag{D.11a}$$

Similarly, at the strong absorption limit, insert Equations D.8b and D.9b into Equation D.10 to obtain

$$\begin{aligned}\left[I_{l,\mathrm{b,u}}(T_\mathrm{u}) - I_l(0)\right]\rho_\mathrm{u} S_\mathrm{u}^{1/2} = \left[I_{l,\mathrm{b}}(0) - I_l(0)\right]&\left[\int_{S^*=0}^{S} \rho^2(S^*)dS^*\right]^{1/2} \\ &+ \int_{S^*=0}^{S}\left[\int_{S^{**}=S^*}^{S} \rho^2(S^{**})dS^{**}\right]^{1/2}\frac{dI_{l,\mathrm{b}}(S^*)}{dS^*}\, dS^*\end{aligned} \tag{D.11b}$$

For known temperature and density distributions in a nonuniform gas, Equations D.11a. and D.11b are solved simultaneously for ρ_u and S_u, which are the equivalent uniform gas density and path length for that band. The $I_{l,\mathrm{b,u}}(T_\mathrm{u})$ is not an additional unknown since the temperature T_u corresponds to ρ_u through the ideal gas law. Then Equation D.7 can be used for any effective bandwidth dependence on ρ_u and S_u (that is, not only at the weak and strong limits) to solve for $I_{l,\mathrm{u}}(S)$. This exactly equals $I_l(S)$ in the nonuniform gas in the weak and strong limits and is usually a good approximation for intermediate absorption values. Once the intensities are found, the radiative transfer is obtained by using the relations for a uniform gas. Evaluating Equations D.11a. and D.11b usually requires numerical integration. Because the Curtis-Godson method requires evaluating at least two integrals for each band along each path, it may be equally feasible to numerically evaluate the nearly exact forms Equation D.5 or D.6.

D: Curtis-Godson Approximation

As originally formulated [Goody and Yung (1989)], the Curtis-Godson method was limited to a small wave number span in an absorption band. The limitation was because of line overlapping and the change in the number of important lines with temperature. It has been shown in Weiner and Edwards (1968) and Plass (1967) that the method gives good results even for conditions with large temperature gradients with the use of wide wave number spans. These references also account for overlapping absorption bands. A band absorption formulation analogous to the Curtis-Godson approximation but involving three parameters was developed by Cess and Wang (1970). The additional parameter enabled the equivalent isothermal gas to give the correct behavior in the linear and square-root limits, and in the logarithmic limit for very strong absorption. The method was used to examine the effects of CO2 and water vapor concentration on the atmospheric temperature profile by Ferland and Howell (1972). The further treatment of radiative transfer along strongly nonisothermal paths is in Vitkin et al. (2000). To try to overcome spectral complexity, a Planck-Rosseland gray model has been developed; it is applied to a hypersonic radiating flow in Sakai et al. (2001).

REFERENCES:

Cess, R. D., and Wang, L. S.: A Band Absorptance Formulation for Nonisothermal Gaseous Radiation, *IJHMT*, vol. 13, no. 3, pp. 547–555, 1970.

Edwards, D. K., and Weiner, M. M.: Comment on Radiative Transfer in Nonisothermal Gases, *Combust. Flame*, vol. 10, no. 2, pp. 202–203, 1966.

Ferland, R. E. and Howell, J. R.: Water Vapor, CO_2 and Particulate Effects on the Atmospheric Temperature Profile, *Proc. 1972 Heat Transfer and Fluid Mechanics Institute*, Stanford University Press, 1972.

Goody, R. M., and Yung, Y. L.: *Atmospheric Radiation*, 2d ed., Oxford University Press, New York, 1989.

Krakow, B., Babrov, H. J., Maclay, G. J., and Shabott, A. L.: Use of the Curtis-Godson Approximation in Calculations of Radiant Heating by Inhomogeneous Hot Gases, *Appl. Opt*., vol. 5, no. 11, pp. 1791–1800, 1966.

Plass, G. N.: Radiation from Nonisothermal Gases, *Appl. Opt*., vol. 6, no. 11, pp. 1995–1999, 1967.

Sakai, T., Tsuru, T., and Sawada, K.: Computation of Hypersonic Radiating Flow-Field over a Blunt Body, *JTHT*, vol. 15, no. 1, pp. 91–105, 2001.

Simmons, F. S.: Band Models for Non-isothermal Radiating Gases, *Appl. Opt*., vol. 5, no. 11, pp. 1801–1811, 1966.

Simmons, F. S.: Application of Band Models to Inhomogeneous Gases, Molecular Radiation and Its Application to Diagnostic Techniques (R. Goulard, ed.), NASA TM X-53711, pp. 113–133, 1968.

Vitkin, E. I., Shuralyov, S. L., and Tamanovich, V. V.: Engineering Procedure for Calculating the Transfer of the Selective Radiation of Molecular Gases, *IJHMT*, vol. 43, no. 11, pp. 2029–2045, 2000.

Weiner, M. M., and Edwards, D. K.: Nonisothermal Gas Radiation in Superposed Vibration-Rotation Bands, *JQSRT*, vol. 8, no. 5, pp. 1171–1183, 1968.

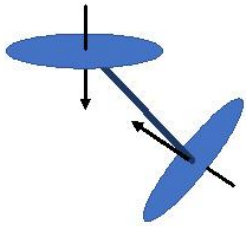

E: THE YIX METHOD

The YIX method (Tan and Howell 1990a, Tan et al. 2000) is a numerical approach that reduces the order of the multiple integrations and has other important attributes. The YIX name is from the shape of the pattern of the integration points for three, two, and four angular directions in a 2D geometry. The integrals over distance are constructed such that results are stored for use in subsequent integrations, allowing integrals to be computed as simple sums.

Subdivide the local intensity integral from the 1D transfer equation so that

$$I = \int_{x=0}^{L} f(x)E_1(x)dx = \sum_{i=1}^{n} \int_{x=x_{i-1}}^{x_i} f(x)E_1(x)dx + \int_{x=x_n}^{L} f(x)E_1(x)dx \tag{E.1}$$

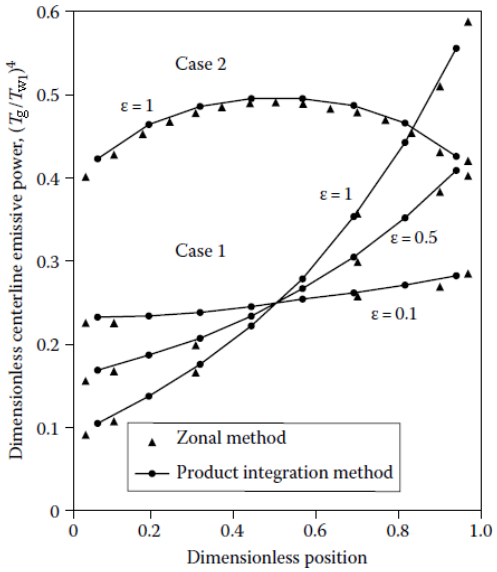

Figure E.1 Centerline dimensionless emissive power in a square enclosure; optical side length τ_D = 1. Case 1, effect of surface emissivity for pure radiation with surfaces at $\vartheta_{w1} = 1$, $\vartheta_{wi} = 0$ for $i = 2$, 3, 4, and case 2, uniform source in medium with $\vartheta_{wi} = 0$ for $i = 1$–4. (From Tan, Z., *JHT*, 111(1), 141, 1989b.)

where $0 = x_0 < x_1 < \ldots < x_n \leq L$ and the individual values of x_i are to be found. The sum accounts for the contribution to I from the subregions from $x = 0$ to x_n. The final term is the contribution in the final interval x_n to L. Each of the integrals over a subregion, $x_{i-1} \leq x \leq x_i$, is expressed as a two-point approximation so that

$$I_i = \int_{x=x_{i-1}}^{x_i} f(x)E_1(x)dx \approx a_i f(x_{i-1}) + b_i f(x_i) \tag{E.2}$$

For $f(x) = 1$ and for $f(x) = x$, Equation E.1 gives the two equations

$$a_i + b_i = \int_{x=x_{i-1}}^{x_i} E_1(x)dx = E_2(x_{i-1}) - E_2(x_i) \tag{E.3}$$

$$a_i x_{i-1} + b_i x_i = \int_{x=x_{i-1}}^{x_i} xE_1(x)dx = x_{i-1}E_2(x_{i-1}) - x_i E_2(x_i) + E_3(x_{i-1}) - E_3(x_i) \tag{E.4}$$

Equations E.3 and E.4 are solved for a_i and b_i, to give

$$a_i = E_2(x_{i-1}) - D(x_i), \quad b_i = D(x_i) - E_2(x_i), \quad \text{and} \quad D(x_i) = \frac{E_3(x_{i-1}) - E_3(x_i)}{x_i - x_{i-1}} \tag{E.5}$$

This approach can be extended to use higher-order approximations of the integrals as provided in Hsu and Tan (1996), but if the intervals $x_i - x_{i-1}$ are small, the two-point approximation is adequate. Substituting Equation E.5 into E.2 and the result into Equation E.1 gives

$$\begin{aligned} I \approx{}& \left[1 - D(x_1)\right] f(0) + \sum_{i=1}^{n-1} \left[D(x_i) - D(x_{i+1})\right] f(x_i) \\ &+ \left[D(x_n) - D(L)\right] f(x_n) + \left[D(L) - E_2(L)\right] f(L) \end{aligned} \tag{E.6}$$

The final simplification that makes this method useful is to let each spatial increment provide the same contribution to the summation in Equation E.6, or $[1 - D(x_1)] = [D(x_i) - D(x_{i+1})] \equiv \beta =$ constant. Substituting into Equation E.6 gives

$$I \approx \beta \left[f(0) + \sum_{i=1}^{n-1} f(x_i) \right] + \left[D(x_n) - D(L)\right] f(x_n) + \left[D(L) - E_2(L)\right] f(L) \tag{E.7}$$

Note that the term $[D(x_n) - D(L)]$ is not equal to β except in the special case when x_{n+1} falls exactly on the boundary at L. This term must be treated separately.

The number of evaluations of the kernel necessary in the original form Equation E.1 has been reduced; only a summation over $f(x_i)$ is necessary over most of the increments in the integration. The kernel evaluations are further reduced by approximating the contribution of the final element where $x_n < x < L < x_{n+1}$ by

$$\begin{aligned} \int_{x=x_n}^{L} E_1(x) f(x)dx &\approx \frac{L - x_n}{x_{n+1} - x_n} \int_{x=x_n}^{x_{n+1}} E_1(x) f(x)dx \\ &\approx \frac{L - x_n}{x_{n+1} - x_n} \left[E_2(x_n) - E_2(x_{n+1})\right] f(x_n), \quad x_n \le L < x_{n+1} \end{aligned} \tag{E.8}$$

This provides an estimate of the contribution of the element lying next to the boundary $x_n < x \le L$, in terms of the more easily calculated contribution of the whole fictitious element $x_n < x < x_{n+1}$. Equation E.7 then becomes

$$I \approx \beta \left[f(0) + \sum_{i=1}^{n-1} f(x_i) \right] + \frac{L - x_n}{x_{n+1} - x_n} \left[E_2(x_n) - E_2(x_{n+1})\right] f(x_n) \tag{E.9}$$

Now, define $Q_i \equiv [E_2(x_{i-1}) - E_2(x_i)]/(x_i - x_{i-1})$ and $P_i \equiv D(x_{i-1}) - E_2(x_{i-1}) - x_{i-1}Q_i - \beta$, and note that $[E_3(x_{n+1}) - E_3(x_n)]/(x_{n+1} - x_n) \approx dE_3(x_n)/dx = -E_2(x_n)$. These relations are substituted into Equation E.9, which becomes, after some algebra using $\xi \equiv D(x_n) - D(x_{n+1})$,

$$I \approx \xi\left[f(0) + \sum_{i=1}^{n-1} f(x_i) \right] + \left[P_{n+1} + LQ_{n+1}\right] f(x_n) \tag{E.10}$$

Once x_1 is specified, the constants D, P, and Q are computed and stored; evaluation of the integral I is then a straightforward summation. The grid spacing is nonuniform and is chosen so that the contribution to the integral from each increment is roughly the same. The integration grid is thus uncoupled from the choice of increment spacing.

An advantage of this method is that $f(x)$ contains the local properties of the medium; if the properties are nonhomogeneous but temperature independent, they are readily incorporated in the solution. Some cases of this type are treated in Tan and Howell (1990). If the properties are temperature dependent, the solution is iterative. The method is readily extended to multidimensional geometries; the exponential integral function E_n is replaced by S_n (Appendix D) in the 2D formulation, as discussed by Tan and Howell. A 2D enclosure with an internal partition is treated by Tan and Howell (1989b), and an anisotropically scattering square medium exposed to a collimated source is analyzed by Tan and Howell (1990b). The method has been applied to radiation with free convection in Tan and Howell (1991), and solutions of the resulting set of equations were obtained using standard linear equation solvers. The method requires precomputation of some coefficients in the solution, but greatly reduces the time for computing the integrals in the radiative source.

REFERENCES:

Hsu, P.-F. and Tan, Z.: Recent benchmarkings of radiative heat transfer within nonhomogeneous participating media and the improved YIX method, in M. P. Mengüç (ed.), *Radiative Transfer I: Proceedings of the First International Symposium Radiative Transfer*, Begell House, New York, 1996.

Tan, Z. and Howell, J. R.: *Radiation Heat Transfer in a Partially Divided Square Enclosure with a Participating Medium*, R. K. Shah (ed.), ASME HTD-vol. 106, pp. 199–203, ASME, New York, 1989b.

Tan, Z. and Howell, J. R.: New numerical method for radiation heat transfer in nonhomogeneous participating media, *JTHT*, 4(4), 419–424, 1990a.

Tan, Z. and Howell, J. R.: Combined radiation and natural convection in a two-dimensional participating square medium, *IJHMT*, 34(3), 785–793, 1991.

Tan, Z.-M., Hsu, P.-F., Wu, S.-H., and Wu, C.-Y.: Modified YIX method and pseudoadaptive angular quadrature for ray effects mitigation, *JTHT*, 14(3), 289–296, 2000.

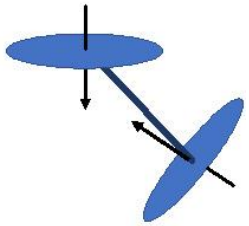

F: CHARTS FOR CO_2, H_2O AND CO EMITTANCE

Alberti et al. (2018) use HITEMP 2010 line-by-line data to compose accurate emittance charts for CO_2, water vapor and CO, along with pressure and overlap corrections for mixtures of these absorbing/emitting gases along with nonparticipating N_2. Aside from the addition of CO to the original Hottel charts (Hottel 1954), the new charts are extended to higher pressures and temperatures. The authors have also constructed curve fits of the new data to allow accurate interpolation, and made available an EXCEL worksheet using these interpolations to allow convenient calculation of the emittance of mixtures of CO_2, H_2O, CO and N_2 at temperatures and pressures within the range of the computed emittance values ($300 < T < 3000$ K and $0.1 < P < 100$ atm). The worksheet is available at ***doi.org/10.1016/j.jqsrt.2018.08.008.***

Prof. Alberti has kindly provided the charts for inclusion here, and they are reproduced below.

For a gas mixture, the total emittance is found from

$$\varepsilon_{tot} = \varepsilon_{H2O} + \varepsilon_{CO2} + \varepsilon_{CO} - \Delta\varepsilon_{CO2}^{H2O} - \Delta\varepsilon_{CO}^{H2O} - \Delta\varepsilon_{CO}^{CO2} + \Delta\varepsilon \qquad \text{(F.1)}$$

In Eq. (F.1), the first three terms are the emittances of the individual gases at their respective pressure-path lengths (bar-cm) and at the mixture temperature, found from Figures F.1 – F.3. These are based on an equivalent pressure, P_E, given by

$$\begin{aligned} P_E^{H2O} &= P_{tot}\left(1 + 5.00 x_{H2O}\right) \\ P_E^{CO2} &= P_{tot}\left(1 + 0.28 x_{CO2}\right) \\ P_E^{CO} &= P_{tot}\left(1 + 0.00 x_{CO}\right) \end{aligned} \qquad \text{(F.2)}$$

where the x_i values are the mole fractions of each component in the mixture with N_2. The next three terms are the binary overlap corrections from Figs. F.4 - F.6, and the final term in Eq. (F.1) is the ternary overlap correction, needed only if more than two gases are present in the mixture. This final term is given by

$$\Delta\varepsilon = \max(\Delta\varepsilon_{CO}^{H2O} + \Delta\varepsilon_{CO}^{CO2} - \varepsilon^{CO} : \varepsilon^{H2O}\varepsilon^{CO2}\varepsilon^{CO}) \qquad \text{(F.3)}$$

Some assumptions are built into the relations for pressure and overlap corrections, but comparisons between emittance values computed from the charts or worksheet and line-by-line calculations have shown that the graphical and worksheet results are within better than 1 percent of the exact LBL values. Alberti et al. (2018) give worked examples to illustrate use of the charts and worksheet.

Tam and Yuen (2019) provide an open-source tool for emittance and absorptance of CO_2-H_2O-N_2-O_2-soot mixtures for combustion calculations. Alberti et al. (2020) provide formulae for gas absorptance of H_2O, CO_2, and CO based on line-by-line calculation and compare with earlier methods.

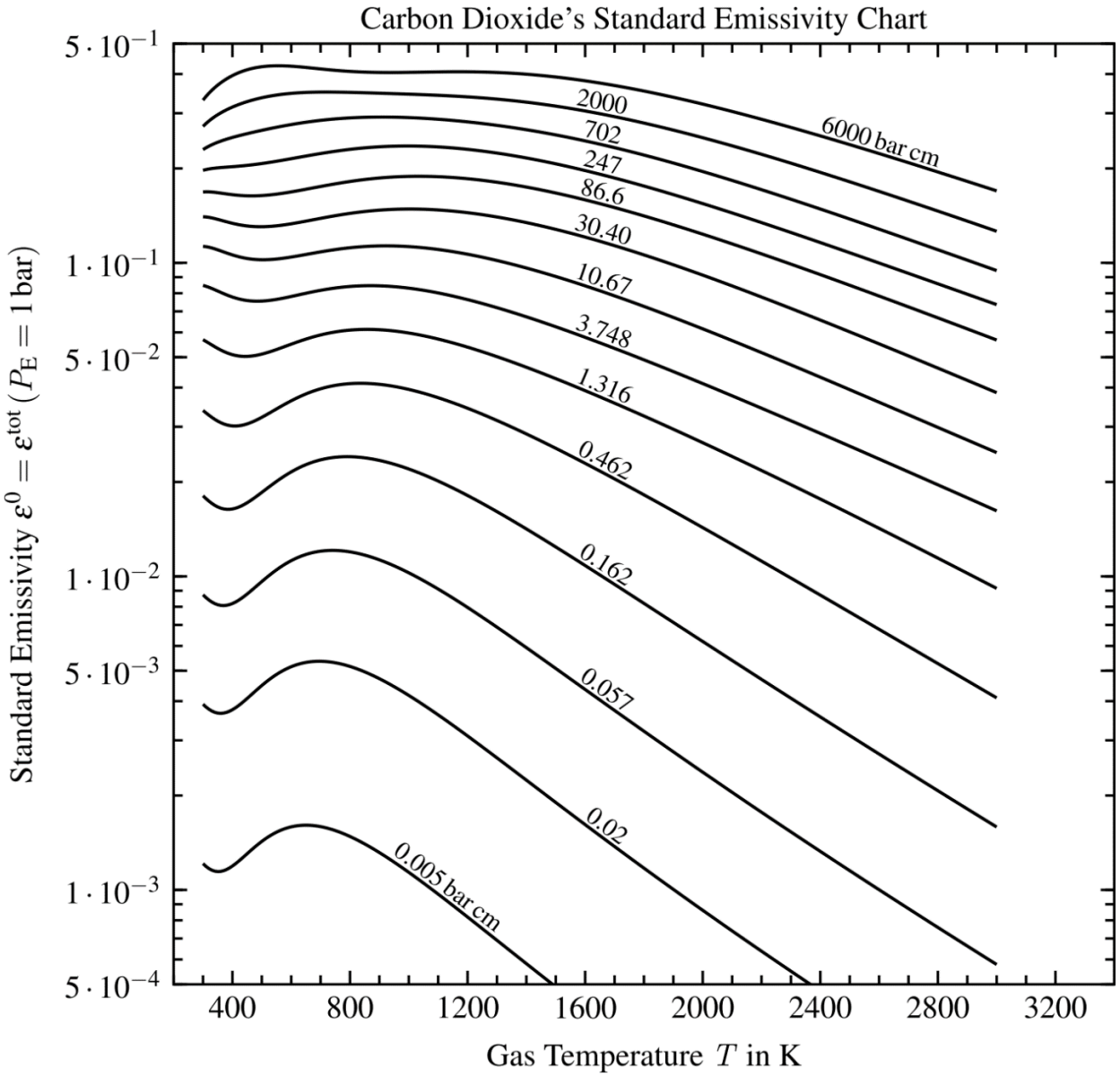

F.1 Emittance of Carbon Dioxide

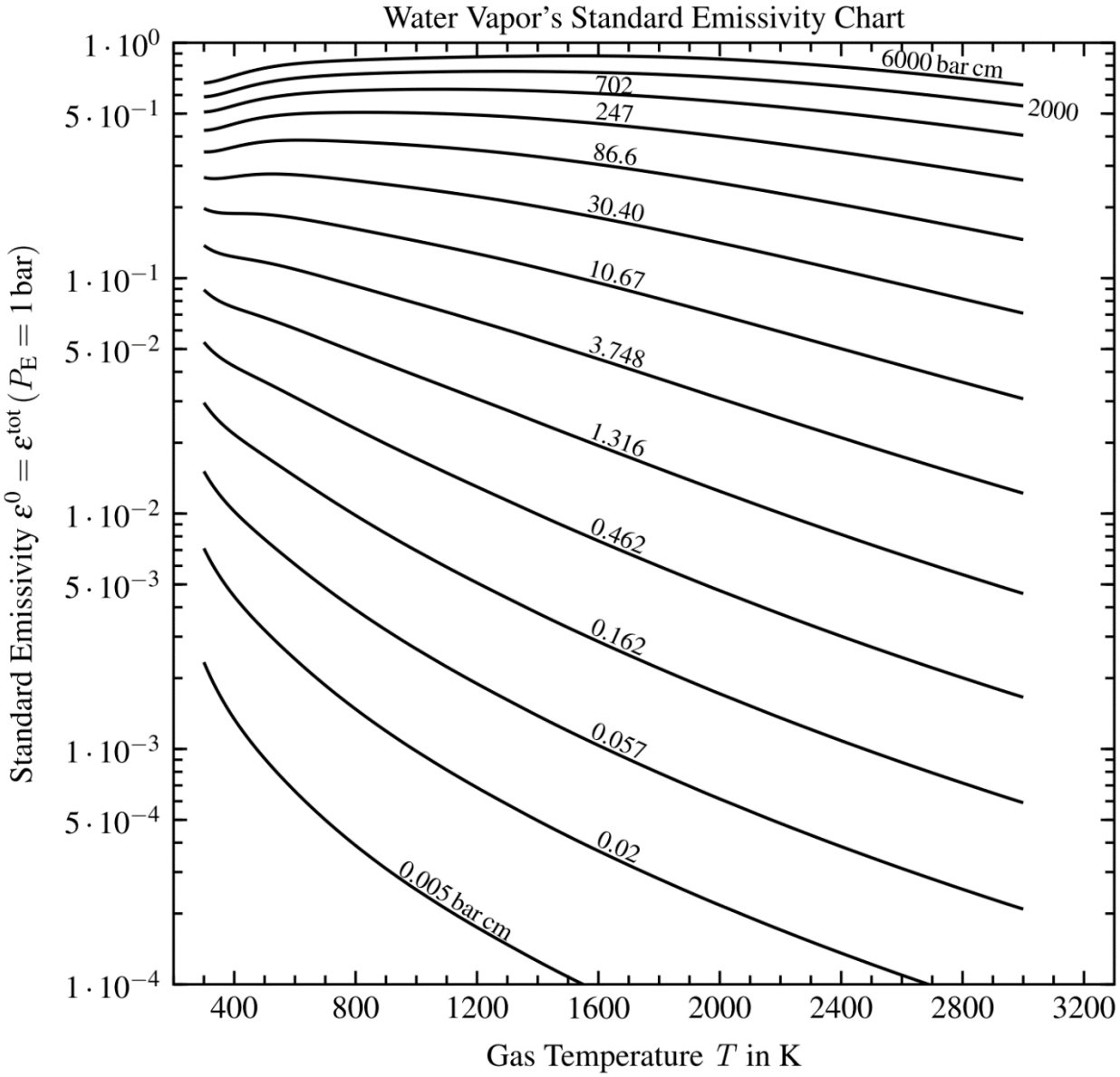

F.2 Emittance of Water Vapor

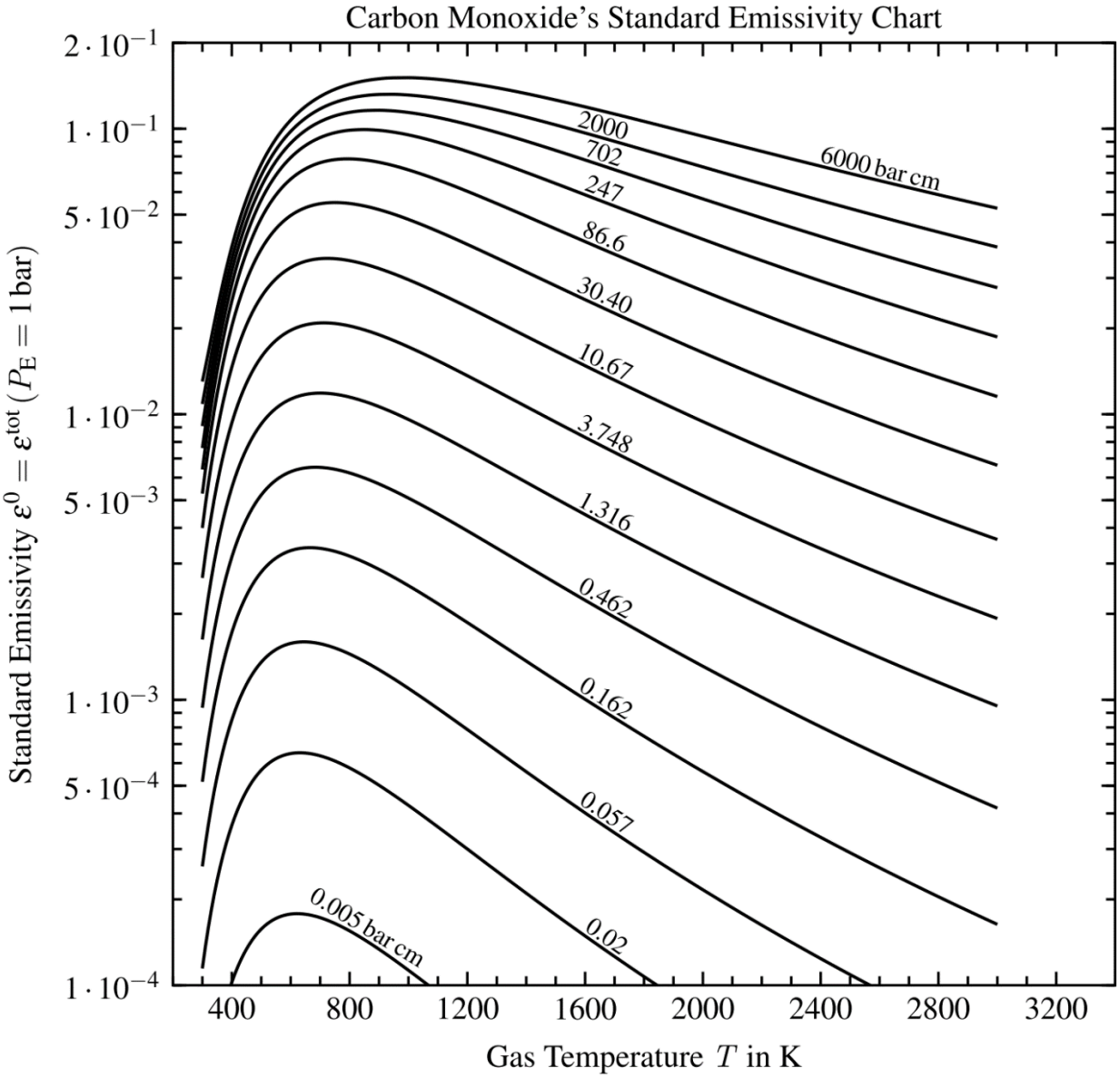

F.3 Emittance of Carbon Dioxide

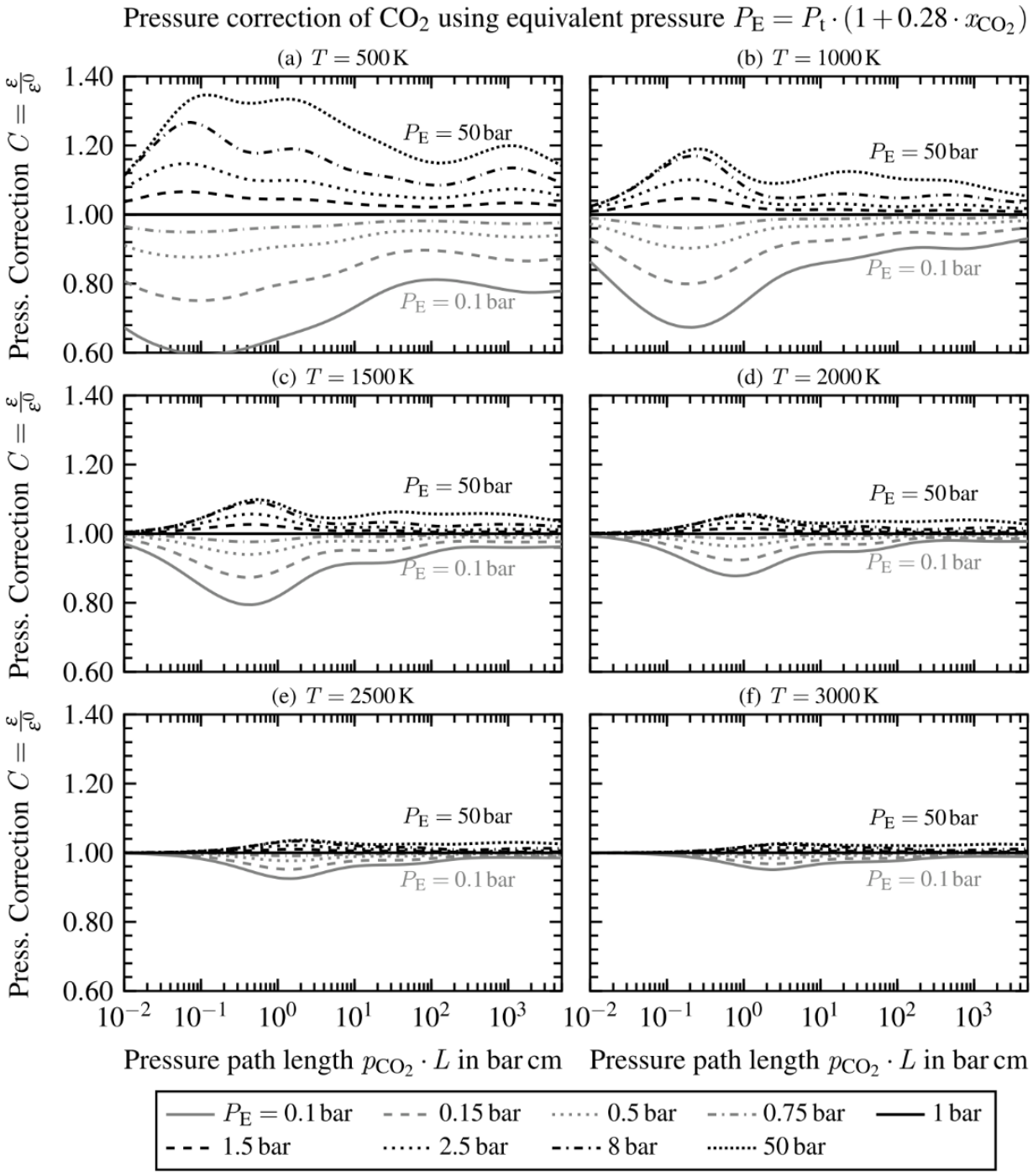

F.4 Pressure Correction for Carbon Dioxide

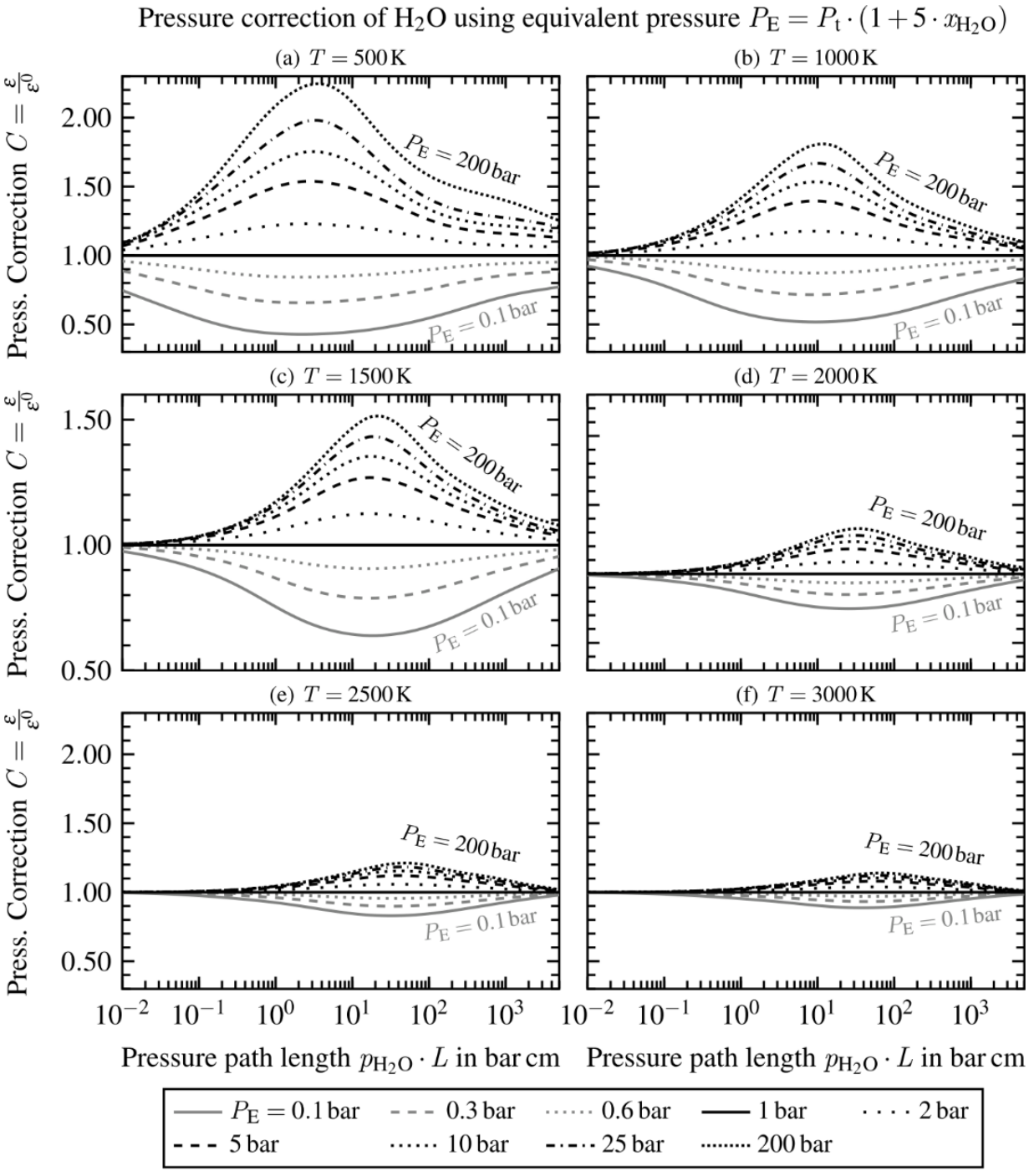

F. 5 Pressure Correction for Water Vapor

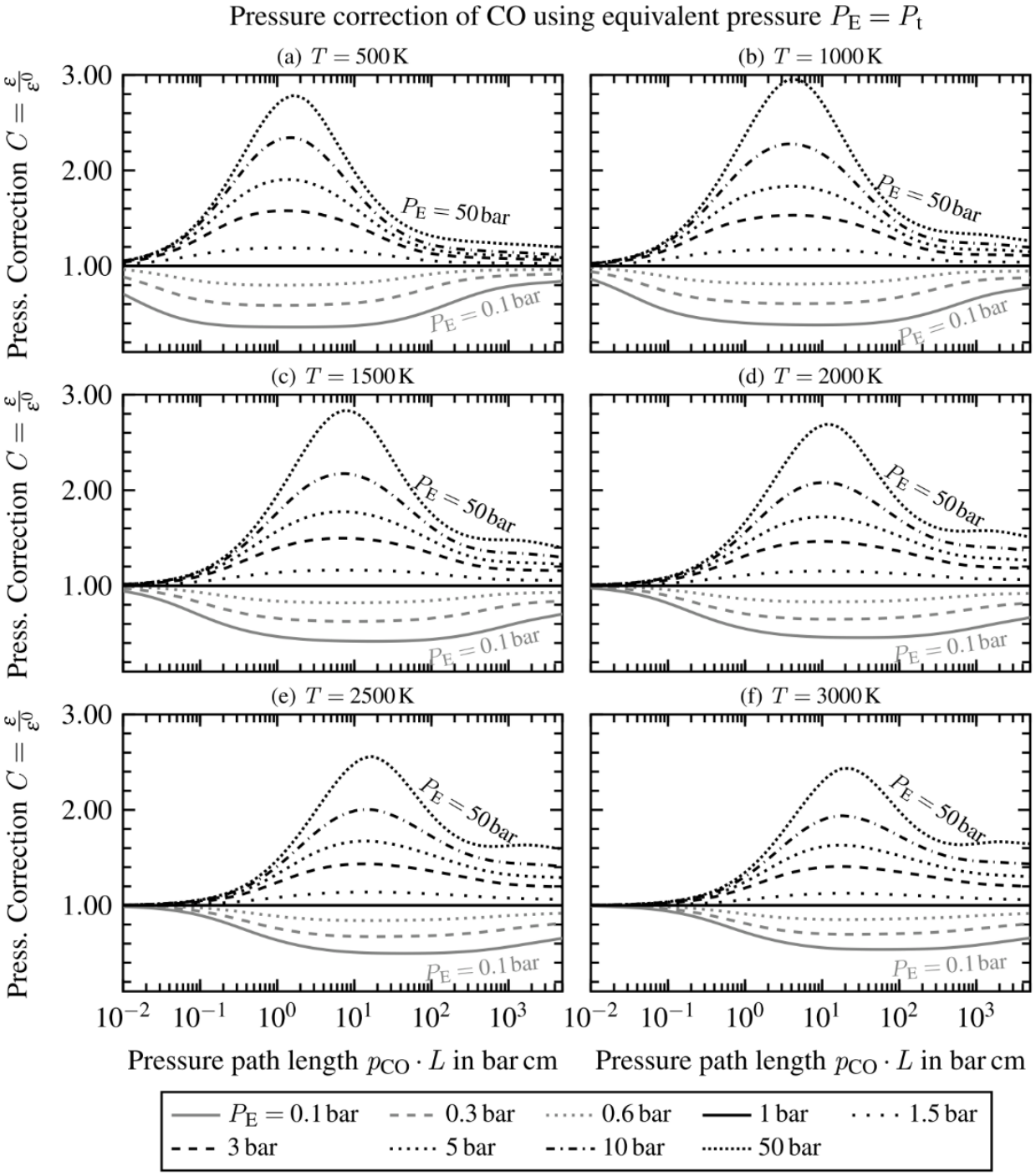

F.6 Pressure Correction for Carbon Monoxide

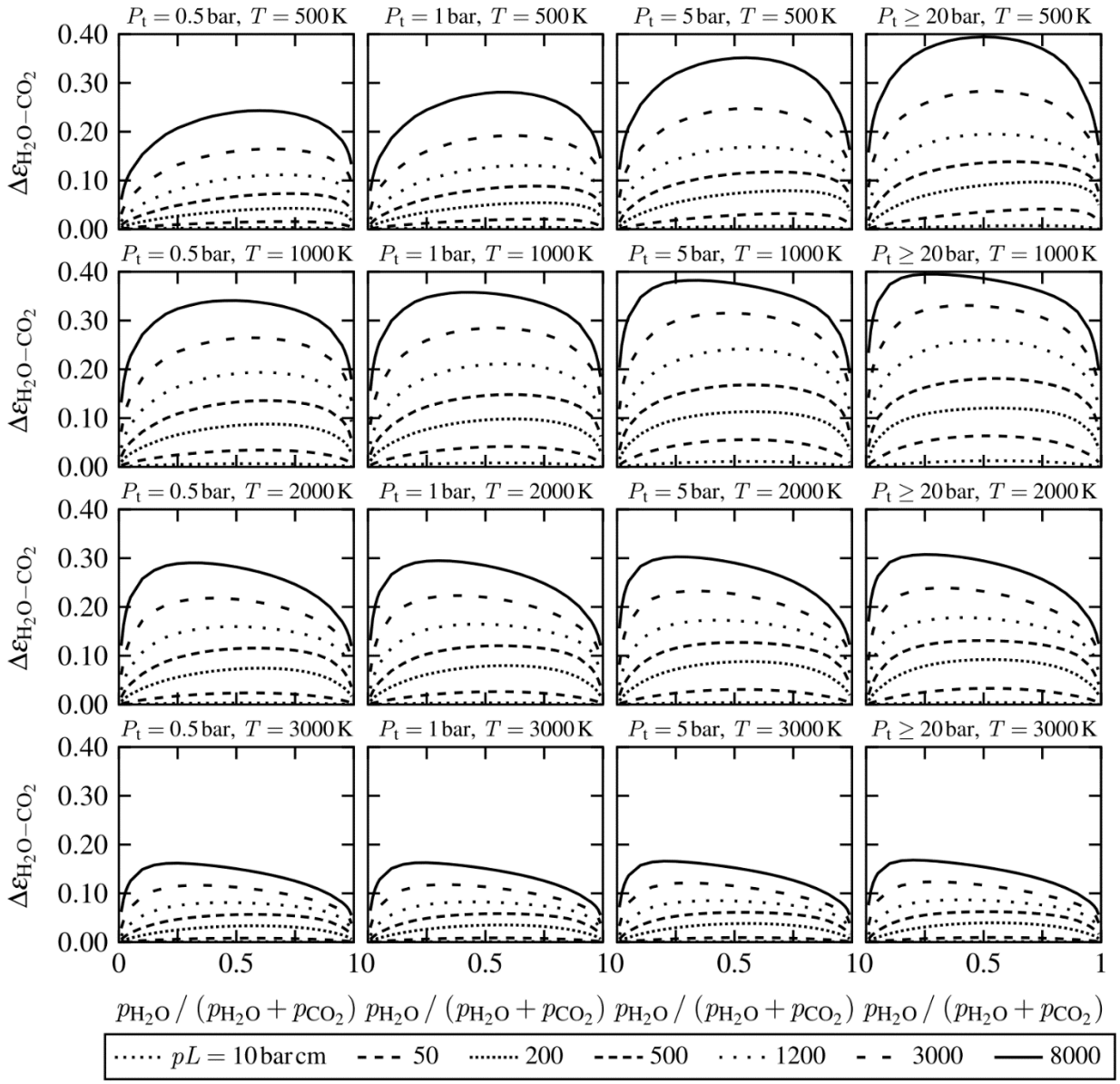

F.7 Overlap Correction for Water Vapor-Carbon Dioxide Mixtures

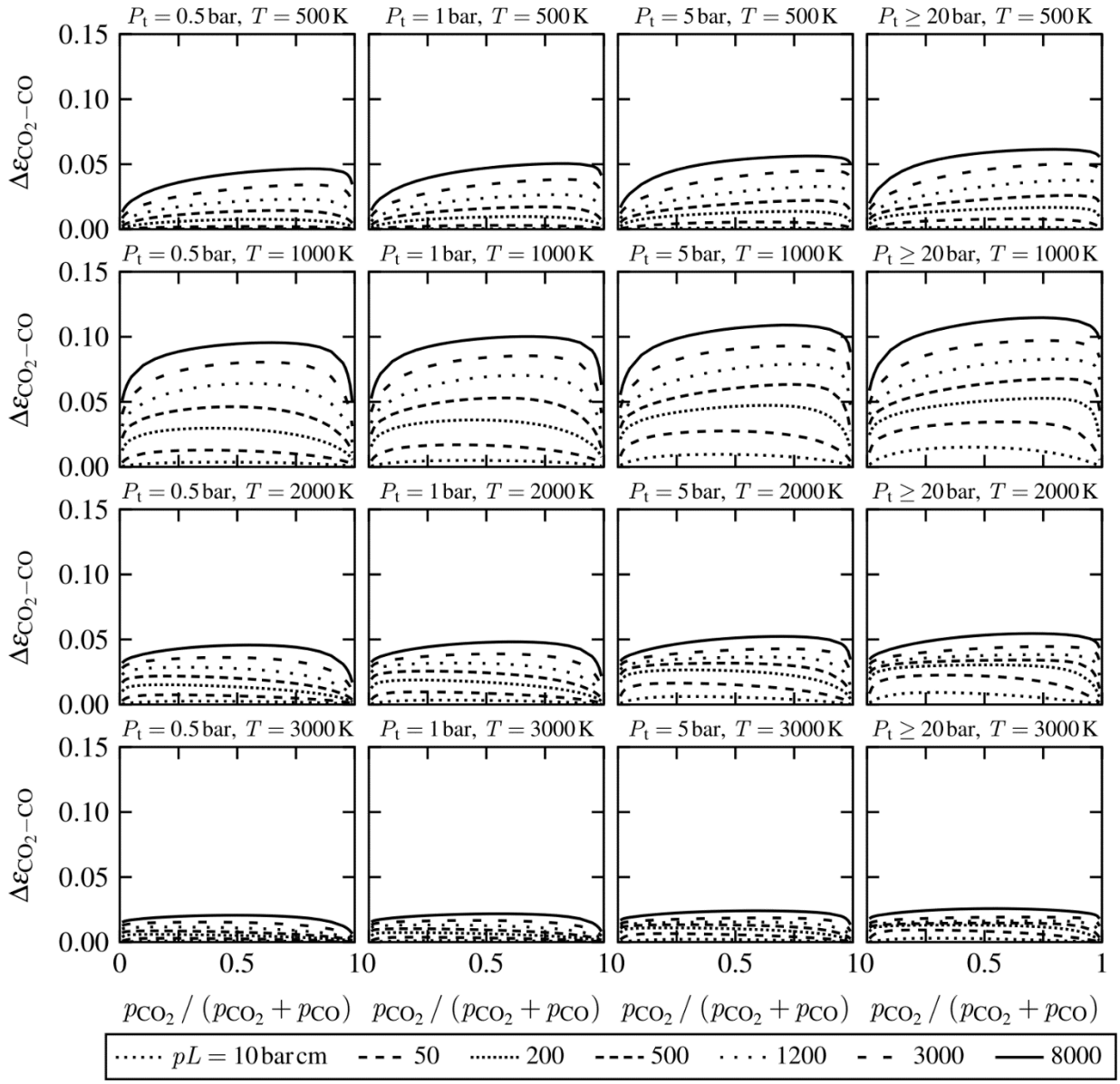

F.8 Overlap Correction for Carbon Dioxide-Carbon Monoxide Mixtures

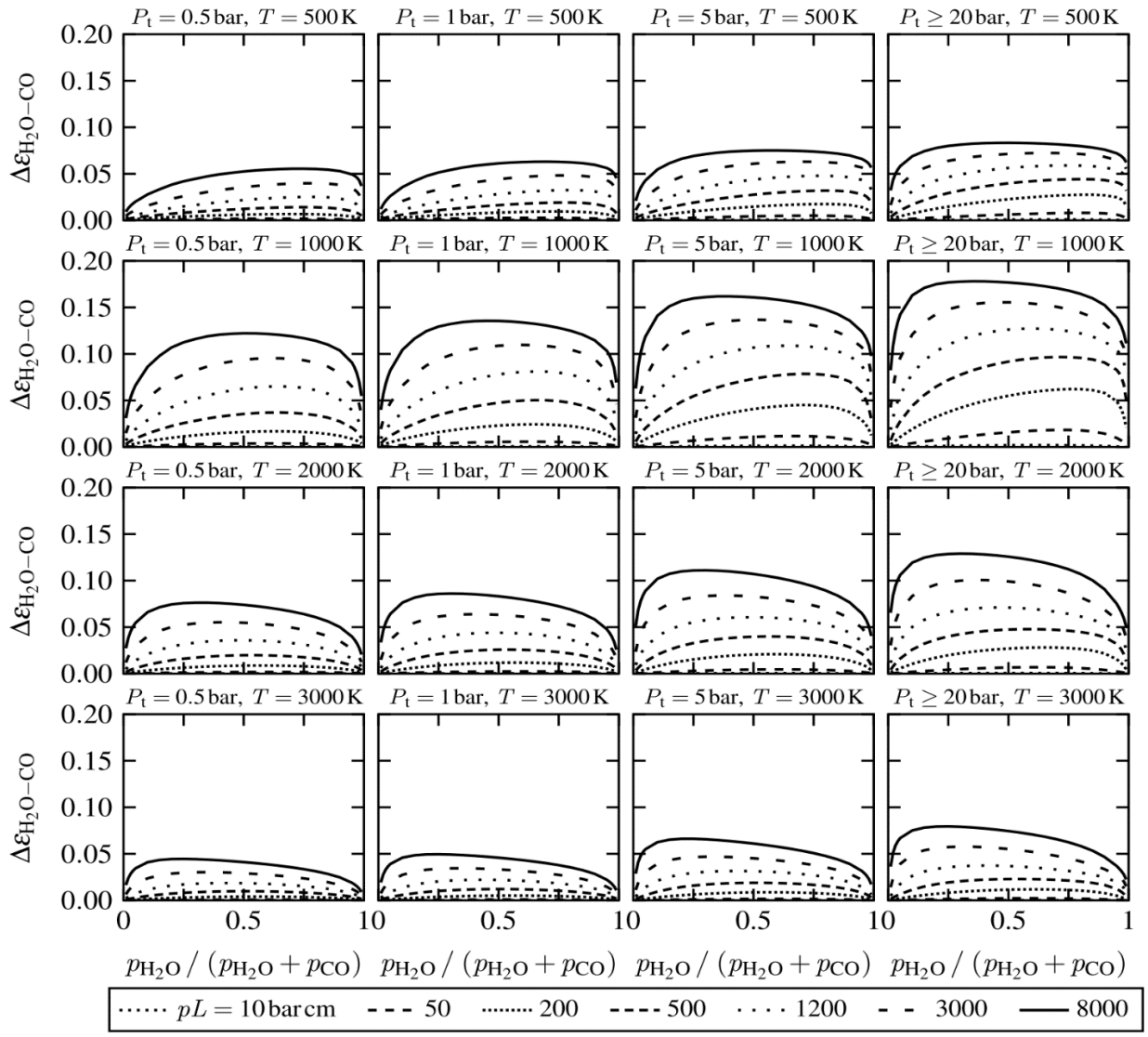

F.9 Overlap Correction for Water Vapor-Carbon Monoxide Mixtures

THE ORIGINAL HOTTEL CHARTS

Hottel's original graphs of the total emittance $\varepsilon(pL_e,T)$ for CO_2 and H_2O (Hottel, 1954; Hottel and Sarofim, 1967) have been widely used since they were published for radiative heat transfer calculations in combustion chambers. They were based on experimental data with extrapolations to high temperatures and large L_e-partial pressure regions based on theory.

Leckner (1972) gives empirical correlations for the total emittance derived from calculations summing narrow band behavior over the spectrum for both water vapor and CO_2. The most accurate expressions from Leckner agree within 5% to values calculated from spectral

data for $T > 400$ K and are in close agreement with Hottel charts for ranges where Hottel based the charts on experimental data. Docherty (1982) compares Leckner's predictions with those of Hottel as well as with more recent experimental data and concludes that Leckner's predictions are more accurate than Hottel charts in the regions where Hottel extrapolated outside the range of experimental data available to him.

Leckner's correlations and equations are functions of p in bar and L_e in cm. The correlation equation is

$$\varepsilon(T, pL_e) = \exp\left\{a_0 + \sum_{j=1}^{M} a_j \left[\log(pL_e)\right]^j\right\} \tag{F.4}$$

where $a_j = c_{0j} + \sum_{i=1}^{N} c_{ij} \left(T/1000\right)^i$ and the values of c_{ij} are in Table F.1 for water vapor and for CO_2.

TABLE F.1
Coefficients c_{ij} for Equation F.4 to Calculate Water Vapor and CO_2 Emittance

j	c_{0j}	c_{1j}	c_{2j}	c_{3j}	c_{4j}
Water vapor, $T > 400$ K, $M = 2$, $N = 2$					
0	−2.2118	−1.1987	0.035596		
1	0.85667	0.93048	−0.14391		
2	−0.10838	−0.17156	0.045915		
Carbon dioxide, $T > 400$ K, $M = 3$, $N = 4$					
0	−3.9781	2.7353	−1.9822	0.31054	0.015719
1	1.9326	−3.5932	3.7247	−1.4535	0.20132
2	−0.35366	0.61766	−0.84207	0.39859	−0.063356
3	−0.080181	0.31466	−0.19973	0.046532	−0.0033086

For water vapor, the pressure correction from Leckner is

$$C_{H_2O} = 1 + (\Lambda_{H_2O} - 1)\Xi_{H_2O} \tag{F.5}$$

where $\Lambda_{H_2O} = \dfrac{\left[1.888 - 2.053\log_{10}(T/1000)\right]P_{E,\,H_2O} + 1.10(T/1000)^{-1.4}}{P_{E,\,H_2O} + \left[1.888 - 2.053\log_{10}(T/1000)\right] + 1.10(T/1000)^{-1.4} - 1}$

and $\Xi_{H_2O} = \exp\left(-\dfrac{\left\{\log_{10}[13.2(T/1000)^2] - \log_{10}(p_{H_2O}L_e)\right\}}{2}\right)$.

The effective pressure is given by $P_{\mathrm{E,\,H_2O}} = P_\mathrm{t}\left[1+4.9(p_{\mathrm{H_2O}}/P_\mathrm{t})(273/T)^{1/2}\right]$ and P_t is the total pressure of the air–H_2O mixture. In the expression for Λ, the T in the expression in square brackets is replaced by 750 if $T < 750$ K.

The pressure correction for CO_2 from Leckner is given by

$$C_{\mathrm{CO_2}} = 1+(\Lambda_{\mathrm{CO_2}}-1)\Xi_{\mathrm{CO_2}} \tag{F.6}$$

where $\Lambda_{\mathrm{CO_2}} = \dfrac{\left[1.00+0.10(T/1000)^{-1.45}\right]P_{\mathrm{E,CO_2}}+0.23}{P_{\mathrm{E,CO_2}}+\left[1.00+0.10(T/1000)^{-1.45}\right]-0.77}$

and $\Xi_{\mathrm{CO_2}} = \exp\left\{-1.47\left[\mu-\log_{10}(p_{\mathrm{CO_2}}L_\mathrm{e})\right]\right\}$.

The effective pressure is given by $P_{\mathrm{E,CO_2}} = P_\mathrm{t}\left[1+0.28(p_{\mathrm{CO_2}}/P_\mathrm{t})\right]$, where P_t is the total pressure of the air–CO_2 mixture. In the expression for Ξ, $\mu = \log_{10}[0.225(T/1000)^2]$ if $T > 700$ K, and $\mu = \log_{10}[0.054(T/1000)^{-2}]$ if $T < 700$ K.

An empirical expression for the band overlap correction that is in good agreement with the Hottel chart (Leckner 1972) valid for $1000 < T < 2200$ K and all pressures is

$$\Delta\varepsilon = \left(\frac{\zeta}{10.7+101\zeta}-0.0089\zeta^{10.4}\right)\left[\log_{10}(pL_\mathrm{e})\right]^{2.76} \tag{F.7}$$

where $\zeta = p_{\mathrm{H_2O}}/\left(p_{\mathrm{H_2O}}+p_{\mathrm{CO_2}}\right)$, $p = \left(p_{\mathrm{H_2O}}+p_{\mathrm{CO_2}}\right)$ is in bars, and L_e is in cm.

The emergence of the accurate line-by-line data bases (used in generating the charts and spread sheet by Alberti et al. 2018) has largely superseded the pioneering work of Hottel.

Example F.1

A container with effective radiation thickness of L_e = 2.4 m contains a mixture of 15 volume percent of CO_2, 20% H_2O vapor, and the remainder air. The total pressure of the gas mixture is 1 atm, and the gas temperature is 1200 K. What is the emittance of the gas?

The partial pressures of the gases are equal to the mole fraction of each times the total pressure. The mole fraction in an ideal gas mixture is equal to the volume fraction, so the partial pressures are $p_{CO_2} = 0.15$, $p_{H_2O} = 0.20$, and p_{air} = 0.65 atm. For water vapor, the a_j values are $a_j = c_{0j} + \sum_{i=1}^{N} c_{ij}\left(T/1000\right)^i$, giving a_1 = −3.599, a_2 = 1.766, and a_3 = −0.248. Using Equation F.4 (remembering to convert the pressures to bars), $\varepsilon_{H_2O}(T, pL_e) = \exp\left\{a_0 + \sum_{j=1}^{M} a_j\left[\log(pL_e)\right]^j\right\} = 0.313$.

A similar calculation for CO_2 gives $\varepsilon(CO_2)$ = 0.155. No pressure correction is necessary because the total pressure is 1 atm. The overlap correction is calculated using

$$\zeta = \frac{p_{H_2O}}{p_{H_2O}+p_{CO_2}} = \frac{0.20}{0.15+0.20} = 0.571$$

and

$$\left(p_{H_2O} + p_{CO_2}\right)L_e = (0.15 + 0.20)\,(\text{atm}) \times 1.01325\,(\text{bar/atm}) \times 240\,(\text{cm})$$
$$= 85.1(\text{bar} \times \text{cm}).$$

Substituting results in

$$\Delta\varepsilon = \left(\frac{\zeta}{10.7 + 101\zeta} - 0.0089\zeta^{10.4}\right)\left[\log_{10}(pL_e)\right]^{2.76} = 0.051$$

The total emittance of the gas mixture is then

$$\varepsilon_{\text{mixture}} = \varepsilon_{H_2O} + \varepsilon_{CO_2} - \Delta\varepsilon = 0.313 + 0.155 - 0.051 = 0.417$$

Using the spreadsheet for the Alberti correlations gives a value of $\varepsilon_{\text{Alberti}} = 0.401$

REFERENCES:

Alberti, M., Weber, R., and Mancini, M.: Gray gas emissivities for H_2O-CO_2-CO-N_2 mixtures, *JQSRT*, 219, 274-291, Nov. 2018.

Alberti, M., Weber, R., and Mancini, M.: New formulae for gray gas absorptivities of H_2O, CO_2, and CO, *JQSRT* 255, 107227, 2020.

Docherty, P.: Prediction of gas emissivity for a wide range of process conditions, Paper R5, *Proceedings of the Seventh International Heat Transfer Conference*, vol. 2, pp. 481–485, Munich, Germany, 1982.

Hottel, H. C.: Radiant heat transmission, Chapter 4, in W. H. McAdams (ed.), *Heat Transmission*, 3rd edn., McGraw-Hill, New York, 1954.

Hottel, H. C. and Sarofim, A. F.: *Radiative Transfer*, McGraw–Hill, New York, 1967.

Leckner, B.: Spectral and total emissivity of water vapor and carbon dioxide, *Combust. Flame*, 19, 33–48, 1972.

Tam, W.C. and Yuen, W. W.: OpenSC – an Open-source Calculation Tool for Combustion Mixture Emissivity/Absorptivity, NIST Technical Note 2064, *National Institute of Standards and Technology*, Sept. 2019.

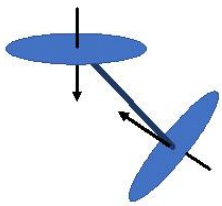

G. RADIATIVE TRANSFER IN POROUS AND DISPERSED MEDIA

Radiative transfer in porous and dispersed media is reviewed in Tien (1988), Dombrovsky (1996), Baillis-Doermann and Sacadura (1998), Howell (2000), Kamiuto (1999, 2008), Nakouzi (2012), and Schoegl (2012) which provide extensive bibliographies. Many early models neglected the effect of anisotropic and/or dependent scattering that have been found important in some applications. If the porous structure is well defined, newer models have moved toward numerical and statistical modeling approaches that incorporate the detailed porous structure and its thermal properties. Considering radiative transfer among the structural elements provides detailed radiative transfer results but does not yield simplified engineering heat transfer correlations. If the structural elements are translucent, refraction at the solid-fluid interfaces must be considered as well as the external and internal reflections that occur at these interfaces (see book Section 17.5.3). Almost always, the structural elements are so closely spaced that dependent scattering occurs (book Section 10.8). The assumption of independent scattering has been shown to fail for systems with low porosity and for packed beds [Singh and Kaviany (1994)], and deviations from independent scattering theory have been found at porosities as high as 0.935.

A less detailed engineering approach has been to assume that the porous material can be treated as a continuum. This depends on the minimum porous bed or medium dimension, L, relative to the particle or pore diameter, D_p or D_pore, and the particle size parameter $\xi = \pi D_P/\lambda$. For most practical systems the porous material is many pore or particle diameters in extent (L/D_pore or $L/D_\mathrm{p} > \sim 10$), and the pores or particles are large relative to the wavelengths of the important radiative energy ($\xi > \sim 5$). In this case, the porous medium may be treated as continuous, and the effective radiative properties are measured by averaging over the pore structure. Traditional radiative transfer analysis methods for translucent media can then be applied without using detailed element-to-element modeling. When temperature gradients are large and/or the thermal conductivity of the elements is small, the assumption of isothermal elements may not be accurate [Singh and Kaviany (1994)]. Combustion in some liquid- and gas-fueled porous burners occurs within the porous structure, producing large temperature gradients; temperatures within the porous medium can increase by over 1000 K within a few pore diameters.

The energy equation for porous media analysis depends on the complexity of the problem to be solved. To determine the energy transfer between the porous solid and a flowing fluid, energy equations are written for both the solid and the fluid, with a convective transfer term providing the coupling between the two equations. This approach permits calculation of the differing bed and fluid temperatures. If the fluid is transparent (no absorption or scattering) the radiative flux divergence is only in the equation for the absorbing and radiating solid structure of the porous material. In this case, the energy equations (in one dimension) become, for the fluid and solid phases,

$$\rho u c_\mathrm{p} \frac{dT_f}{dx} - \frac{d}{dx}\left(k_\mathrm{f} \frac{dT_\mathrm{f}}{dx} \right) - \dot{q} + h_\mathrm{v}(T_\mathrm{f} - T_\mathrm{s}) = 0 \qquad \text{(G.1)}$$

$$\frac{d}{dx}\left(k_s \frac{dT_s}{dx}\right) - \frac{dq_r}{dx} + h_v(T_f - T_s) = 0 \tag{G.2}$$

The h_v is the volumetric convective heat transfer coefficient, and $\dot{q}$ is the volumetric energy source in the fluid from combustion or other internal energy sources. The properties are effective properties that depend on the structure of the solid and the flow configuration. If multiple species are present, as for combustion, additional terms for species diffusion must be included in the fluid-phase equation. The coupling of Equations G.1 and G.2 through the convective transfer terms shows that radiation affects both the solid and fluid temperature distributions even when a radiation term is only in the solid energy equation.

If there is no fluid within the porous medium, a single energy equation is used for the temperature distribution of the solid structure. Then Equations G.1 and G.2 reduce to the steady form of Equation 11.3 of the text with no viscous dissipation. Alternatively, if the fluid flow rate is sufficiently large, the volumetric heat transfer coefficient becomes large and the local fluid and solid temperatures become essentially equal; then Equations G.1 and G.2 combine to give

$$\rho u c_p \frac{dT}{dx} - \frac{d}{dx}\left(k_{eff} \frac{dT}{dx}\right) + \frac{dq_r}{dx} - \dot{q} = 0 \tag{G.3}$$

In this equation, k_{eff} is the effective thermal conductivity of the fluid-saturated porous medium, and the other properties are corrected for the porosity and are on a per unit of total volume basis.

Most analyses of radiative transfer in porous media rely on solving the radiative transfer equation (RTE) and it is necessary to measure or predict the effective continuum radiative properties of the porous medium. This can be done by direct or indirect measurements, or by predicting the properties using models of the geometrical structure and surface properties of the porous structural material. Most radiative property measurements are made by inferring the detailed properties from measurement of radiative transmission or reflection by the porous material. Measured and predicted properties of various packed beds are discussed in Howell (2000), and the properties of open-cell foam insulation are studied in Baillis et al. (2000). Haussener et al. (2009) use computerized tomography to determine the physical characteristics of a packed bed of $CaCO_3$ particles, and then use forward Monte Carlo to determine the spectral scattering and absorption coefficients as well as the spectral phase function. Although the results were independent of the reflectivity characteristics of the system boundaries (specular or diffuse), they were strongly dependent on the assumed reflectivity characteristics of the particles. Barreto et al. (2020) use a Monte Carlo technique with a Henyey-Greenstein phase function to analyze radiative energy transfer through highly porous silicon carbide foams and compare the results with measured transmittance and reflectance from samples.

Solutions are difficult when the radiative mean free path is of the order of the overall bed dimensions. Simplifying assumptions cannot be made, such as an optically thick medium, and in this case a complete solution of the RTE may be required. The two-flux method is often used when one-dimensional radiative transfer is assumed; however, if the particles in the bed are absorbing, this method does not give satisfactory results [Singh and Kaviany (1994)]. If the solid structure of the porous medium has a defined shape it is possible to use conventional surface-to-

surface radiative interchange analysis. This is used in Antoniak et al. (1996) and Palmer et al. (1996) with a Monte Carlo cell-by-cell analysis to simulate radiative transfer among arrays of geometric shapes. Some research has tried to define an effective radiative conductivity that can be combined with heat conduction. For use in optically thick systems with porosity between 0.4 and 0.5, composed of opaque solid spherical particles with surface emissivity ε_r and thermal conductivity of the solid k_s, the radiative conductivity can be approximated by [Singh and Kaviany (1991, 1994), Kaviany (1991)]:

$$k_r = 4D_p\sigma T^3\left\{0.5756\varepsilon_r \tan^{-1}\left[1.5353(k_s^*)^{0.8011}/\varepsilon_r\right]+0.1843\right\} \qquad \text{(G.4)}$$

where $k_s^* = k_s/(4D_p\sigma T^3)$. This is reasonably accurate for both diffuse and specular reflecting particles [the constants in (G.4) are specifically for diffuse surfaces] and is weakly dependent on bed porosity.

An early work on radiation transfer in dispersed media was by Viskanta and Mengüç (1989). Baillis and Sacadura (1996, 2000) have expanded the concept and provided a thorough literature search. Carvajal et al. (2019) compare many standard radiation models for conduction-radiation transfer through high-density insulation and compare predictions with NIST certified values for fiber board. Transport phenomena, including radiation models in solid-gas foams were given by Pilon et al. (2001) and for glass foams the state-of-the-art was discussed by Federov and Pilon (2002). Further applications to foams were reported in several studies by Baillis's group [Loretz et al. (2008); Randrianalisoa et al. 2006; Randrianalisoa and Baillis (2010, 2014); Kaemmerlen et al. (2010); Coquard et al. (2012)]. Diagnosis of foamy and bubbly media also require understanding of radiative transfer and light scattering concepts, as discussed by Wong and Mengüç (2002); Vaillon et al. (2004); Aslan et al. (2006); Swamy et al. (2007); and Gay et al. (2010). Monographs on dispersed systems summarize many formulations and applications specific to practical problems [Dombrovsky and Baillis (2010), Cunsolo et al. (2017)]. The case of long cylindrical fibers in random orientations is analyzed for the geometric optics region using a detailed Monte Carlo analysis in Nisipeanu and Jones (2003). Particle suspensions in liquid are studied in Ma et al. (2015). Ates et al. (2017) examine the effect of gray vs. nongray particle properties in fluidized bed combustors. Liu et al. (2019) provide an alternative to solving the RTE based on the use of a radiation distribution function (the ratio of the absorbed power by particle *j* to the totally emitted radiative power from the source particle *i).* Wu et al. (2020) use a similar approach based on an approximation function model. Wehinger (2019) examines the importance of radiation in fixed-bed reactors. Hashemi and Hashemi (2019) performed a numerical study of 2-D premixed methane-air combustion in a combined porous free-flame burner and compared the results with experiment. Ghorashi et al. (2019, 2020) study a combined porous-free flame burner both numerically and experimentally. Jia et al. (2020) use analysis and experiment to determine the suitability of porous media burners using natural gas fuel for potential use in natural gas stoves. Caetano et al. (2020) measured the angular distribution of radiation from porous burners of zirconia and silicon carbide. Omidi and Emami (2020) measure thermal efficiency, power, and NO_x emission vs. equivalence ratio in a metallic porous media premixed burner. Habib et al (2021) experimentally study methane and biogas combustion in a porous burner. Wang et al. (2020) use a Monte Carlo algorithm to find a graded-porosity medium for use in a central solar power absorber.

REFERENCES:

Antoniak, Z. L., Palmer, B. J., Drost, M. K., and Welty, J. R.: Parametric Study of Radiative Heat Transfer in Arrays of Fixed Discrete Surfaces, *JHT*, vol. 118, no. 1, pp. 228–230, 1996.

Aslan, M. M., Crofcheck, C., Tao, D., and Mengüç, M. P.: Evaluation of Micro Bubble Size and Gas Holdup in Two Phase Gas-Liquid Columns via Scattered Light Measurements, *JQSRT*, vol. 101, pp. 527–539, 2006.

Ates, C., Selçuk, N., Ozen, G., and Kulah, G.: Benchmarking grey particle approximations against nongrey particle radiation in circulating fluidized bed combustors, , 71(5), 467-484, 2017.

Baillis, D., and Sacadura, J.F.: Heat Transfer in Open Cell Foam Insulations, *JHT*, vol. 118, no. 1, pp. 292-298, 1996.

Baillis-Doermann, D., and Sacadura, J. F.: Thermal Radiation Properties of Dispersed Media: Theoretical Prediction and Experimental Characterization, *JQSRT*, vol. 67, no. 5, pp. 327-363, 2000.

Baillis, D., Raynaud, M., and Sacadura, J. F.: Determination of Spectral Radiative Properties of Open-Cell Foam: Model Validation, *JTHT*, vol. 14, no. 2, pp. 137–143, 2000.

Barreto, G., Canhoto, P., and Collares-Pereira, M.: Combined experimental and numerical determination of the asymmetry factor of scattering phase functions in porous volumetric solar receivers, *Solar Energy Materials and Solar Cells*, 206, 110327, March 2020.

Caetano, N. R., Lorenzini, G., Lhamby, A. R., Guillet, V. M. M., Klunk, M. A., Rocha, L. A. O.: Experimental Assessment of Thermal Radiation Behavior Emitted by Solid Porous Material, *Int. J. Heat Technology*, 38(1), 1-8, 2020.

Carvajal, S. A., Garboczi, E. J., and Zarr, R. R.: Comparison of models for heat transfer in high-density fibrous insulation, *J. Research National Institute of Standards and Technology*, 124, 124010, 2019.

Coquard, R., Rochais, D., and Baillis, D.: Conductive and Radiative Heat Transfer in Ceramic and Metal Foams at Fire Temperatures, *Fire Tech.*, vol. 48 no. 3, pp. 699-732, 2012.

Cunsolo, S., Coquard, R., Baillis, D., and Nicola Bianco, N.: Radiative properties modeling of open cell solid foam: Review and new analytical law, *IJTS*, 104, 12-134, 2016.

Dombrovsky, L. A.: *Radiation Heat Transfer in Disperse Systems*, Begell House, New York, 1996.

Dombrovsky, L.A., and Baillis, D.: Thermal Radiation in Disperse Systems: An Engineering Approach, Begell House, 2010.

Fedorov, A.G., and Pilon, L.: Glass Foams: Formation, Transport Properties, and Heat, Mass, and Radiation Transfer, *J. Non-Crystalline Solids*, vol. 311, no. 2, pp. 154-173, 2002.

Gay, B., Vaillon R., and Menguc, M. P.: Polarization Imaging of Multiply-scattered Radiation Based on Integral-Vector Monte Carlo Method, *JQSRT*, vol. 111, pp. 287-294, 2010.

Ghorashi, A., Hashemi, A., Hashemi, M., and Mollamahdi, M.: Experimental study on pollutant emissions in the novel combined porous-free flame burner, *Energy*, 162, 517-525, 2018.

Ghorashi, A., Hashemi, A., Hashemi, M., Hashemi, A., and Mollamahdi, M.: Numerical study on the combustion characteristics in a porous-free flame burner for lean mixtures, *J. Mechanical Engng. Sci*, 1989-1996, Nov. 2019.

Habib, R., Yadollahi, B., Doranehgard, M. H., Li, L. K. B., and Karimi, N.: Unsteady ultra-lean combustion of methans and biogas in a porous burner- An experimental study, *Appl. Thermal Engineering*, 182, 116099, 2021.

Hashemi, S. V., and Hashemi, S. A.: Investigation of the premixed methane–air combustion through the combined porous-free flame burner by numerical simulation, *Proc. Institution Mechanical Engineers, Part A: J. Power and Energy*, Jan. 9, 2019.

Haussener, S., Lipiński, W., Petrasch, J., Wyss, P., and Steinfeld, A.: Tomographic Characterization of a Semitransparent-Particle Packed Bed and Determination of Its Thermal Radiative Properties, *JHT*, vol. 131, no. 7, pp. 072701–072712, July 2009.

Howell, J. R.: Radiative Transfer in Porous Media, in K. Vafai (ed.), *Handbook of Porous Media*, Chap. 7, Marcel Dekker, New York, 2000.

Jia, Y., Zhou, W., Tang, J., and Luo, Y.: Numerical and Experimental Study on Combustion Performance of an Infrared Radiation Burner with Porous Metal Plaque, in Z. Wang et al. (eds.), *Proc. 11th International Symposium on Heating, Ventilation and Air Conditioning (ISHVAC 2019), Environmental Science and Engineering*, Springer Nature Singapore Pte Ltd., 299-307, 2020.

Kaemmerlen, A., Vo, C., Asllanaj, F., Jeandel, G., and Baillis, D.: Radiative Properties of Extruded Polystyrene Foams: Predictive Model and Experimental Results, *JQSRT*, vol. 111. no. 6, pp. 865-877, 2010.

Kamiuto, K.: Modeling of Elementary Transport Processes and Composite Heat Transfer in Open-Cellular Porous Materials, in *Trends in Heat, Mass and Momentum Transfer*, U. Ramchandran, exec. ed., vol. 5, pp. 141–161, *Research Trends*, Trivandrum, India, 1999.

Kamiuto, K.: Modeling of Composite Heat Transfer in Open-Cellular Porous Materials at High Temperatures, in A. Achsner, G. E. Murch, and M. J. S. de Lemos (eds.), *Cellular and Porous Materials: Thermal Properties Simulation and Prediction*, Wiley-VCH, Weinheim, 2008.

Kaviany, M.: *Principles of Heat Transfer in Porous Media*, Springer-Verlag, New York, 1991.

Liu, B., Zhao, J., and Liu, L.: Continuum approach based on radiation distribution function for radiative heat transfer in densely packed particulate system, *JQSRT*, 253, 107028, Sept. 2020.

Loretz, M., Coquard, R., Baillis, D., and Maire, E.: Metallic Foams Radiative Properties/Comparison between Different Models, *JQSRT*, vol. 109, no. 1, pp. 16-27, 2008.

Ma, C.Y., Zhao, J.M., Liu, L.H., and Zhang, L.: GPU-Accelerated Inverse Identification of Radiative Properties of Particle Suspensions in Liquid by Monte Carlo, *Proc. 5th Int. Symp. Computational Thermal Radiation in Participating Media*, Albi, France, 1-3 April 2015.

Mujeebu, M. A., Abdullah, M. Z., Abu Bakar, M. Z., Mohamad, A. A., Muhad, R. M. N., and Abdullah, M. K.: Combustion in porous media and its applications – A comprehensive survey, *J. Environmental Management*, 90, 2287-2312, 2009.

Mujeebu, M. A.: Combustion in Porous Media for Porous Burner Application, in *Convective Heat Transfer in Porous Media*, Mahmoudi, Y., Hooman, K., and Vafai, K. (eds.), Taylor and Francis-CRC Press, 2020.

Nakouzi, S.: *Modelization du Procédé de Cuisson de Composites Infusés par Chauffage Infra Rouge*, doctoral thesis, Institut Clément Ader, Ecole des Mines d'Albi, l'Université de Toulouse, Albi, France, 2012.

Nisipeanu, E. and Jones, P.: Monte Carlo Simulation of Radiative Heat Transfer in Course Fibrous Media, *JHT*, vol. 125, pp. 748-752, 2003.

Omidi, M. and Emami, M. D.: Experimental investigation of premixed combustion and thermal efficiency in a porous heating burner, *Int. J. Energy Res.*, accept. 18 July, 2020.

Palmer, B. J., Drost, M. K., and Welty, J. R.: Monte Carlo Simulation of Radiative Heat Transfer in Arrays of Fixed Discrete Surfaces Using Cell-to-Cell Photon Transport, *IJHMT*, vol. 39, no. 13, pp. 2811–2819, 1996.

Pilon, L., Fedorov, A.G., and Viskanta, R.: Steady-state Thickness of Liquid–gas Foams, *J. of Colloid and Interface Science*, vol. 242, no. 2, pp. 425-436, 2001.

Randrianalisoa, J., and Baillis, D.: Radiative Properties of Densely Packed Spheres in Semitransparent Media: A New Geometric Optics Approach, *JQSRT*, vol. 111, no. 10, pp. 1372-1388, 2010.

Randrianalisoa, J.H., and Baillis, D.: Analytical Model of Radiative Properties of Packed Beds and Dispersed media, *IJHMT*, vol. 70, pp. 264-275, 2014.

Randrianalisoa, J.H., Dombrovsky, L.A., Lipiński, W., and Timchenko, V.: Effects of Short-Pulsed Laser Radiation on Transient Heating of Superficial Human Tissues, *IJHMT*, vol. 78, pp. 488-497, 2014.

Schoegl, I.: Radiation Effects on Flame Stabilization on Flat Flame Burners, *Comb.and Flame*, vol. 159, no. 9, pp. 2817-2828, 2012.

Singh, B. P., and Kaviany, M.: Independent Theory versus Direct Simulation of Radiative Heat Transfer

in Packed Beds, *IJHMT*, vol. 34, pp. 2869–2881, 1991.
Singh, B. P., and Kaviany, M.: Effect of Solid Conductivity on Radiative Heat Transfer in Packed Beds, *IJHMT*, vol. 37, no. 16, pp. 2579–2583, 1994.
Swamy, J.N., Crofcheck, C., and Mengüç, M.P.: A Monte Carlo Ray Tracing Study of the Polarized Light Propagation in Liquid Foams, JQSRT, vol. 101, pp. 527-539, 2007.
Tien, C. L.: Thermal Radiation in Packed and Fluidized Beds, *JHT*, vol. 110, pp. 1230–1242, 1988.
Vaillon, R., Wong, B.T., and Mengüç, M.P.: Polarized Radiative Transfer in a Particle-laden Semi-transparent Medium via a Vector Monte Carlo Method, *JQSRT*, vol. 84, pp. 383-394, 2004.
Wang, P., Li, J. B., Zhou, L., and Liu, D. Y.: Acceptance-rejection sampling based Monte Carlo ray tracing in anisotropic porous media, *Energy*, 199, 117455, May 2020.
Wu, H., Gui, N., Yang, X., Tu, J., and Jiang, S.: An approximation function model for solving effective radiative heat transfer in packed bed, *Annals of Nuclear Energy*, 135, 107000, 2020.
Viskanta, R., and Mengüç, M. P.: Radiative transfer in dispersed media, *ASME Appl. Mechanics Rev.*, vol. 42, pp. 241–259, 1989.
Wehinger, G. D.: Radiation matters in fixed-bed CFD simulations, *Chemie Ingenieur Technik*, 91(5),583-591, 2019.
Wong, B., and Mengüç, M. P.: Depolarization of Radiation by Foams, *JQSRT*, vol. 73, nos. 2–5, pp. 273–284, 2002.

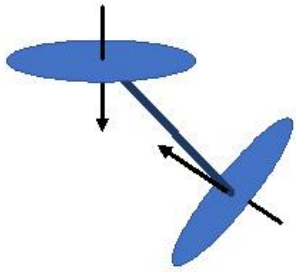

H. BENCHMARK SOLUTIONS FOR VERIFICATION OF RADIATION SOLUTIONS

TABLE H.1 Incident radiation $4\pi\bar{I}$ and z-component of radiative flux q_z in cube of side length $2c$ exposed to uniform diffuse incident radiation q_i on bottom surface $z = -c$ with nonhomogeneous gray extinction coefficient $\beta = (0.05/c) + (0.45/c)\ \{[1-(x^2/c^2)][1-(y^2/c^2)][1-(z^2/c^2)]\}^2$, isotropic scattering, and scattering albedo ω. Results tabulated along line z, $x = y = 0$. Results by numerical quadrature using 17 quadrature points (QM17) [Wu et al. (1996)] (origin of coordinates is at cube center).

	$4\pi\bar{I}(z)/q_i(-c)$		$q_z(z)/q_i(-c)$	
$z/(2c)$	ω = 1.0	ω = 0.5	ω = 1.0	ω = 0.5
−0.49529	2.0674	2.0205	0.9466	0.9746
−0.47534	1.9955	1.9427	0.9410	0.9691
−0.44012	1.8730	1.8107	0.9246	0.9525
−0.39076	1.7066	1.6302	0.8883	0.9150
−0.32884	1.5055	1.4120	0.8251	0.8478
−0.25635	1.2837	1.1745	0.7359	0.7508
−0.17562	1.0588	0.9416	0.6311	0.6355
−0.08924	0.8487	0.7345	0.5259	0,5197
0.00000	0.6667	0.5657	0.4325	0.4180
0.08924	0.5196	0.4374	0.3566	0.3374
0.17562	0.4081	0.3451	0.2987	0.2778
0.25635	0.3280	0.2813	0.2560	0.2357
0.32884	0.2729	0.2384	0.2252	0.2066
0.39076	0.2365	0.2100	0.2033	0.1867
0.44012	0.2131	0.1917	0.1882	0.1733
0.47534	0.1989	0.1803	0.1785	0.1647
0.49529	0.1914	0.1744	0.1734	0.1602

TABLE H.2 Integrated intensity $4\pi\bar{I}$ and surface heat flux distributions q_z, in cylinder with diameter $2r_o$ = height z_o exposed to uniform collimated incident flux $q_i = 1$ on top surface $z = 0$ (positive z extends vertically downward) with nonabsorbing gray homogeneous isotropic scattering, scattering coefficient σ_s, and optical thickness $\tau_{zo} = \sigma_s z_o = 0.25$. Results tabulated along radius $0 < r < r_o$ at z_1 and z_2, and along axial position $0 < z < z_o$ at r_1 and r_2. Results by numerical quadrature using 17 quadrature points (QM17) [Hsu et al. (1999)]

τ_r/τ_{ro}	$4\pi\bar{I}(\tau_r,\tau_{z1})$	$4\pi\bar{I}(\tau_r,\tau_{z2})$	$q_z^-(\tau_r,0)$	$q_z^+(\tau_r,\tau_{zo})$	τ_z/τ_{zo}	$4\pi\bar{I}(\kappa_{r1},\kappa_z)$	$4\pi\bar{I}(\tau_{r2},\tau_z)$	$q_r^+(\tau_{ro},\tau_z)$
0.015625	1.08356	0.85828	0.04490	0.81969	0.015625	1.08356	1.04819	0.02810
0.078125	1.08344	0.85819	0.04484	0.81964	0.078125	1.09101	1.04359	0.03485
0.140625	1.08313	0.85790	0.04464	0.81944	0.140625	1.08377	1.03439	0.03913
0.203125	1.08260	0.85742	0.04434	0.81915	0.203125	1.07618	1.02194	0.04052
0.265625	1.08188	0.85678	0.04390	0.81873	0.265625	1.06548	1.00914	0.04168
0.328125	1.08096	0.85595	0.04337	0.81824	0.328125	1.05352	0.99588	0.04252
0.390625	1.07980	0.85490	0.04271	0.81761	0.390625	1.04008	0.98229	0.04302
0.453125	1.07844	0.85370	0.04194	0.81689	0.453125	1.02603	0.96805	0.04293
0.515625	1.07688	0.85233	0.04106	0.81609	0.515625	1.01082	0.95352	0.04252
0.578125	1.07509	0.85076	0.04006	0.81519	0.578125	0.99534	0.93892	0.04194
0.640625	1.07303	0.84899	0.03892	0.81417	0.640625	0.97851	0.92381	0.04088
0.703125	1.07059	0.84686	0.03749	0.81286	0.703125	0.96127	0.90835	0.03942
0.765625	1.06747	0.84405	0.03557	0.81106	0.765625	0.94304	0.89258	0.03771
0.828125	1.06363	0.84070	0.03334	0.80902	0.828125	0.92268	0.87656	0.03583
0.890625	1.05879	0.83654	0.03064	0.80660	0.890625	0.90140	0.85956	0.03307
0.984375	1.04819	0.82775	0.02527	0.80204	0.984375	0.85828	0.82775	0.02462

[a] $\tau_{r1}=\tau_{ro}/64$, $\tau_{r2}=63\tau_{ro}/64$, $\tau_{z1}=\tau_{zo}/64$, $\tau_{z2}=63\tau_{zo}/64$.

Table H.3 Listing of Benchmark Solution References: Absorbing/Emitting/scattering Media in Simple Enclosures

Geometry	Method	Parameter Range	Boundary Conditions	Comments	Reference
3-D, Cube	Finite element	Given spectral property variation, $\kappa(x,y,z)$; $\omega = 0, 0.9$	Cold, black walls, isothermal medium, isotropic scattering	Compares with YIX and MC solutions.	Burns et al. (1995)
2-D square enclosure	Analytical	All optical thickness	One hot wall, three cold walls; cold medium	Analytical solution; best reference for checking methods in 2-D	Crosbie and Shrenker (1982)
3-D, cube	Analytical	All optical thickness; all ω	One hot wall, 5 cold walls; cold medium, isotropic scattering	Analytical solution; best reference for checking methods in 3-D	Crosbie and Shrenker (1984)
3-D, cube	YIX	$\kappa(x,y,z)$; ω=0 or prescribed linear anisotropic	Cold, black walls, isothermal medium, no or anisotropic scattering	Discussion of error sources in YIX solution relative to exact analytical solution of Crosbie and Shrenker (1984)	Hsu and Tan (1996)
3-D, cube	Numerical quadrature	$\kappa(x,y,z)$; $\omega = 0.5, 1.0$	One hot wall, 5 cold walls; cold gray medium, isotropic scattering	Results in Table F.2	Hsu et al. (1999)
Cylinder with height = diameter	Numerical quadrature	$\tau = \sigma_s z_0 = 0.25$	Cold gray nonabsorbing medium, isotropic scattering, black cold walls except hot top.	Results in Table F.1	Wu et al. (1999)
3-D, cube	Discrete transfer and MC	Given spectral property variation, $\kappa(x,y,z)$; $\omega = 0, 0.5, 0.9$	Cold, black walls, isothermal medium, linear anisotropic scattering	Examines error as a function of angular quadrature	Henson et al. (1997)
3-D, cube	YIX, MC	Given spectral property variation, $\kappa(x,y,z)$; $\omega = 0, 0.9$	All cold, black walls, or 1 hot, 5 cold walls; isothermal medium, isotropic scattering		Hsu and Farmer (1997)
1-D, and 2-D, square	Product Integration	1-D; $\tau = 0.1$, 0.5, 1.0, 3.0 and 3 anisotropic scattering values. 2-D: $\tau = 1$	3-D: 3 sdjacent cold black or diffuse gray walls; 1 hot wall, linear ansotropic scattering. Or, 4 cold black or diffuse gray walls, uniform internal generation, linear anisotropic scattering.	Proposes method to reduce order of integrations required for solution.	Tan (1998)

2-D square enclosure	M_1. S_{32}	$\tau = 5$	Black surfaces	Planar radiation sources at various locations within medium.	Gonzalez et al. (2008)
2-D square enclosure	S_4, S_6, M_1, P_1	$\tau = 0 – 10$, $\omega = 0 - 1$	One hot wall, three cold walls, all black	Compares accuracy of each method with analytical solution of Crosbie and Shrenker (1982)	Tencer and Howell (2013)
2-D square and 3-D cubical	S_8 and S_{16} for 2-D; S_4, S_8 and S_{12} for 3-D.	$\tau = 1$, pure scattering	Black surfaces; One hot wall, three cold walls, isotropic scattering for 2-D; 1 hot, 5 cold walls, Henyey-Greenstein phase function for 3-D	General discussion of factors affecting accuracy of DOM with many references	Coelho (2014)
Annulus between concentric spheres	Analytical derivation with numerical evaluation of weighting functions	Any value of τ or β, $\omega = 0 - 1$ all radius ratios, all boundary temperatures.	Black or gray boundaries, gray medium, linear anisotropic scattering.	Compares results with prior solutions using various methods	Le Dez and Sadat (2015)

Some other benchmark solutions are in Spuckler and Siegel (1996), Olson et al. (2000), Tan et al. (2000), Gonzalez et al. (2009), Joseph et al. (2009)

REFERENCES

Burns, S. P., Howell, J. R., and Klein, D. E.: Finite Element Solution for Radiative Heat Transfer with Nongray, Nonhomogeneous Radiative Properties, *ASME HTD*-vol. 315, pp. 3–10, 1995.

Coelho, P.J.: Advances in the Discrete Ordinates and Finite Volume Methods for the Solution of Radiative Heat Transfer Problems in Participating Media, *JQSRT*, vol. 145, 241-246, 2014.

Crosbie, A. L., and Schrenker, R. G.: Radiative Transfer in a Two-Dimensional Rectangular Medium Exposed to Diffuse Radiation, *JQSRT*, vol. 31, no. 4, pp. 339-372, 1984.

Crosbie, A. L., and Schrenker, R. G.: Exact Expressions for Radiative Transfer in a Three-Dimensional Rectangular Geometry, *JQSRT*, vol. 28, pp. 507-526, 1982.

González, M., Velarde, P., and Garćıa-Fernández, C.: First Comparison of Two Radiative Transfer Methods: M1 and Sn Techniques, *ASP Conference Series*, Vol. 385, Nikolai V. Pogorelov, Edouard Audit, and Gary P. Zank, eds., 2008.

González, M., Garćıa-Fernández, C, and Velarde, P.: 2D Numerical Comparison between S_n and M_1 Radiation Transport Methods, *Annals of Nuclear Energy*, vol. 36, no. 7, pp. 886-895, 2009.

Henson, J. C, Malasekekera, W. M. G., and Dent, J. C.: Comparison of the Discrete Transfer and Monte Carlo Methods for Radiative Heat Transfer in Three-Dimensional, Nonhomogeneous Participating Media, *Num. Heat Transfer*, Part A, vol. 32, no. 1, pp. 19-36, July, 1997.

Hsu, P.-f., and Tan, Z.: Recent Benchmarkings of Radiative Heat Transfer within Nonhomogeneous Participating Media and the Improved YIX Method, Proc. Int. Symp. on Radiation Transfer, ed. by M.P. Mengüç, Kusadasi, Turkey, pp.107-126, Begell House, Inc. NY, August 1995,

Hsu, P.-f, and Farmer, J. T.: Benchmark Solutions of Radiative Heat Transfer within Nonhomogeneous Participating Media Using the Monte Carlo and YIX Method, *JHT*, vol. 119, no. 1, pp. 185-188, 1997.

Hsu, P.-f., Tan, Z. -M., Wu, S. -H., and Wu, C. -Y.: Radiative Heat Transfer in the Finite Cylindrical Homogeneous and Nonhomogeneous Scattering Media Exposed to Collimated Radiation, *Numer. Heat Trans*, vol. 31, no. 8, pp. 819–836, 1999.

Le Dez, V., and Sadat, H.: Radiative Transfer in a Semitransparent Medium Enclosed in a Spherical Annulus, *Int. J. Thermal Sci.*, vol. X, no XX, 2015.

Joseph, D., Perez, P., El Hafi, M., and Cuenot, B.: Discrete Ordinates and Monte Carlo Methods for Radiative Transfer Simulation Applied to Computational Fluid Mechanics Combustion Modeling, JHT, vol. 131, no. 5, pp. 052701-1 to 052701-9, May 2009.

Olson, G. L., Auer, L. H., and Hall, M. L.: Diffusion, P1, and Other Approximate Forms of Radiation Transport, *JQSRT*, vol. 64, pp. 619-634, 2000.

Spuckler, C. M., and Siegel, R.: Two-Flux and Diffusion Methods for Radiative Transfer in Composite Layers, *JHT*, vol. 118, no. 1, pp. 218-222, 1996.

Tan, Z.: Radiative Heat Transfer in Multidimensional Emitting, Absorbing, and Anisotropic Scattering Media-Mathematical Formulation and Numerical Method, *JHT*, vol. l1l, no. l, pp.14l -147, 1989.

Tan, Z. -M., Hsu, P. -F., Wu, S. -H., and Wu, C. -Y.: Modified YIX Method and Pseudoadaptive Angular Quadrature for Ray Effects Mitigation, *JTHT*, vol. 14, no. 3, pp. 289-296, 2000.

Tencer, J. and Howell, J.R.: A Parametric Study of the Accuracy of Several Radiative Transport Solution Methods for a Set of 2-D Benchmark Problems, *Proc. ASME 2013 Summer Heat Transfer Conf.*, Minneapolis, July 14-19, 2013.

Wu, S. -H., Wu, C. -Y., and Hsu, P. -F.: Solutions of Radiative Heat Transfer in Nonhomogeneous Participating Media Using the Quadrature Method, HTD-vol. 332, vol. 1, pp. 101–108, 1996.

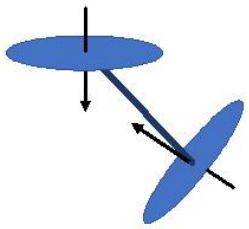

I: INTEGRATION METHODS

I.1: NUMERICAL INTEGRATION METHODS

Integration methods are discussed for use in numerical solutions of pure radiation or combined-mode problems. For radiative exchange, the integrals are often functions of two position variables, and integration is over one or both. For example, the configuration factor dF_{di-dj} from position $\mathbf{r}_i$ on surface i to position $\mathbf{r}_j$ on surface j appears in the integral over surface j to obtain F_{di-j} in the form [see Equation 4.12 in the text]

$$F_{di-j}(\mathrm{r}_i) = \int_{Aj} dF_{di-dj}(\mathrm{r}_i, \mathrm{r}_j) = \int_{Aj} K(\mathrm{r}_i, \mathrm{r}_j) dA_j \tag{I.1}$$

Many ways can be used to numerically approximate an integral. Because the integrands in radiative enclosure formulations are usually well behaved at the end points, *closed* numerical integration forms are often used that include the end points. *Open* methods do not include the end points and can be used when end-point values are indeterminate, such as for improper integrals that yield finite values when integrated. In analyses including convection and/or conduction, the numerical integration will usually use the grid spacing imposed by the differential terms. In some situations, it is enough to use numerical integration methods that have regular grid spacing. However, uneven spacings are often advantageous to place more points in regions where functions have large variations, or to adequately follow irregular boundaries. *Gaussian quadrature* can be used for variable grid spacing. Simpler schemes such as the *trapezoidal rule* or *Simpson's rule* may be adequate for some problems. These often employ uniform grid spacing and are closed, whereas Gaussian quadrature is open. The trapezoidal rule can readily be used with a nonuniform grid size. Textbooks on numerical methods provide detailed presentations of the many available integration methods and their relative accuracies, advantages, and disadvantages. Libraries of computer codes and computational software packages have many subroutines for single or multidimensional numerical integrations that can be applied directly.

I.1.1 TRAPEZOIDAL RULE

The *trapezoidal rule* is a closed numerical integration method that can easily employ a variable increment size. Consider the function in Figure I.1, where an equal grid spacing of Δz is shown for the integration range from z_0 to z_N. In the trapezoidal rule each pair of adjacent points, such as $f(x,z_j)$ and $f(x,z_{j+1})$, is connected by a straight line. Then the integral from z_j to z_{j+1} is approximated by

$$\int_{zj}^{z_{j+1}} f(x,z)dz \approx (z_{j+1} - z_j)\frac{f_j(x) + f_{j+1}(x)}{2}$$

This approximation can be made for each interval between grid points, so an irregular grid spacing can be used. For *equally sized increments*, the sum over all intervals gives the approximation

$$\int_{z_0}^{z_N} f(x,z)\,dz \approx \Delta z\left[\frac{1}{2} f_0(x) + \sum_{j=1}^{N-1} f_j(x) + \frac{1}{2} f_N(x)\right] \tag{I.2}$$

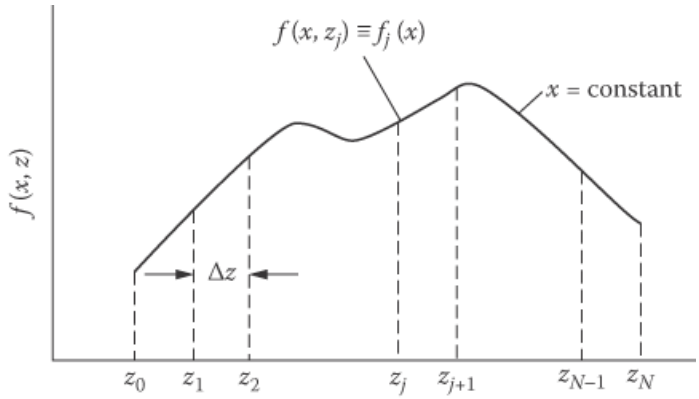

FIGURE I.1 Numerical integration of the function f(x, z) with respect to z for a fixed x.

EXAMPLE I.1

Using the ring-to-ring configuration factor, evaluate the configuration factor from a ring element on the interior of a right circular cylinder to the cylinder base for the geometry in Figure I.2 when $x = r$. Use the trapezoidal rule and compare the result with the analytical solution.

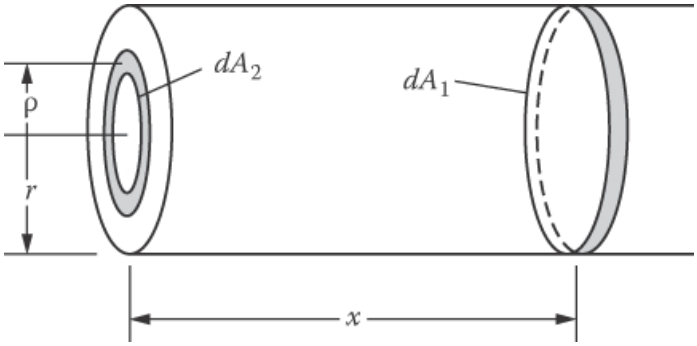

FIGURE I.2 Geometry for configuration factor from ring element on interior of cylinder to ring element on base.

The factor from dA_1 to a ring dA_2 on the base surface is

$$dF_{d1-d2}(X,R) = \frac{2XR(1+X^2-R^2)\,dR}{[(1+X^2+R^2)^2-4R^2]^{3/2}} \tag{I.3}$$

where $X = x/r$ and $R = \rho/r$. For this example, $X = 1$, so $f_j(X = 1, R_j)$ for Figure I.2 is given by

$$f_j(X=1,R_j) \equiv f_j(1) = \frac{2R_j(2-R_j^2)}{(4+R_j^4)^{3/2}}$$

where $R_j = j\Delta R$ and $\Delta R = 1/N$. Letting $f_j(X=1, j\Delta R) \equiv f_j(1)$,

$$f_0(1) = 0, \quad f_j(1) = \frac{2j\Delta R[2-(j\Delta R)^2]}{[4+(j\Delta R)^4]^{3/2}}, \quad f_N(1) = \frac{2}{5^{3/2}}$$

These terms are substituted into Equation I.2, and for $N = 5$ yields $F_{d1-2}(X=1) = (1/5)[(1/2\times 0 + 0.09794 + 0.18225 + 0.23451 + 0.23500 + (1/2)\times 0.17889] = 0.16783$

The exact configuration factor is in Appendix C of the text as

$$F_{d1-2}(X=1) = \frac{X^{*2} + \frac{1}{2}}{(X^{*2}+1)^{1/2}} - X^*, \quad X^* = \frac{x}{2r} = \frac{X}{2} = \frac{1}{2}$$

which gives $F_{d1-2}(X=1) = F_{d1-2}(X^*=0.5) = 0.17082$. Larger numbers of increments improve the accuracy as follows:

N	$F_{d1-2}(X=1)$	% Error
5	0.16783	−1.75
10	0.17007	−0.44
50	0.17079	−0.02
100	0.17081	−0.006
200	0.17082	0

I.1.2 SIMPSON'S RULE

The usual Simpson's rule is obtained by passing a parabola through three adjacent grid points. For equally spaced increments the integral from z_j to z_{j+2} is approximated by

$$\int_{z_j}^{z_{j+2}} f(z)dz \approx \frac{\Delta z}{3}(f_j + 4f_{j+1} + f_{j+2})$$

Because this uses two Δz increments, the repeated application for a range with many grid points requires an *even* number of increments (an odd number of points). For N equally spaced increments in Figure I.1, the result is

$$\int_{z_o}^{z_N} f(z)dz \approx \frac{\Delta z}{3}(f_0 + 4f_1 + 2f_2 + 4f_3 + \cdots + 4f_{N-1} + f_N) \qquad \text{(I.4)}$$

If an odd number of increments must be used, Simpson's rule can be applied over an even number of increments, and the trapezoidal rule used for the remaining increment.

If the curve in Figure I.1 goes through a sharp cusplike peak, it may not be accurate to apply Simpson's rule if the peak is at the central point of the three adjacent points; the cusplike behavior is not accurately approximated by a parabolic curve. Simpson's rule could be used for two increments on each side of the peak. Care should be used in selecting a suitable integration scheme for each application.

Higher-order approximations have been developed by passing a cubic curve through four adjacent points, a fourth-order curve through five adjacent points, etc. These yield the *Newton-Cotes closed integration formulas* of which the trapezoidal and Simpson's rules are the first two. Using a cubic curve through four adjacent points is called *Simpson's second rule*,

$$\int_{z_j}^{z_{j+3}} f(z)dz \approx \frac{3\Delta z}{8}(f_j + 3f_{j+1} + 3f_{j+2} + f_{j+3}) \tag{I.5}$$

In most instances, the functions inside the integrals of the integral equations are complicated algebraic quantities. This is because they involve a configuration factor. There is usually little chance that an analytical solution can be found, so a numerical solution is used. Consider the simultaneous integral equations in Equations 5.21.1 and 5.21.2 of Example 5.21 in the text. With $T_1(x)$ and $T_2(y)$ specified, the right sides are known functions of x and y. Starting with Equation 5.21.1, a distribution for $q_2(y)$ is assumed as a first trial. Then the integration is carried out numerically for various x values to yield $q_1(x)$ at these x locations. This $q_1(x)$ distribution is inserted into Equation 5.21.2 and a $q_2(y)$ distribution is determined. This $q_2(y)$ is used to compute a new $q_1(x)$ from Equation 5.21.2 and the process is continued until $q_1(x)$ and $q_2(y)$ are no longer changing as the iterations proceed.

To perform the integrations in a computer solution, an accurate integration subroutine is required. Many subroutines are available, and they may require functions such as $q_1(x)$ and $q_2(y)$ evaluated at many evenly or unevenly spaced values of the x- and y-coordinates. The values can be obtained by curve fitting the $q_1(x)$ and $q_2(y)$ after each iteration with standard subroutines such as cubic splines. The $q_1(x)$ and $q_2(y)$ are then interpolated at the x and y values called for by the integration subroutine. A precaution should be noted. A quantity such as $J_j\ dF_{dk-dj}$ may go through rapid changes in magnitude because of the geometry involved in the configuration factor; for example, dF_{dk-dj} may decrease rapidly as the distance increases between dA_k and dA_j For small separation distances, there can be a strong peak in the integration kernel. Care should be taken that the integration method is accurate for the functions involved. The integration should be done on each side of a sharp peak and not passed through it.

The Monte Carlo method of Chapter 14 in the text can be used for evaluating integrals, and some discussion of the methodology is given there.

Direct solvers for a set of simultaneous equations can also be used for integral equations. The integrals are expressed in finite-difference form to provide a set of simultaneous equations for the unknowns at each increment position as in Example I.2.

Example I.2

For integral Equation 5.19.1 of Example 5.19 of the text, derive a set of simultaneous algebraic equations to determine $J_2(\xi)$ for $I = 4$. For simplicity, divide the length into four equal increments ($\Delta\eta = 1$) and use the trapezoidal rule for integration.

When Equation 5.19.1 is applied at the end of the tube where $\xi = 0$, the relation is obtained:

$$\begin{aligned} &J_2(0) - \left[\frac{1}{2}J_2(0)K(|0-0|) + J_2(1)K(|1-0|) + J_2(2)K(|2-0|)\right. \\ &\left. + J_2(3)K(|3-0|) + \frac{1}{2}J_2(4)K(|4-0|)\right](1) = q_2 \end{aligned} \tag{I.6}$$

The quantity in brackets is the trapezoidal-rule approximation for the integral. The $K(|\eta-\xi|) = dF(|\eta-\xi|)/d\eta$ is the algebraic expression within the braces of Equation 5.19.2. The $J_2(0)$ terms in Equation I.6 are grouped together to provide the first of Equation I.7. The other four equations are the finite-difference equations at the other incremental positions along the enclosure:

$$\begin{aligned}
&J_2(0)\left[1-\frac{1}{2}K(0)\right]-J_2(1)K(1)-J_2(2)K(2)-J_2(3)K(3)-\frac{1}{2}J_2(4)K(4)=q_2\\
&-\frac{1}{2}J_2(0)K(1)+J_2(1)\left[1-K(0)\right]-J_2(2)K(1)-J_2(3)K(2)-\frac{1}{2}J_2(4)K(3)=q_2\\
&-\frac{1}{2}J_2(0)K(2)-J_2(1)K(1)+J_2(2)\left[1-K(0)\right]-J_2(3)K(1)-\frac{1}{2}J_2(4)K(2)=q_2\\
&-\frac{1}{2}J_2(0)K(3)-J_2(1)K(2)-J_2(2)K(1)+J_2(3)\left[1-K(0)\right]-\frac{1}{2}J_2(4)K(1)=q_2\\
&-\frac{1}{2}q_{o,2}(0)K(4)-q_{o,2}(1)K(3)-q_{o,2}(2)K(2)-q_{o,2}(3)K(1)+q_{o,2}(4)\left[1-\frac{1}{2}K(0)\right]=q_2
\end{aligned} \qquad \text{(I.7)}$$

These equations are solved for J_2 at the five surface locations. From symmetry, and with q_2 uniform along the enclosure, it is possible to simplify the solution for this example by using $J_2(0) = J_2(4)$ and $J_2(1) = J_2(3)$.

Equations such as Equation I.7 are first solved for a moderate number of increments along the surfaces. Then the increment size is reduced, and the solution is repeated. This is continued until sufficiently accurate, $J(\xi)$ values are obtained. Equations I.7 use the trapezoidal rule as a simple numerical approximation to the integrals. More accurate numerical integration schemes can be used, which may reduce the number of increments required for enough accuracy.

Example I.2 has only one integral equation. For the situation with two integral equations in Equations 5.21.1 and 5.21.2 of text Example 5.21, each surface can be divided into increments and equations written at each incremental location. This yields N simultaneous equations for the total of N positions on both plates that are solved simultaneously for the $q_1(x)$ and $q_2(y)$. This procedure is an alternative to the iterative solution described previously. The solver for the system of simultaneous equations may work by iteration.

I.1.3 Other Numerical Integration Methods

Additional numerical integration techniques include Romberg integration, in which the trapezoidal rule is utilized. The integration is performed with a small number of increments and is then repeated for twice the number of increments by adding the contributions from the additional points, four times the number of increments, etc. The sequence of integration results is extrapolated to an improved result using Richardson extrapolation [see Press et al. (1992)]. The process is continued until desired convergence accuracy is achieved in the extrapolated result.

Gaussian integration is very useful; this is an open integration method using an array of unevenly spaced points. The uneven points can be positioned between a fixed grid of evenly or variably spaced points. This can be done by curve fitting, such as by cubic splines, for the individual portions of the curve between the fixed grid points. Values of the integrand at positions between the grid points for use in the Gaussian method are interpolated using the spline coefficients.

Many numerical integration subroutines have been written for computer use and the software can be readily applied. Curve-fitting software routines are available that can be used in conjunction with Gaussian or other techniques, requiring interpolation to obtain unevenly spaced values of the function being integrated. Some subroutines perform multidimensional integrations. Computational software packages for mathematics provide numerical integration using, for example, Romberg integration, Simpson's rule, and adaptive methods; singular and infinite end points are also treated.

Fan et al. (2019) examine fast algorithms for solving the steady state integral form of the RTE based on fast Fourier transforms for homogeneous media and a recursive skeletonization-factorization technique for inhomogeneous media. They show that a unique solution to the RTE exists and provide sample solutions for isotropic and anisotropic scattering in 2- and 3D. Zhou et al. (2020) propose methods to subtract singularities in integrated forms of the RTE for use in analytical and numerical solutions.

I.2: ANALYTICAL INTEGRATION METHODS FOR ENCLOSURES

The unknown wall heat fluxes or temperatures along the surfaces of an enclosure are found from solutions of single or simultaneous integral equations. The integral equations in the formulations up to now are linear; that is, the unknown q, J, or T^4 variables always appear to the first power (note that T^4 is the linear variable rather than T). For linear integral equations, there are various numerical and analytical solution methods; these are discussed in mathematics texts.

For some simple geometries and special conditions, the integral equations describing radiative transfer among surfaces may be solved analytically. Such solutions are usually limited to single-surface or two-surface enclosures, so are not described here in detail.

If the kernel of the integral equation is *separable*, that is, $K(\mathbf{r}_j,\mathbf{r}_k) = F_j(\mathbf{r}_j)F_k(\mathbf{r}_k)$, then $F_k(\mathbf{r}_k)$ may be removed from the integral over $\mathbf{r}_j$, possibly simplifying analytical or numerical integration. However, the kernel in radiation problems usually is *not* separable. The general theory of solution of integral equations using separable kernels is in Hildebrand (1992) and an application using a separable exponential approximation to the kernel (Usiskin and Siegel 1960), allowing reduction of the integral equation to a differential equation, is in Buckley (1927, 1928).

The *variational method* (Hildebrand 1992) may be applied if the kernel is *symmetric*, that is, $K(\xi,\eta) = K(\eta,\xi)$. This approach has been used for radiation in a cylindrical tube (Usiskin and Siegel 1960) and for radiative exchange between infinitely long parallel plates of finite width (Sparrow 1960).

An approximate solution may be obtained through a *Taylor series expansion* (Krishnan and Sundaram 1960, Perlmutter and Siegel 1963), which works well if the kernel $K\left(\left|\xi-\eta\right|\right)$ decays rapidly as $\xi - \eta$ increases as for the cylindrical geometry illustrated in Figure 5.19. The integrand of the integral equations then becomes a series that may be truncated after a few terms and then integrated term by term, reducing the integral equation to a differential equation. Applications are in Choi and Churchill (1985) and Qiao et al. (2000).

The *method of Ambartsumian* can be applied if the temperature or heat flux boundary conditions can be approximately described by an exponential variation or a sum of exponentials, allowing transformation of the integral equation into an initial value problem (Ambartsumian 1942, Kourganoff 1963, Crosbie and Sawheny 1974, 1975).

The problem of finding the intensity leaving a circular opening in a spherical cavity exposed to external uniform heat flux incident on element dA_2, $q_e(dA_2)$, and with a prescribed internal temperature distribution $T(dA_1)$ on the cavity surface has been solved analytically (Jakob 1957, Sparrow and Jonsson 1962). If the internal surface of the cavity has emissivity ε, then the intensity leaving an element dA_1* through the cavity opening in a direction is found to be

$$I\left(dA_1^*\right) = \frac{J_1(dA_1^*)}{\pi} = \frac{\varepsilon\sigma T_1^4\left(dA_1^*\right)}{\pi} + \frac{\frac{1}{\pi}\left(\frac{1-\varepsilon}{4\pi R^2}\right)\left[\int_{A_1}\varepsilon\sigma T_1^4(dA_1)dA_1 + \int_{A_2} q_e(dA_2)dA_2\right]}{1-\left(1-\varepsilon\right)A_1/4\pi R^2} \tag{I.8}$$

All these analytical methods become intractable when multiple surfaces are present, and numerical solution techniques are almost always required for more realistic cases.

I.2.1 Exact Solution of Integral Equation for Radiation from a Spherical Cavity

Radiation from a spherical cavity as in Figure I.3a was analyzed by Jakob (1957) and Sparrow and Jonsson (1962). The spherical shape leads to a relatively simple integral-equation solution because there is an especially simple configuration factor between elements on the inside of a sphere. For the two differential elements dA_j and dA_k in Figure I.3b,

$$dF_{dj-dk} = \frac{\cos\theta_j \cos\theta_k}{\pi S^2} dA_k \tag{I.9}$$

Since the sphere radius is normal to both dA_j and dA_k, the distance between these elements is $S = 2R\cos\theta_j = 2R\cos\theta_k$. Then, Equation I.9 becomes

$$dF_{dj-dk} = \frac{dA_k}{4\pi R^2} = \frac{dA_k}{A_s} \tag{I.10}$$

where A_s is the surface area of the entire sphere. If dA_j exchanges with the finite area, then Equation I.10 becomes

$$F_{dj-k} = \frac{1}{4\pi R^2}\int_{A_k} dA_k = \frac{A_k}{4\pi R^2} = \frac{A_k}{A_s} \tag{I.11}$$

Equation I.11 is *independent of* dA_j, so dA_j can be replaced by any finite area A_j to give

$$F_{j-k} = \frac{A_k}{4\pi R^2} = \frac{A_k}{A_s} \tag{I.12}$$

The configuration factor from any area to any area is simply the fraction of the total sphere area that the *receiving* area occupies.

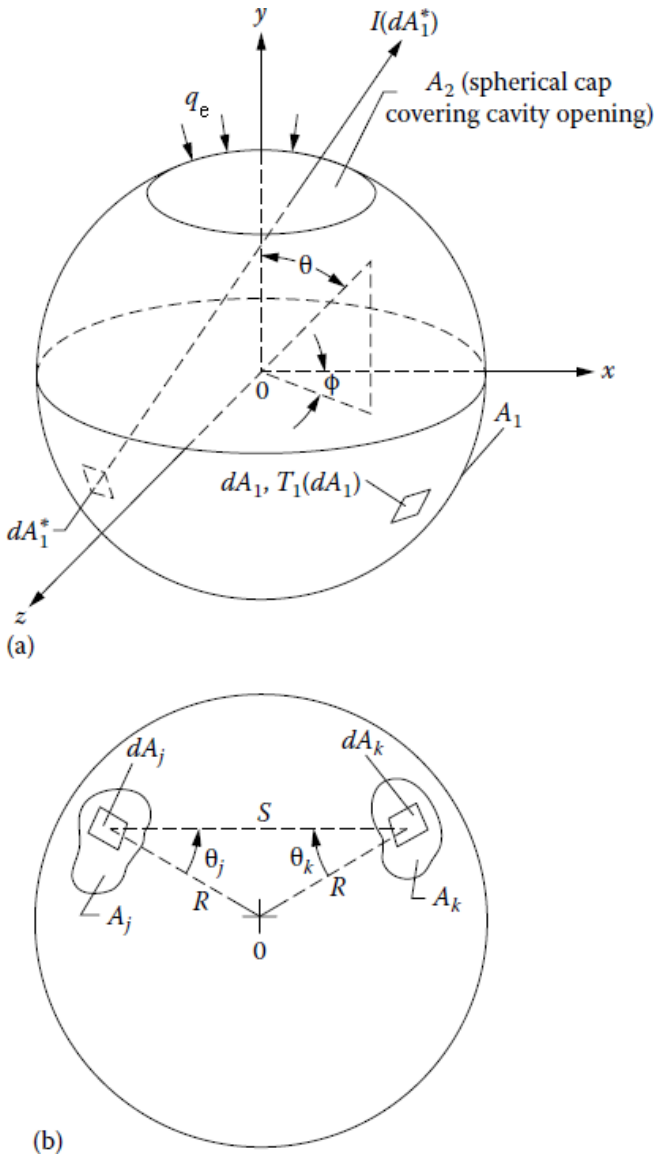

Figure I.3 Geometry for radiation within spherical cavity, (a) spherical cavity with diffuse entering radiation q_e and with surface at variable temperature T_1 and (b) area elements on spherical surface.

Consider the spherical cavity in Figure I.3a with a temperature distribution $T_1(dA_1)$ and a total surface area A_1. The spherical cap that would cover the cavity opening has area A_2. Assume there is diffuse radiative flux q_e (per unit area of A_2) entering through the cavity opening; the q_e can vary over A_2. It is desired to compute the radiation intensity $I(dA_1^*)$ leaving the cavity at a specified location and in a specified direction, as shown by the arrow in Figure I.3a. The desired intensity results from the diffuse flux leaving dA_1^* and equals $J_1(dA_1^*)/\pi$. The $J_1(dA_1^*)$ is found by applying Equation 5.58:

$$J_1\left(dA_1^*\right)-\left(1-\varepsilon_1\right)\int_{A_1}J_1\left(dA_1\right)dF_{d1^*-d1}-\left(1-\varepsilon_1\right)\int_{A_2}q_e\left(dA_2\right)dF_{d1^*-d2}=\varepsilon_1\sigma T_1^4\left(dA_1^*\right) \tag{I.13}$$

and an exact solution will be found. The *F* factors from Equation I.9 are substituted to give

$$J_1\left(dA_1^*\right)-\frac{1-\varepsilon_1}{4\pi R^2}\int_{A_1}J_1\left(dA_1\right)dA_1=\frac{1-\varepsilon_1}{4\pi R^2}\int_{A_2}q_e\left(dA_2\right)dA_2+\varepsilon_1\sigma T_1^4\left(dA_1^*\right) \tag{I.14}$$

To solve Equation I.14, a trial solution $J_1\left(dA_1^*\right)=f\left(dA_1^*\right)+C$ is assumed, where $f(dA_1^*)$ is an unknown function of the location of dA_1^*, and *C* is a constant. Substituting into Equation I.14 gives

$$f\left(dA_1^*\right)+C-\frac{1-\varepsilon_1}{4\pi R^2}\int_{A_1}f\left(dA_1\right)dA_1-\frac{1-\varepsilon_1}{4\pi R^2}CA_1=\frac{1-\varepsilon_1}{4\pi R^2}\int_{A_2}q_e\left(dA_2\right)dA_2+\varepsilon_1\sigma T_1^4\left(dA_1^*\right) \tag{I.15}$$

From the two terms that are functions of local position, $f\left(dA_1^*\right)=\varepsilon_1\sigma T_1^4\left(dA_1^*\right)$. The remaining terms are equated to determine *C*. This gives the desired result as an exact solution:

$$I\left(dA_1^*\right)=\frac{J_1\left(dA_1^*\right)}{\pi}=\frac{\varepsilon_1\sigma T_1^4\left(dA_1^*\right)}{\pi}+\frac{\frac{1}{\pi}\left[\frac{1-\varepsilon_1}{4\pi R^2}\right]\left[\int_{A_1}\varepsilon_1\sigma T_1^4\left(dA_1\right)dA_1+\int_{A_2}q_e\left(dA_2\right)dA_2\right]}{1-\left(1-\varepsilon_1\right)A_1/4\pi R^2} \tag{I.16}$$

I.3 NUMERICAL SOLUTION METHODS FOR NONLINEAR EQUATIONS

Most nonlinear equations for mixed-mode problems with radiation can be cast in the form

$$\left[\mathrm{A}_{ij}\right]\left[\vartheta_j\right]+\left[\mathrm{B}_{ij}\right]\left[\vartheta_j^4\right]=\left[\mathrm{C}_i\right] \tag{I.17}$$

It is important to examine the relative values of the elements A_{ij} and B_{ij}. If the A_{ij} are comparatively large, the problem can be treated as linear in ϑ_j; conversely, for large B_{ij}, the problem can be treated as linear in ϑ_j^4. When the coefficients *A* and *B* are approximately equal, other treatments are in order.

If we define $A_{ij}^*=A_{ij}+B_{ij}\vartheta_j^3$, Equation I.17 becomes

$$\left[A_{ij}\right]\left[\vartheta_j\right]+\left[B_{ij}\right]\left[\vartheta_j^4\right]=\left[A_{ij}+B_{ij}\vartheta_j^3\right]\left[\vartheta_j\right]=\left[A_{ij}^*\right]\left[\vartheta_j\right]=\left[C_i\right] \tag{I.18}$$

This is a set of linear algebraic equations with coefficients A_{ij}^* that are variable and nonlinear. The equations cannot be solved by elimination or direct matrix inversion, because the A_{ij}^* are

temperature dependent and thus are not known. Some numerical solution methods are now discussed.

I.3.1 Successive Substitution Methods

I.3.1.1 Simple Successive Substitution (SSS)

A simple solution method is to assume an initial set of temperatures $\vartheta_j^{(0)}$ and use them to compute $\left[A_{ij}^*\left(\vartheta_j^{(0)}\right)\right]$. This provides values for the elements in the matrix of coefficients, leaving the temperature vector $[\vartheta_j]$ as the unknown. Equation I.18 is then solved for a new set of temperatures $\left[\vartheta_j^{(n+1)}\right]$ from

$$\left[A_{ij}^*\left(\vartheta_j^{(n)}\right)\right]\left[\vartheta_j^{(n+1)}\right]=\left[C_i\right] \tag{I.19}$$

This process is continued until the difference between successive temperature sets is less than an acceptable error, indicating convergence. A difficulty is that this method depends on an accurate initial guess for $[\vartheta_j]$. An inaccurate guess can lead to unstable iterations that may diverge rapidly. For an extended discussion of some of the pitfalls of SSS, see Howell (2017).

I.3.1.2 Successive Underrelaxation

The simple successive substitution (SSS) method can be modified to obtain convergence in many cases if Equation I.17 is written as

$$\left[A_{ij}^*\left(\vartheta_j^{*(n)}\right)\right]\left[\vartheta_j^{(n-1)}\right]=\left[C_i\right] \tag{I.20}$$

where the $A_{ij}^*\left(\vartheta_j^{*(n)}\right)$ are computed at each iteration by using a modified temperature

$$\vartheta_j^{*(n)}=\alpha\vartheta_j^{(n)}+(1-\alpha)\vartheta_j^{(n-1)} \tag{I.21}$$

The α is a weighting coefficient, or *relaxation parameter*, in the range $0 \le \alpha \le 1$. When $\alpha = 1$, the successive underrelaxation (SUR) method reduces to SSS; when $\alpha < 1$, the new guess is weighted toward the previous guess (i.e., underrelaxed), and oscillations between iterations are damped. If possible, the α should be chosen or found that provides optimized convergence. Decreasing α usually provides slower convergence, but greater assurance that convergence will occur. Sometimes decreasing α somewhat will increase convergence by reducing oscillatory behavior. Values of $\alpha \approx 0.3$ are reported by Cort et al. (1982) to provide rapid convergence in many cases.

I.3.1.3 Regulated Successive Underrelaxation

Cort et al. (1982) proposed a method of regulated successive underrelaxation (RSUR) that allows the underrelaxation factor α to be chosen and modified for successive iterations. They recommend the following: (1) Initialize α = 1; (2) solve Equation I.21 for $\vartheta_j^{*(n)}$ (for the first iteration, an initial guess $\vartheta_j^{(0)}$ must be provided); (3) solve Equation I.20 for ϑ_j^{n+1}; (4) calculate

$$\nu^{(n+1)} = \left[\sum_{j=1}^{N} \left(\vartheta_j^{(n+1)} - \vartheta_j^{(n)} \right)^2 \right]^{1/2} \tag{I.22}$$

$$R^{(n+1)} = \left[\sum_{j=1}^{N} \left(\vartheta_j^{(n+1)} \right)^2 \right]^{1/2} \tag{I.23}$$

and if $\nu^{(n+1)} > \nu^{(n)}$ or if $\nu^{(n+1)} > (1/3)R^{(n+1)}$, reduce α by 0.1; and (5) repeat steps (2) through (4) until convergence.

Equation I.22 checks for divergence of the solution between iterations, and Equation I.23 is used to see whether the residual error after each iteration is smaller than a measure of the root-mean-square temperature over the region of the solution. The latter check eliminates slowly oscillating but converging solutions that pass the test of Equation I.22 but converge very slowly.

Another approach is to rewrite Equation I.17 in the form

$$A_{ii}\vartheta_i^{(n+1)} + B_{ii}\left(\vartheta_i^{(n+1)}\right)^4 = C_i - \sum_{j=1}^{N}(1-\delta_{ij})\left[A_{ij}\vartheta_j^{(n+1)} + B_{ij}\left(\vartheta_j^{(n+1)}\right)^4 \right] \equiv D_i \tag{I.24}$$

where δ_{ij} is the Kronecker delta. An initial set of temperatures $\vartheta_j^{(0)}$ is guessed, and D_i is evaluated based on this set. Then the $\vartheta_j^{(1)}$ are found by iterative solution of Equation I.24 and are used to evaluate the next set of D_i. This process is repeated to solve for $\vartheta_i^{(n)}$ until convergence. Tan (1989) points out that, for a given value of i, Equation I.24 is a quartic equation with a single real positive root $\vartheta_i^{(n+1)}$ given by

$$\vartheta_i^{(n+1)} = \frac{y^{1/2}}{2}\frac{p-2}{(p-1)^{1/2}+1} \tag{I.25}$$

where $p = 2\left(1 + \dfrac{4D_i}{B_{ii}y^2}\right)^{1/2}$, $y = \dfrac{2r}{(s+r)^{2/3} + (s-r)^{1/3}[(s+r)^{1/3} + (s-r)^{1/3}]}$

and $r = \dfrac{1}{2}\left(\dfrac{A_{ii}}{B_{ii}}\right)^2$, $s = \left[r^2 + \left(\dfrac{4D_i}{3B_{ii}}\right)^3 \right]^{1/2}$.

Thus, for each set of D_i, the $\vartheta_i^{(n+1)}$ can be found directly from the nonlinear Equation I.24 rather than by an inner iteration and then can be used to evaluate new D_i and continue to the next main

iteration. This method is quite fast and can be combined with the SUR technique to determine succeeding approximations to provide a method that is *both* stable and fast.

I.3.2 Newton–Raphson-Based Methods for Nonlinear Problems

I.3.2.1 Modified Newton–Raphson

A modified Newton–Raphson (MNR) method is in Ness (1959) for the class of nonlinear problems encountered here. Starting from Equation I.17,

$$\left[A_{ij}\right]\left[\vartheta_j\right]+\left[B_{ij}\right]\left[\vartheta_j^4\right]-\left[C_i\right]=0 \tag{I.26}$$

an initial approximate temperature $\vartheta_j^{(0)}$ is guessed at each node. A correction factor δ_j is then computed so that $\vartheta_j=\vartheta_j^{(0)}+\delta_j$. This ϑ_j is used to compute a new δ_j, and this process is continued until δ_j becomes smaller than a specified value. The δ_j are found by solving the set of linear equations:

$$[f_{ij}][\delta_j]+[f_i]=0 \tag{I.27}$$

where

$$f_i=\sum_{j=1}^{N}\left[A_{ij}\vartheta_j^{(0)}+B_{ij}\left(\vartheta_j^{(0)}\right)^4\right]-C_i \tag{I.28}$$

and

$$f_{ij}=A_{ij}+4B_{ij}\left(\vartheta_j^{(0)}\right)^3 \tag{I.29}$$

The MNR method may not converge if a poor initial temperature set is chosen.

7.5.3.2.2 Accelerated Newton–Raphson

Cort et al. (1982) proposed a method in which the amount of change in ϑ_i at each iteration is adjusted to accelerate convergence. They recommended that the f_{ij} in the MNR method be replaced by

$$f_{ij}=A_{ij}+\frac{4B_{ij}}{[1-(\beta/3)]}\left(\vartheta_j^{(0)}\right)^{(3-\beta)} \quad \beta\geq 0 \tag{I.30}$$

This effectively modifies the slope of the changes in ϑ_j with respect to iteration number compared with that used in the MNR method. For $\beta = 0$, the accelerated Newton–Raphson (ANR) method reduces to MNR. If β is too large, oscillations and divergence between iterations may occur. For $\beta = 0.175$, the number of iterations to provide a given accuracy for a particular

problem was reduced from 28 using MNR to 12 using ANR, and reductions in computer time of up to 80% were obtained. A starting value of $\beta = 0.15$ is recommended by Cort et al.

7.5.3.3 Applications of the Numerical Methods

Results using the aforementioned methods were compared in Cort et al. (1982) for some typical radiation–conduction problems with temperature-dependent properties and internal energy generation. Consideration was limited to surfaces with radiative exchanges to black surroundings at a single temperature, and the solutions were by finite elements. Because the example problems in this section showed that even complicated radiation–conduction–convection problems with multiple surfaces reduce to the same general form of Equations 1.17, the conclusions probably apply to a broader class of problems than was studied. In Costello and Shrenk (1966), a linearized solution is proposed that speeds convergence over the MNR method. For problems that are either conduction or radiation dominated or where both modes are important, the method performed well, providing a factor-of-ten improvement in solution speed. It was found that the SUR method gave convergence with the fewest iterations and the least computer time; RSUR was useful to find the optimum value of the relaxation parameter α for use in the SUR method. For the Newton–Raphson method, ANR was always faster than MNR, but neither method was as fast as SUR.

In Howell (1992, 2017), the convergence ranges and behavior of equations of the form of Equations I.17 are discussed, and the various solution methods of this chapter are examined. Nonlinear equations of this type can have behavior characterized by bifurcations and chaos of successive iterations so that steady solutions carried out by SSS, SUR, etc., may not converge. This is true whether the equations are cast as radiation dominated or first-order temperature dominated or the equations used are in mixed form such as Equation I.18. Decreasing the relaxation factor extends the range of convergence, but often will not yield a solution for some ranges of parameters without unacceptable computer time. For conduction–radiation problems, bifurcation–chaos behavior results from the numerical method chosen and the equation form and does not imply that multiple physical solutions can exist. However, when there is coupling between radiation and the flow field, as in combined radiation and free convection, multiple physical steady-state solutions may exist. The particular flow configuration reached in a steady state analysis may depend on the initial conditions chosen and the set of velocity and temperature fields that are traversed in reaching steady state. In some cases, no steady solution is reached; it may be possible to solve for the steady-state solution by using a fully transient solution that proceeds to the final steady state from physically specified initial conditions.

Numerical solution techniques for steady-state and transient combined-mode problems with surface–surface radiative exchange are examined and discussed by Hogan and Gartling (2008). Three techniques that sequentially solve for radiative transfer followed by solution of the energy equation with a radiative source term are compared with a fully coupled solution. For the two example problems studied, the fully coupled method always produced the most accurate solution,

although execution time made it unattractive for very large problems. A semi-implicit technique with a Newton type of update appeared to be the best choice for very large problems.

The finite-difference and finite-element numerical procedures that have been described used radiative enclosure theory with finite or infinitesimal areas to obtain a set of simultaneous equations with configuration factors for radiative exchange between surface areas. Convection was specified in terms of a heat transfer coefficient for each area; for example, for radiation exchange inside a tube with a flowing transparent gas, the heat transfer coefficient inside the tube is obtained from available results from tube flow analyses or experimental correlations. For some situations, however, convection is quite dependent on the surface temperatures, such as for free convection, or the geometry is complex so that convective heat transfer correlations are not available with desired accuracy. In these cases, analyses have been made where convection is solved simultaneously with radiation as the flow and surface temperatures are strongly coupled; conduction may also be included, such as for free convection and radiation from a cooling fin as discussed in Section 7.4.3 of the book. To solve for the convection heat transfer, the methods of computational fluid mechanics are used.

Another consideration is that the analysis may not use configuration factors. The radiative exchange in an enclosure can be computed directly by a ray-tracing technique such as a Monte Carlo method (Chapter 14 of the book). This may be necessary if the surfaces are not diffuse so that configuration factors do not apply. Another solution method where radiation is followed along directions is by use of discrete ordinates. The discrete ordinates method, discussed in Chapter 12, was developed for enclosures filled with a medium that is not transparent, but rather absorbs, emits, and scatters radiation. If radiative participation by the medium is omitted, the method can be applied to enclosures containing a transparent medium such as a convecting nonradiating gas. In this method, the angular directions from each surface element are divided into a finite number, and radiation is followed along these discrete directions to evaluate the radiative exchange. In Tan et al. (1998), discrete ordinates are used in combination with the SIMPLE computer algorithms developed for computational fluid mechanics (Patankar 1980) to simultaneously solve the mass, momentum, and energy equations along with radiation transfer between surfaces.

For natural convection combined with radiation, many computational methods have been used for simultaneously solving the fluid flow and energy equations with radiative exchange. In Zhao et al. (1992), free convection and radiation were analyzed for heated cylinders in a rectangular enclosure. In Dehghan and Behnia (1996), net radiation enclosure analysis was used for the radiative transfer, and the flow and energy equations were placed in finite-difference form and solved with a pseudo transient method to analyze free convection in a cavity with a local heated area on one vertical wall. A vented cavity with a discrete heat source was analyzed by Yu and Joshi (1999) using the numerical methods from Patankar (1980); this study included combined radiation exchange, conduction, and natural convection, with the gas in the cavity being transparent. Free convection of transparent air in a heated vertical channel with one or more vents in one wall was analyzed by Moutsoglou et al. (1992). The flow and energy equations were

solved by using finite-difference computational methods as developed by Patankar and Spalding (1972) and van Doormall and Raithby (1983).

REFERENCES:

Ambarzumian, V. A.: Diffusion of light by planetary atmospheres, *Astron. Zh.*, 19, 30–41, 1942.

Buckley, H.: On the radiation from the inside of a circular cylinder: Part I, *Philos. Mag.*, 4, 753–762, 1927; Part II, *Philos. Mag.*, 6, 447–457, 1928.

Choi, B. C. and Churchill, S. W.: A technique for obtaining approximate solutions for a class of integral equations arising in radiative heat transfer, *Int. J. Heat Fluid Flow*, 6(1), 42–48, 1985.

Cort, G. E., Graham, H. L., and Johnson, N. L.: Comparison of methods for solving non-linear finite element equations in heat transfer, ASME Paper 82-HT-40, *Proc. 21st National Heat Transfer Conf.*, Seattle, August 1982.

Costello, F. A. and Schrenk, G. L.: Numerical solution to the heat-transfer equations with combined conduction and radiation, *J. Comput. Phys.*, 1, 541–543, 1966.

Crosbie, A. L. and Sawheny, T. R.: Application of Ambarzumian's method to radiant interchange in a rectangular cavity, *JHT*, 96, 191–196, 1974.

Crosbie, A. L. and Sawheny, T. R.: Radiant interchange in a nonisothermal rectangular cavity, *AIAA J.*, 13(4), 425–431, 1975.

Dehghan, A. A. and Behnia, M.: Combined natural convection-conduction and radiation heat transfer in a discretely heated open cavity, *JHT*, 118(1), 56–64, 1996.

Fan, Y., An, J. and Yin, L.: Fast algorithms for integral formulations of steady-state radiative transfer equation, *J. Computational Physics*, 380(1), 191-211, Jan. 2018.

Hildebrand, F. B.: *Methods of Applied Mathematics*, 2nd edn., Dover, New York, 1992.

Hogan, R. E. and Gartling, D. K.: Solution strategies for coupled conduction/radiation problems, *Commun. Numer. Methods Eng.*, 24(6), 523–542, June 2008.

Howell, J. R.: Modern computational methods in radiative heat transfer, in K. T. Yang and W. Nakayama (eds.), *Computers and Computing in Heat Transfer Science and Engineering*, pp. 153–171, CRC Press, Boca Raton, FL, December 1992.

Howell, J. R.: The effect of bifurcation on numerical calculation of conjugate heat transfer with radiation, *JQSRT*, 196, 242-245, 2017.

Jakob, M.: *Heat Transfer*, vol. II, Wiley, New York, 1957.

Kourganoff, V.: *Basic Methods in Transfer Problems*, Dover, New York, 1963.

Krishnan, K. S. and Sundaram, R.: The distribution of temperature along electrically heated tubes and coils, I. Theoretical, *Proc. R. Soc. Lond., Ser. A*, 257(1290), 302–315, 1960.

Moutsoglou, A., Rhee, J. H., and Won, J. K.: Natural convection-radiation cooling of a vented channel, *IJHMT*, 35(11), 2855–2863, 1992.

Ness, A. J.: Solution of equations of a thermal network on a digital computer, *Solar Energy*, 3(2), p. 37, 1959.

Patankar, S. V.: *Numerical Heat Transfer and Fluid Flow*, Hemisphere, Washington, DC, 1980.

Patankar, S. V. and Spalding, D. B.: A calculation procedure for heat, mass, and momentum transfer in three-dimensional parabolic flows, *IJHMT*, 15, 1787–1806, 1972.

Perlmutter, M. and Siegel, R.: Effect of specularly reflecting gray surface on thermal radiation through a tube and from its heated wall, *JHT*, 85(1), 55–62, 1963.

Press, W. H., Flannery, B. P., Teukolsky, S. A., and Vetterling, W. T.: *Numerical Recipes in C: The Art of Scientific Computing*, 2d ed., Cambridge University Press, London, 1992.

Qiao, H., Ren, Y., and Zhang, B.: Approximate solution of a class of radiative heat transfer problems, *JHT*, 122(3), 606–612, 2000.

Sparrow, E. M.: Application of variational methods to radiation heat-transfer calculations, *JHT*, 82(4), 375–380, 1960.

Sparrow, E. M. and Jonsson, V. K.: *Absorption and Emission Characteristics of Diffuse Spherical Enclosures*, NASA TN D-1289, Washington, DC, 1962.

Tan, Z., Przekwas, A. J., Wang, D., Srinivasan, K., and Sun, R.: Numerical simulation of coupled radiation and convection for complex geometries, Paper AIAA-98-2677, *Seventh AIAA/ASME Joint Thermophysics and Heat Transfer Confeerence*, Albuquerque, NM, June 1998.

Usiskin, C. M. and Siegel, R.: Thermal radiation from a cylindrical enclosure with specified wall heat flux, *JHT*, 82(4), 369–374, 1960.

van Doormall, J. P. and Raithby, G. D.: Enhancements of the simple method for predicting incompressible fluid flows, *Numer. Heat Transfer*, 7, 147–163, 1983.

Yu, E. and Joshi, Y. K.: Heat transfer in discretely heated side-vented compact enclosures by combined conduction, natural convection, and radiation, *JHT*, 121(4), 1002–1010, 1999.

Zhou, R.-R., Li, B.-W., Wang, W.-K., and Sun, Y.-A.: Improved integration strategies for the singularity subtraction method to solve radiative integral transfer equations with specified temperature field, *IJTS*, 149, 106158, 2020.

Zhao, Z., Poulikakos, D., and Ren, Z.: Combined natural convection and radiation from heated cylinders inside a container, *JTHT*, 6(4), 713–720, 1992.

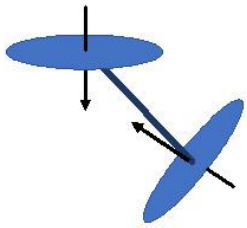

J: RADIATIVE COOLING

Under certain conditions, enhanced cooling by radiation from surfaces is useful. This can be achieved if the emission from the surface is enhanced at the longer wavelengths where most of the cooling (radiative energy loss) takes place. In addition, it is desirable to minimize the radiative energy gain of a given surface at the same time. This can be realized by decreasing the solar absorption and increasing the IR emission of the surface. Such spectrally selective surfaces can also be useful where it is desirable to cool an object exposed to incident radiation from any high-temperature source. Common situations are objects exposed to the sun, such as a hydrocarbon storage tank, a cryogenic fuel tank in space, the roof and facades of a building, or electronic equipment which gets hot due to internal heat generation. There are several studies published over the years on enhanced radiative cooling during nighttime {Catalanotti et al. (1975); Granqvist et al. (1982); Eriksson and Granqvist (1982); Berdahl et al.(1983); and Smith (2009) and his colleagues [Gentle et al. (2013)], and Family et al. (2020).}.

Few natural materials have the desired radiative spectral characteristics. Radiative cooling can be enhanced using tailored properties of surfaces in both the spectral and directional sense (see Section 3.4 of the text).

The largest impact of radiative cooling would be on buildings, which consume more than one-third of the energy in the US, as well as in most energy intense countries. Air-conditioning requirements and costs are significant. If a passive system could be employed to help minimize these costs, it would be a significant help in improving energy efficiency. Buildings receive energy mostly from sun and emit at about room temperatures. This means that most radiation incident on buildings, which cause radiation gain, is near visible wavelengths. If the buildings themselves are assumed to be at about 300 K temperature, then their emission wavelength peaks around 10 μm, following the Wien Law. The Earth's atmosphere has a transparency window for electromagnetic waves between 8 and 13 μm that coincides with the peak thermal radiation wavelength at these temperatures. Therefore, buildings can lose radiation quite effectively through this atmospheric transparency window, particularly under clear sky conditions, both day and night!

A number of studies on radiative cooling are discussed by Zhu et al. (2013). It is important to achieve not only night-time cooling, but also daytime cooling. Given that there will be solar absorption during the times that cooling is most desirable, a detailed energy balance is needed to determine a surface equilibrium temperature that is below ambient. To achieve this, Zhu et al. have shown that it is necessary to achieve over 88 percent solar radiation reflection during the day.

To achieve solar cooling, we need a 'designer' surface that has large reflectivity in the spectral region of visible (short) wavelenghts to block the peak solar energy but has large absorptivity/emissivity at far-infrared (longer) wavelengths, where the surface emission peaks. For these "spectrally/directionally selective" surfaces, we can use a performance parameter. This parameter is defined as the ratio of its directional total absorptivity $\alpha_s(\theta_i, \phi_i, T_i)$ for incident solar energy to its hemispherical total emissivity $\varepsilon(T)$. With small $\alpha_s(\theta_i, \phi_i, T_i)/\varepsilon(T)$, a surface can radiate enegy quite effectively (See Equation 3.46 of the text).

A highly reflecting material such as a polished metal or a metallic coated surface can be considered for these applications. Although such materials would reflect much of the incident energy in the visible range, they do not effectively radiate at longer wavelengths. This yields a poor desired behavior for the energy balance in the vacuum of outer space and may not provide a low α_s/ε. Paints, such as white paint, are an example of a useful spectrally selective surface [Dunkle (1963)], as they do not only reflect the incident solar radiation predominant at short wavelengths, but also radiate well at the longer wavelengths characteristic of the relatively low body temperature. Performance should be evaluated including convective cooling, which may dominate over radiant emission.

Radiative cooling is also part of thermal control in outer space, which needs (sometimes exotic) spectrally selective surfaces. Among them, the optical solar reflector (OSR) is a mirror composed of a glass layer silvered on the back side. The glass, being transparent in the short wavelength region, $\lambda<\sim2.5\mu m$, that includes the visible range, lets the silver reflect incident radiation in this spectral region. The small fraction of short-wavelength energy that is absorbed by the silver, and the energy absorbed by the glass at longer wavelengths, are radiated away by the glass in the longer-wavelength infrared region where glass emits well.

Commonly used thin plastic sheets for solar reflection are Kapton, Mylar, and Teflon with silver or aluminum coating on the backside. Fused-silica second-surface mirrors and polished metals are essentially stable in orbit. Metalized Teflon, aluminized Kapton, and some light-colored paints darken over a long period of time, degrading their performance as discussed by Hall and Fote (1992).

The performance of a CuO pigment coating has been investigated and compared against that of a white TiO_2 pigment, which is widely used as a white pigment (Gonome et al., 2014). They also measured results for CuO coatings and compared against the measured results for TiO_2-pigmented coating. The performance of CuO pigment was found to be much higher than that of TiO_2 pigment, though the CuO coating shows a darker, almost black color (Gonome et al., 2014). Titanium dioxide white paint is superior as an external solar-selective coating to polyvinyl fluoride film with an aluminized coating 12 μm thick on the underside. These are the types of materials among many others that are used for spacecraft thermal control (Henninger, 1984).

The most common material system currently used for low thrust, radiation-cooled rockets or spacecrafts is a niobium alloy (C-103) with a fused silica coating (R-512A or R-512E) for oxidation protection. However, significant amounts of fuel film cooling are usually required to keep the material below its maximum operating temperature of 1370°C, degrading engine performance.

A new class of high-temperature, oxidation-resistant materials is being developed for radiation-cooled rocket engines, with the thermal margin to reduce or eliminate fuel film cooling, while still exceeding the life of silicide-coated niobium. Rhenium coated with iridium is the most developed of these high-temperature materials, as discussed by Reed et al. (1993) from NASA Lewis in the early 1960s. They also studied other material systems, which may offer more thermal margin and/or oxidation resistance, such as hafnium carbide/tantalum carbide matrix composites and ceramic oxide-coated iridium/rhenium chambers. Reed et al. discussed a chamber fabricated from pure iridium that would eliminate the rhenium/iridium diffusion mechanism, but there are concerns about its structural integrity as a rocket engine. A tantalum-

10% tungsten alloy and woven carbon-carbon fibers could serve as high-temperature substrates but require a suitable oxidation-resistant coating for long life applications. Platinum-10% rhodium alloy and grain-stabilized platinum are excellent oxidation resistant materials that could be considered for very long life (tens of hours), but relatively low temperature (1650 °C) applications. Cermets and intermetallic compounds have also been considered for high temperature rocket operation, but there is a very limited experience base with them.

There are many materials that have absorption peaks at different wavelengths. Rare earth metals can be used as selective emitters in the infrared region due to their high absorption in this region [Rose et al. (1996); Licciulli et al. (2003); Wijewardane and Goswami (2012)]. Commonly, these metals are used as composites by mixing with other materials such as ceramics or titania because of the rarity of these metals. The problem with these composites is that at higher temperatures gray-body like emission from other constituents' starts to dominate the rare earth metal's selective emission. For applications, which require peaks of various wavelengths the absorption peaks must be tuned or shifted and the answer falls in the nano-scale. Nano sized metal particles embedded in insulators or a semiconductor matrix, as reviewed by Wijewardane and Goswami, (2012).

In addition to spectral tuning, we can also consider directional tuning of surfaces. For example, an emitting surface can be constructed to emit strongly in preferred direction, while reducing emission into unwanted directions. This approach is based on the possibility of designing a regular micro-roughness (a "grating") that would provide selective emission [Sentenac and Greffet (1994); Greffet and Henkel (2007)]. The grating dimension is of the same order of the predominant radiation wavelength. Indeed, this concept was shown experimentally and theoretically for different polarization settings [Arnold et al. (2012); see references cited]. If the objective of the designer surface is to absorb primarily from a certain direction, then it can be constructed that way; also, the fabrication can be performed for it to absorb poorly in other directions. If the surface is used for solar absorption, then it would, based on the Kirchhoff law for directional properties, emit strongly toward the sun but weakly in other directions. It can absorb about the same energy as a nondirectional absorber, yet its total emission would be less than a typical surface. Coherent directional and spectral emission concepts have been explored by Greffet's group over the years [Carminati and Greffet (1999); Greffet et al. (2002); Joulain et al. (2005); Laroche et al. (2006); Arnold et al. (2012) and references therein]. Recent calculations carried out by Didari and Menguc (2015) also suggest that the shape and size of the extrusions on the surfaces can alter the far-field emission. These concepts were discussed briefly in Chapter 16 and are likely to be used for selective emission in the future.

Recently, the concept of radiative cooling was explored by the Fan group [Zhu et al. (2013)]. By modifying the structure of silicon nanowire array on an aluminum substrate, they observed significant emissivity/absorptivity enhancement in the far-infrared. Their feature size ranged from sub-micron to 10 nm range, and they demonstrated that the color of the sample did not change noticeably. Zhu et al. also applied their idea of radiation cooling to solar cells, which is a very important area to enhance the performance of PV-panels (Zhu et. al. 2014). Kecebas et al. (2017, 2020) examine using multiple alternating layers of high- and low-refractive index materials to enhance radiative cooling. See also Section 19.1.1.2 of the text for further discussions and references on optimized PV cell enhancement.

REFERENCES

Arnold, C., Marquier, F., Garin, M., Pardo, F., Collin, S., Bardou, N., Pelouard, J-L., and Greffet, J.-J., Coherent thermal emission by two-dimensional silicon carbide gratings, *Phys. Rev. B*, vol. 86, 035316, 2012.

Berdahl, P., Martin, M., and Sakkal, F.: Thermal performance of radiative cooling panels, *IJHMT*, vol. 26, no. 6, pp. 871–880, 1983.

Carminati, R., and Greffet, J. -J.: Near-field effects in spatial coherence of thermal sources, *Phys. Rev. Lett.*, vol. 82, no. 8, pp. 1660–1663, 1999.

Catalanotti, S., Cuomo, V., Piro, G., Ruggi, D., Silvestrini, V., and Troise, G.: The Radiative Cooling of Selective Surfaces, *Sol. Energy*, vol. 17, 83, 1975.

Didari, A., and Mengüç, M. P.: Near-Field Thermal Emission between Corrugated Surfaces Separated by Nano-Gaps, *JQSRT*, 158, 43-51, 2015.

Dunkle, R. V.: Thermal Radiation Characteristics of Surfaces, in J. A. Clark (ed.), *Theory and Fundamental Research in Heat Transfer*, pp. 1–31, Pergamon Press, New York, 1963.

Eriksson, T. S., and Granqvist, C. G.: Radiative Cooling Computed for Model Atmospheres, *Applied Optics*, vol. 21, no. 23, 1982.

Family, R. and Mengüç, M. P.: Materials for radiative cooling: A review, *Procedia Environmental Sciences*, 38, 752 – 759, 2017.

Family, R., Celik, S., and Mengüç, M. P.: Coupled heat transfer analysis and experiments to evaluate the radiative cooling potential of concrete and green roofs for buildings, *Heat and Mass Transfer*, 56, 2605-2617, 2020.

Gentle, A. R., Dybdal, K. L., and Smith, G. B.: Polymeric Mesh for Durable Infra-red Transparent Convection Shields: Applications in Cool Roofs and Sky Cooling, *Solar Energy Materials and Solar Cells*, vol. 115, pp. 79–85, 2013.

Gonome, H., Baneshi, M., Okajima, J., Komiya, A., and Maruyama, S.: Controlling the Radiative Properties of Cool Black-color Coatings Pigmented with CuO Submicron Particles, *JQSRT*, Special Issue on Micro- and Nano-scale Radiative Transfer, vol. 132, pp. 90-98, 2014.

Granqvist, C. G., Hjortsber, A., and Eriksson, T. S.: Radiative Cooling to low temperatures with selectively IR-Emitting surfaces, Thin *Solid Films*, vol. 90, pp. 187-190, 1982.

Greffet, J. -J., and Henkel, C.: Coherent Thermal Radiation, *Contemporary Phys.*, vol. 48, no. 4, pp. 183–194, July–August 2007.

Greffet, J. -J., Carminati, R., Joulain, K., Mulet, J. -P., Mainguy, S., and Chen, Y.: Coherent Emission of Light by Thermal Sources, *Nature*, vol. 416, pp. 61–64, March 7, 2002.

Hall, D. F., and Fote, A. A.: Thermal Control Coatings Performance at Near Geosynchronous Altitude, *JTHT*, vol. 6, no. 4, pp. 665–671, 1992.

Henninger, J. H.: Solar Absorptance and Thermal Emittance of Some Common Spacecraft Thermal-Control Coatings, NASA Reference Publication 1121, 1984.

Kecebas, M. A., Mengüç, M. P., Kosar, A., and Sendur, K.: Passive radiative cooling design with broadband optical thin-film filters, *JQSRT* 198, 179-186, 2017.

Kecebas, M. A., Mengüç, M. P., Kosar, A., and Sendur, K.: Spectrally selective filter design for passive radiative cooling, *JOSA-B*, 37(4), 1173-1182, April 2020.

Joulain, K., Mulet, J. -P., Marquier, F., Carminati, R., and Greffet, J. -J.: Surface Electromagnetic Waves Thermally Excited: Radiative Heat Transfer, Coherence Properties and Casimir Forces Revisited in the Near Field, *Surf. Sci. Rep.*, vol. 57, pp. 59–112, 2005.

Laroche, M., Carminati, R., and Greffet, J. -J.: Near-Field Thermophotovoltaic Energy Conversion, *J. Appl. Phys.*, vol. 100, p. 063704, 2006.

Licciulli, A., Diso, D., Torsello, G., and Tundo, S.: The Challenge of High-performance Selective Emitters for Thermophotovoltaic Applications, *Semiconductor Science and Technology*, vol. 18, pp. 174-183, 2003.

Reed, B., Biaglow J., and Schneider, S.: Advanced Materials for Radiation-Cooled Rockets, in NASA Lewis Research Center, N94-23052, *NASA Propulsion Engineering Research Center, Annual Report 199, Vol. II*, NASA Lewis Research Center, N94-28052, pp. 115-118, Sept. 1993.

Rose, M. F., Adair, P., and Schroeder, K.: Selective Emitters for Thermophotovoltaic Power Systems for Use in Aerospace Applications, *J. Propul. Power*, vol. 12, no. 1, pp. 83–88, 1996.

Sentenac, A., and Greffet, J. -J.: Design of Surface Microrelief with Selective Radiative Properties, *IJHMT*, vol. 37, no. 4, pp. 553–558, 1994.

Smith, G. B.: Amplified radiative cooling via optimised combinations of aperture geometry and spectral emittance profiles of surfaces and the atmosphere, *Solar Energy Materials & Solar Cells*, vol. 93, 1696–1701, 2009.

Wijewardane, S., and Goswami, D. Y.: A Review on Surface Control of Thermal Radiation by Paints and Coatings for New Energy Applications, *Renewable and Sustainable Energy Reviews*, vol. 16, pp. 1863-1873, 2012.

Zhu, L., Raman, A., and Fan, S.: Color-preserving Daytime Radiative Cooling, *Appl. Phys. Letters*, vol. 103, 223902, 2013.

Zhu, L., Raman, A., Wang, K. X., Anoma, M. A. and Fan, S.: Radiative Cooling of Solar Cells, *Optica*, vol. 1, no. 1, July 2014.

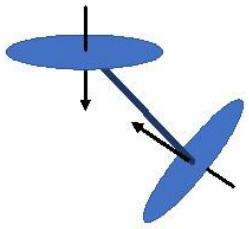

K. RADIATION FROM FLAMES

Combustion consists of chemical reactions in series and in parallel and involving many intermediate species. The composition and concentration of these species cannot be predicted very well unless knowledge is available of the flame reaction kinetics; this detailed knowledge is not usually available or convenient to obtain. Because the flame radiation properties depend on the distributions of temperature and species within the flame, a detailed prediction of radiation from flames is not often possible from knowledge of only the combustible constituents and the flame geometry. It is usually necessary to resort to empirical methods for predicting radiative transfer in systems involving combustion.

Under certain conditions the constituents in a flame emit much more radiation in the visible region than would be expected from their gaseous absorption coefficients. For example, the typical almost transparent blue flame of a Bunsen burner can become a more highly emitting yellow-orange flame by changing the fuel-air ratio. Such luminous emission is usually ascribed to incandescent soot (hot carbon) particles formed because of incomplete combustion in hydrocarbon flames. Alternatively, Echigo et al. (1967) and others have advanced the hypothesis, supported by some experimental facts, that luminous emission from some flames is by emission from vibration-rotation bands of chemical species that appear during the combustion process *prior* to the formation of soot particles. Zimmer and Pereira (2020) compare models for soot formation and radiation from an ethylene coflow flame.

K.1 RADIATION FROM NONLUMINOUS FLAMES

Radiation from the nonluminous portion of the combustion products is well understood. For this the complexities of the chemical reaction are not as important, since it is the gaseous end products above the active burning region that are considered. Most instances are for hydrocarbon combustion, and radiation is from the CO_2 and H_2O absorption bands in the infrared. For flames a meter or more thick, as in commercial furnaces, the emission leaving the flame within the CO_2 and H_2O vibration-rotation bands can approach blackbody emission in the band spectral regions. The gas radiation properties in Chapter 9 can be used to compute the radiative transfer. The analysis is greatly simplified if the medium is well mixed and can be assumed isothermal. A nonisothermal medium can be divided into approximately isothermal zones, and convection can be included if the circulation pattern in the combustion chamber is known. A nonisothermal analysis with convection was carried out in Hottel and Sarofim (1965) for cylindrical flames. In Dayan and Tien (1974), Edwards and Balakrishnan (1973), Modak (1975, 1977), Taylor and Foster (1974), Lefebvre (1984),and Liu et al. (2020), radiation from various types of nonluminous flames (laminar or turbulent, mixed or diffusion) is treated. The flame shape for an open diffusion flame is considered in Annamali and Durbetaki (1975). The local absorption coefficient in nonluminous flames is calculated in Grosshandler and Thurlow (1992) as a function of mixture fraction and fuel composition. Modest (2005) reviews models for radiative transfer in combustion gases.

When considering the radiation from flames, a characteristic parameter is the average temperature of a well-mixed flame as a result of the addition of chemical energy. Well-developed methods exist [Gaydon and Wolfhard (1979)] for computing the theoretical flame temperature from thermodynamic data. The effect of preheating the fuel and/or oxidizer can be included. An ideal theoretical flame temperature T is computed using energy conservation

assuming complete combustion, no dissociation of combustion products, and no heat losses. The energy in the constituents supplied to the combustion process, plus the energy of combustion, is equated to the energy of the combustion products to give,

$$T - T_{ref} = \frac{\left(\text{energy in feed air and fuel above } T_{ref}\right) + \left(\text{energy released by combustion}\right)}{\left(\text{total mass of products}\right) \times \left(\text{mean specific heat of products}\right)} \quad \text{(K.1)}$$

Energy losses by radiation and other means that would lower the flame temperature are not included. Methods for including these effects are in Gaydon and Wolfhard (1979); extinction of a flame by radiative energy loss is analyzed in Ju et al. (2000). A list of ideal theoretical flame temperatures (no radiation or other losses included) is in Table K.1 for various hydrocarbon flames, using data from Gaydon and Wolfhard and from Barnett and Hibbard (1957). Results for complete combustion with dry air are shown, followed by calculated results modified to allow for product dissociation and ionization. The latter are compared with experimental results. The heats of combustion of the substances are also given. Extensive tabulations of similar data for more than 200 hydrocarbons are in Barnett and Hibbard and in Green and Southard (2019). After its average temperature has been estimated, the radiation emitted by a nonluminous flame can be considered, as illustrated by an example.

EXAMPLE K.1 As a result of combustion of ethane in 100% excess air, the combustion products are 4 mol of CO_2, 6 mol of H_2O vapor, 33.3 mol of air, and 26.3 mol of N_2. Assume these products are in a cylindrical region 4 m high and 2 m in diameter, are uniformly mixed at a theoretical flame temperature of 1853 K, and are at 1 atm pressure. Compute the radiation from the gaseous region.

The partial pressure of each constituent is equal to its mole fraction:

$$p_{CO_2} = (4/69.6)(1\text{ atm}) = 0.0575\text{atm and } p_{H_2O} = (6/69.6)(1\text{ atm}) = 0.0.0862\text{atm.}$$

The gas mean beam length for negligible self-absorption is, from Equation 11.104,

$$L_{e,0} = 4V/A = 4\left[\pi\left(2^2/4\right)\right] \times 4 / \left[\left(2\pi \times 4\right) + 2\pi\left(2^2/4\right)\right] = 1.6\text{m}.$$

To include self-absorption, a correction factor of 0.9 is applied to give L_e = 0.9(1.6) = 1.44 m. Then $p_{CO2}L_e$ = 0.0575 × 1.44 = 0.0828 atm · m = 8.54 bar-cm, and $p_{H2O}L_e$ = 0.0862 × 1.44 = 0.124 atm · m = 12.8 bar-cm. Using the Alberti et al. (2018) spread sheet (Section 9.4) at ***https://doi.org/10.1016/j.jqsrt.2018.08.008*** gives ε_g = 0.1451. The radiation from the gas region at the theoretical flame temperature is,

$$Q = \varepsilon_g \sigma T_g^4 A = 0.1451 \times 5.6704 \times 10^{-8} \times 1853^4 \times 10\pi = 3050\text{kW}$$

TABLE K.1 Heat of combustion and flame temperature for hydrocarbon fuels [Gaydon and Wolfhard (1979); Barnett and Hibbard (1957); Lide (2008)]

		Maximum flame temperature, K (combustion with dry air at 298 K)		
Fuel	Heat of combustion kJ/kg	Theoretical (complete combustion)	Theoretical (with dissociation and ionization)	Experimental
Carbon monoxide (CO)	10.1×10^4	1756	1388	
Hydrogen (H_2)	14.1×10^4	2400	2169	
Methane (CH_4)	5.53×10^4	2328	2191	2158

Ethane (C_2H_6)	5.19×10^4	2338	2244	2173
Propane (C_4H_8)	5.03×10^4	2629	2250	2203
n-Butane (C_4H_{10})	4.95×10^4	2357	2248	2178
n-Pentane (C_5H_{12})	4.53×10^4	2360	2250	
Ethylene (C_2H_4)	5.03×10^4	2523	2375	2253
Propylene (C_3H_6)	4.89×10^4	2453	2323	2213
Butylene (C_4H_8)	4.53×10^4	2431	2306	2208
Amylene (C_5H_{10})	4.50×10^4	2477		
Acetylene (C_2H_2)	5.00×10^4	2859	2607	
Benzene (C_6H_6)	4.18×10^4	2484	2363	
Toluene ($C_6H_5CH_3$)	4.24×10^4	2460	2344	

REFERENCES

Annamali, K., and Durbetaki, P.: Characteristics of an Open Diffusion Flame, *Combust. Flame*, vol. 25, pp. 137–139, 1975.

Barnett, H. C., and Hibbard, R. R. (eds.): *Basic Considerations in the Combustion of Hydrocarbon Fuels with Air*, NACA Rept. 1300, 1957.

Dayan, A., and Tien, C. L.: Radiant Heating from a Cylindrical Fire Column, *Combust. Sci. Technol.*, vol. 9, pp. 41–47, 1974.

Echigo, R., Nishiwaki, N., and Hirata, M.: A Study on the Radiation of Luminous Flames, *Eleventh Symp.* (*Int.*) *Combust.*, pp. 381–389, The Combustion Institute, 1967.

Edwards, D. K., and Balakrishnan, A.: Thermal Radiation by Combustion Gases, *IJHMT*, vol. 16, no. 1, pp. 25–40, 1973.

Gaydon, A. G., and Wolfhard, H. G.: *Flames, Their Structure, Radiation, and Temperature*, 4th ed., Chapman and Hall, London, 1979.

Green, D. W. and Southard, M. Z. (eds.): *Perry's Chemical Engineers' Handbook*, 9th ed., McGraw-Hill, New York, 2019.

Grosshandler, W. L., and Thurlow, E. M.: Generalized State-Property Relations for Nonluminous Flame Absorption Coefficients, *JHT*, vol. 114, no. 1, pp. 243–249, 1992.

Lefebvre, A. H.: Flame Radiation in Gas Turbine Combustion Chambers, *IJHMT*, vol. 27, no. 9, pp. 1493–1510, 1984.

Lide, D. R. (ed.): *Handbook of Chemistry and Physics*, 88th ed., CRC Press, Boca Raton, 2008.

Liu, F., Consalvi, J.-L., Coelho, P. J., Andre, F., Gu, M., Solovjov, V., and Webb, B. W.: The impact of radiative heat transfer in combustion processes and its modeling – with a focus on turbulent flames, *Fuel*, 281, 118555, 2020.

Modak, A.: Nonluminous Radiation from Hydrocarbon-Air Diffusion Flames, *Combust. Sci. Technol.*, vol. 10, pp. 245–259, 1975.

Modak, A.: Thermal Radiation from Pool Fires, *Combust. Flame*, vol. 29, no. 2, pp. 177–192, 1977.

Modest, M. F.: Radiative Heat Transfer Models in Combustion Gases, in *Annual Review of Heat Transfer*, Hemisphere, New York, pp. 23–47, 2005.

Taylor, P. B., and Foster, P. J.: The Total Emissivities of Luminous and Non-luminous Flames, *IJHMT*, vol. 17, pp. 1591–1605, 1974.

Zimmer, L. and Pereira, F.: Limitations of simplified models to predict soot formation in laminar flames. *J. Braz. Soc. Mech. Sci. Eng.* **42,** 340, 2020.

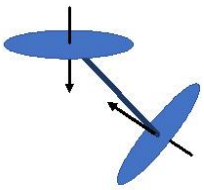

M. REFERENCES TO REVIEWS AND HISTORICAL PAPERS

L: COMMERCIAL CODES FOR RADIATION

L.1 CODES FOR CONFIGURATION FACTORS

Many computer programs are available that use one or more of the methods outlined in Chapter 4 of the text for numerical calculation of configuration factors. Examples are FACET (Shapiro 1983), which uses area integration and contour integration; VIEW (Emery 1986), which can be used with the NASTRAN thermal analysis code; a program that relies on the computer-graphical analog to the unit-sphere method (Alciatore et al. 1989), and VIEW3D. The latter program provides factors between a differential element and an arbitrary 3D object. The program TSS (Thermal Simulation System, Chin et al. 1992), developed under NASA sponsorship, incorporates an advanced graphical user interface for displaying configurations. The CHAPARRAL program (Glass 1995) incorporates FACET for 2D factors and uses the hemicube method for computing 3D factors in very large surface element arrays. Many commercially available thermal analysis programs such as COMSOL, FLUENT, FIDAP, NEVADA, and OpenFOAM also incorporate configuration factor computation using various methods, sometimes with choices among methods.

These and other computer codes provide a means to generate configuration factors for complex geometries and are invaluable for radiative analyses. Their accuracy can be assessed by comparison of computed results with the analytical expressions developed here for simpler geometries that can be used for test cases. Several different numerical methods for calculating configuration factors in complex configurations are compared by Emery et al. (1991) for computing speed, accuracy, and convenience. The geometries range from surfaces almost unobstructed in their view, to highly obstructed intersecting surfaces. The methods compared include double integration, Monte Carlo, contour integration, and projection techniques. If the view is not too complex, methods based on contour integration are found to be successful. The advent of massively parallel computers is making Monte Carlo methods (Chapter 14) particularly attractive for computing configuration factors. Walker et al. (2010, 2012) and Walker (2013) have examined the use of parallel Monte Carlo using either standard central processing units (CPUs) or graphical processing units (GPUs) and find good speed and accuracy in comparison with finite-element-based numerical integration for computing configuration factors for complex geometries. They employ superimposed primitives for fast rendering of many common objects.

L.2: Codes and Data for Molecular and Atomic Gas Spectral Properties

Property data is available from accessible on-line sources. These are continually updated and improved. More information on the databases is in Section 9.3.5.3 of the text. The databases themselves can be accessed at:

Jacquinet-Husson, N. et al., The 2015 edition of the GEISA spectroscopic database, J. Molecular Spectroscopy 327, 31-72, Sept. 2017.). The 2019 version of GEISA is accessible at CDS-ESPRI:Home.

Laux, C. O.: Radiation and nonequilibrium collisional-radiative models, in D. Fletcher, J.-M. Charbonnier, G. S. R. Sarma, and T. Magin (eds.), *Physico-Chemical Modeling of High Enthalpy and Plasma Flows*, von Karman Institute Lecture Series 2002-07, Rhode-Saint-Genèse, Belgium, 2002. [SPECAIR User Manual, ver. 3.0, 2012 (latest version online)]. Code available at *www.specair-radiation.net*/

Kramida, A., Ralchenko, Y., Reader, J. and NISTASDTeam: NIST Atomic Spectra Database (version 5.0), [Online]. Available: *physics.nist.gov/asd* (accessed April 27, 2015), National Institute of Standards and Technology, Gaithersburg, MD, 2012.

Rothman, L. S., Gordon, I. E., Barbe, A. et al., The HITRAN 2012 molecular spectroscopic database, *JQSRT* 130, 4–50, 2013. (For most recent version (2012) see www.cfa.hitran.com. Accessed April 27, 2015).

Rothman, L. S., Gordon, I. E., Barber, R. J., Dothe, H., Gamache, R. R., Goldman, A., Perevalov, V., Tashkun, S. A., and Tennyson, J.: HITEMP, the high-temperature molecular spectroscopic database, *JQSRT*, 111(15), 2139–2150, 2010. Data available on-line at https://hitran.org/hitemp/

L.3: CFD-BASED CODES

Most of the major commercially available computational fluid dynamics (CFD) codes employ one or more choices of methods for handling radiative transfer within a participating medium. For example, the ANSYS CFD code packages FLUENT and CFX between them provide choice from among surface–surface, diffusion, P_1, discrete transfer, discrete ordinates, and Monte Carlo solvers. The COMSOL built-in Heat Transfer module incorporates spectral surface properties for surface-surface exchange in simple geometries, and uses the Rosseland approximation, P_1 approximation or the discrete ordinate method (DOM) for radiation in participating media. OpenFOAM, a free online CFD code includes P_1 and finite volume models, plus a configuration factor calculator for transparent medium problems.

Various models may be included for treating anisotropic scattering and spectral medium property variations, although these features are not available for all solvers. These and competing codes continue to add features and capabilities, and careful comparison is warranted of the required capabilities for a problem or application.

L.4 FINITE DIFFERENCE TIME-DOMAIN METHOD

The FDTD method is probably the most common approach for simulation of scattering problems (Wriedt 2009), and for nanoscale radiation interactions with textured surfaces (Heltzel et al. 2005. 2007; 2008). The method was first introduced by Yee (1966), where time-dependent Maxwell equations are solved to calculate electromagnetic scattering in both time and space domains. The derivatives of Maxwell equations in space and time are approximated by a finite difference scheme and discretized in both space and time domains. The equations are solved numerically with appropriate boundary conditions and particle or surface properties using a fully explicit scheme.

FDTD methods were reviewed by Schlager and Schneider (1995) and Taflove (2007). This approach is commercially available, as more than 25 companies were listed by Taflove. There are several other open source development projects, which are listed at the corresponding Wikipedia site. It is also used extensively for simulations of metamaterials as discussed by Veselago et al. (2006). This method computes the solution in a finite domain, like the FEM, and so a far zone transformation must be invoked to calculate fields in far-field. The method is popular because of its conceptual simplicity and ease of implementation but has disadvantages like those of the FEM including limitations in accuracy, mathematical complexity, and the need to repeat computations for different angles of incidence. The FDTD approach can be applied to arbitrary geometries with different properties.

Maxwell equations are discretized using the FDTD method. In order to present the implementation of FDTD, the Maxwell equations are written in terms of electrical displacement and magnetic fields D_x, D_z, and H_y, respectively. They are considered for a transverse magnetic (TM) wave, in which the only nonzero component of magnetic field is H_y, that is, propagation along the z-axis. They are

$$\frac{\partial D_{\mathrm{x}}}{\partial t} = -\frac{\partial H_{\mathrm{y}}}{\partial z} \tag{L.1}$$

$$\frac{\partial D_{\mathrm{z}}}{\partial t} = \frac{\partial H_{\mathrm{y}}}{\partial x} \tag{L.2}$$

$$D_{\mathrm{x}}(\omega) = \bar{\varepsilon}_0 \bar{\varepsilon}_{\mathrm{r}}(\omega) E_{\mathrm{x}}(\omega) \tag{L.3}$$

$$D_{\mathrm{z}}(\omega) = \bar{\varepsilon}_0 \bar{\varepsilon}_{\mathrm{r}}(\omega) E_{\mathrm{z}}(\omega) \tag{L.4}$$

$$\frac{\partial H_{\mathrm{y}}}{\partial t} = \frac{1}{\mu_0}\left(\frac{\partial E_{\mathrm{z}}}{\partial x} - \frac{\partial E_{\mathrm{x}}}{\partial z}\right) \tag{L.5}$$

The first order finite difference representation of the fields in Equations L.1, L.2, and L.5 are written in discrete time domain as

$$\frac{D^{n+1/2}_{\mathrm{x}i+1/2,k} - D^{n-1/2}_{\mathrm{x}i+1/2,k}}{\Delta t} = -\frac{H^{n}_{\mathrm{y}i+1/2,k+1/2} - H^{n}_{\mathrm{y}i+1/2,k-1/2}}{\Delta z} \tag{L.6}$$

$$\frac{D^{n+1/2}_{\mathrm{z}i,k+1/2} - D^{n-1/2}_{\mathrm{z}i,k+1/2}}{\Delta t} = -\frac{H^{n}_{\mathrm{y}i+1/2,k+1/2} - H^{n}_{\mathrm{y}i-1/2,k+1/2}}{\Delta x} \tag{L.7}$$

$$\frac{H^{n+1}_{\mathrm{y}i+1/2,k+1/2} - H^{n}_{\mathrm{y}i+1/2,k+1/2}}{\Delta t} = \frac{E^{n+1/2}_{\mathrm{z}i+1,k+1/2} - E^{n+1/2}_{\mathrm{z}i,k+1/2}}{\mu_0 \Delta x} - \frac{E^{n+1/2}_{\mathrm{x}i+1/2,k+1} - E^{n+1/2}_{\mathrm{x}i+1/2,k}}{\mu_0 \Delta z} \tag{L.8}$$

If the Yee cell size is kept small, the central differences are said to have second-order accuracy or second-order behavior (Δx^2 terms can be ignored). Furthermore, we can rewrite Equations L.6 through K.8 as

$$D^{n+1/2}_{\mathrm{x}i+1/2,k}(k) = D^{n-1/2}_{\mathrm{x}i+1/2,k}(k) - \frac{\Delta t}{\Delta z}\left[H^{n}_{\mathrm{y}i+1/2,k+1/2} - H^{n}_{\mathrm{y}i+1/2,k-1/2}\right] \tag{L.9}$$

$$D^{n+1/2}_{\mathrm{z}i,k+1/2}(k) = D^{n-1/2}_{\mathrm{z}i,k+1/2}(k) - \frac{\Delta t}{\Delta x}\left[H^{n}_{\mathrm{y}i+1/2,k+1/2} - H^{n}_{\mathrm{y}i-1/2,k+1/2}\right] \tag{L.10}$$

$$H^{n+1}_{\mathrm{y}i+1.2,k+1/2} = H^{n}_{\mathrm{y}i+1.2,k+1/2} + \frac{\Delta t}{\mu_0 \Delta x}\left[E^{n+1/2}_{\mathrm{z}i+1,k+1/2} - E^{n+1/2}_{\mathrm{z}i,k+1/2}\right] - \frac{\Delta t}{\mu_0 \Delta z}\left[E^{n+1/2}_{\mathrm{x}i+1/2,k+1} - E^{n+1/2}_{\mathrm{x}i+1/2,k}\right] \tag{L.11}$$

In the *xz* plane of interest, the 1D wave equation is

$$\left(\frac{\partial}{\partial x} - \frac{1}{c}\frac{\partial}{\partial t}\right) E_{\mathrm{z}} = 0 \tag{L.12}$$

$$\left(\frac{\partial}{\partial z} - \frac{1}{c}\frac{\partial}{\partial t}\right) E_{\mathrm{x}} = 0 \tag{L.13}$$

They can be easily discretized using only the field components on, or just inside the mesh wall, yielding an explicit finite difference equation at time step $n + 1$:

$$E_{z_{1,k+1/2}}^{n+1} = E_{z_{2,k+1/2}}^{n} + \frac{c\Delta t - \Delta x}{c\Delta t + \Delta x}\left(E_{z_{2,k+1/2}}^{n+1} - E_{z_{1,k+1/2}}^{n}\right) \tag{L.14}$$

$$E_{x_{i+1/2,1}}^{n+1} = E_{x_{i+1/2,2}}^{n} + \frac{c\Delta t - \Delta z}{c\Delta t + \Delta z}\left(E_{x_{i+1/2,2}}^{n+1} - E_{x_{i+1/2,1}}^{n}\right) \tag{L.15}$$

where $E_{z_{i,k+1/2}}^{n}$ and $E_{x_{i+1/2,k}}^{n}$, respectively, refer to the *i*, *k*th electric component of Yee cell in *z* and *x* direction, and *c* is the speed of light.

The numerical algorithm for Maxwell's curl equations requires that the time increment Δt have a specific bound relative to the space increments Δx, Δy, and Δz. The time increment must obey the following bound, known as Courant–Friedrichs–Lewy (CFL) stability criterion:

$$\Delta t \le \min\left\{\left(c\sqrt{\frac{1}{(\Delta x)^2} + \frac{1}{(\Delta y)^2} + \frac{1}{(\Delta z)^2}}\right)^{-1}\right\} \tag{L.16}$$

The difficulty in working with FDTD is due mainly to the imposition of the boundary conditions. The choice of boundary conditions is the key to an accurate FDTD simulation. There are various techniques to achieve the aim of simulating a geometry that extends to infinity in all dimensions, thereby eliminating reflections from the actual physical edges. In FDTD these are known as absorbing boundary conditions or ABCs as they absorb or attenuate waves (electric or magnetic) as they approach the edge of the actual problem geometry. Which method you use (known as Dirichlet, periodic, Mur, Mie/Fang superabsorption, perfectly matched layers (PML), convolution PML (CPML), etc.) will very much depend on the nature of the waves, their incidence angle, and their wavelength relative to the geometry size. Choosing the best ABC for an FDTD simulation is crucial as it can minimize the overall problem space, that is, the number of grid cells in the *x*, *y*, and *z* dimensions, and thereby reduce computation time (Didari and Mengüç 2014, 2015).

FDTD has found applications in several diverse areas of mechanical engineering such as near-field thermal radiation (see Datas et al. 2013, Didari and Mengüç 2014, 2015), microelectronics, with applications in energy-conversion devices, nanothermal manufacturing, as well as in electrical engineering such as antenna imaging design and bioelectromagnetic device development.

MATLAB by Mathworks is a particularly powerful tool for developing FDTD solutions because of its inherent support for matrices and arrays. FDTD algorithms implemented in MATLAB only need a single iteration per time-step to cover the complete spatial space (1D, 2D, or 3D). A fast Fourier transform (FFT) can be applied at any point in time or space to produce a frequency domain solution without an additional frequency "sweep." This is achieved by applying a broadband excitation pulse at some appropriate point within the problem geometry and then applying an FFT to the resultant time-domain response.

Implementing FDTD programmatically through MATLAB (or similar open source solutions such as GSVIT) allows complete independence over problem parameter definition, particularly in near-field thermal radiation research where arbitrary geometries and multiple dispersive materials may be used (Didari and Mengüç 2014, 2015). In addition, the application of FDTD to light scattering aerosols and the relevant literature review was reported by Sun et al. (2013) and Datas et al. (2013).

In the last few years, MATLAB and other FDTD solvers have embraced parallel computation, both through support for multiple CPU cores and by harnessing the power of graphics processing units (GPU) with their hundreds of processing cores. These developments have made possible finely gridded simulations over large 2D or 3D geometries by dramatically reducing simulation

times (by factors between 10 and 200). As one of the weaknesses of FDTD is numerical accuracy due to the discrete representations of electromagnetic fields, faster execution time allows proportional reduction in the discretization steps in both space and time.

Recent FDTD studies of near field thermal radiation have shown that modeling geometries separated by nanogaps in orders of a few tens of nanometers is also possible using the FDTD method, which is a promising factor in this field since analytical methods may not be easily available for some geometries due to geometry asperities; however, a tradeoff needs to be found between the accuracy and the simulation time requirements when working in such small scales (Didari and Mengüç 2014, 2015). Note that, for complex particles, these relations can be used for experimental determination of the phase function coefficients. Agarwal and Mengüç (1991) carried out an extensive numerical and experimental research to determine these parameters from experiments for polystyrene latex particles. A similar experimental study was conducted for coal particles by Mengüç et al. (1994).

L.5: AVAILABLE ON-LINE CODES AND DATABASES (Links checked as of 8/25/2019)

On-line resources are available for aid in computing many useful functions for radiation. These include:

CONFIGURATION FACTORS BETWEEN SURFACES:

FACET (Shapiro et al. 1983): **www.oecd-nea.org/tools/abstract/detail/nesc9578**

VIEW (Emery 1986): **https://bit.ly/2kOYJjO**

VIEW3D (Walton 1986): **www.View3d.sourceforge.net**

Catalog (Howell, 1982 on line: More than 350 factors, many with calculator):
www.ThermalRadiation.net/indexCat.html

LINE-BY-LINE SPECTRAL DATA

HITRAN 2016 (Gordon et al. 2017): **www.cfa.harvard.edu/hitran//**

HITEMP 2010 (Rothman et al. 2013): **https://hitran.org/hitemp/**

SPECAIR (Laux 2002) : **www.specair-radiation.net/**

GEISA (Jacquinet-Husson et al. 2017):

https://geisa.aeris-data.fr/line-transition-parameters-2019/

NIST Atomic Spectra (Kramida et al. 2012): **https://www.physics.nist.gov/asd**

GAS EMITTANCE FOR CO_2, H_2O, CO MIXTURES

Alberti et al. (2018), Spread sheet under "Supplementary Data" at:
doi.org/10.1016/j.jqsrt.2018.08.008

SCATTERING

M. REFERENCES TO REVIEWS AND HISTORICAL PAPERS

References to scattering literature and codes: **https:www.scattport.org/index.php**

Mie scattering calculator (Prahl,2009) : **https://omlc.org/calc/mie_calc.html**

T-matrix for irregular particles (Mishchenko et al. 2013): at
https://www.giss.nasa.gov/staff/mmishchenko/t_matrix.html

OpenDDA: Discrete dipole approximation for Agglomerates, (McDonald et al. 2009):
www.opendda.org
ADDA: Discrete dipole code for agglomerates, Yurkel
https://github.com/adda-team/adda
Add-on package for MATLAB (Nieminen et al.2007):
www.physics.uq.edu.au/people/nieminen/software.html

REFERENCES:

Agarwal, B. M. and Mengüç, M. P.: Single and multiple scattering of collimated radiation in an axisymmetric system, *IJHMT*, 34(3), 633–647, 1991.

Alberti, M., Weber, R., and Mancini, M.: Gray gas emissivities for H_2O-CO_2-CO-N_2 mixtures, *JQSRT*, 219, 274-291, Nov. 2018.

Alciatore, D., Lipp, S., and Janna, W. S.: Closed-form solution of the general three-dimensional radiation configuration factor problem with microcomputer solution, *Proceedings of the 26th National Heat Transfer Conference*, Philadelphia, PA, August 1989.

Chin, J. H., Panczak, T. D., and Fried, L.: Spacecraft thermal modeling, *Int. J. Numer. Methods Eng*., 35, 641–653, 1992.

Datas, A., Hirashima, D., and Hanamura, K.: FTDT simulation of near-field radiative heat transfer between thin films supporting surface phonon polaritons: Lessons learned, *J. Thermal Sci. Technol*., 8(1), 91–105, 2013.

Didari, A. and Mengüç, M. P.: Analysis of near-field radiation transfer within nano-gaps using FDTD method, *JQSRT*, 146, 214–226, 2014.

Didari, A. and Mengüç, M. P.: Near-field thermal emission between corrugated surfaces separated by nano-gaps, *JQSRT*, 158, 43–51, 2015.

Emery, A. F.: VIEW—A radiation view factor program with interactive graphics for geometry definition (Version 5.5.3), 1986.

Emery, A. F., Johansson, O., Lobo, M., and Abrous, A.: A comparative study of methods for computing the diffuse radiation viewfactors for complex structures, *JHT*, 113(2), 413–422, 1991.

Glass, M. W.: *CHAPARRAL: A Library for Solving Large Enclosure Radiation Heat Transfer Problems*, Sandia National Laboratory Report SAND95-2049, Albuquerque, NM, August 1995.

Gordon, I. E., et al. (eds): The HITRAN 2016 molecular spectroscopic databas**e**, *JQSRT*, 203, 3-69, 2017.

Heltzel, A., Battula, A., Howell, J. R., and Chen, S.: Nanostructuring borosilicate glass with near-field enhanced energy using a femtosecond laser pulse, *J. Heat Transfer*, Special Issue on *Nanoscale Heat Transfer*, 129, 53–59, January 2007.

Heltzel, A., Chen, S., and Howell, J. R.: Surface plasmon-based nanopatterning assisted by gold nanospheres, *Nanotechnology*, 19(2), January 2008.

Heltzel, A., Theppakuttai, S., Howell, J. R., and Chen, S.: Analytical and experimental investigation of laser-microsphere interaction for nanoscale surface modification, *J. Heat Transfer*, 127(11), 1231–1235, 2005.

Howell, J. R.: ***Catalog of Radiation Configuration Factors,*** McGraw-Hill Book Company, New York, 1982; later eds. published in electronic form on-line.

Jacquinet-Husson, N. et al., The 2015 edition of the GEISA spectroscopic database, *J. Molecular Spectroscopy* 327, 31-72, Sept. 2017. (GEISA database updated in 2019)

Kramida, A., Ralchenko, Y., Reader, J. and NISTASDTeam: NIST Atomic Spectra Database (version 5.0), [Online]. National Institute of Standards and Technology, Gaithersburg, MD, 2012.

Laux, C. O.: Radiation and nonequilibrium collisional-radiative models, in D. Fletcher, J.-M. Charbonnier, G. S. R. Sarma, and T. Magin (eds.), *Physico-Chemical Modeling of High Enthalpy and Plasma Flows*, von Karman Institute Lecture Series 2002-07, Rhode-Saint-Genèse, Belgium, 2002.

McDonald, J., Golden, A., and Jennings, G.: OpenDDA: A high-performance computational framework for the discrete dipole approximation, *Int. J. High Perf. Comp. Appl*. 23(1), 42–46, 2009

Mengüç, M. P., Manickavasagam, S., and D'sa, D. A.: Determination of radiative properties of pulverized coal particles from experiments, *FUEL*, 73(4), 613–625, 1994.

Mishchenko, M. I., Videen, G., Khlebtsov, N. G., and Wriedt, T.: Comprehensive T-matrix reference database: A 2012–2013 update, *JQSRT*, 123, 145–152, 2013.

Nieminen, T. A., Loke, V. L. Y., Stilgoe, A. B., Knöner, G., Branczyk, A. M., Heckenberg, N. R., and Rubinsztein-Dunlop, H.: Optical tweezers computational toolbox, *J. Opt. A*, 9, S196–S203, 2007.

M. REFERENCES TO REVIEWS AND HISTORICAL PAPERS

Prahl, S.: Mie scattering calculator, http://omlc.ogi.edu/calc/mie_calc.html (accessed April 16, 2015). Oregon Medical Laser Center, Portland, OR, 2009.

Rothman, L. S., Gordon, I. E., Barbe, A. et al., The HITRAN 2012 molecular spectroscopic database, *JQSRT*, 130, 4–50, 2013.

Shapiro, A. B.: FACET—A computer view factor computer code for axisymmetric, 2d planar, and 3d geometries with shadowing, UCID-19887, University of California, Lawrence Livermore National Laboratory, Livermore, CA, August 1983

Shlager, K. L. and Schneider, J. B.: A Selective Survey of the Finite-Difference Time-Domain Literature, *IEEE Antennas Propag. Mag*., 37(4), 39-56, Aug. 1995.

Sun, W., Videen, G., Fu, Q., and Hu, Y.: Scattered-field FDTD and PSTD algorithms with CPML absorbing boundary conditions for light scattering by aerosols, *JQSRT*, 131, 166–174, 2013.

Taflove, A.: *Advances in FDTD Techniques and Applications in Photonics*, *Photonics North 2007*, Ottawa, Ontario, Canada, June 4, 2007.

Veselago, V., Braginsky, L., Shklover, V., and Hafner, C.: Negative refractive index materials, *J. Comput. Theoret. Nanosci.*, 3, 1–30, 2006.

Walker, T.: The use of primatives in the calculation of radiative view factors, PhD dissertation, School of Chemical and Biomolecular Engineering. University of Sydney, Sydney, New South Wales, Australia, December 2013.

Walker, T., Xue, S.-C., and Barton, G. W: Numerical determination of radiative view factors using ray tracing, *JHT*, 132(7), 072702-1–072702-6, 2010.

Walker, T., Xue, S.-C., and Barton, G. W: A robust Monte Carlo-Based ray-tracing approach for the calculation of view factors in arbitrary three- dimensional geometries, *Comput. Thermal Sci*., 4(5), 425–442, 2012.

Walton, G.N.: Algorithms for Calculating Radiation View Factors Between Plane Convex Polygons with Obstructions, National Bureau of Standards NBSIR 863463, Gaithersburg, MD, 1986.

Wriedt, T.: Light scattering theories and computer codes, *JQSRT*, 110, 833–843, 2009.

Yee, K. S.: Numerical solution of initial value problems involving Maxwell's equations in isotropic media, *IEEE Trans. Antennas Propag*., 14, 302–307, 1966.

Yurkin, M. A. and Hoekstra, A. G.: The discrete-dipole-approximation code ADDA: Capabilities and known limitations, *JQSRT*, 112(13), 2234–2247, 2011.

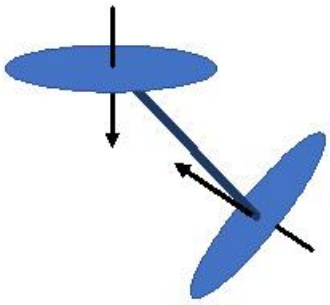

M. REFERENCES TO REVIEWS AND HISTORICAL PAPERS

M.1 GENERAL

Bone, W. A., and Townsend, D. T. A.: *Flame and Combustion in Gases*, Longmans, Green, London, 1927.

Born, M., Wolf, E., and Bhatia, A. B.: *Principles of Optics*, 7th expanded ed., Cambridge University Press, New York, 1999.

Breene, R. G.: *Theories of Spectral Line Shapes*, John Wiley and Sons, New York, 1981.

Carslaw, H. S., and Jaeger, J. C.: *Conduction of Heat in Solids*, 2d ed., Clarendon Press, Oxford, UK, 1959.

Coakley Jr, J. A. and Yang, P.: *Atmospheric Radiation: A Primer with Illustrative Solutions*, John Wiley & Sons, New York, 2014.

Garbuny, M.: *Optical Physics*, 2nd printing, Academic Press, New York, 1967.

Glassman, I., Yetter, R. A., and Glumac, N. G.: *Combustion*, 5th ed., Elsevier Science/Academic Press, Burlington, MA 2018.

Griem, H. R.: *Principles of Plasma Spectroscopy*, Cambridge University Press, 2005.

Hecht, E.: *Optics*. 4th ed., Pearson Education, Inc., Upper Saddle River, USA, 2002.

Herzberg, G.: *Molecular Spectra and Molecular Structure*, 2d ed., 3 vols., Krieger, Malabar, FL, 1992.

Howell, J. R.: The development of engineering radiative heat transfer, *IMECE2002-33131*, 73-78, IMECE, New Orleans, Nov. 2002.

Howell, J. R., Hall, M. J., and Ellzey, J. L.: Combustion of Hydrocarbon Fuels within Porous Inert Media, *Prog. Energy Comb. Science*, vol. 22, pp. 121–145, 1996.

Khalil, E. E.: *Modelling of Furnaces and Combustors*, Energy and Engineering Science Series, Gupta, A.K. and Lilley, D.G. (eds.), Abacus Press, Tunbridge Wells, U.K., 1982.

Kittel, C.: *Introduction to Solid State Physics*, John Wiley & Sons, Hoboken, 2005.

Kourganoff, V.: *Basic Methods in Transfer Problems*, Dover, New York, 1963.

Kuneš, J.: *Dimensionless Physical Quantities in Science and Engineering*, Elsevier, New York, 2012.

Kuo, K.: *Principles of Combustion*, 2nd ed., John Wiley & Sons, 2005.

Landau, L. D. and Lifshitz, E. M.: *Electrodynamics of Continuous Media*, Addison-Wesley, Reading, MA, 1960.

Law, C. K.: *Combustion Physics*, Cambridge University Press, 2006 (on-line, July 2010).

MacRobert, T. M.: *Spherical harmonics*, 3rd edn. Pergamon Press, New York, 1967.

Maier, S. A.: *Plasmonics: Fundamentals and Applications*, Springer, New York, 2007.

Majumdar, A.: Scanning Thermal Microscopy, *Ann. Rev. of Matls Sci.*, vol. 29, pp. 505–585, 1999.

Mandel, L. and Wolf, E.: *Optical Coherence and Quantum Optics*, Cambridge University Press, Cambridge, 1995.

Mandelbrot, B. B.: *Les Objets Fractals: Forme, Hasard et Dimension*, Flammarion, Paris, 1975.

Mandelbrot, B. B.: *The Fractal Geometry of Nature*, W. H. Freeman, San Francisco, CA, 1983.

Mark, J.C.: The spherical harmonics method. Part I. Atomic Energy Report No. MT 92, *National Research Council of Canada*, 1944.

Mohr, P. J., Newell, D. B., and Taylor, B. N.: CODATA recommended values of the fundamental physical constants: 2014, *Rev. Mod. Phys*., 88, 035009, July-Sept. 2014.

Novotny, J. L., and Hecht, B.: *Principles of Nano-optics*, University Press, Cambridge, 2006.

Patankar, S. V.: *Numerical Heat Transfer and Fluid Flow*, Hemisphere, Washington, DC, 1980.

Penner, S. S.: *Quantitative Molecular Spectroscopy and Gas Emissivities*, Addison-Wesley, Reading, MA, 1959.

Shen, J., and Tang, T.S., *Spectral and High-Order Methods with Applications*, Science Press, Beijing, 2006.

Stone, J. M.: *Radiation and Optics*, McGraw–Hill, New York, 1963.

Tien, C. L., and Cunnington, G. R.: Cryogenic Insulation Heat Transfer, in T. F. Irvine, Jr., and J. P. Hartnett (eds.), *Advances in Heat Transfer*, 9, 349–417, Academic Press, New York, 1973.

Turns, S. R.: *An Introduction to Combustion; Concepts and Applications*, McGraw-Hill, New York, 2011.

Vincenti, W. G, and Kruger Jr., C. H.: *Introduction to Physical Gas Dynamics*, Corrected Ed., Krieger Publishing Company, Malabar, FL, 1986.

Williams, F. A.: *Combustion Theory*, 2nd ed., Taylor and Francis, New York, 1994.

Yeh, P.: *Optical Waves in Layered Media*, John Wiley & Sons, Hoboken, 2005.

Zel'dovich, Ya. B., and Raizer, Yu. P.: *Physics of Shock Waves and High-Temperature Hydrodynamic Phenomena*, vol. 1, pt. II, Academic Press, New York, 1966.

M.2 INVERSE METHODS

Alifanov, O. M.: *Inverse Heat Transfer Problems*, Springer, Berlin, 1994.

Alifanov, O. M., Artyukhin, E. A., and Rumyantsev, S. V.: *Extreme Methods for Solving Ill-Posed Problems with Applications to Inverse Heat Transfer Problems*, Begell House, New York, 1995.

Beck, J. V., Blackwell, B., and St. Clair, Jr., C. R.: *Inverse Heat Conduction: Ill-Posed Problems*, Wiley-Interscience, New York, 1995.

Beckman, F. S.: The Solution of Linear Equations by the Conjugate Gradient Method, in A. Ralston and H. S. Wilf (eds.), *Mathematical Methods for Digital Computers*, John Wiley and Sons, New York, 62–72, 1960.

França, F. H. R., Howell, J. R., Ezekoye, O. A., and Morales, J. C.: Inverse design of thermal systems, in J. P. Hartnett and T. F. Irvine (eds.), *Advances in Heat Transfer*, vol. 36, 1, pp. 1–110, Academic Press, Waltham, MA, 2002.

Hansen, P. C., *Rank-Deficient and Discrete Ill-Posed Problems: Numerical Aspects of Linear Inversion*, SIAM, Philadelphia, 1998.

M. REFERENCES TO REVIEWS AND HISTORICAL PAPERS

Kushner, H. J. and Clark, D. S.: *Stochastic Approximation Methods for Constrained and Unconstrained Systems*, Springer, New York, 1978.

Özişik, M. N., and Orlande, H. R. B.: *Inverse Heat Transfer: Fundamentals and Applications*, Taylor and Francis, New York, 2000.

Morozov, V. A.: *Methods for Solving Incorrectly Posed Problems*, Springer-Verlag, New York, 1984.

Tikhonov, A. N.: Solution of Incorrectly Formulated Problems and the Regularization Method, *Soviet Math. Dokl.*, 4, 1035–1038, 1963. [Engl. trans. *Dokl. Akad. Nauk. SSSR*, 151, 501–504, 1963.]

Vogel, C.R.: *Computational Methods for Inverse Problems*, SIAM, Philadelphia, 2002.

M.3 RADIATIVE TRANSFER

M.3.1 GENERAL

Amber, I. and O'Donovan, T. S.: Natural convection induced by the absorption of solar radiation: A review, *Renewable and Sustainable Energy Reviews*, 82, 3526–3545, 2018.

Cess, R. D.: The interaction of thermal radiation with conduction and convection heat transfer, in T. F. Irvine, Jr. and J. P. Hartnett (eds.), *Advances in Heat Transfer*, vol. 1, pp. 1–50, Academic Press, New York, 1964

Ficker, T.: General Model of Radiative and Convective Heat Transfer in Buildings: Part I: Algebraic Model of Radiative Heat Transfer, *Acta Polytechnica*, 59(3), 211-233, 2019.

Frank, M. and Klar, A.: Radiative heat transfer and applications for glass production processes, in A. Farina, A. Klar, R. M. M. Mattheijj, A. Mikelić, N. Siedow, and A. Fasano (eds.), *Mathematical Models in the Manufacturing of Glass, Proceedings of the C.I.M.E. Summer School*, pp. 57–134, Springer, Terme, Italy, 2008.

Hottel, H. C.: Radiant Heat Transmission, in W. H. McAdams (ed.), *Heat Transmission*, 3d ed., McGraw-Hill, New York, 1954.

Hottel, H. C, and Sarofim, A. F.: *Radiative Transfer*, McGraw–Hill, New York, 1967.

Hottel, H. C., Sarofim, A. F., Wankat, P. C., Noble, J. J., Silcox, G. D., and Knaebel, K. S.: Heat and Mass Transfer, in D. W. Green and R. H. Perry (eds.), *Perry's Chemical Engineer's Handbook*, 8th ed., Chap. 5, pp. 5-16–5-43, McGraw-Hill, 2008.

Lee, S. -C, and Cunnington, G. R.: Theoretical Models for Radiative Transfer in Fibrous Media, in *Ann. Rev. Heat Transfer*, vol. IX, Chap. 3, pp. 159–218, Begell House, New York, 1998.

Modest, M. F.: *Radiation heat transfer*. 3rd ed., Academic Press, Waltham, MA, 2013.

Özişik, M. N.: *Radiative Transfer, and Interactions with Conduction and Convection*, John Wiley & Sons, New York, 1973.

Sparrow, E. M.: On the Calculation of Radiant Interchange between Surfaces, in W. Ibele (ed.), *Modern Developments in Heat Transfer*, pp. 181–212, Academic Press, New York, 1963b.

Sparrow, E. M., and Cess, R. D.: *Radiation Heat Transfer*, augmented edition, Hemisphere, Washington, DC, 1978.

Stewart, S. M. and Johnson, R. B.: *Blackbody Radiation: A History of Thermal Radiation Computational Aids and Numerical Methods*, CRC Press, Boca Raton, 2016.

Tencer, J. and Howell, J.R.: Coupling Radiative Heat Transfer with Other Heat Transfer Modes, *J. Brazilian Society Engng Sci*, 38(5), 1473-1487, June 2016.

Timoshenko, V. P., and Trenev, M. G.: A Method for Evaluating Heat Transfer in Multilayered Semitransparent Materials, *Heat Transfer—Sov. Res*., vol. 18, no. 5, pp. 44–57, 1986.

Viskanta, R.: Radiation Transfer and Interaction of Convection with Radiation Heat Transfer, in Thomas F. Irvine, Jr., and James P. Hartnett (eds.), *Advances in Heat Transfer*, vol. 3, pp. 175–251, Academic Press, New York, 1966.

Viskanta, R., and Anderson, E. E.: Heat Transfer in Semi-transparent Solids, in J. P Hartnett and T. F. Irvine, Jr. (eds.), *Advances in Heat Transfer*, vol. 11, pp. 317–441, Academic Press, New York, 1975.

Viskanta, R., and Mengüç, M. P.: Radiation Heat Transfer in Combustion Systems, *Prog. Energy Combust. Sci.*, vol. 13, pp. 97–160, 1987.

Viskanta, R.: *Radiative Transfer in Combustion Systems: Fundamentals and Applications*, Begell House, New York, 2005.

M.3.2 ATMOSPHERIC RADIATION

Bohren, C.W. and Clothiaux, E.E.: *Fundamentals of Atmospheric Radiation*, John Wiley & Sons, New York, 2006.

Coakley Jr, J. A., and Yang, P.: *Atmospheric Radiation: A Primer with Illustrative Solutions*, John Wiley & Sons, New York, 2014.

Duffie, J. A., and Beckman, W. A.: *Solar Energy Thermal Processes*, 3d ed., Wiley, New York, 2006.

Goody, R. M., and Yung, Y. L.: *Atmospheric Radiation*, 2d ed., Oxford University Press, New York, 1989.

Kondratyev, Ya. K.: *Radiation in the Atmosphere*, Academic Press, New York, 1969.

Liou, K.-N.: *An Introduction to Atmospheric Radiation*, 2nd ed., Academic Press, 2002

Petty, G.W.: *A First Course in Atmospheric Radiation*, 2nd ed., Sundog Publishing, Madison, WI., 2006.

M.3.3 INVERSE SOLUTIONS IN RADIATION

Daun, K. J., Ertürk, H., and Howell, J. R.: Inverse Design Methods for High-Temperature Systems, *Arabian J. Sci. and Tech*, 27(2C), 3–48, 2003.

M. REFERENCES TO REVIEWS AND HISTORICAL PAPERS

Daun, K. J., Ertürk, H., Howell, J. R., Gamba, M. and Hosseini Sarvari, M.: The Use of Inverse Methods for the Design and Control of Radiant Sources, *JSME International Journal*, ser. B, 46(4), 470–478, 2003.

França, F. H. R., Howell, J. R., Ezekoye, O. A., and Morales, J. C.: Inverse Design of Thermal Systems, in J. P. Hartnett and T. F. Irvine (eds.), *Advances in Heat Transfer*, 36(1), 1–110, Elsevier, 2002.

Hansen, P. C.: *Rank-Deficient and Discrete Ill-Posed Problems: Numerical Aspects of Linear Inversion*, SIAM, Philadelphia, PA, 1998.

Kennedy, J. and Eberhart, R.: Particle swarm optimization, *Proc. ICNN'95 – Intl. Conf. on Neural Network*s, pp. 1942-1948, IEEE, Nov. 1995.

Vogel, C. R.: *Computational Methods for Inverse Problems*, SIAM, Philadelphia, PA, 2002.

Wing, G. W.: *A Primer on Integral Equations of the First Kind*, SIAM, Philadelphia, PA, 1991.

M.3.4 k-DISTRIBUTION AND SLWSGG METHODS

André, F. and Vaillon, R.: Generalization of the *k*-moment Method Using the Maximum Entropy Principle; Application to the NBKM and Full Spectrum SLMB Gas Radiation Models, *JQSRT*, 113(12), 1508–1520, 2012.

André, F., Solovjov, V.P., Hou, L., Vaillon, R., and Lemonnier, D.: The Generalized k-Moment Method for the Modeling of Cumulative k-Distributions of H_2O at High Temperature, *JQSRT* 143, 92-99, 2014a.

André, F., Hou, L., Roger, M., and Vaillon, R.: The Multispectral Gas Radiation Modeling: A New Theoretical Framework Based on a Multidimensional Approach to *k*-Distribution Methods, *JQSRT*, vol. 147, pp. 178-195, 2014b.

Badger, J., Webb, B. W., and Solovjov, V. P.: An exploration of advanced SLW modeling approaches in comprehensive combustion predictions, *Combustion Sci. and Tech.*, 208757754 pub. On line, DOI: 10.1080/00102202.2019.1678907, 22 Oct. 2019.

Cai, J. and Modest, M. F.: Improved full-spectrum *k*-distribution implementation for inhomogeneous media using a narrow-band database, *JQSRT*, 141, 65-72, July 2014.

Guo, J., Li, X., Huang, X., Liu, Z., and Zheng, C.: A full spectrum k-distribution based weighted-sum-of gray-gases model for oxy-fuel combustion, *IJHMT*, 90, 218-226, Nov. 2015.

Denison, M. K. and Webb, B. W.: The spectral line weighted-sum-of-gray-gases model—A review, in M. P. Mengüç (ed.), *Radiative Transfer—I, Proceedings of the First International Symposium on Radiative Transfer*, pp. 193–208, Begell House, New York, 1996.

Howell, J. R.: Non-equilibrium Radiative Transfer Models: k-Distribution, *von Karman Institute Lecture Series STO-AVT-218-VKI, Radiation and Gas-Surface Interaction Phenomena in High-Speed Re-Entry*, University of Illinois at Urbana Champagne, April 2014.

Modest, M.F.: The Treatment of Nongray Properties in Radiative Heat Transfer: From Past to Present, *JHT*, 135(6) 061801-1 through 061801-12. doi:10.1115/1.40235, 2013.

Solovjov, V. P., Webb, B. W., and André, F.: Radiative Properties of Gases, in Kulacki, F. ed., *Handbook of Thermal Science and Engineering*, 1-74, Springer, 2017.

Wang, C., He, B., Modest, M. F., and Ren, T.: Efficient full-spectrum correlated-k-distribution look-up table, *JQSRT*, 219, 108–116, 2018.

M.3.5 MATHEMATICAL RESOURCES

Abramowitz, M. and Stegun, I. A.: *Handbook of Mathematical Functions*, Dover, New York, 1965.

Altaç, Z.: Integrals Involving Bickley and Bessel Functions in Radiative Transfer, and Generalized Exponential Integral Functions, *JHT*, vol. 118, no. 3, pp. 789–792, 1996.

Breig, W. F., and Crosbie, A. L.: Numerical Computation of a Generalized Exponential Integral Function, *Math. Comput*., vol. 28, no. 126, pp. 575–579, 1974.

Chang, S. L., and Rhee, K. T.: Blackbody Radiation Functions, *Int. Comm. Heat Mass Transfer*, vol. 11, pp. 451–455, 1984.

Chung, T. J.: Integral and integrodifferential systems, in W. J. Minkowitz, E. M. Sparrow, G. E. Schneider, and R. H. Pletcher (eds.), *Handbook of Numerical Heat Transfer*, Chapter 14, Wiley, New York, 1988.

M.3.6 MICROSCALE-NANOSCALE

Basu, S., Chen, Y.B., and Zhang, Z.M.: Microscale Radiation in Thermophotovoltaic Devices- A Review, *Int. J. Energy Research*, vol. 31, no. 6-7, 689-716, 2007.

Boltasseva, A., and Shalaev, V.: Fabrication of Optical Negative-index Metamaterials: Recent Advances and Outlook, *Metamaterials*, vol. 2, pp. 1-17, 2008.

Cai, W. and Shalaev, V.: *Optical Metamaterials: Fundamentals and Applications*, Springer, New York, 2010.

Carey, V. P., Chen, G., Grigoropoulos, C., Kaviany, M., and Majumdar, A.: A Review of Heat Transfer Physics, *Nanosc. Microsc. Therm.*, vol. 12, pp. 1–60, 2008.

Chen, G.: *Nanoscale Energy Transport and Conversion*, Oxford University Press, New York, 2005.

Cahill, D.G., Ford, W.K., Goodson, K.E., Mahan, G.D., Majumdar, A., Maris, H.J., Merlin, R., and Phillpot, S.R.: Nanoscale thermal transport, *J. Appl. Phys*. vol. 93, pp. 793–818, 2003.

M. REFERENCES TO REVIEWS AND HISTORICAL PAPERS

Cahill, D.G. et al.: Nanoscale thermal transport II. 2003–2012, *Appl. Phys. Revs*, vol. 1, 011305, 2014.

Corbitt, S., Francoeur, M., and Raeymaekers, B.: Implementation of Optical Dielectric Metamaterials: A Review," *JQSRT*, **158**, 3-16, 2015.

Family, R. and Mengüç, M.P.: Materials for radiative cooling: A review, *Procedia Environmental Sciences*, 38, 752 – 759, 2017.

Francoeur, M.: Thermal fundamentals, Chap. 4 in *Micro Energy Harvesting*, Briand, D., Yeatman, E. and Roundy, S. (eds.) Wiley-VCH, 2015.

Fu, C. J. and Zhang, Z. M.: Thermal radiative properties of metamaterials and other nanostructured materials: A review, *Frontiers of Energy and Power Engineering in China*, 3(1), 11-26, 2009.

Greffet, J. -J., Carminati, R., Joulain, K., Mulet, J. -P., Mainguy, S., and Chen, Y.: Coherent Emission of Light by Thermal Sources, *Nature*, vol. 416, pp. 61–64, March 7, 2002.

Liu, X., Wang, L., and Zhang, Z.M.: Near-Field Thermal Radiation: Recent Progress and Outlook, *Nanoscale and Microscale Thermophysical Engineering*, 19(2), 98-126, 2015

Narayanaswamy, A., and Chen, G.: Direct Computation of Thermal Emission from Nanostructures, *Ann. Rev. Heat Transfer*, vol. 14, pp. 169–195, 2005.

Otey, C. R., Zhu, L., Sandhu, S., and Fan, S.: Fluctuational electrodynamics calculations of near-field heat transfer in non-planar geometries: A brief overview, *JQSRT*, Special Issue on *Micro- and Nano-scale Radiative Transfer*, 132, 3–11, 2014.

Raether, H.: *Surface Plasmons on Smooth and Rough Surfaces and on Gratings*, Springer-Verlag, Berlin, 1988.

Rytov, S. M.: *Theory of Electric Fluctuations and Thermal Radiation*, Air Force Cambridge Research Center, Bedford, MA, 1959.

Rytov, S. M., Kravtsov, Y. A., and Tatarskii, V. I.: *Principles of Statistical Radiophysics 3: Elements of Random Fields*, Springer, Berlin, Heidelberg, New York, 1989.

Shi, L., Dames, C., Lukes, J.R., Reddy, P., Duda, J., Cahill, D.G., Lee, J., Marconnet, A., Goodson, K.E., Bahk, J.-H., Shakouri, A., Prasher, R.S., Felts, J., King, W.P., Han, B., and Bischof, J.C.: Evaluating Broader Impacts of Nanoscale Thermal Transport Research, *Nanoscale and Microscale Thermophysical Engineering*, 19(2), 127-165, 2015

Taflove, A.: *Advances in FDTD Techniques and Applications in Photonics*, *Photonics North 2007*, Ottawa, Ontario, Canada, June 4, 2007.

Wong, B. T. and Mengüç, M. P.: *Thermal Transport for Applications in Micro- and Nanomachining*, Springer, Berlin, Germany, 2008.

Zhang, Z. M.: *Nano/Microscale Heat Transfer*, McGraw-Hill, New York, 2007.

M.3.7 PROPERTIES

Bernath, P. and Rothman, L.: HITRAN2016 Special Issue, *JQSRT*, 203, 1-582, Dec. 2017.

Fox, M: *Optical Properties of Solids*, Oxford University Press, Oxford, UK, 2001.

Fu, C. J. and Zhang, Z. M.: Thermal radiative properties of metamaterials and other nanostructured materials: A review, *Frontiers of Energy and Power Engineering in China*, 3(1), 11-26, 2009.

Gordon, I. E., et al. (eds): The HITRAN 2016 molecular spectroscopic database, *JQSRT*, 203, 3-69, 2017.

Kunitomo, T.: Present status of research on radiative properties of materials, *Int. J. Thermophys*., 5(1), 73–90, 1984.

Palik, E. D. (ed.): *Handbook of Optical Constants of Solids*, vols. I-IV, Elsevier, New York, 1998.

Reed, B., Biaglow, J., and Schneider, S.: *Advanced Materials for Radiation-Cooled Rockets*, vol. II, pp. 115–118, NASA Propulsion Engineering Research Center, Annual Report 199, NASA Lewis Research Center, N94-28052, Washington, DC, September 1993.

Rothman, L. S., Jacquemart, D., Barbe, A., et al.: The *HITRAN* 2004 Molecular Spectroscopic Database, *JQSRT*, vol. 96, pp. 139–204, 2005. For most recent version (2012) see www.cfa.harvard.edu/hitran//.

Rothman, L.S., Gordon, I.E., Barber, R.J., Dothe, H., Gamache, R.R., Goldman, A., Perevalov, V., Tashkun, S.A., and Tennyson, J.: "HITEMP, the High-temperature Molecular Spectroscopic Database," *JQSRT*, vol. 111, no. 15, 2139.2150 , 2010.

Rumble, J. R., (ed.): *Handbook of Chemistry and Physics*, 100th edn., CRC Press, Boca Raton, FL, 2018-2019.

Svet, D. I.: *Thermal Radiation; Metals, Semiconductors, Ceramics, Partly Transparent Bodies, and Films*, Consultants Bureau, Plenum Publishing, New York, 1965.

Tien, C. L.: Thermal Radiation Properties of Gases, in T. F. Irvine, Jr., and J. P. Hartnett (eds.), *Advances in Heat Transfer*, vol. 5, pp. 253–324, Academic Press, New York, 1968.

Touloukian, Y. S., and Ho, C. Y. (eds.): Thermophysical Properties of Matter, TRPC Data Services. Volume 7, *Thermal Radiative Properties: Metallic Elements and Alloys*, Touloukian, Y. S. and DeWitt, D. P. (1970); Volume 8, *Thermal Radiative Properties: Nonmetallic Solids*, Touloukian, Y. S. and DeWitt, D. P. (1972a); Volume 9, *Thermal Radiative Properties: Coatings*, Touloukian, Y. S., DeWitt, D. P., and Hernicz, R. S. (1972b), Plenum Press, New York.

Warren, S. G. and Brandt, R. E.: Optical constants of ice from the ultraviolet to the microwave: A revised compilation, *J. Geophys. Res.*, 113, D14220, 2008. (Tables of values available at *www.atmos.washington.edu/ice_optical_constants*)

Wood, W. D., Deem, H. W., and Lucks, C. F.: *Thermal Radiative Properties*, Plenum Press, New York, 1964.

M.3.8 RTE SOLUTION METHODS

Tencer, J. and Howell, J.R.: Coupling Radiative Heat Transfer with Other Heat Transfer Modes, *J. Brazilian Society Engng Sci*, 38(5), 1473-1487, June 2016.

M. REFERENCES TO REVIEWS AND HISTORICAL PAPERS

M.3.8.1 FINITE ELEMENT

Nice, M. L.: Application of Finite Element Method to Heat Transfer in a Participating Medium, in T. M. Shih (ed.), *Numerical Properties and Methodologies in Heat Transfer*, pp. 497–514, Hemisphere, Washington, DC, 1983.

M.3.8.2 FINITE VOLUME

Chai, J. C., and Patankar, S. V.: Finite Volume Method for Radiation Heat Transfer, in W. Minkowycz and E. Sparrow (eds.), *Advances in Numerical Heat Transfer*, vol. 2, 109-141, Taylor and Francis, London, 2000.

Mathur, S. R., and Murthy, J. Y.: Unstructured Finite Volume Methods for Multi-mode Heat Transfer, in W. J. Minkowycz and E. M. Sparrow (eds.), *Advances in Numerical Heat Transfer*, vol. 2, pp. 37–70, Taylor and Francis, New York, 2000.

M.3.8.3 DISCRETE ORDINATES

Balsara, D.: Fast and accurate discrete ordinates methods for multidimensional radiative transfer. Part I, basic methods, *JQSRT*, 69, 671-707, 2001.

Carlson, B. G. and Lathrop, K. D.: Transport theory—The method of discrete ordinates, in H. Greenspan, C. N. Kelber, and D. Okrent (eds.), *Computing Methods in Reactor Physics*, Chapter 3, Gordon & Breach, New York, 1968.

Lathrop, K. D.: Use of discrete ordinate methods for solution of photon transport problems, *Nucl. Sci. Eng*., 24, 381–388, 1966.

M.3.8.4 MONTE CARLO

Barker, E., and Kelsey, J.: *Recommendation for Random Number Generation Using Deterministic Random Bit Generators*, NIST Special Publication 800-90A Revision 1, 109 pp., National Institute of Standards and Technology, Gaithersburg, MD, June 2015.

Burns, P. J. and Pryor, D. V.: Surface radiative transport at large scale via Monte Carlo, in C.-L. Tien (ed.), *Annual Review of Heat Transfer*, IX, Chapter 7, pp. 79–158, Begell House, New York, 1998.

Cashwell, E. D. and Everett, C. J.: *A Practical Manual on the Monte Carlo Method for Random Walk Problems*, Pergamon, New York, 1959.

Chen, G. and Boyd, I. D.: Statistical error analysis for the direct simulation Monte Carlo method. *J. Computational Physics*, 126, 434-448, 1996.

Dauchet, J., Bezian, J.-J., Blanco, S., Caliot, C., Charon, J., Coustet, C., El Hafi,, M., Eymet, V., Farges, O., Forest, V., Fournier, R., Galtier, M., Gautrais, J., Khuong, A.,Pelissier, L., Benjamin Piaud, B., Maxime Roger, M., Guillaume Terrée, G., and Sebastian Weitz, S.: Addressing nonlinearities in Monte Carlo, *Scientific Reports* 8, 13302, 2018.

Ertürk, H., and Howell, J. R.: Monte Carlo methods for radiative transfer, in: *Handbook of Thermal Science and Engineering*, F. Kulacki, ed., pp. 1-43, Springer, Cham, 2017.

Farmer, J. T., and Howell, J. R.: Monte Carlo Strategies for Radiative Transfer in Participating Media, in J. P. Hartnett and T. Irvine, (eds.), *Advances in Heat Transfer*, vol. 31, pp. 1–97, Acadamic Press, San Diego, 1998.

Fournier, R., Blanco, S., Eymet, V., El Hafi, M., and Spiesser, C.: Radiative, conductive and convective heat transfers in a single Monte Carlo algorithm, *J. Physics*: Conf. Series, 676(1), 012007, 2016.

Haji-Sheikh, A., and Sparrow, E. M.: Probability Distributions and Error Estimates for Monte Carlo Solutions of Radiation Problems, in T. F. Irvine, W. E. Ibele, J. P. Hartnett, and R. J. Goldstein (eds.), *Progress in Heat and Mass Transfer*, vol. 2, pp. 1–12, Pergamon, Oxford, 1969.

Haji-Sheikh, A.: Monte Carlo Methods, in W. J. Minkowycz, E. M. Sparrow, G. E. Schneider, and R. H. Pletcher (eds.), *Handbook of Numerical Heat Transfer*, Chap. 16, pp. 672–723, Wiley Interscience, New York, 1988

Haji-Sheikh, A., and Howell, J. R.: Monte Carlo Methods, in W. J. Minkowycz, E. M. Sparrow, and J. Y. Murthy (eds.), *Handbook of Numerical Heat Transfer*, 2d ed., Chap. 8, pp. 249–296, Wiley Interscience, New York, 2006.

Halton, J. H.: A Retrospective and Prospective Survey of the Monte Carlo Method, *SIAM Rev*., vol. 12, no. 1, pp. 1–63, 1970.

Hammersley, J. M., and Handscomb, D. C.: *Monte Carlo Methods*, Wiley, New York, 1964.

Howell, J. R.: The Monte Carlo method in radiative heat transfer, *JHT*, 120(3), 547–560, 1998.

Mahan, J. R., *The Monte Carlo Ray-Trace Method in Radiation Heat Transfer and Applied Optics*. John Wiley & Sons, New York, 2018.

Metropolis, N., and Ulam, S.: The Monte Carlo Method, *J. Am. Stat. Assoc*., vol. 44, no. 247, pp. 335–341, 1949.

Schreider, Yu. A. (ed.): *Method of Statistical Testing—Monte Carlo Method*, American Elsevier, New York, 1964.

Taussky, O. and Todd, J.: Generating and testing of pseudo-random numbers, in H. A. Meyer (ed.), *Symposium on Monte Carlo Methods*, pp. 15–28, Wiley, New York, 1956.

Walters, D. V., and Buckius, R. O.: Monte Carlo Methods for Radiative Heat Transfer in Scattering Media, in C. -L. Tien (ed.), *Annual Review of Heat Transfer*, vol. 5, Chap. 3, pp. 131–176, CRC Press, Boca Raton, 1994.

Wing, G. W.: *A Primer on Integral Equations of the First Kind*, SIAM, Philadelphia, 1991.

Yang, W.-J., Taniguchi, H., and Kudo, K.: Radiative Heat Transfer by the Monte Carlo Method, in J. P. Hartnett and T. F. Irvine

(eds.), *Advances in Heat Transfer*, vol. 27, pp. 1–215, Academic Press, San Diego, 1995.
Yarbrough, D. W., and Lee, C. -L.: Monte Carlo Calculation of Radiation View Factors, in F. R. Payne et al. (eds.), *Integral Methods in Science and Engineering 85*, pp. 563–574, Hemisphere, Washington, DC, 1985.

M.3.8.5 LATTICE BOLTZMANN

Asinari, P., Mishra, S.C., and Borchiellini, R.: A lattice Boltzmann formulation for the analysis of radiative heat transfer problems in a participating medium, *Numerical Heat Transfer-A, Fundamentals*, 57(2), 126-146, March 2010.
Guo, Z. L. and Shu, C.: *Lattice Boltzmann Method and Its Applications in Engineering.* World Scientific Publishing, 2013.
Krüger, T., Kusumaatmaja, H., Kuzmin, A., Shardt, O., Silva, G., and Viggen, E. M.: *The Lattice Boltzmann Method: Principles and Practice.* Springer Verlag, 2017.
McHardy, C. B.: A lattice Boltzmann method for the simulation of light transfer in turbid media and its application in computational studies on microalgae growth kinetics, Dr. Eng. Dissertation, Technischen Universität Berlin, 2019.
McHardy, C., Horneber, T., and Rauh, C.: New lattice Boltzmann method for the simulation of three-dimensional radiation transfer in turbid media, *Optics Express*, 16999-17017, 24(15), 25 Jul 2016.
Succi, S.: *The Lattice Boltzmann Method for Fluid Dynamics and Beyond*, Oxford University Press, 2001.

M.3.9 SCATTERING

Baillis, D., and Sacadura, J.F., Thermal Radiation Properties of Dispersed Media: Theoretical Prediction and Experimental Characterization, *JQSRT* 67, 327-363, 2000.
Barber, P. W., and Hill, S. S.: *Light Scattering by Particles: Computational Methods*, World Scientific, Singapore, 1990.
Bayvel, L. P., and Jones, A. R.: *Electromagnetic Scattering and Its Applications*, Applied Science, London, pp. 5–6, 1981.
Beckmann, P., and Spizzichino, A.: *The Scattering of Electromagnetic Waves from Rough Surfaces*, Macmillan, New York, 1963.
Bohren, C., and Huffman, D.: *Absorption and Scattering of Light by Small Particles*, Wiley-Interscience, New York, 1983.
Charalampopoulos, T. T.: Morphology and dynamics of agglomerated particulates in combustion systems using light scattering techniques, *Prog. Energy Combust. Sci.*, 18, 13–45, 1992.
Doicu, A., Wriedt, T., and Eremin, Y. A.: *Light Scattering by Systems of Particles*, Springer, Heidelberg, 2006.
Dombrovsky, L. A. and Baillis, D.: *Thermal Radiation in Disperse Systems: An Engineering Approach*, Begell House, Redding, PA, 2010.
Frisad, J. R. and Kragh, H.: On Ludvig Lorenz and his 1890 treatise on light scattering by spheres, *Eur. Phys. J.- H*, 44(2), 137–160, Aug. 2019.
Henyey, L. G., and Greenstein, J. L.: Diffuse Radiation in the Galaxy, *Astrophys. J.*, vol. 88, pp. 70–83, 1940.
Kerker, M.: *The Scattering of Light and Other Electromagnetic Radiation*, Academic Press, New York, 1961.
Mie, G.: Beiträge zur Optik trüber Medien, speziell kolloidaler Metallösungen, *Ann. Phys.*, vol. 330, pp. 377–445, 1908.
Mie, G.: Optics of Turbid Media, *Ann. Phys.*, vol. 25, no. 3, pp. 377–445, 1908.
Mishchenko, M. I., Hovenier, J. W., and Travis, L. D.: *Light Scattering by Nonspherical Particles*, Academic Press, New York, 2000.
Mishchenko, M. I., Travis, L. D., and Lacis, A. A.: *Scattering, Absorption, and Emission of Light by Small Particles*, Cambridge University Press, London, 2002.
Mishchenko, M. I., Travis, L. D., and Lacis, A. A.: *Multiple Scattering of Light by Particles: Radiative Transfer and Coherent Back Scattering*, Cambridge Press, New York, 2006.
Rayleigh, Lord: On scattering of light by small particles, *Philos. Mag.*, 41, 447–454, 1871.
Rayleigh, Lord: On the incidence of electric and aerial waves upon small obstacles in the form of ellipsoids or elliptic cylinders and on the passage of electric waves through a circular aperture in a conducting screen, *Phil. Mag.*, 44, 28–52, 1897.
Rother, T.: *Electromagnetic Wave Scattering on Nonspherical Particles, Basic Methodology and Simulations*, Springer Series Optical Sciences, 2009.
Schuerman, D. W. (ed.): *Light Scattering by Irregularly Shaped Particles*, Plenum Press, State University of New York at Albany, NY, 1979.
Stokes, G. G.: On the Composition and Resolution of Streams of Polarized Light from Different Sources, *Trans. Camb. Phil. Soc.*, vol. 9, pp. 399–424, 1852. (Reprinted in *Mathematical and Physical Papers*, vol. 3, Cambridge University Press, pp. 233–258, London, 1901.)
Tang, K., Yang, Y., and Buckius, R. O.: Theory and Experiments on Scattering from Rough Interfaces, in C. -L. Tien (ed.), *Annual Review of Heat Transfer*, vol. X, Chap. 3, pp. 101–140, Begell House, 1999b.
Tien, C. L., and Drolen, B. L.: Thermal Radiation in Particulate Media with Dependent and Independent Scattering, *Annual Review of Numerical Fluid Mechanics and Heat Transfer*, vol. 1, pp. 1–32, Hemisphere, Washington, DC, 1987.
Tsang, L., Kong, J. A., and Ding, K. H.: *Scattering of Electromagnetic Waves*, Wiley, New York, 2000.
Van de Hülst, H. C: *Light Scattering by Small Particles*, Wiley, New York, 1957; Dover Publications, New York, 1981.
Xu, R.: *Particle Characterization: Light Scattering Methods*, Springer, 2001.

M. REFERENCES TO REVIEWS AND HISTORICAL PAPERS

M.4 POROUS MEDIA

Abdul, M., Abdullaha, M., and Abu Bakarb, M.: Combustion in porous media and its applications—A comprehensive survey. *J. Environmental Management*, 90:2287-2312, 2009.

Howell, J. R., Hall, M. J., and Ellzey, J. L.: Combustion of hydrocarbon fuels within porous inert media, *Prog. Energy Comb. Sci.*, 22(2), 121–145, 1996.

Kamal, M. M. and Mohamad, A. A.: Combustion in porous media, a review, *J. Power and Energy* 220(5), 487–508, 2006.

Lu, J. and Lu, W-q.: Review: Heat and mass transfer in porous medium, Mathematic/numerical models and research directions, *Int. J. Petrochemic. Sci. Eng.* 3(3), 97-100, 2018.

Mishra, N. K., Muthukumar, P., and Panigrahy, S.: A review on clean combustion within porous media, in *Air Pollution and Control*, N. Sharma et al. eds., pp. 209-224, Springer Link, 2018.

Mujeebu, M. A., Abdullah, M. Z., Abu Bakar, M. Z., Mohamad, A. A., Muhad, R. M. N., and Abdullah, M. K.: Combustion in porous media and its applications – A comprehensive survey, *J. Environmental Management*, 90, 2287-2312, 2009.

Mujeebu, M. A.: Combustion in porous media for porous burner application, in *Convective Heat Transfer in Porous Media*, Mahmoudi, Y., Hooman, K., and Vafai, K. (eds.), Taylor and Francis-CRC Press, 2020.

Tien, C. L. and Drolen, B. L.: Thermal radiation in particulate media with dependent and independent scattering, in *Annual Review of Numerical Fluid Mechanics and Heat Transfer*, vol. 1, pp. 1–32, Hemisphere, Washington, DC, 1987.

Xu, H. J., Xing, Z. B., Wang, F. Q., and Cheng, Z. M.: Review on heat conduction, heat convection, thermal radiation and phase change heat transfer of nanofluids in porous media: Fundamentals and applications, *Chem. Engng. Sci* 195, 462-483, 2019.

M.5 GLOBAL WARMING

Crutzen, P. J.: Albedo enhancement by stratospheric sulfur injections: A contribution to resolve a policy dilemma? *Clim. Change.* 77, 211–219, 2006.

Dombrovsky, L. A. and Kokhanovsky, A. A.: The influence of pollution on solar heating and melting of a snowpack, *JQSRT* 233, 42-51, Aug. 2019.

Maslowski, W., Kinney, J. C., Higgens, M., and Roberts, A.: The future of Arctic sea ice, *Ann. Rev. Earth Planet. Sci*., 40, 625–654, 2012.

Ocean Studies Board. *Climate intervention: Reflecting sunlight to cool the earth*, National Research Council, National Academies Press, 260 pp., Washington DC, 2015.

World Meteorological Organization Statement on the State of the Global Climate in 2019, WMO-No. 1248, 2020.

M.6 AVAILABLE COMPUTER CODES

Alberti, M., Weber, R., and Mancini, M.: Gray gas emissivities for H_2O-CO_2-CO-N_2 mixtures, *JQSRT*, 219, 274-291, Nov. 2018. EXCEL spreadsheet for emissivity calculation under *Supplemental Materials* at *DOI: 10.1016/j.jqsrt.2018.08.008.*

Emery, A. F.: VIEW—A radiation view factor program with interactive graphics for geometry definition (Version 5.5.3), 1986, available at https://bit.ly/2kOYJjO (accessed 9/23/2019).

Flatau, P. J.: SCATTERLIB (atol.ucsd.edu/scatlib/scatterlib.htm, accessed May 26, 2015), 2009.

Kneizys, F. X., Shettle, E. P., Gallery, W. O., Chetwynd, J. H., Jr., Abreu, L. W., Selby, J. E. A., Fenn, R. W., and McClatchey, R. A.: Atmospheric transmittance/radiance: Computer code LOWTRAN 5, Paper 697, *Optical Physics Div., Air Force Geophysics Lab.*, Hanscom AFB, 21 Feb. 1980.

Laux, C.O., Radiation and nonequilibrium collisional-radiative models, von Karman Institute Lecture Series 2002-07, D. Fletcher, J.-M. Charbonnier, G.S.R. Sarma, and T. Magin (eds.), *Physico-Chemical Modeling of High Enthalpy and Plasma Flows*, Von Karman Institute for Fluid Dynamics, Rhode-Saint-Genèse, Belgium, 2002. SPECAIR program available at www.specair-radiation.net/.)

McDonald, J., Golden, A., and Jennings, G.: OpenDDA: A high-performance computational framework for the discrete dipole approximation, *Int. J. High Perf. Comp. Appl.* 23(1), 42–46, 2009. www.science.uva.nl/research/scs/Software/adda/.

Prahl, S.: Mie scattering calculator, omlc.ogi.edu/calc/mie_calc.html (accessed April 16, 2015). Oregon Medical Laser Center, Portland, OR, 2009.

Sandia National Laboratories: International workshop - measurements and computations of turbulent nonpremixed flames - CH4/H2/N2 jet flames, 2018. www.sandia.gov/TNF/DataArch/DLRflames.html

Shapiro, A. B.: FACET—A computer view factor computer code for axisymmetric, 2d planar, and 3d geometries with shadowing, UCID-19887, University of California, Lawrence Livermore National Laboratory, Livermore, CA, August 1983 (LLNL Methods Development Group, www.oecd-nea.org/tools/abstract/detail/nesc9578/, accessed 1/19/2019). (Check)

Wriedt, T.: Electromagnetic scattering programswww.t-matrix.de/, accessed April 27, 2015, 2010.

M.7 HISTORICAL REFERENCES

M. REFERENCES TO REVIEWS AND HISTORICAL PAPERS

Agassi, J.: The Kirchhoff-Planck Radiation Law, *Science*, 156, pp. 30-37, April 1967.

Ambarzumian, V. A.: Diffusion of Light by Planetary Atmospheres, *Astron. Zh*., vol. 19, pp. 30–41, 1942.

Aschkinass, E.: Heat Radiation of Metals, *Ann. Phys*., 17, no. 5, pp. 960–976, 1905.

Barr, E. S.: Historical Survey of the Early Development of the Infrared Spectral Region, *Am. J. Phys*., 28, no. 1, pp. 42–54, 1960.

Beer, A.: Bestimmung der Absorption des rothen Lichts in farbigen Flüssigkeiten. (Determination of the absorption of red light in colored liquids). *Annalen der Physik und Chemie (in German).* 86(5): 78–88, 1852.

Boltzmann, L.: Ableitung des Stefan'schen Gesetzes, betreffend die Abhängigkeit der Wärmestrahlung von der Temperatur aus der electromagnetischen Lichttheorie, *Ann. Phys*., ser. 2, vol. 22, pp. 291–294, 1884.

Bouguer, Pierre: *Essai d'Optique, sur la gradation de la lumiere*, Claude Jombert, Paris, 16–22, 1729.

Chandrasekhar, S.: *Radiative Transfer*, Dover, New York, 1960.

Charle, M.: *Les Manuscripts de Léonard de Vinci, Manuscripts C, E, et K de la Bibliothèque de l'Institute Publiés en Facsimilés Phototypiques*, Ravisson-Mollien, Paris. 1888. (Referenced in Knowles Middleton, W. E.: Note on the Invention of Photometry, *Am. J. Phys*., vol. 31, no. 3, pp. 177–181, 1963.)

Crepeau, J.: A Brief History of the T^4 Law, *Proc. HT 2009; 2009 Summer Heat Transfer Conf*., Paper HT2009-88060, San Francisco, July 2009.

d'Aguillon, F., S. J.: Opticorum Libri Sex, Antwerp, 1613. (Referenced in Knowles Middleton, W. E.: Note on the Invention of Photometry, *Am. J. Phys*., 31(3), 177–181, 1963.

Davisson, C, and Weeks, J. R., Jr.: The Relation between the Total Thermal Emissive Power of a Metal and Its Electrical Resistivity, *JOSA*, 8(5), 581–605, 1924.

Draper, J. W.: On the Production of Light by Heat, *Phil. Mag*., ser. 3, 30, 345–360, 1847.

Drude, P.: Zur Elektronentheorie der Metalle, *Annalen der Physik*, 306(3): 566–613., 1900.

Drude, P.: Zur Elektronentheorie der Metalle; II Teil: Galvanomagnetische und Thermomagnetische Effecte, *Annalen der Physik*, 308(11): *369-402*, 1900b.

Eckert, E.: Das Strahlungsverhaltnis von Flachen mit Einbuchtungen und von zylindrischen Bohrungen, *Arch. Waermewirtsch*., vol. 16(5), 135–138, 1935.

Eckert, E.R.G.: Messung der Gesamtstrahlung von Wasserdampf und Kohlnesaure in Mischung mit nichtstrahlung Gasen bei temperaturen bis 1300ºC, *VDI Forshungshefte*, 387, 1-20, 1937.

Eddington, A. S.: *The Internal Constitution of the Stars*, Cambridge University Press, 1926.

Einstein, A.: Über einen die Erzeugung und Verwandlung des Lichtes betreffenden heuristischen Gesichtspunkt, *Annalen der Physik.* 17(6), 132–148, 1905.

Fabry, C. and Perot, A.: Theorie et applications d'une nouvelle methode de spectroscopie interferentielle, *Ann. Chim. Phys.* 16(7), *1899.*

Frisad, J. R. and Kragh, H.: On Ludvig Lorenz and his 1890 treatise on light scattering by spheres, *Eur. Phys. J.- H,* 44(2), 137–160, Aug. 2019.

Gardon, R.: A Review of Radiant Heat Transfer in Glass, *J. Am. Ceram. Soc.*, 44(7), pp. 305–312, 1961.

Hadamard, Jacques: Sur les problèmes aux dérivées partielles et leur signification physique, *Princeton University Bulletin*. 49–52, 1902.

Hagen, E. and Rubens, H.: Metallic reflection, *Ann. Phys.*, 1(2), 352–375, 1900. (See also E. Hagen and H. Rubens: Emissivity and electrical conductivity of alloys, *Deutsch. Phys. Ges. Verhandl*., 6(4), 128–136, 1904.)

Hale, G. E.: Sir Arthur Schuster, *Astrophysical J.*, 81(2), March 1935.

Heaviside, O.: On the electromagnetic effects due to the motion of electrification through a dielectric, *Phil. Mag. S.5* 27: 324, 1889.

Heaviside, O.: On the forces, stresses, and fluxes of energy in the electromagnetic field, *Phil. Trans. Royal Soc. A* 183:423–80, 1892.

Herschel, William; Investigation of the Powers of the prismatic Colours to heat and illuminate Objects; with Remarks, that prove the different Refrangibility of Radiant Heat. To which is added, an Inquiry into the Method of viewing the Sun advantageously, with Telescopes of large Apertures and high magnifying Powers, *Trans. Roy. Soc. (London)*, 90, Pt. II, pp. 255-326 plus 16 plates, 1800.

Horvath, H.: Gustav Mie and the Scattering and Absorption of Light by Particles: Historic Development and Basics, *JQSRT*, 110, no. 11, pp. 787–799, July 2009.

Horvath, H., (ed.): Light Scattering: Mie and More–Commemorating 100 Years of Mie's 1908 Publication, *JQSRT Special Issue*, 110, no. 11, 2009b.

Huggins, W. and Miller, W. A., Notes on the lines in the spectra of some of the fixed stars, *Proc. Royal Society of London*, 12, 444-445, 1862 – 1863.

Jeans, Sir J.: On the Partition of Energy between Matter and the Ether, *Phil. Mag*., vol. 10, pp. 91–97, 1905.

Kirchhoff, G.: Appendix, Über das Verhältniß zwischen dem Emissionsvermögen und dem Absorptionsvermögen der Körper für Wärme und Licht, in *Untersuchungen über das Sonnenspectrum und die Spectren der chemischen Elemente*, Ferd. Dümmler's Verlagsbuchhandlung, Berlin, pages 22-39, 1862.

Lambert, J. H.: *Photometrie: Photometria, sive de mensura et gradibus luminus, colorum et umbrae*, (1760) republished by Verlag von Wilhelm Engelmann, Leipzig, 1892.

Langley, S. P.: Experimental Determination of Wave-Lengths in the Invisible Prismatic Spectrum, *Mem. Natl. Acad. Sci*., 2, pp. 147–162, 1883.

Lebedev, P.: Untersuchungen über die Druckkräfte des Lichtes, *Annalen der Physik*, 4th Series, 6, 433-458, 1901.

Lewis, H. R.: Einstein's Derivation of Planck's Radiation Law, *Am. J. Phys*., 41(1), pp. 38–14, 1973.

M. REFERENCES TO REVIEWS AND HISTORICAL PAPERS

Lilienfeld, P.: Gustav Mie: The Person, *Appl. Opt.*, 30, no. 33, pp. 4696–4698, 1991.

Lorenz, L., Über die Identität der Schwingungen des Lichtes mit den Elektrischen Strömen. *Ann. der Physik und Chemie*, 131, 243-263, 1867a.

Lorenz, L., On the identity of the vibrations of light with electrical currents. *Phil. Mag*., 34, 287-301, 1867b.

Lorenz, L.: Lysbevaegelsen i og uden for en af plane Lysbolger belyst Kugle, *Det Kongelige Danske Videnskabernes Selskabs Skrifter*, 6. Raekke, 6. Bind, 1890, 1, pp. 1–62. (see Classical Papers at www.t-matrix.de/)

Lorenz, L: Sur la lumière réfléchie et réfractée par une sphère (surface) transparente, in Oeuvres scientifiques de L. Lorenz." revues et annotées par H. Valentiner. Tome Premier, Libraire Lehmann & Stage, Copenhague, 1898, pp. 403–529. (see Classical Papers at www.t-matrix.de/)

Lummer, O. and Pringsheim, E., *Verhandl. Der Deutschen Physikal. Gesells*., 1, 23 and 215, 1899.

Lummer, O. and Pringsheim, E., *Verhandl. Der Deutschen Physikal. Gesells.*, 2, 163, 1900.

Maxwell, J. C.: A Dynamical Theory of the Electromagnetic Field, in W. D. Niven (ed.), *The Scientific Papers of James Clerk Maxwell*, vol. 1, Cambridge University Press, London, 1890.

McRea, W.H.: Obituary, Edward Arthur Milne, *The Observatory*, 70, 225-232, Dec. 1950.

Metropolis, N., and Ulam, S.: The Monte Carlo Method, *J. Am. Stat. Assoc*., 44, no. 247, pp. 335–341, 1949.

Mie, G.: Beiträge zur Optik trüber Medien, speziell kolloidaler Metallösungen, *Ann. Phys.*, 330, 377–445, 1908.

Mie, G.: Optics of Turbid Media, *Ann. Phys*., 25(3), 377–445, 1908.

Milne, F. A.: Thermodynamics of the Stars, in *Handbuch der Astrophysik*, 3, pp. 65–255, Springer-Verlag, OHG, Berlin, 1930.

Mott, N. F., and Zener, C.: The Optical Properties of Metals, *Cambridge Philos. Soc. Proc*., pt. 2, vol. 30, pp. 249–270, 1934.

Nobili, L. and Melloni, M.: New Experiments in Caloric, performed by means of the Thermomultiplier, *Am. J. Sci. and Arts*, 1, pp. 185-180, 1833. (Trans. from *Annales de Chim. et de Phys.*, Oct. 1831.)

Nusselt, W.: Graphische Bestimmung des Winkelverhaltnisses bei der Wärmestrahlung, *VDI Z*., vol. 72, p. 673, 1928.

Park, D. and Epstein, H.T.: On the Planck Radiation Formula, *Am. J. Phys*., vol. 17, pp. 301-302, 1949.

Planck, M.: Distribution of Energy in the Spectrum, *Ann. Phys*., vol. 4, no. 3, pp. 553–563, 1901.

Planck, M.: *The Origin and Development of the Quantum Theory*, 1918 Nobel Prize Address delivered June, 2, 1920, Oxford at the Clarendon Press, 1922.

Planck, M.: *The Theory of Heat Radiation*, 2nd. ed. (trans. by M. Masius), Dover, New York, 1959.

Poljak, G.: Analysis of the Heat Exchange by Radiation Between Gray Surfaces by the Saldo Method, *Tech. Phys. USSR*, 1, no. 5/6, pp. 555-590, 1935.

Rayleigh, Lord: On Scattering of Light by Small Particles, *Philos. Mag*., 41, pp. 447–454, 1871.

Rayleigh, Lord: The Law of Complete Radiation, *Phil. Mag*., 49, pp. 539–540, 1900.

Rayleigh, Lord: The dynamical theory of gases and of radiation, *Nature*, 72, 54-55, 1905a.

Rayleigh, Lord: The constanty of radiation as calculated from molecular data, *Nature*, 72, 243-244, 1905b.

Rosseland, S.: *Theoretical Astrophysics: Atomic Theory and the Analysis of Stellar Atmospheres and Envelopes*, Clarendon Press, Oxford, 1936.

Rytov, S. M.: *A Theory of Electric Fluctuations and Thermal Radiation*, USSR Academy of Sciences, Moscow, 1953, republished Air Force Cambridge Research Center, Bedford, MA, 1959.

Schuster, A.: Radiation through a Foggy Atmosphere, *Astrophys. J*., 21, pp. 1–22, 1905.

Schwarzschild, K.: Equilibrium of the Sun's Atmosphere, *Ges. Wiss. Gottingen Nachr., Math-Phys. Klasse*, vol. 1, pp. 41–53, 1906.

Saunders, O. A.: Notes on Some Radiation Heat Transfer Formulae, *Proc. Phys. Soc. London*, 41, pp. 569–575, 1929.

Schmidt, E., and Eckert, E. R. G.: Über die Richtungsverteilung der Wärmestrahlung von Oberflächen, *Forsch. Geb. Ingenieurwes*., 6(4), pp. 175–183, 1935.

Stark, J.: Der Dopplereffekt bei den kanalstrahlen und die spektra der positiven atomionen, *Physikalische Zeitschrift*, 6, 892–897, 1905.

Stefan, J.: Über die beziehung zwischen der wärmestrahlung und der temperatur, *Sitzber. Akad. Wiss. Wien*, 79(2), 391–428, 1879.

Stokes, G. G.: On the Composition and Resolution of Streams of Polarized Light from Different Sources, *Trans. Camb. Phil. Soc.*, vol. 9, pp. 399–424, 1852. (Reprinted in *Mathematical and Physical Papers*, vol. 3, Cambridge University Press, pp. 233–258, London, 1901.)

Tikhonov, A. N.: On the stability of inverse problems, *Dokl. Akad. Nauk SSSR*, 39(5), 195–198, 1943.

Tikhonov, A. N.: Solution of incorrectly formulated problems and the regularization method, *Soviet Math. Dokl*., 4, 1035–1038, 1963. [Engl. trans. *Dokl. Akad. Nauk. SSSR*, 151, 501–504, 1963.]

Townsend, A. A.: The Effects of Radiative Transfer on Turbulent Flow of a Stratified Fluid, *J. Fluid Mech.* vol. 4, no. 4, pp. 361-375, Aug. 1958.

Tyndall, James: *Heat Considered as a Mode of Motion being a Course of Twelve Lectures*, D. Appleton and Company, New York,1865.

Wien, W.: Temperatur und Entropie der Strahlung, *Ann. Phys*., ser. 2, vol. 52, pp. 132–165, 1894.

Wien, W.: Über die Energievertheilung im Emissionsspectrum eines schwarzen Körpers, *Ann. Phys*., ser. 3, vol. 58, pp. 662–669, 1896.

Zerefos, C. S., Tetsis, P., Kazantzidis, A., Amiridis, V., Zerefos, S. C., Luterbacher, J., Eleftheratos, K., Gerasopoulos, E., Kazadzis, S., and Papayannis, A.: Further evidence of important environmental information content in red-to-green ratios as depicted in paintings by great masters, *Atmos. Chem. Phys*.14, 2987-3015, 2014.

N: A HISTORY OF THERMAL RADIATION AND SHORT BIOGRAPHIES

N.1 HISTORY OF THERMAL RADIATION

The historical development of the blackbody relations differs from the sequence in which they are presented *Thermal Radiation Heat Transfer*. The derivation of the approximate spectral distributions of Wien and of Rayleigh and Jeans, the Stefan–Boltzmann law, and Wien's displacement law are all presented as logical consequences of the fundamental spectral distribution of intensity derived by Max Planck. However, these relations were formulated *prior* to publication of Planck's work (1901) and were originally derived through complex thermodynamic arguments (see the Timeline following the biographies below.)

Joseph Stefan (1879) proposed, after study of some experimental results, that emissive power was related to the fourth power of the absolute temperature of a radiating body. His student, Ludwig Eduard Boltzmann (1884), was able to derive the same relation by analyzing a Carnot cycle in which radiation pressure was assumed to act as the pressure of the working fluid.

Wilhelm Carl Werner Otto Fritz Franz (Willy) Wien (1894, 1896) derived the displacement law by consideration of a piston moving within a mirrored cylinder. He found that the spectral energy density in an isothermal enclosure and the spectral emissive power of a blackbody are both directly proportional to the fifth power of the absolute temperature when "corresponding wavelengths" are chosen. He later derived his spectral distribution of intensity through thermodynamic argument plus assumptions concerning the absorption and emission processes (1896). Lord Rayleigh (1900) and Sir James Jeans (1905) based their spectral distribution on the assumption that the classical idea of equipartitioning of energy was valid.

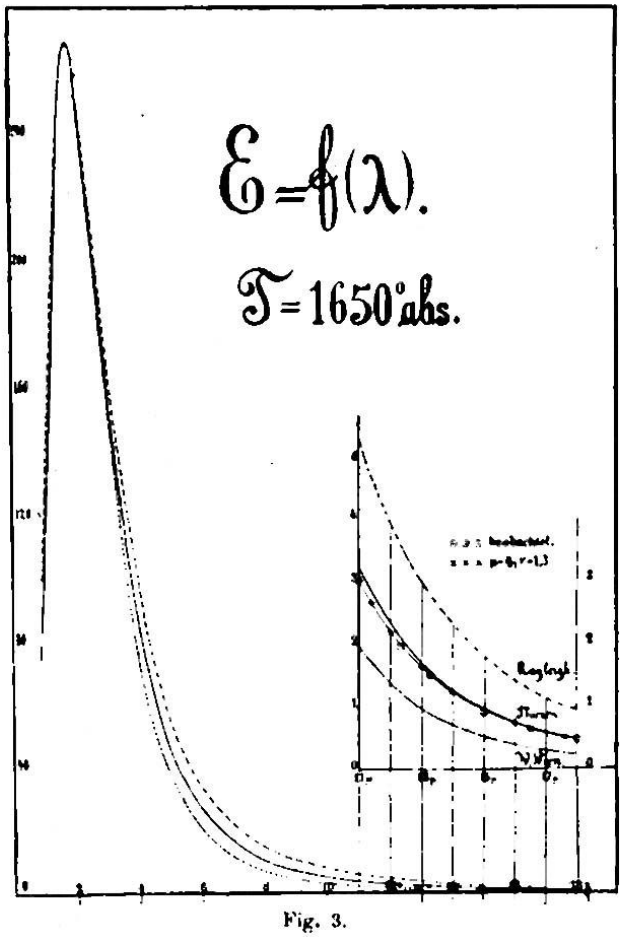

Fig. 3.

Careful measurements of the blackbody spectral distribution by Otto Lummer and Ernst Pringsheim (1900) (and some theoretical considerations) indicated that Wien's expression for the spectral distribution was invalid at high temperatures and/or large wavelengths. This led Planck to an investigation of harmonic oscillators that were assumed to be the emitters and absorbers of radiant energy. The figure from Lummer and Pringsheim shows, at the lower right, the disagreement between the Rayleigh, Wien, and experimental data at large λT values. Various further assumptions about the average energy of the oscillators led Planck to derive both the Wien and Rayleigh–Jeans distributions. Planck finally found an empirical equation that fit the measured energy distributions over the entire spectrum. In determining what modifications to the theory would allow derivation of this empirical equation, he was led to the assumptions that form the basis of quantum theory. His equation leads directly to all the results derived previously by Wien, Stefan, Boltzmann, Rayleigh, and Jeans.

Gustav Mie used the EM theory to predict the scattering coefficient and phase function for radiation interacting with small spherical particles (1908a, b), and a historical overview of his contributions is in Horvath (2009a).

Short biographies of the major historical contributors to the theory and practice of thermal radiation energy transfer abridged from various sources are given below, along with a timeline that sets the sequence of their accomplishments For an interesting and informative comprehensive review of the history of the field of thermal radiation, the article by Barr (1960) is recommended. Howell (2002) gives a review of the development of radiation energy transfer. Lewis (1973) and Crepeau (2009) discuss the derivation of Planck law, and Stewart and Johnson (2016) give a historical overview of Planck's Law and the computational methods historically invoked in computing it in various forms.

REFERENCES

Barr, E. S.: Historical survey of the early development of the infrared spectral region, *Am. J. Phys*., 28(1), 42–54, 1960.

Boltzmann, L.: Ableitung des Stefan'schen Gesetzes, betreffend die Abhängigkeit der Wärmestrahlung von der Temperatur aus der electromagnetischen Lichttheorie, *Ann. Phys*., *Ser. 2*, 22, 291–294, 1884.

Crepeau, J.: A brief history of the T^4 law, Paper HT2009-88060, *Proceedings of the HT 2009; 2009 Summer Heat Transfer Conference*, San Francisco, CA, July 2009.

Horvath, H. (ed.): Light scattering: Mie and more–commemorating 100 years of Mie's 1908 publication, *JQSRT*, 110(11), 783–786, 2009a.

Horvath, H.: Gustav Mie and the scattering and absorption of light by particles: Historic development and basics, *JQSRT*, 110(11), 787–799, July 2009b.

Howell, J. R.: The development of engineering radiative heat transfer, *IMECE2002-33131*, 73-78, IMECE, New Orleans, Nov. 2002.

Jeans, Sir. J.: On the partition of energy between matter and the ether, *Phil. Mag*., 10, 91–97, 1905.

Lewis, H. R.: Einstein's derivation of Planck's radiation law, *Am. J. Phys*., 41(1), 38–14, 1973.

Lummer, O. and Pringsheim, E.: Über die Strahlung des Schwarzen Körpers für Lange Wellen, *Verhandlungen der Deutschen Physikalischen Gesellschaft.* **2**, 163-180, 1900.

Mie, G.: Beiträge zur Optik trüber Medien, speziell kolloidaler Metallösungen, *Ann. Phys.*, 330, 377–445, 1908a.

Mie, G.: Optics of turbid media, *Ann. Phys*., 25(3), 377–445, 1908b.

Planck, M.: Distribution of energy in the spectrum, *Ann. Phys*., 4(3), 553–563, 1901.

Rayleigh, Lord: The law of complete radiation, *Phil. Mag*., 49, 539–540, 1900.

Stefan, J.: Über die beziehung zwischen der wärmestrahlung und der temperatur, *Sitzber. Akad. Wiss. Wien*, 79(2), 391–428, 1879.

Stewart, S. M. and Johnson, R. B.: *Blackbody Radiation: A History of Thermal Radiation Computational Aids and Numerical Methods*, CRC Press, Boca Raton, 2016.

Wien, W.: Temperatur und Entropie der Strahlung, *Ann. Phys*., *Ser. 2*, 52, 132–165, 1894.

Wien, W.: Über die Energievertheilung im Emissionsspectrum eines schwarzen Körpers, *Ann. Phys*., *Ser. 3*, 58, 662–669, 1896.

M.2: BIOGRAPHIES OF FIGURES IN THE DEVELOPMENT OF RADIATION THEORY

August Beer (1825-1863) was a German physicist. In 1852, he published a paper on the absorption of red light in colored aqueous solutions of various salts. He showed that the intensity of light transmitted through a solution at a given wavelength decays exponentially with increasing path length and the solute concentration.

Ludwig Eduard Boltzmann (1844-1906) made seminal contributions to the kinetic theory of gases and on heat transfer by radiation, but is probably best known for his invention, independently of J. Willard Gibbs, of statistical mechanics and the formulation of entropy on a microscopic basis. He derived Stefan's fourth power law for radiation emission by considering a heat engine with light as the working fluid. He committed suicide in 1906, probably because of depression (he was subject to what we now call bipolar disorder) brought on by broad criticism of his work. Boltzmann's epitaph in the Central Cemetery in Vienna reads

Ludwig Boltzmann
1844-1906
$S = k \ln W$

Pierre Bouguer (1698-1758) first discovered the law in 1729 of exponential decay of light intensity through an absorbing medium (in his case, the atmosphere), now often called the Beer-Lambert Law. He was an accomplished naval architect (known as "the Father of Naval Architecture), beating out Euler for a prize by the French Academy of Sciences for a paper on the masting of ships. Craters on the Moon and Mars are named after him.

Robert Wilhelm Eberhard Bunsen (1811-1899) investigated spectra emitted by heated elements using a spectrometer designed with Gustav Kirchhoff. They discovered cesium and rubidium using the device. Bunsen developed gas-analytical methods and was a pioneer in photochemistry. With his laboratory assistant, Peter Desaga, he developed the Bunsen burner. John Tyndall was one of his graduate students.

Nicolas Leonard Sadi Carnot (1796-1832) was the son of Napoleon's Minister of War ("the Great Carnot"), and was educated as a military engineer. In 1824, he published his only paper, "Reflexions on the Motive Power of Fire, and on Machines Fitted to Develop that Fire," which outlined one form of the second law as well as a reasoned form of the first law. His analysis of the most efficient possible cycle efficiency and a cycle that has this efficiency carry his name. His analysis was based on caloric theory, although unpublished notes indicate that he had begun to doubt that theory. He died of cholera at age 36, having provided probably the single most important contribution to classical thermodynamics.

Anders Celsius (1701-1744), although primarily an astronomer, introduced a thermometer scale with 0 at the boiling point of water, and 100 at the freezing point. The scale was reversed after his death to provide the present Celsius scale (formerly called the centigrade scale). Celsius showed that the boiling point of water varied with atmospheric pressure, and introduced corrections to the temperature scale to account for this.

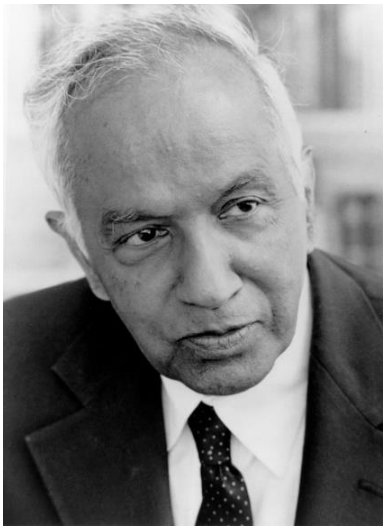

Subrahmanyan Chandrasekhar (1910-1995) won the Nobel Prize in 1938 for his work on the structure and evolution of stars, later showing star progression toward becoming a black hole. His uncle was Chandrasekhara Venkata Raman who won the 1930 Nobel Prize in Physics for his work on Raman scattering of photons. His book *Radiative Transfer* (1960) outlines the discrete ordinates method (DOM) now used extensively in thermal radiation transfer and introduces methods for treating scattering using Stoke's parameters.

Photo courtesy of University of Chicago Photographic Archive, [apf1-09456], Special Collections Research Center, University of Chicago Library.

Louis de Broglie (1892-1987) did not originally envisage a career in science. He entered the Sorbonne in Paris taking a course in history and graduated at 18 with an arts degree. However, he became interested in mathematics and physics and chose to study for a degree in theoretical physics.

De Broglie was awarded his undergraduate degree in 1913 but his career was put on hold by World War I. His doctoral thesis put forward his theory of electron waves, based on the work of Einstein and Planck. It proposed the theory for which he is best known, the particle-wave duality theory that matter has the properties of both particles and waves. The wave nature of the electron was experimentally confirmed in 1927.

His was awarded the Nobel Prize in 1929 and continued to work on extensions of wave mechanics. He questioned whether the statistical nature of quantum physics reflects an ignorance of the underlying theory or whether statistics is all that can be known.

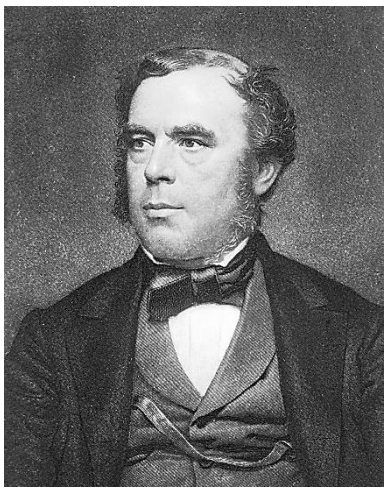

John William Draper (1811-1882) was an English-born American scientist. In 1847 he observed the *Draper point* of 798 K at which the emission from a heated object becomes visible to the human eye. In his 1847 paper he presented data on the emission vs. temperature from a heated object (replotted here on an absolute scale) but failed to recognize the fourth-power dependence, because an absolute temperature scale was not yet in use.

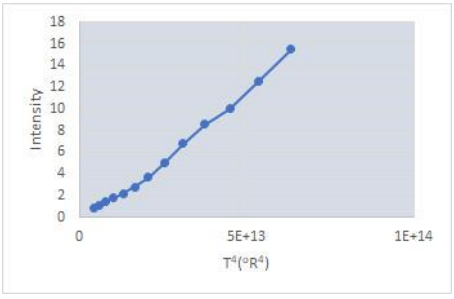

He is credited with taking the one of the first photographic portraits in 1839. An image of his sister from 1840 is considered the oldest surviving portrait photo. He took the first detailed photograph of the moon in 1840.

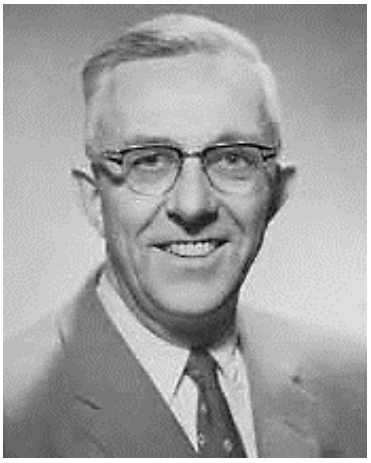

Ernst Rudolph George (ERG) Eckert (1904-2004) was born in Prague. After earning his Dr. Ing. in 1927, he moved to Danzig to work with Ernst Schmidt at the Engine Laboratory. He researched radiation from solids and gases, and published measurements of directional emissivity from various materials as well as directional reflectivity of blackbody radiation. He also developed optical methods for obtaining configuration factors. In 1937, he turned to measurement of the emissivity of CO_2-N_2 mixtures as well as water vapor at various temperatures and partial pressures. His later career was spent in investigating high-speed flows. He spent a long and productive career in Germany, Czechoslovakia, and the U.S. at NASA Lewis (now Glenn) Research Center and from 1951 at the University of Minnesota.

Albert Einstein (1879-1955) of course is best known for his theory of relativity and for promulgating the world's most famous equation, relating energy and mass through $E=mc^2$. His 1921 Nobel Prize in Physics, however, was "for his services to theoretical physics, and especially for his discovery of the law of the photoelectric effect." The latter effect, which experimentally showed the presence of quantum energy in incident radiation, was a major impetus to the acceptance of quantum theory and provided support for Planck's hypothesis of the existence of quantum energy states needed in his derivation of the blackbody distribution.

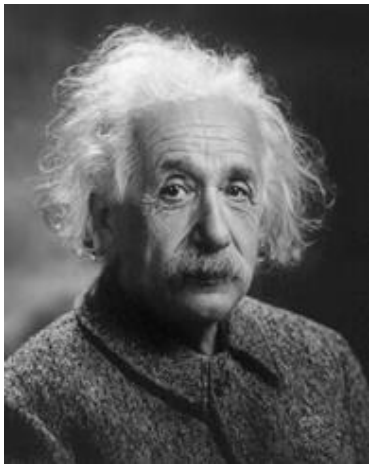

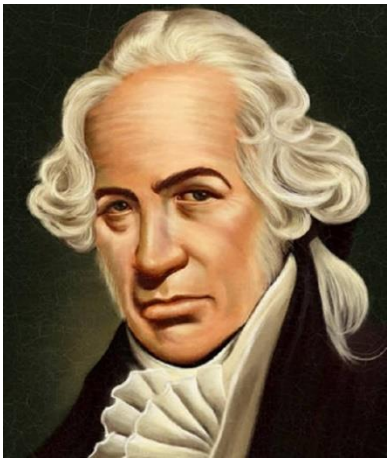

Gabriel Daniel Fahrenheit (1686-1736) developed both an alcohol and mercury thermometer, as well as the temperature scale that bears his name. He was the first to calibrate thermometers with a reproducible scale; previously, each thermometer had an arbitrary scale. His original scale for the alcohol thermometer used the zero point at the temperature of an equal mixture by weight of ice and salt, and 90 degrees as the temperature of the human body, resulting in 30 degrees for the freezing point of water. Later, the mercury thermometer allowed expansion of the scale to the boiling point of water at 212 degrees, and the rest of the scale was revised to 98.6 degrees for the body temperature and the freezing point of water to 32 degrees.

Maurice Paul Auguste Charles Fabry (1867-1945) received his doctorate from the University of Paris in 1892 for his work on interference fringes, which established him as an authority in the field of optics and spectroscopy. He explained the phenomenon of interference fringes and together with Alfred Pérot he invented the Fabry–Pérot interferometer in 1899, making possible the accurate measurement of wavelength and refractive index. In 1904, he was appointed Professor of Physics at the University of Marseille, where he spent 16 years. While studying the light spectra of the Sun and stars with the interferometer, Fabry and Henri Buisson demonstrated in 1913 that solar ultraviolet radiation is filtered out by an ozone layer in the upper atmosphere.

Joseph Thomas Gier (1910-1961) received his undergraduate degree in Mechanical Engineering at UC Berkeley in 1933, followed by a Master of Engineering degree in 1940. He was initially employed as a laboratory technician under Llewellyn Boelter. After serving as a lecturer and researcher, Gier was promoted to Associate Professor of Electrical Engineering at UC Berkeley in 1951, becoming the first tenured African-American professor in the University of California system. He formed a fruitful partnership with Robert V. Dunkle, a Mechanical Engineering professor in 1943. Together they developed instrumentation to characterize the radiative properties of surfaces and conceived of spectral-selectivity to improve the performance of solar collectors.

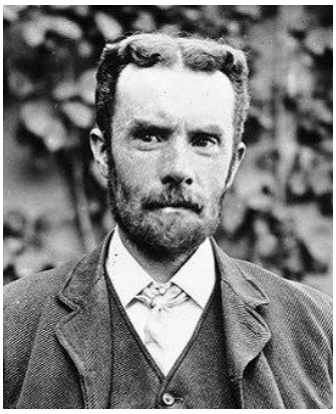

Oliver Heaviside (1850-1925) was a self-taught engineer/mathematician/physicist who invented methods for solving differential equations and made many contributions to vector calculus. In 1888/9, he reformulated Maxwell's twenty field equations into a more manageable and now generally used set of four equations in terms of four variables. Heaviside was often at odds with his employer and the scientific community but made important contributions to physics, astronomy, and mathematics.

William Herschel (1738-1822) was a German-born British astronomer. He constructed his first large telescope in 1774 and spent nine years carrying out sky surveys to investigate double stars. In March 1781 he discovered the planet Uranus.

He pioneered the use of astronomical spectrophotometry, measuring stellar spectral distributions. In 1800, he discovered the presence of infrared radiation in sunlight by passing it through a prism and holding a thermometer just beyond the red end of the visible spectrum. It showed a higher temperature than the visible spectrum, implying energy in then unknown infrared portion of the spectrum. He improved the measurement of the rotation period of Mars, and determined that the Martian polar caps vary seasonally,

Hoyt Clarke Hottel (1903-1998) was a Professor at MIT from 1928 until his death and became an Emeritus Professor in 1968. He developed gas emissivity charts for the important combustion gases, the crossed-string method for determining configuration factors in 2D geometries, and in 1927 papers established the engineering basis for treating radiation in furnaces, including the zone method. Hottel also contributed to the fields of combustion and solar energy.

Margaret Lindsay Huggins (1848-1915) was a pioneer in measuring stellar spectra. She, along with her husband William Huggins, was the first to show that the stars were indeed suns, based on the similarity of their emission spectra with that of the Sun (especially spectral lines of magnesium and calcium). Their instrumentation was based on a spectroscope model proposed by Bunsen and Kirchhoff. Observations of Sirius showed a slight Doppler shift in the measured spectra, which indicated that it was moving away from the Earth. This eventually led to the discovery of the expanding universe.

Christiaan Huygens (1629-1695) was born and died at The Hague. His father had studied natural philosophy and was a diplomat. Christiaan gained access through him to the top scientific circles of the times. He studied law and mathematics at the University of Leiden and the College of Orange at Breda.

In 1654 his attention was directed to the improvement of the telescope. In 1655, using one of his own lenses, he detected the first moon of Saturn. His astronomical observations required some exact means of measuring time, and this led him in 1656 to invent the pendulum clock. His reputation was now so great that in 1665, Louis XIV offered him a pension if he would live in Paris, which became his place of residence. In 1670 he had a serious illness which resulted in leaving Paris for Holland. By 1671 he returned to Paris. In 1672 Louis XIV invaded the Low Countries and Huygens found himself in the position of being in an important position in Paris at a time France was at war with his own country. Scientists of this era felt themselves above political wars and Huygens, with much support from his friends, continued his work.

The first watch regulated by a balance spring was made under Huygens's directions, and presented by him to Louis XIV. He returned to Holland in 1681 and devoted himself to the construction of lenses of enormous focal length, and he discovered the achromatic telescope eye piece which is known by his name.

In 1689 he came from Holland to England in order to make the acquaintance of Newton, whose *Principia* had been published in 1687. Huygens fully recognized the merits of the work but believed any theory incomplete which did not explain gravitation by mechanical means and so didn't accept Newton's theory of universal gravitation which "appears to me absurd." On his return in 1690 Huygens published his treatise on light in which the wave theory was expounded and explained. The immense reputation of Newton led to disbelief in any theory which he rejected, and to the general adoption of Newton's corpuscular theory over wave ideas.

In the final years of his life Huygens composed one of the earliest discussions of extraterrestrial life, published after his death as the *Cosmotheoros* (1698).

James Hopwood Jeans (1877-1946) was educated in London. Initially interested in the classics, he soon turned towards mathematics.

Jeans went to Trinity College Cambridge in 1896 on a mathematical scholarship. As an undergrad he gained experience in experimental physics in the Cavendish Laboratory during 1899-1900. During recovery from tuberculosis in 1902 and 1903 he worked on his first major text *The Dynamical Theory of Gases*. Planck had announced in 1900 his formula on black-body radiation, but Jeans was strongly opposed to Planck's results.

He held a series of positions between 1900 and 1906, and during this period he published his second major text *Theoretical Mechanics* (1906). He published *The Mathematical Theory of Electricity and Magnetism* in 1908 while in the United States. In 1909 he returned to England and held the post of Lecturer in Applied Mathematics at Cambridge until he retired in 1912. Jeans continued work and wrote *Radiation and Quantum Theory* in 1914. In this work he showed that he had come to accept Planck's black-body formula. He died in September 1946.

Gustav Robert Kirchhoff (1824 -1887) had a broad influence on physics and engineering. He proposed in 1859 and provided a proof in 1861 that, in simple terms, "For an arbitrary body emitting and absorbing thermal radiation in thermodynamic equilibrium, the emissivity is equal to the absorptivity." This was shown to apply for spectral, directional, and total properties. He first described the ideal radiation emitter in 1862 and called it the *schwarzer körper* (blackbody) because, as the perfect emitter, it must also be the perfect absorber and thus a zero reflector that would appear black to the eye.

He, along with Robert Bunsen used a prism to analyze the spectrum emitted by heated samples. Applying this new research tool, they discovered two new elements, cesium (1860) and rubidium (1861). He also promulgated the laws of electrical circuit analysis.

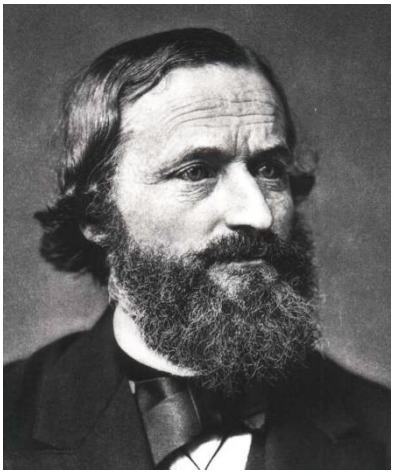

Johann Heinrich Lambert (1728-1777) was a self-taught mathematician, astronomer, logician, and philosopher. Aside from his work in radiation, he offered the first proof that π was an irrational number. In 1758, he published his first book, describing the exponential decay of light, followed in 1760 by his more complete book *Photometrie* that describes the exponential decay as well as the cosine dependence of the emission from a diffuse surface.

Pyotr Nikolaevich Lebedev (1866-1912) was the first to measure radiation pressure on a solid body (1899) at Moscow State University which he published in 1901. The measurements of the tiny force (Solar radiation exerts about 9 μPa at the Earth's orbit) were fairly inaccurate (off by about 20 percent) but provided the first experimental confirmation of Maxwell's theory of electromagnetism. He also performed important experiments on millimeter-wave radiation, He created the first school of science in Russia, now part of the Russian Academy of Science. A crater on the far side of the moon is named for him.

Gilbert Newton Lewis (1875- 1946) was a precocious child who learned to read at age three. At age 13 he entered the prep school of the University of Nebraska and continued to the University. After his second year, he transferred to Harvard, where he concentrated in chemistry, getting his B.A. in 1896 and Ph.D. in 1899.

After earning his Ph.D., he studied under Wilhelm Ostwald at Leipzig and Nernst at Göttingen. In 1905 MIT appointed him to the faculty. He became assistant professor in 1907, associate professor on 1908, and full professor in 1911. He left MIT to become dean of the College of Chemistry at UC Berkeley in 1912.

In 1908 he published the first of several papers on relativity, in which he derived the mass-energy relationship in a different way from Einstein's. In 1913, he was elected to the National Academy of Sciences, but in 1934 he resigned in a dispute over internal politics. In 1926, he coined the term "photon" for the smallest unit of radiant energy. He died at 70 of a heart attack while working in his laboratory.

Ludvig Valentin Lorenz (1829-1891) was a Danish chemical engineer who became interested in physics. Because he published in Danish, his work went unrecognized for many years. He published the relation between the density of a pure transparent material and light refraction in 1869. He also derived the correct velocity of light from electromagnetic theory. In 1890 he preceded Gustav Mie in proposing a theory of light scattering from spherical particles, sometimes now called the Lorenz-Mie theory.

Otto Richard Lummer (1860-1925) (left) and **Ernst Pringsheim (1859-1917)** (right). Lummer received the Ph.D. under Helmholtz in 1882 and joined the University of Berlin as lecturer in physics in 1886. He became professor in 1896 and in 1905 was appointed full professor of theoretical physics at the University of Breslau, where his close collaborator Ernst Pringsheim had preceded him by six months. In 1898, Lummer and Ferdinand Kurlbaum had published an account of their cavity radiation source (*hohlraum*), used largely unchanged for radiation measurements to the present. It was a hole in the wall of a platinum box, divided by diaphragms, with its interior blackened.

Pringsheim's doctoral dissertation of 1882 determined the direction of his research- heat and light radiation. Despite his appointment in theoretical physics at Breslau, Pringsheim's scientific production was largely experimental. At Berlin it was characterized first by a period of research done alone and then in cooperation with Lummer after 1896. He developed the radiometer into a useful instrument for measuring infrared radiation.

In 1896, Lummer and Pringsheim turned to investigations of thermal radiation. Continuing Wien's work, Pringsheim assisted Lummer in implementing Kirchhoff's concept of the blackbody They verified the Stefan-Boltzmann law for the temperature dependence of total radiated energy. They then measured the spectral distribution of the radiation energy with the aid of a hohlraum.

In September 1900 they published a paper stating the "invalidity of the Wien-Planck spectral equation." Such negative statements were the main stimuli for Planck to seek a new radiation expression.

James Clerk Maxwell (1831-1879), along with his many extremely important contributions in electromagnetic theory and other fields of science, formulated the kinetic theory of gases. He is often considered the most influential physicist after Einstein and Newton.

He described the propagation of an electromagnetic wave using a system of 20 equations, and showed that the speed of electromagnetic wave propagation was equal to the speed of light, implying that light was itself an electromagnetic wave.

Working with Clausius, he used a statistical approach to find the velocity distribution in an assembly of gas molecules at a given temperature (later derived using the maximum entropy principle by Boltzmann, and now called the Maxwell-Boltzmann distribution). He also observed the relationships among thermodynamic properties embodied in Maxwell's Relations.

Gustav Adolf Feodor Wilhelm Ludwig Mie (1868-1957) was a professor of physics with a strong background in mathematics. He researched colloids at the University of Greifswald in North-Eastern Germany. One of his PhD students investigated the scattering and attenuation of light by gold colloids. Mie used his knowledge of the Maxwell equations and solutions of very similar problems in the literature to treat the theoretical problem of scattering and absorption of light by a small absorbing sphere. Since these calculations were done by hand, Mie had to limit his theoretical results to three terms in infinite expansions, and this limited treatment to particles smaller than 200 nm at visible wavelengths. Mie's paper was hardly noticed for the next 50 years. He developed the Mie system of units in 1910 with the basic units Volt, Ampere, Coulomb and Second (VACS-system).

Edward Arthur Milne (1896-1950) was an English astrophysicist who worked on radiation pressure and the generation of white dwarf stars. **Arthur Stanley Eddington (1882-1944),** also English, investigated the importance of nuclear reactions in stellar structure. The pair provided a second solution to the radiative transfer equation (after Schuster-Schwarzschild) based on a two-flux (rather than two intensity) model.

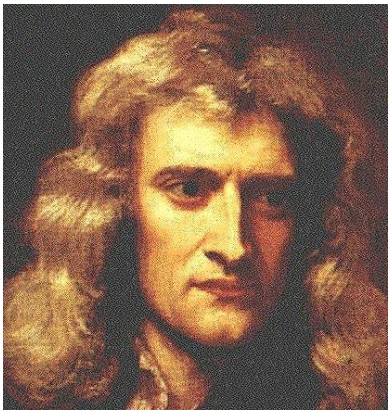

Isaac Newton (1643-1727) established the fundamentals of calculus, as well as his laws of mechanics and gravitation, and fundamental studies of the behavior of light. His laws of mechanics form a major part of the thermodynamic understanding of mechanical work in classical thermodynamics. He built the first practical reflecting telescope, and developed a theory of color based on obervations of the prismatic visible spectrum. Newton argued that the geometric nature of reflection and refraction of light could only be explained if light was made of particles, referred to as corpuscles, because waves do not tend to travel in straight lines, and refraction was caused by accelerating of the corpuscles due to attraction by the denser medium. He explained why the particles were partially refracted and partially reflected at a glass (prism) surface by noting that the particles had "fits of attraction and fits of repulsion." His corpuscular theory was gradually superseded by the wave theory of Huygens, which proved more successful in explaining many observed phenomena. Measurements of the speed of light in vacuum and then in media with nonunity refractive index showed that light speed is lower, not greater in such media, putting the final nail in the corpuscular theory. Modern arguments about wave-particle duality have reopened the wave-particle controversy.

Alexander Pope wrote the famous epitaph:

Nature and nature's laws lay hid in night;
God said "Let Newton be" and all was light.

Leopoldo Nobili (1784-1835) (left) and **Macedonio Melloni (1798-1854)** (right) developed a thermopile-based radiometer read by a galvanometer, and investigated radiation from various sources. They showed (1831) that different surfaces emitted differing amounts of radiation at the same temperature, and that the radiometer reacted similarly to light sources and heated surfaces.

Max Planck (1858-1947) laid the basis for quantum mechanics and was the forerunner of modern physics based on that theory. He studied with Helmholtz, and was impressed with the powerful conclusions that could be drawn from the Second Law. He originally developed his blackbody spectral distribution based on the observation that the denominator in classically derived distributions such as that of Wien needed to be slightly smaller to fit the experimental data. His attempts to explain the theoretical basis of his proposed spectral energy equation led him to hypothesize the existance of quantized energy levels, a concept at odds with all of classical physics and thermodynamics. He was forced to accept Boltzmann's interpretation of the Second Law as a statistical rather than an absolute law.

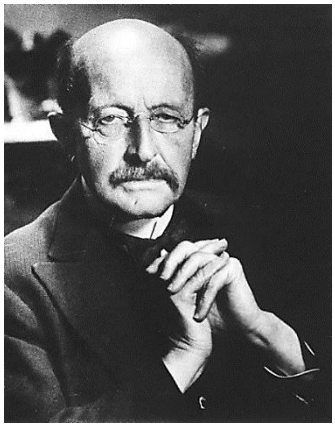

Pierre Prevost (1759-1839) was born in the Republic of Geneva, and skittered between the church, law, education, travel, and philosophy before concentrating on physical science after meeting Lagrange in Berlin. In 1791, he proposed that the radiation from a body is emitted regardless of the presence or absence of other bodies ("Prevost's Law"). He also commented on how radiative equilibrium between a body and its surroundings is obtained.

William John Macquorn Rankine (1820-1872) was born in Edinburgh, Scotland. He wrote practical treatises on thermodynamics, including the first systematic treatment of steam engine theory, and the exposition of what we now call the Rankine cycle. He proposed the Rankine absolute temperature scale in 1859. He was also a poet, writing *The Mathematician in Love*, and a song writer, composing such ballads as *They Never Shall Have Gibraltar.*

Svein Rosseland (1894-1985) was a theoretical astrophysicist who followed early education in Norway with a fellowship at the Institute of Physics in Copenhagen in 1920, where he met many pioneers in atomic physics, including Neils Bohr. In 1924, he published the paper describing the opacity coefficient of stellar matter, now known as the Rosseland coefficient. He made important contributions to theoretical astrophysics throughout his career. His 1936 text, *Theoretical Astrophysics*, may be his most important work. He left occupied Norway in 1941 to the US and then England, finally returning to Norway in 1946.

Photo courtesy of Creative Commons-Oslo Museum

Sergei Mikhailovich Rytov (1908-1996) contributed to the development of near-field radiation transfer concepts with his pioneering studies on fluctuational electrodynamics. Earlier in his career, he developed an approximate solution of Maxwell's equations to describe the propagation of an electromagnetic wave through a turbulent atmosphere, and was a pioneer in the field of radiophysics. This work has widely been used in inverse techniques for determining the phase function and scattering coefficient of scattering media from remote signals. Later, he developed the description of the effect of thermal fluctuations in electrodynamics and published some of the most cited papers and and a book on the subject.

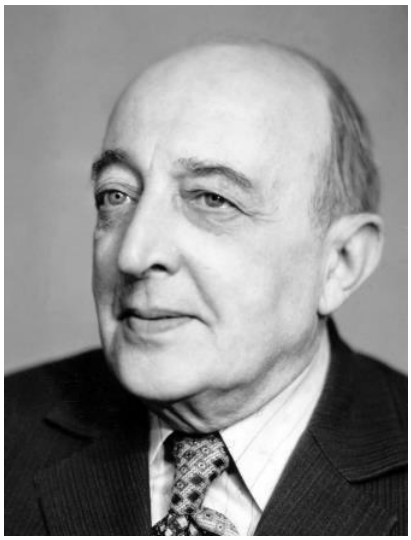

Erwin Rudolf Josef Alexander Schrödinger (1887-1961) was a Nobel Prize-winning (1933) Austrian physicist who developed fundamental results in quantum theory. The Schrödinger equation describes the wave function of a particle and how it changes dynamically in time. He did not like the consequences that flow from interpreting the equation, and said "I don't like it, and I'm sorry I had anything to do with it." He wrote in various fields of physics: statistical mechanics and thermodynamics, physics of dielectrics, color theory, electrodynamics, general relativity, and cosmology. He made several attempts to construct a unified field theory and is also known for his "Schrödinger's cat" thought-experiment.

Franz Arthur Friedrich Shuster (1851-1934) studied with Kirchhoff, Maxwell, Helmholtz and Rayleigh among others. He is credited with initial work on predicting antimatter and the eleven-year sunspot cycle. **Karl Schwarzschild (1873-1916)** worked on radiative pressure on small particles, atomic spectra, laid the foundation for the theory of black holes, and generalized the theory of the Stark effect. Schuster and Schwarzchild developed the two-stream model of radiative transfer in one-dimensional systems. The model is based on assuming a different uniform intensity in the forward and backward hemisphere of directions.

Johannes Stark (1874-1957) received the Nobel Prize in 1919 for his "discovery of the Doppler effect in canal rays and the splitting of spectral lines in electric fields", the latter effect on lines now called Stark broadening. His request in 1907 as a journal editor for a review article by the relatively (!!) unknown Albert Einstein led Einstein along a path to his General Theory of Relativity. Stark later became a strong advocate of Adolph Hitler and the Nazi party and was a main figure in the *Deutsch Physik* movement, seeking to remove Jewish scientists (including Einstein) and their contributions from German physics.

Following WW II, Stark was classified as a "major offender," and was given a four-year (suspended) sentence by a denazification court.

Josef Stefan (1835-1893) was born in Austria and attended elementary school in Klagenfurt, where he showed his talent. In 1845, he entered the Klagenfurt Lyceum and graduated top of his class. He left for Vienna in 1853 to study mathematics and physics and earned his qualification for university teaching in mathematical physics at the University of Vienna in 1858.

Stefan published nearly 80 scientific articles, mostly in the Bulletins of the Vienna Academy of Sciences. He is best known for originating Stefan's law in 1879, which states that the total radiation from a black body is proportional to the fourth power of its absolute thermodynamic temperature *T*. In 1884, the law was derived from a thermodynamic analysis by Stefan's student Ludwig Boltzmann and hence is known as Stefan–Boltzmann law. The law is now usually derived from Planck's law of black body radiation.

Using his law, Stefan determined the temperature of the Sun's surface to be 5,430 °C (9,810 °F), comparable to the presently accepted average value of 5780K. This was the first reasonable prediction of the temperature of the Sun.

John William Strutt, Lord Rayleigh (1842-1919) was one of the very few members of higher nobility who won fame as an outstanding scientist. He entered Cambridge in 1861 where he read mathematics, and his exceptional abilities enabled him to overtake his better prepared competitors. From then on, he devoted his full time to science.

In 1859, John Tyndall had discovered that bright light scattering off nanoscopic particulates was faintly blue-tinted. He conjectured that a similar scattering of sunlight gave the sky its blue hue, but he could not explain the preference for blue light, nor could atmospheric dust explain the intensity of the sky's color.

In 1871, Rayleigh published two papers on the color and polarization of skylight to quantify Tyndall's effect in water droplets in terms of the volumes and refractive indices of particulates. In 1881 with the benefit of James Clerk Maxwell's 1865 proof of the electromagnetic nature of light, he showed that his equations followed from electromagnetism. In 1899, he showed that they applied to individual molecules, with the terms containing particulate volumes and refractive indices replaced with terms for molecular polarizability.

In 1879 he was appointed to follow Maxwell as Professor of Experimental Physics and Head of the Cavendish Laboratory at Cambridge. He left Cambridge in 1884 to continue his experimental work and from 1887 to 1905 he was Tyndall’s successor as Professor of Natural Philosophy in the Royal Institution of Great Britain.

His first researches were mainly mathematical, concerning optics and vibrating systems, but his later work ranged over almost the whole field of physics, covering sound, wave theory, color vision, electrodynamics, electromagnetism, light scattering, flow of liquids, hydrodynamics, density of gases, viscosity, capillarity, elasticity, and photography. He was a Fellow of the Royal Society (1873) and won the Nobel Prize for 1904. He died on June 30, 1919.

William Thomson, Lord Kelvin (1824-1907) became Professor of Natural Philosophy in 1846 at the University of Glasgow at age 22, and remained there for 53 years. He established the first physics teaching laboratory, and was responsible for the quote “I often say that when you can measure what you are speaking about, and express it in numbers, you know something about it; but when you cannot measure it, when you cannot express it in numbers, your knowledge is of a meagre and unsatisfactory kind.” Of course, he also said “Radio has no future," "X-rays are clearly a hoax," and "The aeroplane is scientifically impossible.”

He suggested his eponymous absolute temperature scale in 1848 based on Carnot’s work. While working on the laying of the Atlantic cable, he found time to publish work in 1849 (at age 25) that included the first use of the words *thermodynamic* and *mechanical energy*. By 1850 he had abandoned the caloric theory, and worked with Joule to extend Joule’s earlier experiments to examine the expansion of gases, leading to the measurement and introduction of the Joule-Thomson coefficient.

His interest in thermal conduction and thermodynamics led him to an incorrect estimate of the age of the Earth as 20 to 400 million years (and not infinite). His estimate was incorrect because it neglected the

effect of radioactive decay and the internal convection of the core, both unknown at the time. (The presently accepted value is $4.54\times10^9 \pm 1\%$ years.)

He was elevated to the House of Lords in 1892, the first scientist so honored.

Andrey Nikolayevich Tikhonov (1906-1993) was a Russian mathematician. He graduated from Moscow State University with a PhD in 1927. He immediately made important contributions to topology and mathematical physics and proved the fundamental uniqueness of the heat equation. Of most importance to this book is the method he developed for solving ill-posed inverse problems. He is credited with being the first to develop the method now known as *Tikhonov regularization* in 1963 although others (e.g., Phillips, 1962) developed very similar methods at nearly the same time.

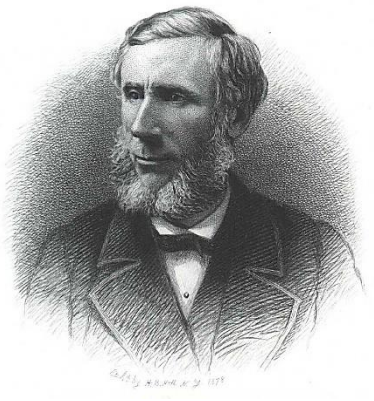

John Tyndall (1820-1893) was chiefly an experimentalist. From 1853 to 1887 he was professor of physics at the Royal Institution of Great Britain in London. His experiments on radiation and the radiation absorption of gases were the basis for his 1872 book *Contributions to Molecular Physics in the Domain of Radiant Heat* and are also described in his 1863 text *Heat Considered as a Mode of Motion*. He proposed that differing types of molecules have differing absorptions of infrared radiation because their molecular structures give them differing oscillating resonances and that the absorption behavior of molecules is quite different from that of the atoms composing the molecules. For example, nitric oxide (NO) absorbed more than a thousand times more infrared radiation than either nitrogen (N_2) or oxygen (O_2). He also observed that – no matter whether a gas is a weak absorber of broad-spectrum radiant heat – any gas will strongly absorb the radiant heat coming from a separate body of the same type of gas, demonstrating a kinship between the molecular mechanisms of absorption and emission. He observed that moist air was a much better radiation absorber than dry air and speculated on what this meant in terms of meteorology and climate.

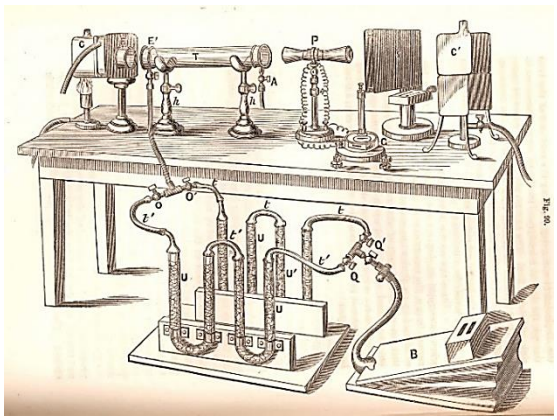

Tyndall's apparatus for measuring the difference in radiation absorptance of moist and dry air. The moist or dry air is pumped from a bag (B) into a cylinder (T) enclosed at each end with a rock salt window. C is a blackbody source; P is a radiometer connected to a galvanometer (G). A secondary high temperature source (burner heated) C' could also be viewed by the detector if the intervening screen was removed. (From Tyndall 1865).

Stanislaw Ulam (1909-1984) was a Polish-born scientist who worked at Los Alamos on the nuclear weapons Manhattan Project during WW II. Following recovery from serious brain surgery, in 1947 he brought forth the idea of implementing statistical techniques for modeling the individual histories of neutrons during their supercritical reactions as a substitute for solving the very complex equations otherwise required, now known as the Monte Carlo method. He developed the idea along with John von Neumann, Enrico Fermi, Nicholas Metropolis and others. Metropolis and Ulam published the first paper in the open literature on the method in 1949.

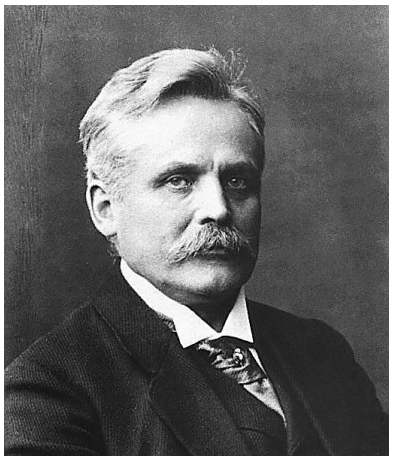

Wilhelm Carl Werner Otto Fritz Franz (Willy) Wien (1864-1928) was born in East Prussia to a landholding family. He studied mathematics and physics at the Universities of Göttingen and Berlin. Between 1883 and 1885, he worked in Hermann von Helmholtz's laboratory and in 1886, he took a doctorate with a thesis on diffraction and on the influence of materials on the color of refracted light.

In 1893, he announced what would later be called the law of displacement: that the product of wavelength and absolute temperature for a blackbody is constant. In 1896, he proposed a formula which described the spectral composition of radiation from an ideal body, which he called a black body. This work impelled Max Planck to propose quantum effects to bring Wien's distribution into agreement with experimental measurements. It also earned Wien the 1911 Nobel Prize in physics. In the late 1890s, Wien studied cathode rays, confirming that they were made of fast-moving negatively charged particles, or electrons, that were about two thousand times lighter than hydrogen atoms. He then analyzed *canal rays* which pass through a perforated cathode, finding that they were the positive equivalent of electrons and we now recognize them as streams of positive ions moving in the opposite direction to the electrons in the cathode ray tube. Twenty years later this research led to the development of mass spectrography.

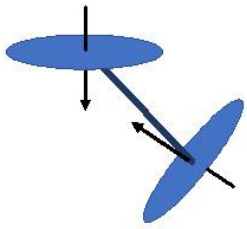

O: TIMELINE OF IMPORTANT EVENTS IN RADIATION

1672 **Isaac Newton** publishes his corpuscular theory of light (based on ideas of "corpuscularism" originally set forth by **Rene Descartes** in 1637) positing that light is composed of individual corpuscles that travel in straight lines and have intrinsic characteristics such as color.

1690 **Christiaan Huygens** publishes a treatise on the wave theory of light, which can explain effects such as diffraction and very slowly displaces Newton's theory.

~1700 **Gabriel Daniel Fahrenheit** proposes a reproducible temperature scale for alcohol and mercury thermometers.

1729 **Pierre Bouguer** establishes the exponential attenuation of light through the atmosphere.

1742 **Anders Celsius** proposes a temperature scale based on water's ice and boiling points.

1760 **Johann Lambert**'s book reaffirms Bouguer's exponential attenuation law and describes the cosine law dependence of radiation from a diffuse surface.

1791 **Pierre Prevost** postulates that all bodies radiate energy regardless of the presence of other bodies.

1800 **William Herschel** finds the presence of radiative energy in the previously unknown infrared portion of the spectrum.

1824 **Sadi Carnot** publishes analysis establishing the Second Law of Thermodynamics for ideal reversible heat engines, operating on a cycle now known as the Carnot Cycle.

1831 **Leopoldo Nobili** and **Macedonio Melloni** use the thermopile-based radiometer to demonstrate that light and radiant energy have similar characteristics.

1847 **John William Draper** observes the temperature at which a heated object becomes visible but misses the fourth power dependence of emission in his data, perhaps because the absolute temperature scale had yet to be established.

1848 **Lord Kelvin** proposes an absolute temperature scale based on Carnot's reversible cycle.

1852 **August Beer** shows that the exponential attenuation of light through a solution depends on the concentration of the absorbing solute. The exponential attenuation relation is often called the Beer-Lambert Law, although it was first proposed by Bouguer in 1729.

1859 **W.J.M. Rankine** proposes an absolute temperature scale. **James Tyndall** observes that blue light is preferentially scattered by small particles. **Gustav Kirchhoff** shows that the emissivity and absorptivity of a body in radiative equilibrium must be equal, both on a spectral and total basis. **Kirchhoff** and **Robert Bunsen** show that emission spectra can be used to identify elements from their spectral patterns and develop a spectroscope to identify the presence of trace metals in flame tests. Method leads to discovery of cesium and rubidium as new elements in the following year.

1859-66 **James Clerk Maxwell** develops a heuristic theory of the distribution of velocities among a set of ideal gas particles.

1861 **Gustav Kirchhoff** coins the term *blackbody* for the ideal absorber and emitter of thermal radiation. **Margaret and William Huggins** use a spectroscope based on the Kirchhoff-Bunsen design to demonstrate that stars are far-away suns.

1863 **John Tyndall** makes measurements of total gas absorptance, noting that NO, H_2O, CO_2, CH_4 and others are strong absorbers compared with N_2 and O_2, and indicates that their presence in the atmosphere may well affect climate.

1864 **Maxwell** publishes *A Dynamical Theory of the Electromagnetic Field*, mathematically describing the propagation of electromagnetic waves using twenty differential equations. He also performs a statistical derivation of the velocity distribution of gas molecules.

c.1870 **Ludwig Boltzmann** rederives Maxwell's velocity distribution based on the maximum entropy principle, placing it on a sound theoretical basis. It is now known as the Maxwell-Boltzmann distribution.

1871 **Lord Rayleigh** publishes his conclusions on scattering from small particles and shows that his ideas extend to scattering by molecules.

1879 **Josef Stefan** proposes empirically that emission from a blackbody is proportional to the fourth power of the absolute temperature.

1884 **Boltzmann** provides theoretical justification for Stefan's proposal.

1888/9 **Oliver Heaviside** reduces Maxwell's twenty electromagnetic wave equations to the set of four now used.

1894 **Willy Wien** proposes a thermodynamically based relation between the wavelength and temperature of one ideal blackbody and the "corresponding" wavelength and temperature of another (the "Displacement Law.")

1896 **Wien** proposes a thermodynamically based relation for the spectral distribution of radiation emission from an ideal blackbody.

1899 **Maurice Paul Auguste Charles Fabry** with Alfred Pérot invents the interferometer, allowing accurate measurements of wavelength and refractive index. **Pyotr Nikolaevich Lebedev** makes the first measurement of radiation pressure, providing experimental confirmation of Maxwell' electromagnetic theory.

1900 **Rayleigh** proposes a relation for the spectral distribution of the emission of radiation from an ideal blackbody. However, his relation approaches very large values at short wavelengths, in opposition to experimental data (the "ultraviolet catastrophe".) **Otto Lummer** and **Ernst Pringsheim** provide careful measurements of the spectral emission of radiation from an ideal blackbody and show that both the Wein and Rayleigh distributions lie outside the data error bounds at large or small λT values, respectively.

1901 **Max Planck** proposes a relation for the spectral distribution of emission of radiation from an ideal blackbody that modifies the Wien distribution and agrees with the

Lummer-Pringsheim data. The required assumption of quantized energy states necessary to derive his distribution leads to the beginning of quantum theory.

1905 **James Jeans** bolsters Rayleigh's idea of a spectral distribution by invoking the classical idea of the equipartition of energy. **Albert Einstein** explains that the photoelectric effect of electrons ejected from a surface exposed to light cannot be satisfactorily explained by wave theory, but that the incident radiation must have energy quantum characteristics. This gives credence to Planck's quantum energy state hypothesis.

1905-6 **Arthur Schuster** and **Karl Schwarzschild** develop a two-intensity stream model of radiative transfer, giving one of the first analytical solutions to radiative transfer in participating media.

1908 **Gustav Mie** establishes the radiation scattering characteristics of particles.

1909 **Johannes Stark** receives Nobel Prize for discovering the effect of electrical fields on spectral lines.

1921 **E. A. Milne** and **Arthur Eddington** provide a solution to the radiative transfer equation in participating media based on a modified two-stream model.

1923 **Luis de Broglie** hypothesizes that since electromagnetic radiation can be interpreted in terms of particles, then matter particles should also have the characteristics of waves (an extension of the idea of wave-particle duality).

1924 **Svein Rosseland** describes the opacity of stellar matter in terms of the now named Rosseland coefficient.

1926 **Erwin Schrödinger** publishes his wave equation, describing the wave characteristics of particles as predicted to exist by de Broglie, leading to rapid advances in quantum theory. **G.N. Lewis** coins the term *photon* for the particle/wave carrying radiant energy.

1927- **Hoyt Hottel** in a series of papers, chapters and texts provides the engineering basis and combustion gas property values for calculating radiation transfer in combustion furnaces.

1937 **E.R.G. Eckert** measures the emittance of CO_2-N_2 and H_2O-N_2 mixtures.

1947 **Stanislaw Ulam** proposes the Monte Carlo method for modeling neutron interactions, later extended to model thermal radiation.

1953 **Sergei Mikhailovich Rytov** publishes seminal work on the effect of electrical fluctuations on thermal radiation, or fluctuation electrodynamics,

1963 **Andrey Tikhonov** introduces regularization methods to treat ill-posed inverse problem.

Credit for developments in the field since 1965 will await the judgment of historians.

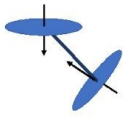

P: ADDITIONAL HOMEWORK

The homework in this Appendix is meant to provide instructors or students an additional range of problems from those in the text for extra assignment or home study. Solutions are in the Solution Manual, available from the publisher.

Chapter 1:

P.1.1 Radiant energy at a wavelength of 2.0 μm is traveling through a vacuum. It then enters a medium with a refractive index of 1.28.

(a) Find the following quantities for the radiation in the vacuum: speed, frequency, and wave number.

(b) Find the following quantities for the radiation in the medium: speed, frequency, wave number, and wavelength.

Answer: (a) 2.9979×10^8 m/s; 1.4990×10^{14} s^{-1}; 5×10^5 m^{-1}. (b) 2.342×10^8 m/s; 1.4990×10^{14} s^{-1}; 6.40×10^5 m^{-1}; 1.5625×10^{-6} m

P.1.2 What range of radiation wavelengths is present within a glass sheet that has a wavelength-independent refractive index of 1.29 when the sheet is exposed in vacuum to incident radiation in the visible range $\lambda_0 = 0.4$–0.7 μm?

Answer: 0.310–0.543 μm

P.1.3 Plot the hemispherical spectral emissive power $E_{\lambda b}$ for a blackbody in air [W/(m^2·μm)] as a function of wavelength (μm) for surface temperatures of 2000 and 6250 K.

P.1.4 A blackbody at 1100 K is radiating in the vacuum of outer space.

(a) What is the ratio of the spectral intensity of the blackbody at $\lambda = 1.0$ μm to the spectral intensity at $\lambda = 4.0$ μm?

(b) What fraction of the blackbody emissive power lies between the wavelengths of $\lambda = 1.0$ μm and $\lambda = 4.0$ μm?

(c) At what wavelength does the peak energy in the radiated spectrum occur for this blackbody?

(d) How much energy is emitted by the blackbody in the range $1.0 \le \lambda \le 4.0$ μm?

Answer: (a) 0.0541; (b) 0.5488.; (c) 2.6344μm; (d) 45484 W/m^2

P.1.5 Solar radiation is emitted by a fairly thin layer of hot plasma near the sun's surface. This layer is cool compared with the interior of the sun, where nuclear reactions are occurring. Various methods can be used to estimate the resulting effective radiating temperature of the sun, such as determining the best fit of a blackbody spectrum to the observed solar spectrum. Use two other methods (as follows), and compare the results to the oft-quoted value of $T_{solar} = 5780$ K.

(a) Using Wien's law and taking the peak of the solar spectrum as 0.50 μm, estimate the solar radiating temperature.

(b) Given the measured solar constant in the Earth's orbit of 1368 W/m^2 and using the "inverse square law" for the reduction in heat flux with distance, estimate the solar temperature. The mean radius of the Earth's orbit around the sun is 149×10^6 km and the diameter of the sun is 1.392×10^6 km.

Answer: (a) 5796 K; (b) 5766 K

P.1.6 A blackbody radiates such that the wavelength at its maximum emissive power is 2.50 μm. What fraction of the total emissive power from this blackbody is in the range $\lambda = 0.7$ to $\lambda = 6$ μm?

Answer: 0.805

P.1.7 A radiometer is sensitive to radiation only in the interval $3.6 \le \lambda \le 8.5$ μm. The radiometer is used to calibrate a blackbody source at 1200 K. The radiometer records that the emitted energy is 5000 W/m^2. What percentage of the blackbody radiated energy in the prescribed wavelength range is the source actually emitting?

Answer: 11.2%

P.1.8 What temperature must a blackbody have for 25% of its emitted energy to be in the visible wavelength region?

Answer: 4,343 K, 12,460 K (Note: two solutions are possible!)

P.1.9 Show that the blackbody spectral intensity $I_{\lambda b}$ increases with T at any fixed value of λ.

P.1.10 A sheet of silica glass transmits 87% of the radiation that is incident in the wavelength range between 0.38 and 2.7 μm and is essentially opaque to radiation having longer and shorter wavelengths. Estimate the percent of solar radiation that the glass will transmit. (Consider the sun as a blackbody at 5780 K.)

If the garden in a greenhouse radiates as a black surface and is at 40°C, what percent of this radiation will be transmitted through the glass?

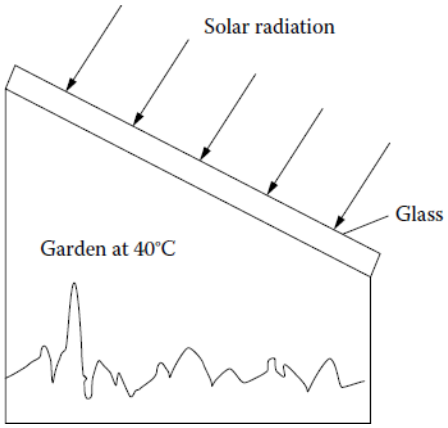

Answer: 75.6%; 0.003%

P.1.11 Derive Wien's displacement law in terms of wave number by differentiation of Planck's spectral distribution in terms of wave number, and show that $T/\eta_{max} = 5099.4$ μm·K.

P.1.12 A student notes that the peak emission of the sun according to Wien's displacement law is at a wavelength of about $\lambda_{max} = C_3/5780$ K = 2897.8/ 5780 = 0.501 μm. Using $\eta_{max} = 1/0.501$ μm, the student solves again for the solar temperature using the result derived in Homework Problem P.1.11. Does this computed temperature agree with the solar temperature? Why? (This is not trivial—put some thought into *why*.)

P.1.13 Derive the relation between the wave number and the wavelength at the peak of the blackbody emission spectrum. (You may use the result of Homework Problem P.1.11.)

Answer: η_{max} (cm^{-1}) = 5682.6/λ_{max} (μm)

P.1.14 A 6 by 10 cm black rectangular sheet of metal is heated uniformly with 2600 W by passing an electric current through it. One face of the rectangle is well insulated. The other face is exposed to vacuum and very cold surroundings. At thermal equilibrium, what fraction of the emitted energy is in the wave number range from 0.40 to 2 μm^{-1}?

Answer: 0.5086

P.1.15 Radiation from a blackbody source at 2,200 K is passing through a layer of air at 12,000 K and 1 atm. Considering only the transmitted radiation (i.e., not accounting for emission by the air), what path length is required to attenuate by 35% the energy at the wavelength corresponding to the maximum emission by the blackbody source? At this λ, take $\kappa_\lambda = 1.2 \times 10^{-1}$ cm^{-1} for air at 12,000 K and 1 atm.

Answer: 3.59 cm

P.1.16 A gas layer at constant pressure P has a linearly decreasing temperature across the layer and a constant mass absorption coefficient κ_m (no scattering). For radiation passing in a normal direction through the layer, what is the ratio I_2/I_1 as a function of T_1, T_2, and L? The temperature range T_2 to T_1 is low enough that emission from the gas can be neglected. The gas constant is R.

Chapter 2:

P.2.1 Using Figure 3.43 of the text, estimate the hemispherical total emissivity of tungsten at 2200 K.
Answer: 0.242.

P.2.2 For a surface with hemispherical spectral emissivity ε_λ, does the maximum of the E_λ distribution occur at the same λ as the maximum of the $E_{\lambda b}$ distribution at the same temperature? (*Hint*: examine the behavior of $dE_\lambda/d\lambda$.) Plot the distributions of E_λ as a function of λ for the data of Figure 2.9 of the text at 600 K and for the property data at 700 K. At what λ is the maximum of E_λ? How does this compare with the maximum of $E_{\lambda b}$?

P.2.3 The surface temperature-independent hemispherical spectral absorptivity of a surface is measured when it is exposed to isotropic incident spectral intensity, and the results are approximated as shown in the following graph. What is the total hemispherical emissivity of this surface when it is at a temperature of 1200 K?

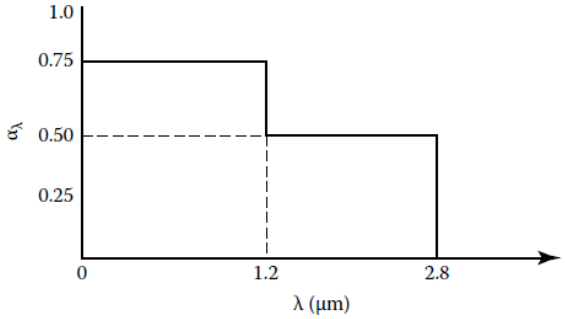

Answer: 0.179.

P.2.4 A white ceramic surface has a hemispherical spectral emissivity distribution at 1500 K as shown. What is the hemispherical total emissivity of the surface at this surface temperature?

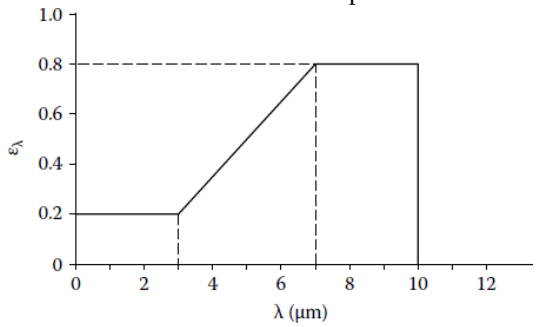

Answer: 0.292.

P.2.5 A surface has the following values of hemispherical spectral emissivity at a temperature of 900 K.

λ (μm)	ε_λ(900 K)
<1	0
1	0
1.5	0.2
2	0.4
2.5	0.6
3	0.8
3.5	0.8
4	0.8
4.5	0.7
5	0.6
6	0.4
7	0.2
8	0
>8	0

(a) What is the hemispherical total emissivity of the surface at 900 K?

(b) What is the hemispherical total absorptivity of the surface at 900 K if the incident radiation is from a gray source at 1800 K that has an emissivity of 0.815? The incident radiation is uniform over all incident angles.

Answer: (a) 0.476; (b) 0.427.

P.2.6 A diffuse surface at 1100 K has a hemispherical spectral emissivity that can be approximated by the solid line shown.

(a) What is the hemispherical-total emissive power of the surface? What is the total intensity emitted in a direction 60° from the normal to the surface?

(b) What percentage of the total emitted energy is in the wavelength range $5 < \lambda < 10$ μm? How does this compare with the percentage emitted in this wavelength range by a gray body at 1100 K with an emissivity $\varepsilon = 0.611$?

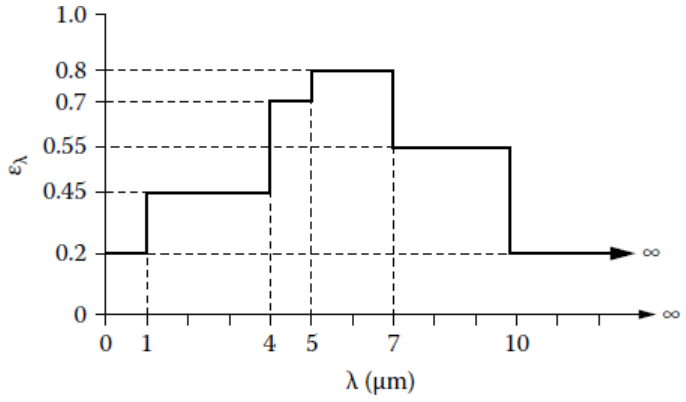

Answer: (a) 44,010 W/m^2; 14,009 W/m^2 · sr: (b) 36.7%; 24.0%.

P.2.7 The ε_λ for a metal at 1100 K is approximated as shown, and it does not vary significantly with the metal temperature. The surface is diffuse.

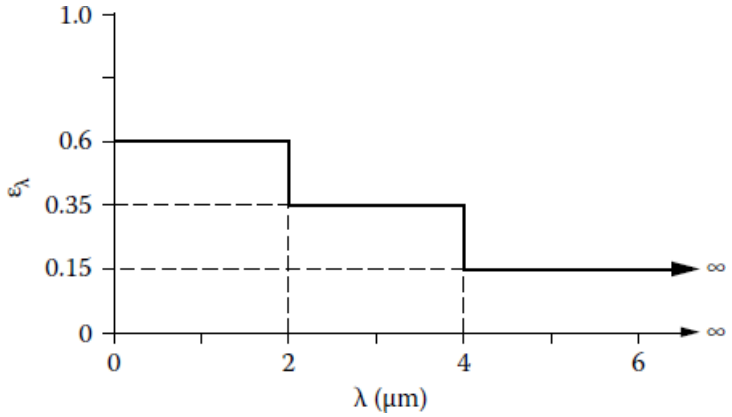

(a) What is α for incident radiation from a gray source at 1100 K with $\varepsilon_{source} = 0.822$?

(b) What is α for incident radiation from a source at 1100 K made from the same metal as the receiving plate?

Answer: (a) 0.285; (b) 0.356.

P2.8 A flat metal plate 0.1 m wide by 1.0 m long has a temperature that varies only along the long direction. The temperature is 900 K at one end, and decreases linearly over the one meter length to 350 K. The hemispherical spectral emissivity of the plate does not change significantly with temperature but is a function of wavelength. The wavelength dependence is approximated by a linear function decreasing from $\epsilon_\lambda = 0.85$ at $\lambda = 0$ to $\epsilon_\lambda = 0.02$ at $\lambda = 10$ □m. What is the rate of radiative energy loss from one side of the plate? The surroundings are at a very low temperature.

Answer: 416.6 W.

Chapter 3:

P.3.1 A smooth hot ceramic dielectric sphere with an index of refraction $n = 1.40$ is photographed with an IR camera. Calculate how bright the image is at locations B and C relative to that at A. (Camera is distant from sphere.)

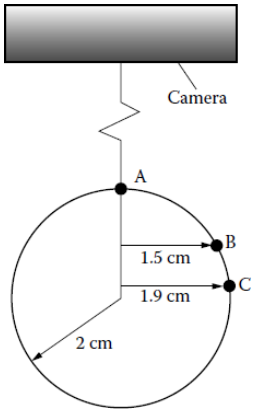

Answer: 0.987; 0.849.

P.3.2 A smooth dielectric material has a normal spectral emissivity of $\varepsilon_{\lambda,n} = 0.765$ at a wavelength in air of 6 μm. Find or estimate values for

(a) The hemispherical-spectral emissivity ε_λ at the same wavelength.

(b) The perpendicular component of the directional-hemispherical-spectral reflectivity $\rho_{\lambda,\perp}(\theta)$ at the same wavelength and for incidence at $\theta = 40°$.

Answer: (a) 0.736; (b) 0.327.

P.3.3 A smooth ceramic dielectric has an index of refraction $n = 1.48$, which is independent of wavelength. If a flat ceramic disk is at 1100 K, how much emitted energy per unit time is received by the detector when it is placed at $\theta = 0°$ or at $\theta = 60°$? Use relations from the EM theory.

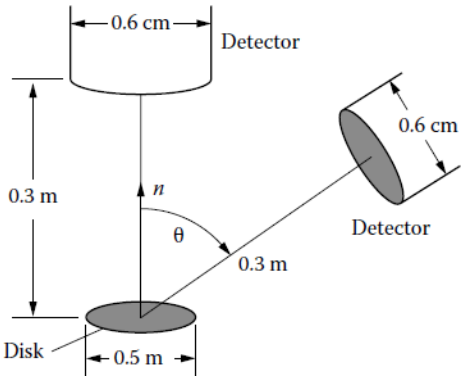

Answer: 15.69×10^{-5} W at $\theta = 0°$; 7.845×10^{-5} W at $\theta = 60°$.

P.3.4 At a temperature of 300 K, these metals have the following resistivities (Table 3.2):

Copper	1.71×10^{-6} Ω-cm
Gold	2.26×10^{-6} Ω -cm
Aluminum	2.71×10^{-6} Ω -cm

What are the theoretical normal total emissivities and hemispherical total emissivities of these metals, and how do they compare with tabulated values for clean, unoxidized, polished surfaces?

Answer: ε_n 0.0131, 0.0157, 0.0168; ε 0.0170, 0.0202, 0.0217.

P.3.5 A clean metal surface has a normal spectral emissivity of $\varepsilon_{\lambda,n} = 0.055$ at a wavelength of 12 μm. Find the value of the electrical resistivity of the metal.

Answer: 2.834×10^{-4} Ω-cm.

P.3.6 Evaluate the normal spectral reflectivity of clean aluminum at 400 K when λ_0 = 6, 12, and 24 μm. For aluminum, the temperature coefficient of resistivity is 0.0039.

Answer: 0.971; 0.980; 0.986.

P.3.7 Polished platinum at 300 K is irradiated normally by a gray-body source at 1200 K. Evaluate its normal total absorptivity α_n. (Use the method of Example 3.4 of the text.)

Answer: 0.0655.

P.3.8 The hemispherical total emissive power emitted by a polished metallic surface is 2500 W/m^2 at temperature T_A. What would you expect the emissive power to be if the temperature were doubled? What assumptions are involved in your answer?

Answer: 80,000 W/m^2.

P.3.9 The following figure gives some experimental data for the hemispherical-spectral reflectivity of polished aluminum at room temperature. Extrapolate the data to λ = 10 μm. Use whatever method you want, but list your assumptions. Discuss the probable accuracy of your extrapolation. (*Hint:* The electrical resistivity of pure aluminum is about $r_e = 2.73 \times 10^{-6}$ Ohm-cm at 293 K. At 10 μm, take $\bar{n} = 33.6 - 76.4i$. You may use any, all, or none of these data as you wish.)

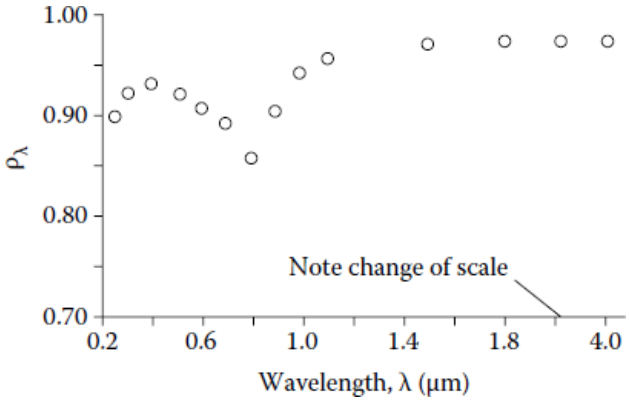

Answer: 0.975.

P.3.10 An unoxidized titanium sphere is heated until it is glowing red. From a distance, it appears as a red disk. From the EM theory how would you expect the brightness to vary across the disk? What would you expect after looking at Figure 3.32 of the text?

P.3.11 Using Hagen–Rubens emissivity relation, plot the normal spectral emissivity as a function of wavelength for a polished aluminum surface used in a cryogenic application at 50 K. What is the normal total emissivity? (*Note*: Do not use any relations valid only near room temperature.)

P.3.12 Metals cooled to very low temperatures approaching absolute zero become superconducting; that is, the value of $r_e(T \approx 0) \approx 0$. Based on EM theory predictions, what is your estimate of the values of the simple refractive index *n*, the absorption index *k*, and the normal spectral and normal total emissivities at such conditions? What assumptions are implicit in your estimates? What assumptions are implicit in your estimates? (The results predicted by the Hagen-Rubens relation, and other results from classical electromagnetic theory, become inaccurate at T < 100 K. Predictions of radiative properties at low absolute temperatures using more exact theoretical approaches are reviewed in Toscano, W. M. and Cravalho, E. G.: Thermal radiative properties of the noble metals at cryogenic temperatures, *JHT*, 98(3), 438–445, 1976.

P.3.13 A smooth polished stainless steel surface must emit a total intensity in the normal direction of 70.0 W/m^2·sr. What is its surface temperature as calculated from equations derived from Hagen–Rubens relations? The r_e of the steel is 11.9×10^{-6} Ohm-cm at 293 K.

Answer: 509 K.

P.3.14 The normal spectral absorptivity of a SiO–Al selective surface can be approximated as shown by the long-dashed line in Figure 3.50 of the text. The surface receives a flux q from the normal direction. The equilibrium temperature of the surface is 1200 K. Assume the hemispherical-spectral $\varepsilon_\lambda = \alpha_\lambda(\theta = 0)$. What is the value of q if it comes from a gray-body source at 4900 K?

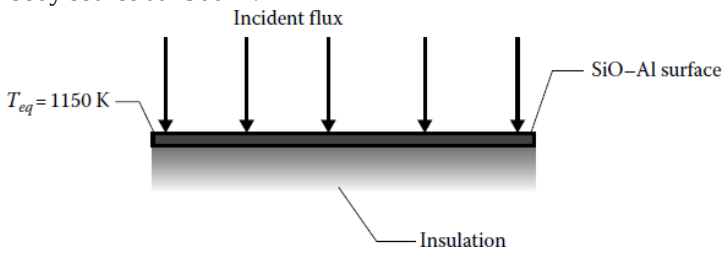

Answer: 12,640 W/m^2.

P.3.15 A directionally selective gray surface has properties as shown below. The $\alpha(\theta)$ is isotropic with respect to the azimuthal angle ϕ.

(a) What is the ratio $\alpha_n(\theta = 0)/\varepsilon$ (the normal directional absorptivity over the hemispherical emissivity) for this surface?

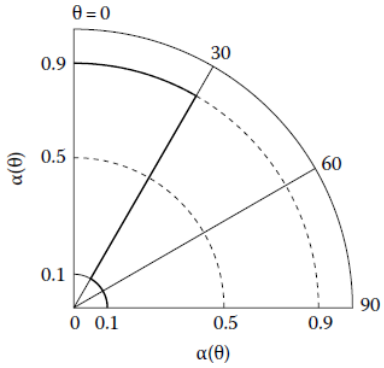

(b) If a thin plate with the aforementioned properties is in Earth orbit around the sun with incident solar flux of 1350 W/m^2, what equilibrium temperature will it reach? Assume that the plate is oriented normal to the sun's rays and is perfectly insulated on the side away from the sun.

(c) What is the equilibrium temperature if the plate is oriented at 40° to the sun's rays?

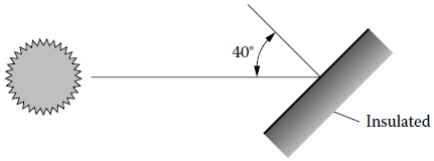

(d) What is the equilibrium temperature if the plate is normal to the sun's rays but is not insulated? Assume the plate is very thin and has the same directional radiation properties on both sides. Neglect radiation emitted by or reflected from the Earth.

Answer: (a) 3.0; (b) 517 K; (c) 297 K; (d) 435 K.

P.3.16 A flat plate in Earth orbit is insulated on one side, and the other side is facing normal to the solar intensity. The incident solar flux is 1350 W/m^2. A coating on the plate surface facing the sun has a total hemispherical emissivity of 0.250 over a broad range of plate temperatures. Surroundings above the plate are at a very low temperature. Telemetry signals to Earth indicate that the plate temperature is 730 K.

(a) What is the normal solar absorptivity α_{solar} of the plate surface facing the sun?

(b) If α_{solar} is independent of angle, what is the plate temperature if the plate is tilted so that its normal is 40° away from the solar direction?

Answer: (a) 2.982; (b) 683 K.

P.3.17 The spectral absorptivity of a SiO–Al selective surface can be approximated as shown below. The surface is in Earth orbit around the sun and has the solar flux 1353 W/m^2 incident on it in the normal direction. What is the equilibrium temperature of the surface if the surroundings are very cold?

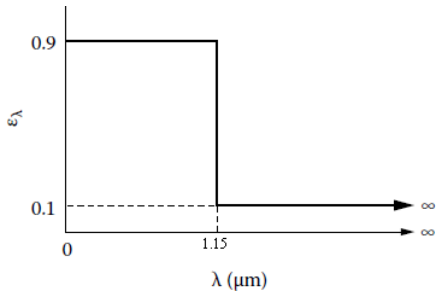

Answer: 672 K.

P.3.18 A thin plate has a directional-gray surface on one side with the directional emissivity shown below on the left. On the other side of the plate is a coating with diffuse-spectral emissivity shown below on the right. The surroundings are at very low temperature. Find the equilibrium temperature of the plate if it is exposed in vacuum to a normal solar flux of 1353 W/m^2 with a solar spectrum equivalent to that of a blackbody at 5780 K when

(a) The directional-gray side is facing normal to the sun.

(b) The diffuse-spectral side is facing normal to the sun.

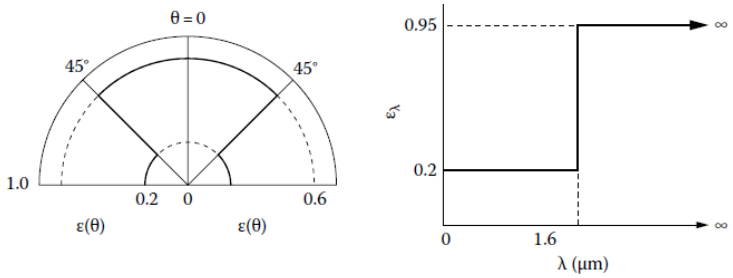

Answer: (a) 376 K; (b) 265 K.

P.3.19 A gray surface has a directional total absorptivity given by $\alpha(\theta) = 0.80 \cos^4 \theta$. This flat surface is exposed to normally incident sunlight of flux 1050 W/m^2. A fluid flows past the back of the thin radiation absorber plate at T_{fluid} = 325 K and with a velocity that gives a heat transfer coefficient of h = 64 W/m^2 · K. What is the equilibrium temperature of this flat-plate radiation collector?

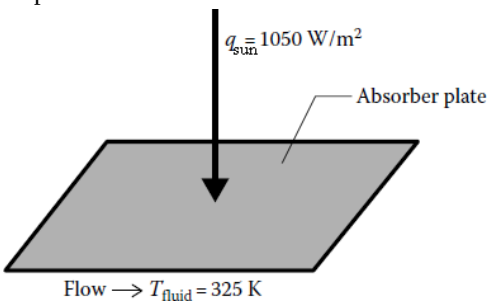

Answer: 335 K.

P.3.20 A plate is coated with a material combining directional and spectral selectivity so that the plate has a normal total solar absorptivity of 0.92 and an IR hemispherical emissivity of 0.040 at long wavelengths. When placed in sunlight normal to the sun's rays, what temperature will the plate reach (neglecting conduction and convection and with no heat losses from the unexposed side of the plate)? What assumptions did you make in reaching your answer? The incident solar flux ("insolation") is 1000 W/m^2.

Answer: 648 K.

P.3.21 A solar water heater consists of a sheet of glass 1 cm thick over a black surface that is assumed in perfect contact with the water below it. Estimate the water temperature for normally incident solar radiation. (Assume that Figure 9.22 of the text can be used for the glass properties and that the glass is perfectly transparent for wavelengths shorter than those shown. Take into account approximately the reflections at the glass surfaces; this is treated in more detail in Chapter 17.)

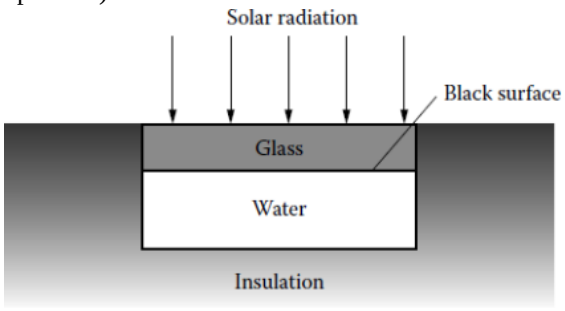

Answer: 389 K.

P.3.22 A gasoline storage tank is receiving sunlight on a somewhat cloudy day so that the incident radiation normal to the top of the tank is 900 W/m^2. The sides are not receiving solar radiation. The tank top and sides are painted with white paint having spectral reflectivity of $\rho_\lambda = 0.9$ for $\lambda < \lambda_{cutoff} = 2$ μm, and $r_l = 0.1$ for $\lambda > \lambda_{cutoff} = 2$ μm

(a) Estimate the average equilibrium temperature that the tank will achieve. (Neglect emitted and reflected radiation from the ground. Do not account for free or forced convection to the air, although this will be appreciable.) The ambient radiating temperature of the surroundings is $T_e = 300$ K.

(b) What is the average tank temperature if the top is painted white as before but the sides have a gray coating with an emissivity of 0.825?

(c) What is the temperature if the entire tank is painted with the gray coating?

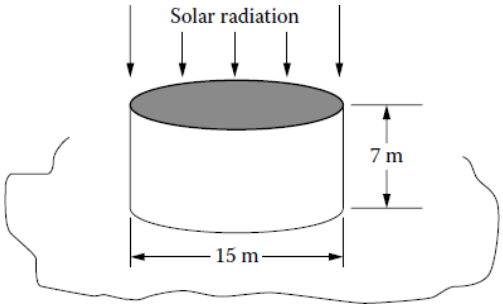

P.3.23 Consider the Earth as a spinning sphere exposed on one hemisphere to solar energy at the solar flux of 1353 W/m^2.

(a) If the average solar absorptivity of the Earth is taken as equal to its emissivity (a gray body), what is the estimated equilibrium temperature of the Earth?

(b) If the solar absorptivity and low-temperature emissivity are taken as the properties of fine snow (Tables B.1, B.2 of the text), what will be the Earth's equilibrium temperature?

(c) If the solar absorptivity and low-temperature emissivity are taken as the properties of plowed soil (Tables B.1, B.2 of the text), what will be the Earth's equilibrium temperature?

(d) Given the results of parts c and d, what do you see as the impact of the melting of polar ice and glaciers due to global warming? Is there a feedback mechanism that tends to increase or mitigate the effects of warming? (For more in-depth discussion, see Maslowski et al. 2012)

Answer: (a) 4.7°C; (b) −133.5°C; (c) 56.3°C.

P.3.24 A flat-plate radiator in space in Earth orbit is oriented normal to the solar radiation. It is receiving direct solar radiation of 1350 W/m^2, radiation emission from the Earth, and solar radiation reflected from the Earth. What must the radiator temperature be to dissipate a total of 3500 W of waste heat from both sides of each 1 m^2 of the radiator?

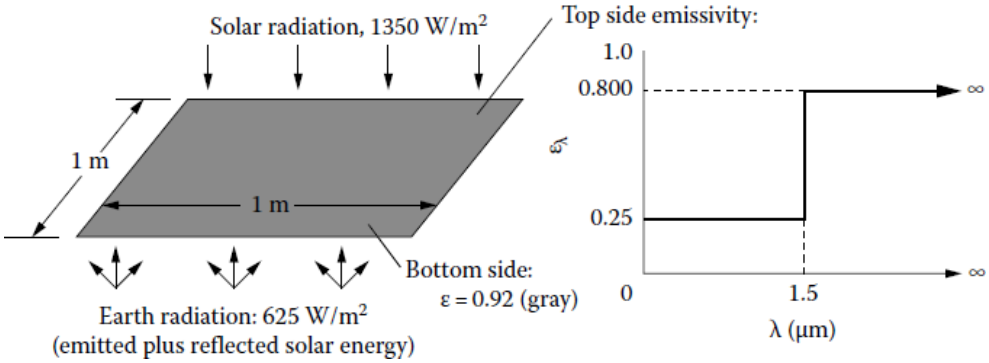

Answer: 450.1. K.

P.3.25 Specimens of metals are prepared by machining the surfaces so that the surface roughness is composed of parallel elements of rms roughness σ_0 with a correlation distance τ between roughness elements as measured by a profilometer. Determine whether geometric optics or complete EM theory should be applied for determining the reflectivity of the surfaces for the cases below for laser radiation of wavelength λ incident on the surface at angle θ in the plane normal to the roughness elements:

Case	rms Roughness, σ_o, μm	Roughness Correlation Length, τ, μm	Angle of Incidence, θ, Degrees	Laser Wavelength, λ, μm
1	5	5	0	1
2	1	5	0	10.2
3	2	5	60	5
4	10	20	85	10.2
5	10	2	30	1

Answer: Cases 2, 4 and 5, EM theory; Case 1, geometric optics; Case 3 on boundary.

P.3.26 A light pipe (refractive index n_2 = 1.3950) of diameter 0.1 cm is placed with its flat end 1 cm from a heated semiconductor wafer. What diameter of the wafer surface is viewed by the light pipe?

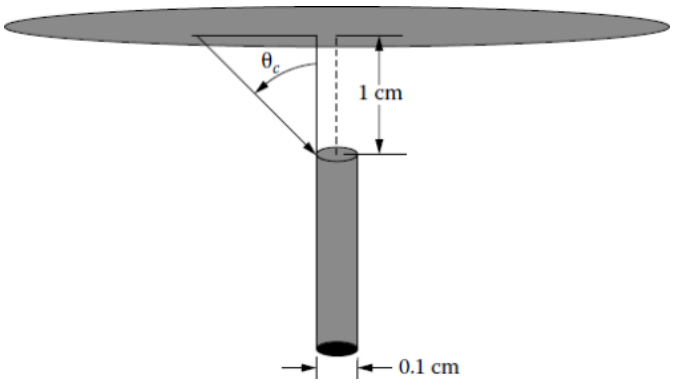

Answer: All values of $0 < \theta < \pi/2$.

Chapter 4:

P.4.1 Derive by any three methods, including use of the factors in Appendix C if you choose, the configuration factor F_{1-2} for the infinitely long geometry shown below in cross section.

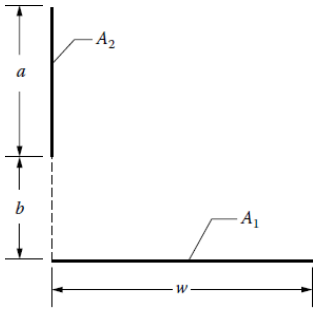

Answer: $F_{1-2} = \{A + (1 + B^2)^{1/2} - [(A + B)^2 + 1]^{1/2}\}/2$,
where
$A = a/w$
$B = b/w$

P.4.2 The configuration factor between two infinitely long directly opposed parallel plates of finite width L is F_{1-2}. The plates are separated by a distance D.

(a) Derive an expression for F_{1-2} by integration of the configuration factor between parallel differential strip elements.

(b) Derive an expression for F_{1-2} by the crossed-string method.

Answer: $\left[1+\left(\frac{D}{L}\right)^2\right]^{1/2} - \left(\frac{D}{L}\right)$.

P.4.3 The configuration factor between two infinitely long parallel plates of finite width L is F_{1-2} in the configuration shown below in cross section.

(a) Derive an expression for F_{1-2} by the crossed-string method.

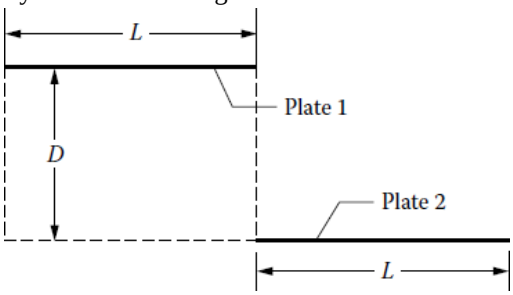

(b) Derive an expression for F_{1-2} by using the results of Homework Problem 4.6 and configuration factor algebra.

(c) Find the configuration factor F_{1-2} for the geometry of infinitely long plates shown below in cross section.

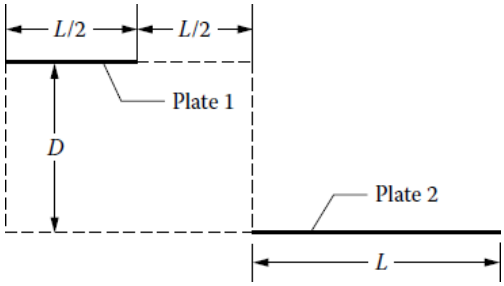

Answer: (a), (b) $\left[1+\left(\frac{D}{2L}\right)^2\right]^{1/2} + \frac{D}{2L} - \left[1+\left(\frac{D}{L}\right)^2\right]^{1/2}$;

(c) $$F_{1\text{–}2} = 2\left[1+\left(\frac{D}{2L}\right)^2\right]^{1/2} - \left[1+\left(\frac{D}{L}\right)^2\right]^{1/2} - \left[\left(\frac{D}{L}\right)^2+\left(\frac{3}{2}\right)^2\right]^{1/2} + \left[\left(\frac{D}{L}\right)^2+\left(\frac{1}{2}\right)^2\right]^{1/2}.$$

P.4.4 (a) For the 2D geometry shown in cross section, derive a formula for $F_{2\text{–}2}$ in terms of r_1 and r_2.

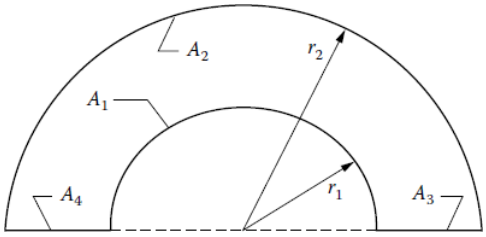

(b) Find $F_{2\text{–}2}$ for the 2D geometry. A_1 is a square (A_1 refers to the total area of the four sides) and A_2 is part of a circle.

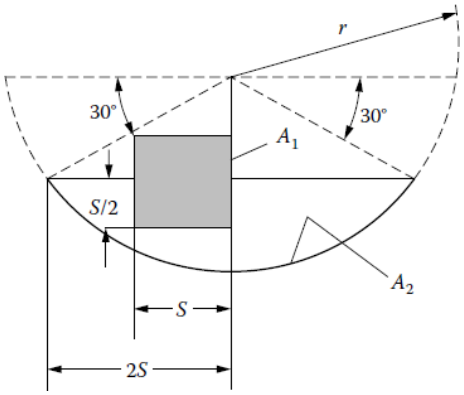

Answer:

(a) $$F_{2\text{–}2} = 1 - \frac{2}{\pi}\left[1-\left(\frac{r_1}{r_2}\right)^2\right]^{1/2} - \frac{2}{\pi}\frac{r_1}{r_2}\sin^{-1}\left(\frac{r_1}{r_2}\right).$$

(b) $F_{2\text{–}2} = 0.1359$.

P.4.5 Compute the configuration factor $F_{1\text{–}2}$ between faces A_1 and A_2 of the infinitely long parallel plates shown below in cross section when the angle β is equal to (a) 30° and (b) 75°.

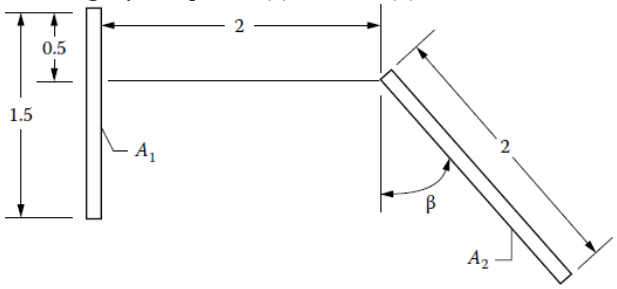

Answer: (a) 0.2752; (b) 0.0915.

P.4.6 A sphere of radius r is divided into two quarter spheres and one hemisphere. Obtain the configuration factors between all areas inside the sphere, $F_{1\text{–}2}$, $F_{2\text{–}2}$, $F_{3\text{–}1}$, $F_{1\text{–}1}$, etc. From these factors find $F_{4\text{–}5}$, where A_4 and A_5 are equal semicircles that are at right angles to each other.

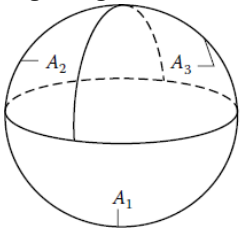

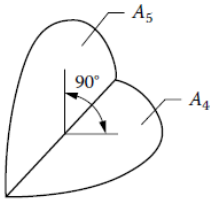

Answer: $F_{4-5} = 0.25$.

P.4.7 For the 2D geometry shown, the view between A_1 and A_2 is partially blocked by an intervening structure. Determine the configuration factor F_{1-2}.

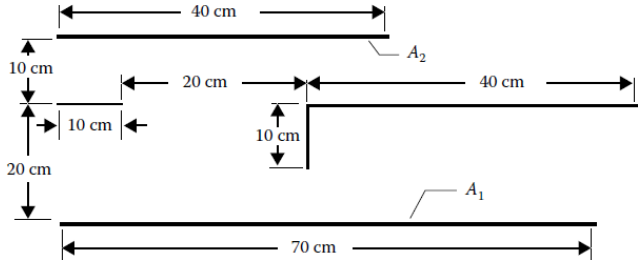

Answer: 0.1815.

P.4.8 The cylindrical geometry shown in cross section is very long in the direction normal to the plane of the drawing. The cross section consists of two concentric three-quarter circles and two straight lines. Obtain the value of the configuration factor F_{2-2}.

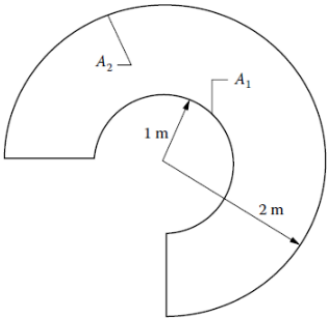

Answer: 0.3547.

P.4.9 Using the relation $F_{3-(1+2)} = F_{3-1} + F_{3-2}$, show whether the relation $F_{(1+2)-3} = F_{1-3} + F_{2-3}$ is also valid.

P.4.10 A plate A_1 in the configuration below is to be moved along positions from $S = 0$ cm to $S = 100$ cm. Plot the configuration factor F_{1-2} versus S for this configuration.

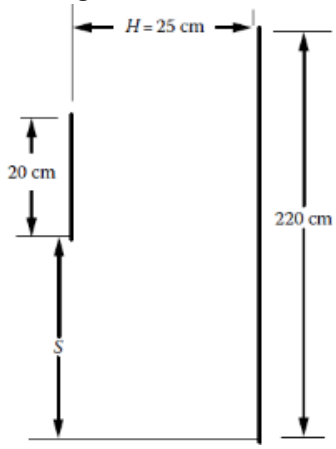

P.4.11 Derive the configuration factor F_{1-2} from a finite rectangle A_1 to an infinite plane A_2 where the rectangle is tilted at an angle η relative to the plane and one edge of the rectangle is in the infinite plane.

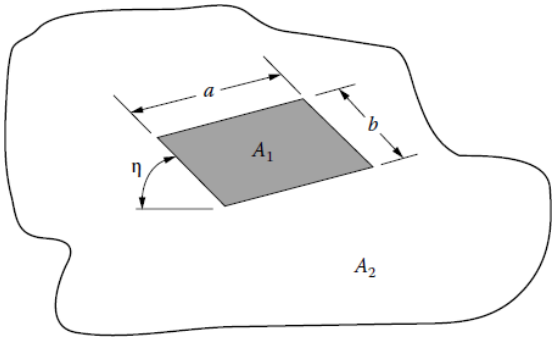

Answer: $F_{1-2} = (1/2)\,(1 - \cos\eta)$.

P.4.12 The four flat plates shown in cross section are very long in the direction normal to the plane of the cross section shown. Obtain the value of the configuration factor F_{1-2}. What are the values of F_{2-1} and F_{1-3}?

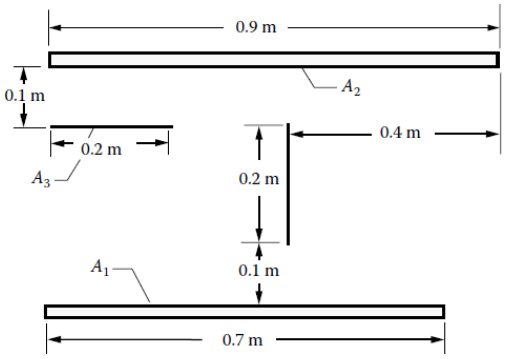

Answer: $F_{1-2} = 0.4260$; $F_{2-1} = 0.3314$; $F_{1-3} = 0.1704$.

P.4.13 A long tube in a tube bundle is surrounded by six other identical equally spaced tubes as shown in cross section below. What is the configuration factor from the central tube to each of the surrounding tubes?

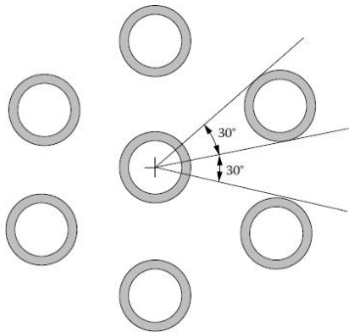

Answer: 0.0844 (>1/12).

P.4.14 Given F_{n-k}, determine the configuration factor between two perpendicular rectangles having a common edge. In terms of this factor, use configuration factor relations to derive the F_{1-8} factor between the two areas A_1 and A_8.

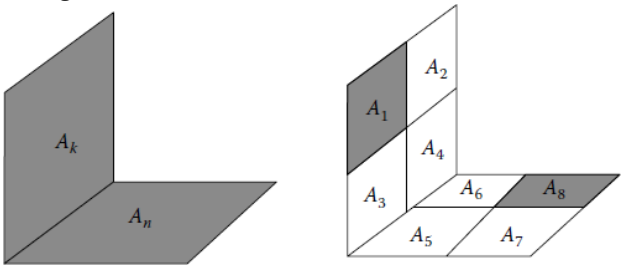

P.4.15 Find F_{1-2} by any two methods for the 2D geometry shown in cross section.

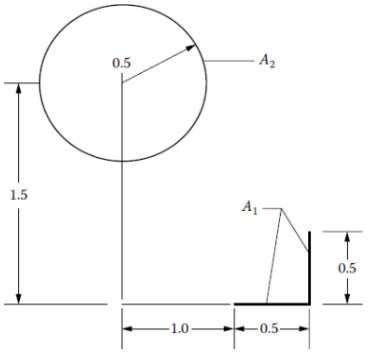

Answer: 0.1974.

P.4.16 Find the configuration factor F_{1-2} from the quarter disk to the parallel planar ring.

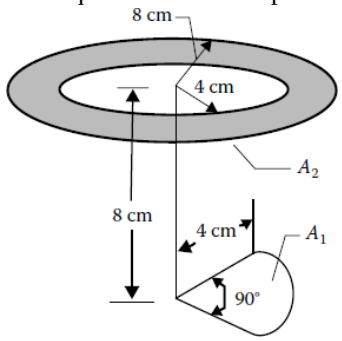

Answer: 0.2973.

P.4.17 Use the crossed-string method to derive the configuration factor between an infinitely long strip of differential width and a parallel infinitely long cylindrical surface.

Answer: $F_{d1-2} = (1/2)\,(\sin\beta_2 + \sin\beta_1)$.

P.4.18 Use the disk-to-disk configuration factor 10 of Appendix C to obtain the factor F_{d1-d2} between the interior surfaces of two differential rings on the interior of a right circular cone.

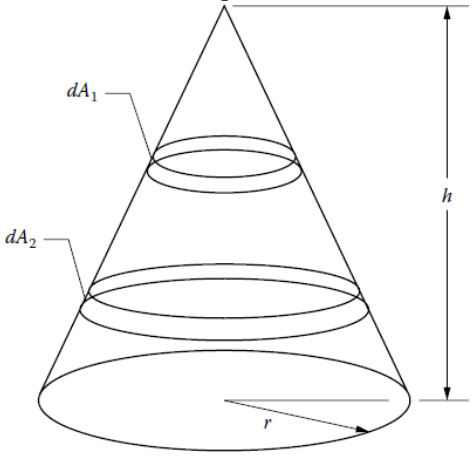

Answer:

$$R \equiv r/h;\ \alpha \equiv \left(R^2+1\right);\ \beta \equiv \left(2R^4 - R^2 - 5\right)$$

$$dF_{d1-d2} = -\frac{\cos\alpha}{2Rx^2}\left\{x - 2y\alpha + \frac{\alpha^{1/2}\left[\alpha x^4 + x^3 y\beta + 3x^2y^2(\beta+8) + xy^3\alpha(6R^2-7) + 2y^4Z^2\right]}{\left[\alpha(x+y)^2 - 4xy\right]^{3/2}}\right\}$$

P.4.19 In terms of disk-to-disk configuration factors, derive the factor between the finite ring A_1 and the finite area A_2 on the inside of a cone.

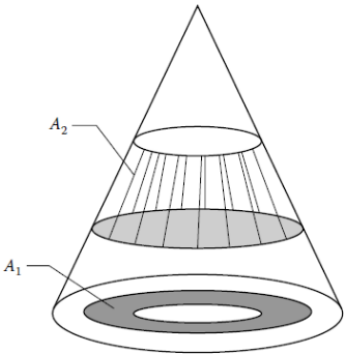

P.4.20 A closed right circular cylindrical shell with base diameter 1 m and height 1 m is located at the center of a spherical shell 1 m in radius.

(a) Determine the configuration factor between the inside of the sphere and itself.

(b) If the top of the cylindrical shell is removed, determine the configuration factor between the inside of the sphere and the inside of the bottom of the cylindrical shell.

Answer: (a) 0.6250; (b) 0.01072.

P.4.21 Show by an algebraic derivation whether the configuration factor from the interior curved surface of the frustum of a cone A_1 to its base A_2 as given in configuration factor C-111 of the configuration factor catalog at ***www.ThermalRadiation.net/ /indexCat.html*** is equivalent to that given in factor C-112.

P.4.22 Obtain the configuration factor dF_{d1-2} in Homework Problem 4.2 by using contour integration.

Answer:
$$F_{d1-2} = \left(\frac{2}{\pi}\right)\left\{\left[\frac{X}{(1+X^2)^{1/2}}\right]\tan^{-1}\left[\frac{Y}{(1+X^2)^{1/2}}\right] + \left[\frac{Y}{(1+Y^2)^{1/2}}\right]\tan^{-1}\left[\frac{X}{(1+Y^2)^{1/2}}\right]\right\}$$

where

$X = L/2H$

$Y = W/2H$

P.4.23 Obtain the value of the configuration factor dF_{d1-2} for the geometry shown. The areas dA_1 and A_2 are parallel.

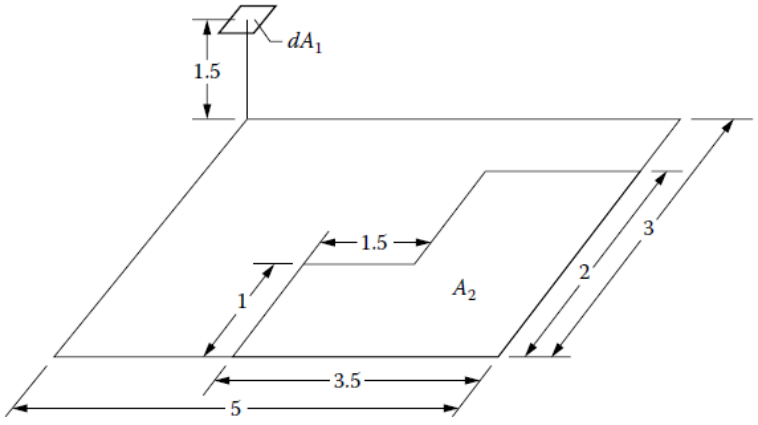

Answer: 0.01261.

P.4.24 For the geometry below and the special case of $l_1 = l_3$, derive algebraic expressions for the factors F_{1-2}, F_{1-3}, and F_{3-3}. Use relations from factors C-77 and C-97 from the online catalog at *www.ThermalRadiation.net/ indexCat.html*.

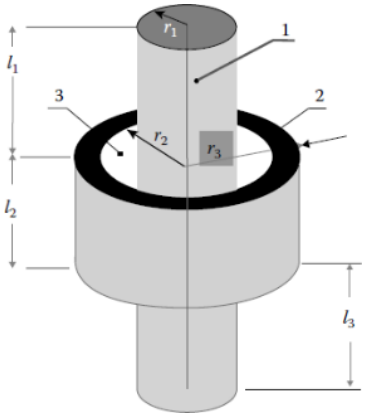

P.4.25 For the infinite parallel cylinders 1 and 2 with plate 3 forming a "deck" between them, find the factors F_{1-2}, F_{1-3}, and F_{2-2} in algebraic form.

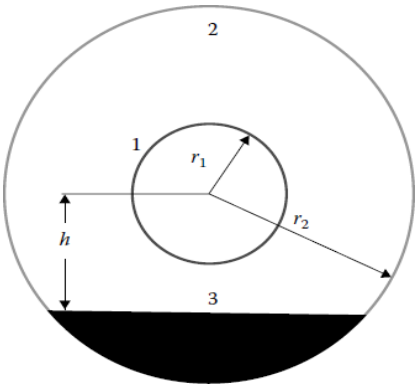

Answer: $F_{1-2} = 1 - F_{1-3} = 1 - \dfrac{\sqrt{r_2^2 - h^2}}{\pi r_1^2} \tan^{-1}\left(\dfrac{\sqrt{\left(r_2^2 - h^2\right)}}{h} \right)$

$$F_{1-3} = \frac{A_3}{A_1} F_{3-1} = \frac{\sqrt{r_2^2 - h^2}}{\pi r_1^2} \tan^{-1}\left(\frac{\sqrt{\left(r_2^2 - h^2\right)}}{h} \right)$$

$$F_{2-2} = 1 - \frac{\pi r_1}{(\pi - \cos^{-1}(h/r_2))} \left\{ 1 - \frac{\sqrt{r_2^2 - h^2}}{\pi r_1^2} \tan^{-1} \frac{\sqrt{r_2^2 - h^2}}{h} \right\}$$

$$- \frac{\sqrt{r_2^2 - h^2}}{(\pi - \cos^{-1}(h/r_2))} \left\{ 1 - \frac{1}{\pi} \tan^{-1} \frac{\sqrt{r_2^2 - h^2}}{h} \right\}$$

P.4.26 Interpreting the figure in Homework Problem P.4.25 as concentric spheres 1 and 2 with a disk 3 inserted between them, find the factors F_{1-2}, F_{1-3}, and F_{2-2} in algebraic form.

Answer: $R = \dfrac{b}{h} = \dfrac{\sqrt{r_2^2 - h^2}}{h}$; $F_{1-2} = 1 - F_{1-3} = 1 - \dfrac{1}{2}\left[1 - \dfrac{1}{(1+R^2)^{1/2}} \right]$

$$F_{1-3} = \frac{1}{2}\left[1 - \frac{1}{(1+R^2)^{1/2}} \right];$$

$$F_{2-2} = 1 - \frac{\pi r_1^2}{r_2^2\left[\pi - \cos^{-1}(h/r_2)\right]}\left(1 - \frac{1}{2}\left[1 - \frac{1}{(1+R^2)^{1/2}}\right]\right)$$

$$- \frac{\pi\left(r_2^2 - h^2\right)}{4r_2^2\left[\pi - \cos^{-1}(h/r_2)\right]}\left(1 - \frac{2r_1^2}{\left(r_2^2 - h^2\right)}\left(1 - \frac{1}{(1+R^2)^{1/2}}\right)\right)$$

Chapter 5:

P.5.1 A rectangular carbon steel billet 1 × 0.5 × 0.5 m is initially at 1150 K and is supported in such a manner that it transfers heat by radiation from all of its surfaces to surroundings at $T_e = 27°C$ (assume the surroundings are black). Neglect convective heat transfer and assume the billet radiates like a blackbody. Also, assume for simplicity that the thermal conductivity of the steel is infinite. How long will it take for the billet to cool to 410 K? (For carbon steel, let $\rho_{cs} = 7800$ kg/m^3 and $c_{cs} = 470$ J/kg · K.)

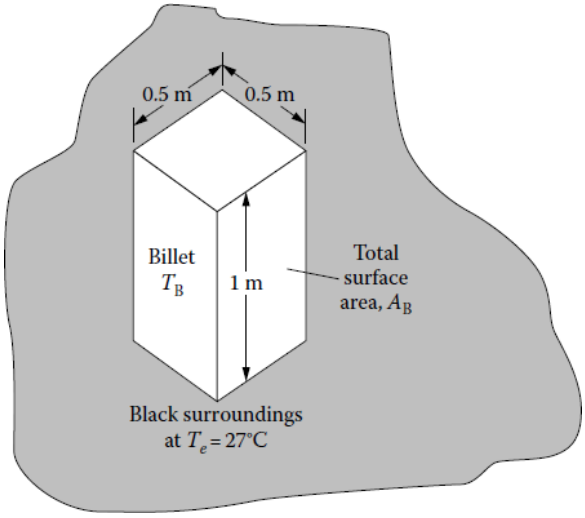

Answer: 9.61 h.

P.5.2 A black circular disk 0.15 m in diameter and well insulated on one side is electrically heated to a uniform temperature. The electrical energy input is 1300 W. The surroundings are black and are at T_e = 500 K. What fraction of the emitted energy is in the wave number region from 0.2 to 1 μm^{-1}?

Answer: 0.680.

P.5.3 A hollow cylindrical heating element is insulated on its outside surface. The element has a 25 cm inside diameter and is 25 cm long. The black internal surface is to be held at 1000 K. The surroundings are in vacuum and are at 400 K. Both ends of the cylinder are open to the surroundings. Estimate the energy that must be supplied to the element (W).

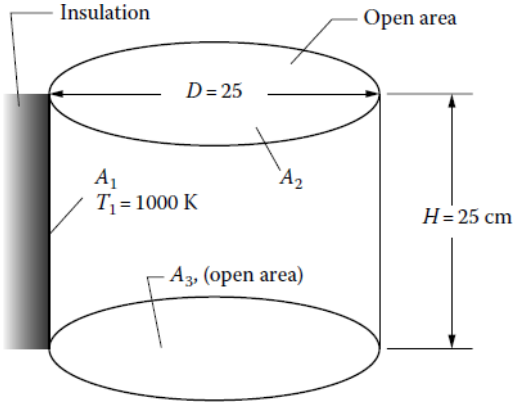

Answer: 4490 W.

P.5.4 The black-surfaced three-sided enclosure shown below has infinitely long parallel sides, with the specified temperatures and energy rate additions. Find Q_1, Q_2, and T_3. (Side 3 is a circular arc).

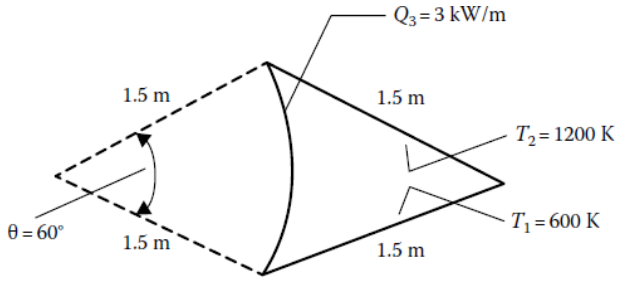

Answers: Q_1 = -123,561 W/m; Q_2 = 120,561 W/m; T_3 = 1032 K.

P.5.5 Two enclosures are identical in shape and size and have black surfaces. For one enclosure, the temperatures of the surfaces are $T_1, T_2, T_3,....,T_N$. For the second, the surface temperatures are $(T_1^4 + k)^{1/4}$, $(T_2^4 + k)^{1/4}$, $(T_3^4 + k)^{1/4}$, ..., $(T_N^4 + k)^{1/4}$, where k is a constant. Show how the heat transfer rates Q_j at any surface A_j are related for the two enclosures.

P.5.6 An enclosure with black interior surfaces has one side open to an environment at temperature T_e. The sides of the enclosure are maintained at temperatures of T_1, T_2, T_3, ..., T_N. How are the rates of energy input to the sides Q_1, Q_2, Q_3, ..., Q_N influenced by the value of T_e? How can the results for $T_e = 0$ be used to obtain solutions for other T_e?

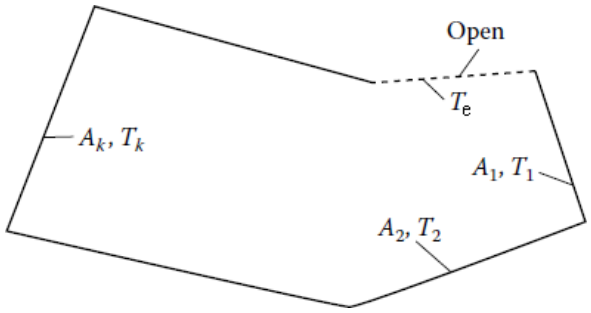

P.5.7 A black 6 cm diameter sphere at a temperature of 1100 K is suspended in the center of a thin 10 cm diameter partial sphere having a black interior surface and an exterior surface with a hemispherical total emissivity of 0.1. The surroundings are at 300 K. A 7.5 cm diameter hole is cut in the outer sphere. What is the temperature of the outer sphere? What is the Q being supplied to the inner sphere? (For simplicity, do not subdivide the surface areas into smaller zones.)

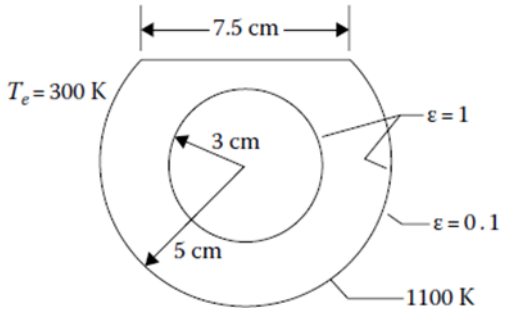

Answer: 988 K; 431 W.

P.5.8 An infinitely long enclosure (normal to the direction shown) is shaped as shown in the following. Assuming that the uniform flux restrictions are met along each surface, find Q_1 and T_2.

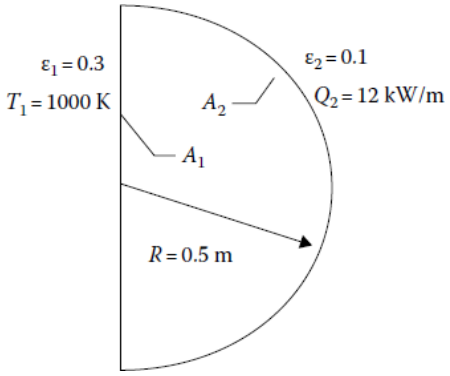

Answers: $Q_1 = -12$ kW/m; $T_2 = 1307$ K.

P.5.9 Two infinitely long diffuse–gray concentric circular cylinders are separated by two concentric thin diffuse–gray radiation shields. The shields have identical emissivities on both sides.

(a) Derive an expression for the energy transferred between the inner and outer cylinders in terms of their temperatures and the necessary radiative and geometric quantities. (Number the surfaces from the inside out; i.e., the inner surface is number 1, the outer surface is number 4.)

(b) Check this result by showing that in the proper limit it reduces to the correct result for four parallel plates with identical emissivities.

(c) Find the percent reduction in heat transfer when the shields are added if the radii for the surfaces are in the ratio 1:2:4:8, and if $\varepsilon_1 = \varepsilon_4 = 0.7$ and $\varepsilon_2 = \varepsilon_3 = 0.1$.

Answer:

(a) $$Q = \frac{A_1\sigma\left(T_1^4 - T_4^4\right)}{G_{12} + \dfrac{A_1 G_{23}}{A_2} + \dfrac{A_1 G_{34}}{A_3}} \text{ where } G_{ab} \equiv \frac{1}{\varepsilon_a} + \frac{A_a}{A_b}\left(\frac{1}{\varepsilon_b} - 1\right).$$

(b) $$Q = \frac{A_1\sigma\left(T_1^4 - T_4^4\right)}{3\left(\dfrac{2}{\varepsilon} - 1\right)}.$$

(c) $Q_{\text{with}}/Q_{\text{without}} = 0.0942$

P.5.10 Consider the gray cylindrical enclosure described in Homework Problem 5.8 of the text with the top in place. A hole 30 cm in diameter is cut in the top. Determine the configuration factors between (a) the base and the hole and (b) the curved wall and the hole. Estimate the radiant energy escaping through the hole. The outside environment is at $T_e \approx 0$ K.

Answer: (a) 0.00238; (b) 0.00238; (c) 2630 W.

P.5.11A thin gray disk with emissivity 0.9 on both sides is in Earth's orbit. It is exposed to normally incident solar radiation (neglect radiation emitted or reflected from the Earth.) What is the equilibrium temperature of the disk? A single thin radiation shield having emissivity 0.05 on both sides is placed as shown. What is the disk temperature? What is the effect on both of these results of reducing the disk emissivity to 0.5? (Assume the surroundings are at zero absolute temperature and that for simplicity, it is not necessary to subdivide the areas.)

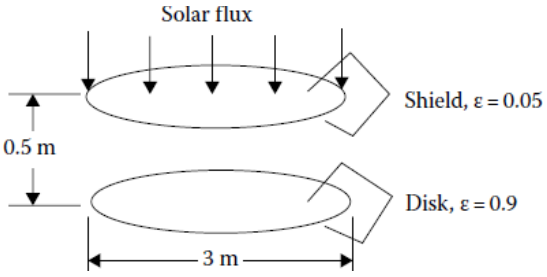

Answer: For unshaded disk, 330.5 K (either value of ε); with shield, 31.1 K ($\varepsilon = 0.05$); 136.1 K (for $\varepsilon = 0.5$).

P.5.12 For the enclosure with four infinitely long parallel walls shown in the following in cross section, calculate the average heat flux on surface 2 (W/m^2). All surfaces are diffuse–gray and are assumed for simplicity to have uniform outgoing flux distributions.

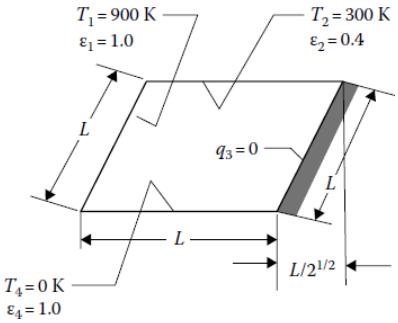

Answer: −4972 W/m^2.

P.5.13 A very long cylinder at temperature T_1 is coaxial with a long square enclosure shown in the following cross section. The conditions on surfaces 1–5 are shown in the table. Find Q_1 and T_2. (For simplicity, do not subdivide the surfaces. Also, note that the configuration factors for this geometry were derived in Homework Problem 4.12 of the text.)

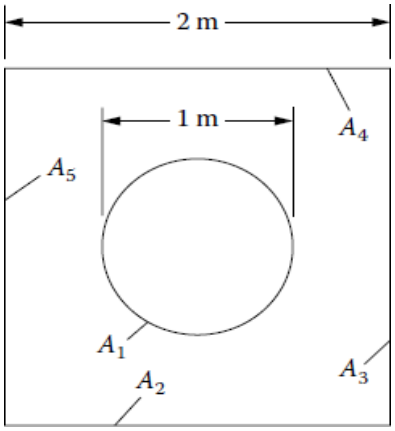

Surface	T(K)	Q (W/m)	ε
1	1100		0.4
2		0	0.5
3	0		1
4	0		1
5	0		1

Answer: $T_2 = 703$ K; $Q_1 = 100$ kW/m.

P.5.14 In a metal-processing operation, a metal sphere at uniform temperature is heated in a vacuum to high temperature by radiative exchange with a circular heating element. The surroundings are cool enough that they do not affect the radiative exchange and may be neglected. The surfaces are diffuse–gray. Derive an expression for the net rate of energy absorption by the sphere. The expression should be given in terms of the quantities shown. For simplicity, do not subdivide the surface areas. Discuss whether this is a reasonable approximation for this geometry with regard to the distribution of reflected energy from the sphere.

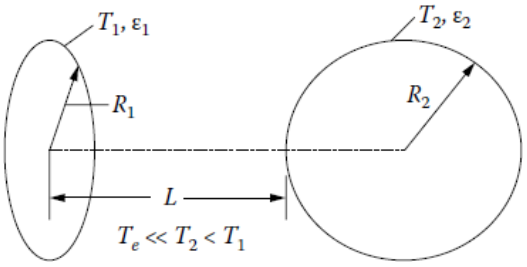

P.5.15 A 10 cm diameter hole extends through the wall of a furnace having an interior temperature of 1350 K. The wall is a 20 cm thick refractory brick. Divide the wall thickness into two zones of equal length and compute the net radiation out of the hole into a room at 300 K. (Neglect heat conduction in the wall.)

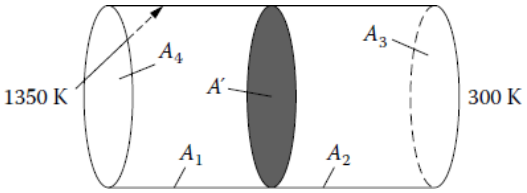

Answer: $T_1 = 1216$ K; $T_2 = 1033$ K; $Q_3 = -560$ W.

P.5.16 A cubical enclosure with edge length of 6 m has a very small sphere placed at its center ($A_{sphere} \ll A_{side}$). The sphere has emissivity $\varepsilon = 0.4$ and is maintained electrically at $T_s = 1300$ K. The interior walls of the cube have the following properties:

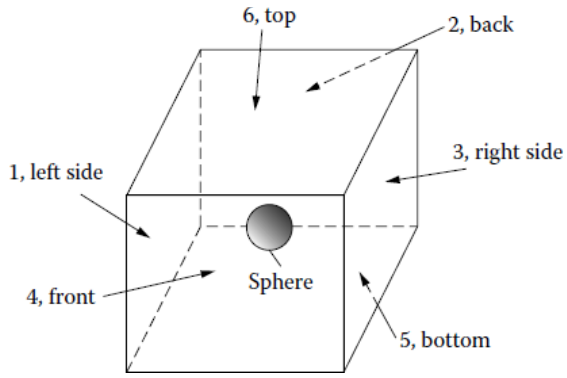

Side	Temperature (K)	Emissivity
1	1100	1.0
2	800	0.5
3	700	0.5
4	400	1.0
5	200	0.2
6	0	1.0

Determine the net q added or removed from each side of the cube and the q added to the sphere. Find the results in kW/m^2. Tabulate all the required configuration factors. (Assume the incident radiation on each surface is uniform.)

Answer: $q_1 = 69.9$ kW/m$_2$; $q_2 = -0.86$ kW/m^2; $q_3 = -6.10$ kW/m^2; $q_4 = -28.0$ kW/m^2; $q_5 = -5.11$ kW/m^2; $q_6 = -29.8$ kW/m^2; $q_s = 54.9$ kW/m^2.

P.5.17 A thin diffuse–gray circular disk with emissivity ε_1 on one side and ε_2 on the other side is being heated in a vacuum by a cylindrical electrical heater with a diameter D. The heater has a diffuse–gray interior surface and is open at both ends.

(a) Derive a formula (which can be in terms of configuration factors) for the net radiative energy rate being gained by the disk while it is being heated. The formula should be in terms of the instantaneous disk temperature and the quantities shown.

For the specific case, T_h = 1200 K; T_e = 300 K; D = 0.50 m; L = 0.80 m; d = 0.30 m; l = 0.10 m; ε_1 = 0.70; ε_2 = 0.85; ε_h = 0.80.

(b) What is the net gain (W) when T_d = 600 K?

(c) What is the equilibrium disk temperature long after the heater is turned on?

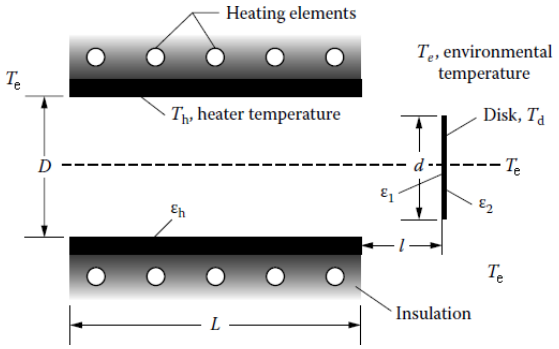

Net gain =

Answer: (a)

$$= \varepsilon_2\sigma\frac{\pi d^2}{4}\left(T_e^4 - T_d^4\right) - \frac{\varepsilon_1\pi d^2}{4}\frac{\left\{\begin{matrix}\sigma T_d^4\left[1-\left(1-\varepsilon_3\right)\left(F_{3-3}+F_{3-1}F_{1-3}\right)\right]-\varepsilon_3F_{1-3}\sigma T_3^4\\ +\sigma T_4^4\left[-F_{1-4}+\left(1-\varepsilon_3\right)\left(F_{3-3}F_{1-4}-F_{3-4}F_{1-3}\right)\right]\end{matrix}\right\}}{1-\left(1-\varepsilon_3\right)\left[F_{3-3}+F_{3-1}F_{1-3}\left(1-\varepsilon_1\right)\right]}$$

(b) 4010 W; (c) 902 K.

P.5.18 A hollow satellite in Earth orbit consists of a circular disk and a hemisphere. The disk is facing normal to the direction to the sun. The surroundings are at T_e = 20 K. The satellite walls are thin. All surfaces are diffuse. The properties are $\alpha_{1,\,solar}$ = 0.95; $\varepsilon_{1,\,infrared}$ = 0.13; ε_2(gray) = 0.80; ε_3(gray) = 0.50; ε_4(gray) = 0.60. What are the values of T_1 and T_4? (Do not subdivide surfaces. Neglect any emitted or reflected radiation from the Earth.)

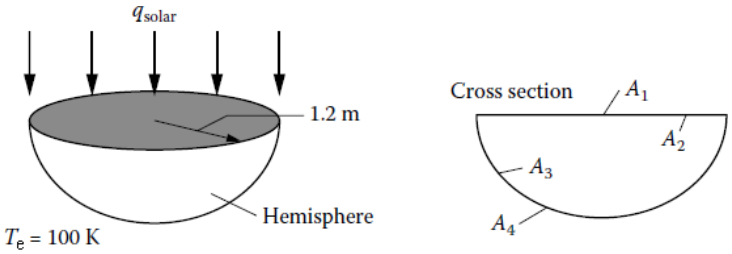

Answer: T_2 = 458 K; T_3 = 345 K.

P.5.19 A space vehicle in orbit around the sun is at the same distance as the Earth. It is a hollow cube with thin walls and is oriented with one side always facing directly toward the sun and the other five sides in the shade. The interior is painted with a coating with ε = 0.60. On the outside, the top is coated with a material with α_{solar} = 0.93 and ε = 0.80, the front and back sides are faced with aluminum foil with ε = 0.04, and the two sides and the bottom have white paint with ε = 0.80. The surroundings are at 0 K. Using as simple a radiation model as is reasonable, obtain the temperatures of the six faces of the cube.

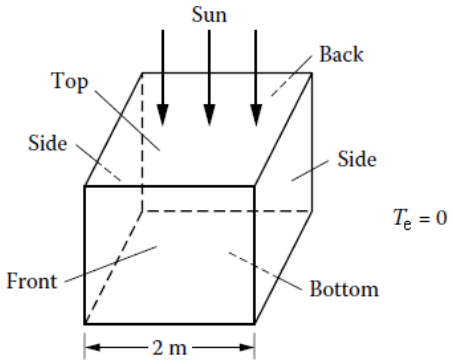

Answer: T_1 (top) = 367 K; T_2 (2 sides, bottom) = 234 K; T_3 (front and back) = 281 K.

P.5.20 Consider two parallel plates of finite extent in one direction. Both plates are perfectly insulated on the outside. Plate 1 is uniformly heated electrically with heat flux q_e. Plate 2 has no external heat input. The environment is at zero absolute temperature.

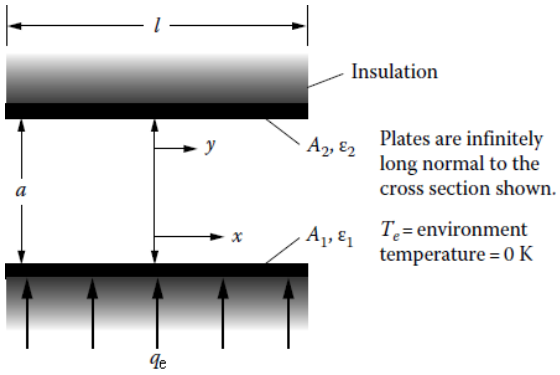

(a) For both plates *black*, show that the integral equations for the surface temperatures are

$$\theta_{b,1}(X) = 1 + \frac{1}{2}\int_{-L/2}^{L/2} \theta_{b,2}(Y)\frac{dY}{\left[(Y-X)^2+1\right]^{3/2}}$$

$$\theta_{b,2}(Y) = \frac{1}{2}\int_{-L/2}^{L/2} \theta_{b,1}(X)\frac{dX}{\left[(X-Y)^2+1\right]^{3/2}}$$

where $X = x/a$, $Y = y/a$, $\theta = \sigma T^4/q_e$, and $L = l/a$.

(b) If both plates are *gray*, show that $\theta_1(X) = \theta_{b,1}(X) + \dfrac{1-\varepsilon_1}{\varepsilon_1}$; $\theta_2(Y) = \theta_{b,2}(Y)$.

P.5.21 A long groove is cut into a metal surface as shown in the following cross section. The groove surface is diffuse–gray and has emissivity ε. The temperature profile along the groove sides, as measured from the apex, is found to be $T(x)$. The environment is at temperature T_e.

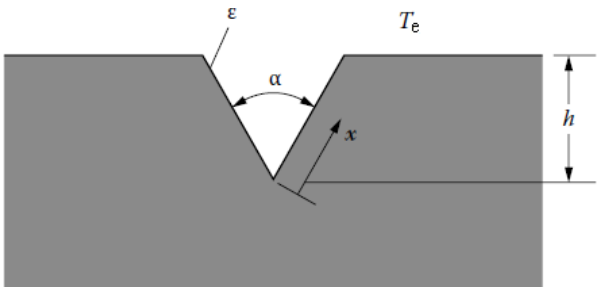

(a) Derive the equations for the heat flux distribution $q(x)$ along the groove surface.

(b) Examine the kernel of the integral equation found in part (a) and show whether it is symmetrical and/or separable.

P.5.22 A hemispherical cavity is in a block of lightly oxidized copper ($\varepsilon_1 = 0.57$) maintained at 800 K in vacuum. The surroundings are at 300 K. Use the integral equation method to compute the outgoing heat flux from the cavity surface.

Answer: 27,140 W/m^2.

P.5.23 A cavity having a gray interior surface S is uniformly heated electrically and achieves a surface temperature distribution $T_{w,0}(S)$ while being exposed to a zero absolute temperature environment, $T_e = 0$. If the environment is raised to T_e and the heating kept the same, what is the surface temperature distribution?

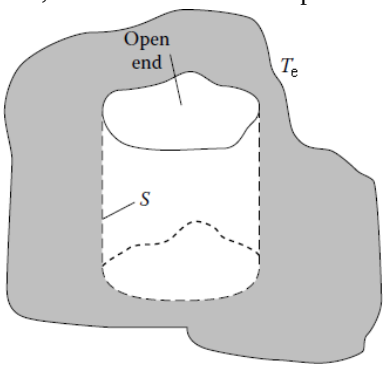

Answer: $T_{w,0}(r) = \left[T_w^4(r) - T_e^4\right]^{1/4}$, where $T_{w,0}(S) = T_w(S, T_e = 0)$.

P.5.24 A gray circular tube insulated on the outside is exposed to an environment at $T_e = 0$ at both ends. The $q(x, T_e = 0)$ has been calculated to maintain the wall temperature at any constant value. Now, let $T_e \approx 0$, and let the wall temperature be uniform at T_w. Show that the $q(x, T_e \neq 0)$ can be obtained as the $q(x, T_e = 0)$ corresponding to the wall temperature $(T_w^4 - T_e^4)^{1/4}$.

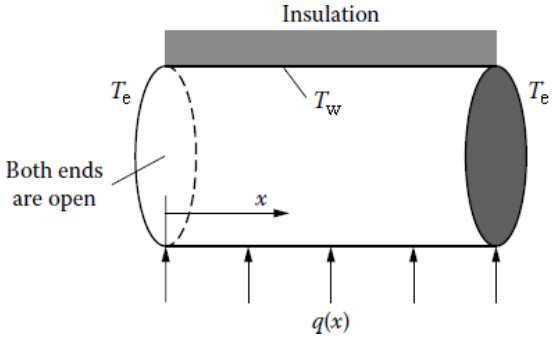

P.5.25 Two infinitely long plates are joined at right angles along one infinite edge. The plates are each of width W, and both have diffuse–gray surfaces with the same emissivity ε. The heat flux supplied to both surfaces is maintained at a uniform value q. Derive an equation for the temperature distribution on each surface and describe

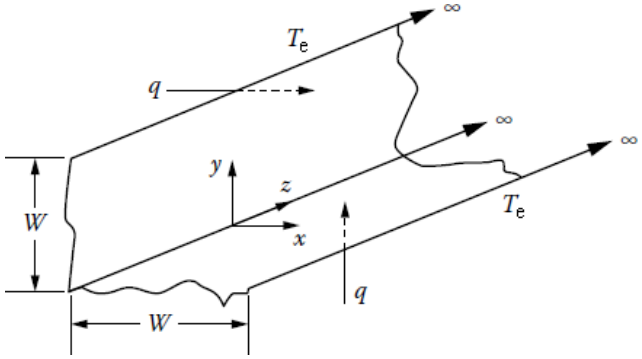

how you would solve for $T(x)$ and $T(y)$. Neglect conduction in the plates and convection to the atmosphere. The surroundings are at temperature T_e.

P.5.26 For the geometry and conditions shown in Problem P.5.25, solve for the unknown distributions of temperature $T_1(y)$ and net radiative heat flux $q_2(x)$ and plot the results.

P.5.27 For the geometry and conditions shown in the following, set up the required integral equations for finding $q_1(y)$, $T_2(z)$, and $T_3(x)$. Put the equations in dimensionless form and discuss how you would go about solving the equations. Which method of Chapter 5 appears most useful?

$T_1(y) = T_1$ = constant; $q_2(z) = 0$ (insulated on the outside); $q_3(x) = q_3$ = constant; $\varepsilon_1(y) = 1.0$; $\varepsilon_2(z) = \varepsilon_3(x) = 0.5$

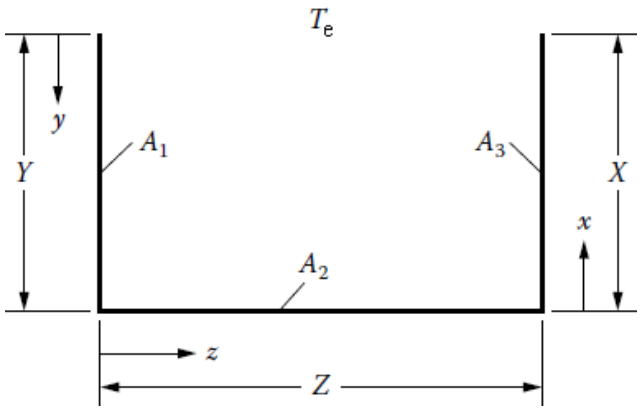

P.5.28 A four-surface enclosure has the properties and temperatures shown in the following. Find the heat flux for each surface and demonstrate that the radiative heat balance is satisfied. Assume that radiosities can be taken as uniform across each surface.

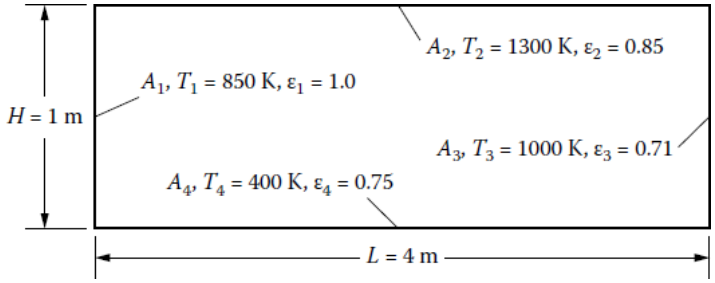

Answer: $q_1 = -54{,}690$ W/m; $q_2 = 108{,}100$ W/m; $q_3 = -16.620$ W/m; $q_1 = -90{,}230$ W/m.

P.5.29 A very long A-frame grain dryer is built with the cross section of an isosceles triangle with the dimensions shown in the following. For solar heating, the right opaque side is exposed to the sun and is black, the left side is insulated. At a particular time, the conditions for the inside surfaces of the dryer are as shown in the table.

(a) What will be the floor temperature T_3 (K)?

(b) What will be the temperature of the insulated wall T_2?

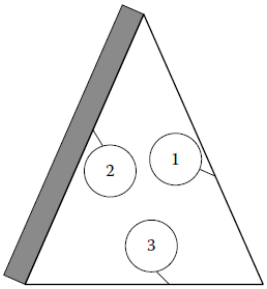

Surface	L (m)	T (K)	q (W/m²)	ε
1	5	450		1.0
2	5		0	0.537
3	3.5		−600	0.35

Answer: (a) 304 K; (b) 437 K.

P.5.30 A radiator is planned to provide heat rejection from a nuclear power plant that is to provide electrical power for a lunar outpost. The radiator will itself will be horizontal on the lunar surface, and condensing working fluid in the power cycle will maintain the uniform surface temperature of the radiator at 800 K. The radiator is

shielded from the nearby lunar outpost by a 1.5 m high vertical insulated plate (see diagram on the next page). The width of the radiator is limited to 2 m. The radiator has a diffuse–gray emissivity of 0.92, while the insulated shield has an emissivity of 0.37. It is expected that the radiator will be quite long. Conduction within the radiator and heat shield can be neglected. For the situation when the radiator is on the night side of the moon,

(a) Set up the equations for finding the heat flux distribution on the radiator, $q_1(x)$, and the temperature distribution on the shield, $T_2(y)$. Note any assumptions.

(b) Solve the equations for $q_1(x)$ and $T_2(y)$. Show that the increment size chosen for solution is small enough that the solutions are grid independent.

(c) If the total heat rejection from the radiator is required to be 1.0 MW, what must be the length of the radiator (m)?

(d) Discuss how the results would change if the influence of incident solar energy on the radiator during daytime is considered.

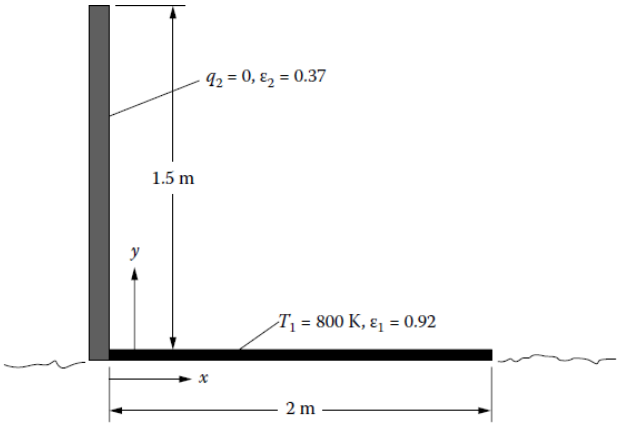

Answers: $T_2(y = 1.5\text{ m}) = 525$ K; $T_2\ (y = 0) = 662$ K; $q_1(x = 0) = 16.5$ kW/m^2; $q_1(x = 2\text{ m}) = 20.8$ kW/m^2; length of radiator = 47.2 m.

Chapter 6:

P.6.1 Two large diffuse parallel plates are maintained at the temperatures T_1 = 1400 K and T_2 = 700 K. The plates are made from the same metal, and their spectral emissivities as a function of wavelength, ε_λ, are approximated as shown by two constant values joined by a linear decrease with wavelength. Compute the net radiant energy flux being transferred from plate 1 to plate 2. What is the energy flux if both plates are assumed gray with an approximate average emissivity of 0.5 applied over the entire spectral range?

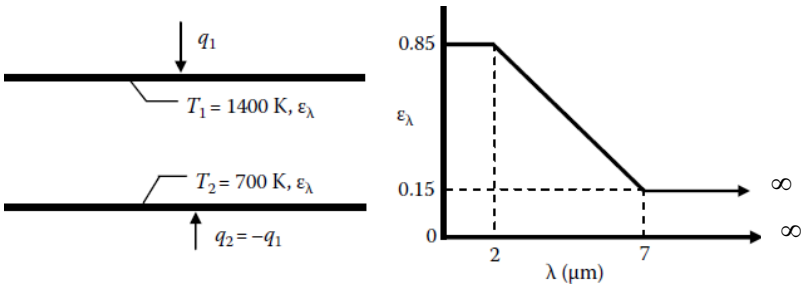

Answer: q_1 = 106,850 W/m^2; $q_{1,gray}$ = 68,073 W/m^2.

P.6.2 Radiation is being transferred across the space between two large parallel plates. Both plates are made of the same metal, and the spectral emissivity of the metal does not depend on temperature. The wavelength variation of the emissivity for both plates is approximated in three steps as shown. The lower plate is maintained at T_2 = 700 K, and the upper plate has a uniform heat addition of q_1 = 60 kW/m^2. What is the temperature, T_1, of the upper plate?

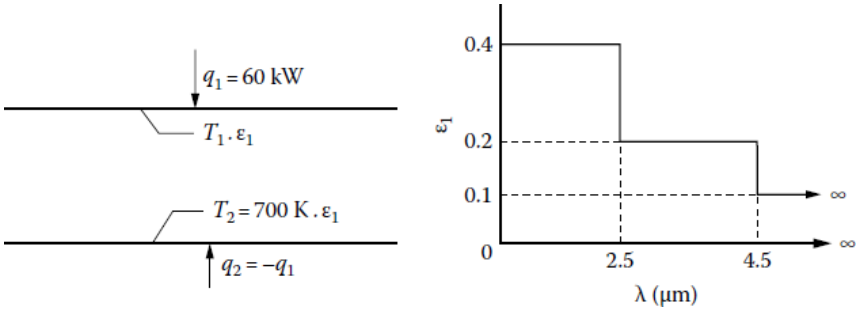

Answer: 1594 K

P.6.3 Consider the enclosure of Homework Problem 5.9 with three walls at different specified temperatures. Compute the radiative heat transfer for the indicated values of hemispherical spectral emissivity. (For simplicity, do not subdivide the three areas into smaller regions.)

Answer: q_1 = 18,480 W/m^2; q_2 = - 24,190 W/m^2; q_3 = - 301 W/m^2.

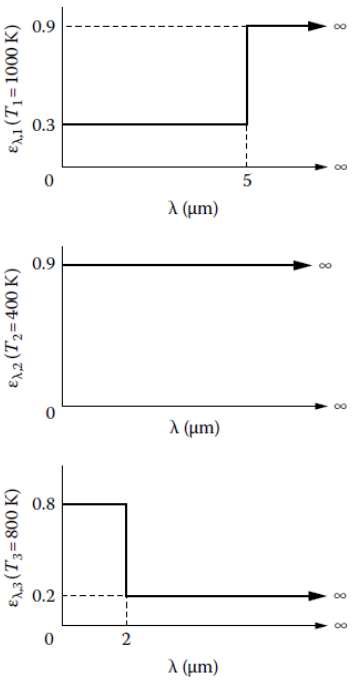

P.6.4 Two parallel plates are of finite width and of infinite length in the direction normal to that shown. The plates are diffuse, but their spectral emissivity varies with wavelength and is approximated by a step function as shown. Both plates are made of the same material, and hence have the same emissivity which is independent of temperature. The plate edge openings are exposed to the environment at T_e = 350 K, and there is energy exchange only from the internal surfaces. Energy is being added to the lower plate, and the upper plate is maintained at a fixed temperature. Obtain values for the temperature of the lower plate, T_1, and for the heat flux q_2 that must be added or removed from the upper plate to maintain its specified temperature. For simplicity, do not subdivide the surface areas.

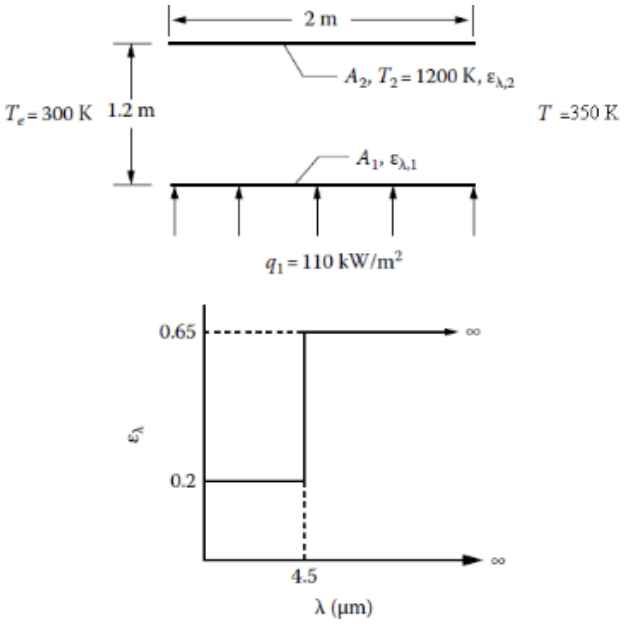

Answer: 1709 K; - 6722 W/m^2.

P.6.5 A sphere and area element are positioned as shown. The sphere is gray but has a nondiffuse emissivity $\varepsilon_s = \mu \cos\theta$, where θ is the angle measured from the normal to the sphere surface and μ is a constant. Set up the integral for the direct radiation from the sphere to the area element in terms of the quantities given.

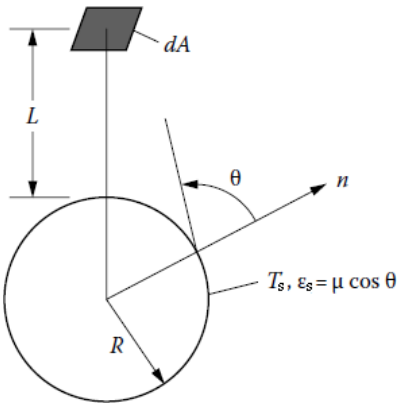

P.6.6 Obtain the result for $F_{1\text{-}1(2)}$ in Example 6.11 by using the crossed-string method. What is $F_{1\text{-}1(2)}$ if A_1 in Figure 6.23 is rotated 45° about its center point? (The geometry remains two-dimensional.)

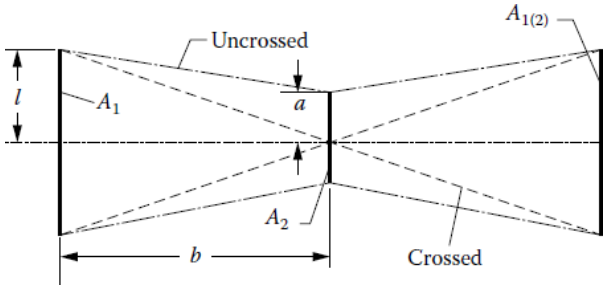

Answer: First part: $F_{1-1(2)} = \left(\sqrt{1+b^{*2}} - \sqrt{(1-a^*)^2 + b^{*2}}\right)$

Second part: $F_{1-1(2)} = \frac{1}{2}\left[2\left(b^{*2}+1/2\right)^{1/2} - \left(\sqrt{a^{*2}+b^{*2}+1-(a^*+b^*)\sqrt{2}} + \sqrt{a^{*2}+b^{*2}+1-(a^*-b^*)\sqrt{2}}\right)\right]$ where a*= a/ *land b** = *b/ l.*

P.6.7 In Figure 6.25, the image $A_{2(3\text{-}4)}$ is shown as a dotted horizontal line on the lower right-hand side of the image diagram. By a suitable construction of rays (actual and through image surfaces) similar to the one shown in the text, show whether $A_{2(3\text{-}4)}$ is where Figure 6.25 indicates it to be.

P.6.8 An equilateral triangular enclosure of infinite length normal to the cross-section shown has black surfaces A_1 and A_2 and a specularly reflecting surface A_3 with reflectivity $\rho_{s,3} = 0.6$. Find the values of $F^S_{1\text{-}1}$, $F^S_{1\text{-}2}$ and $F^S_{1\text{-}3}$.

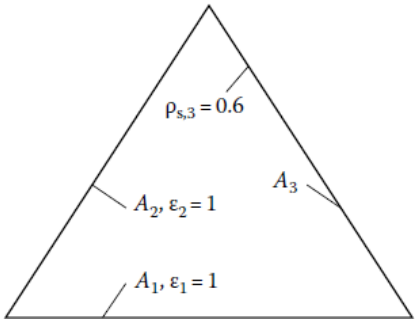

Answer: 0.0938; 0.7562; 0.5000.

P.6.9 (a) What is the value of the sum of the specular configuration factors $\sum_{j=1}^{N} F^S_{1-j}$ for Homework Problem 6.8?

(b) What is the value of the summation $\sum_{j=1}^{N}\left(1-\rho_{s,j}\right)F^S_{1-j}$ for Homework Problem 6.8?

(c) Explain the results of parts (a) and (b) in terms of the definition of $F^S_{1\text{-}j}$. Is the result of part (b) a general relation for all specular enclosures?

Answer: (a) 1.30; (b) 1.00.

P.6.10 An enclosure is made up of three sides as shown. The length L is sufficiently long that the triangular ends can be neglected in the energy balances. Two of the surfaces are black, and the other is a diffuse-gray emitter with emissivity $\varepsilon_1 = 0.10$. What is the energy added, per meter along the length L, to each surface because of radiative exchange within the enclosure for each of the two cases:

(a) area 1 is a diffuse reflector.
(b) area 1 is a specular reflector.

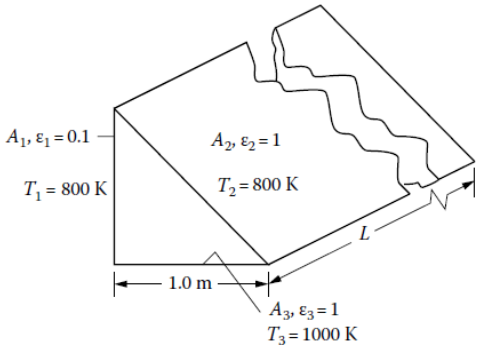

P.6.11 A triangular enclosure has the conditions shown below. Side 3 is a specular reflector.

a) Derive relations for T_1^4, q_2 and q_3.

b) Prove that $q_2 A_2 = - q_3 A_3$.

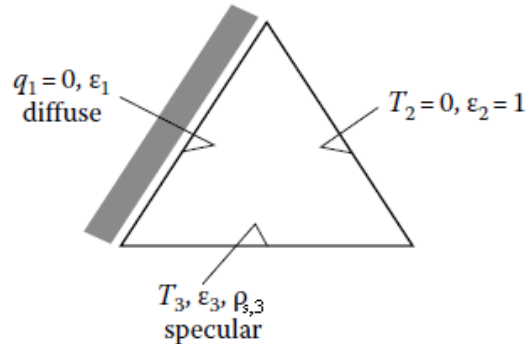

Answer: $T_1^4 = \dfrac{\varepsilon_3 T_3^4 F_{1-3}}{1-\rho_{s,3}F_{1(3)-1}}$; $q_2 = -\varepsilon_3 \sigma T_3^4 \left(\dfrac{F_{1-3}}{1-\rho_{s,3}F_{1(3)-1}} F^s_{2-1} + F_{2-3} \right)$; $q_3 = \varepsilon_3 \sigma T_3^4 \left(1 - \dfrac{\varepsilon_3 F_{1-3}}{1-\rho_{s,3}F_{1(3)-1}} F_{3-1} \right)$.

P.6.12 A two-dimensional rectangular enclosure has gray interior surfaces that are all diffuse emitters. Two opposing surfaces are specular reflectors, while the other two reflect diffusely. Write the set of energy equations to determine Q_1, Q_2, Q_3, and Q_4, including the expressions for the F^S factors in terms of the configuration factors F. (Note: Each F^S will consist of an infinite sum.)

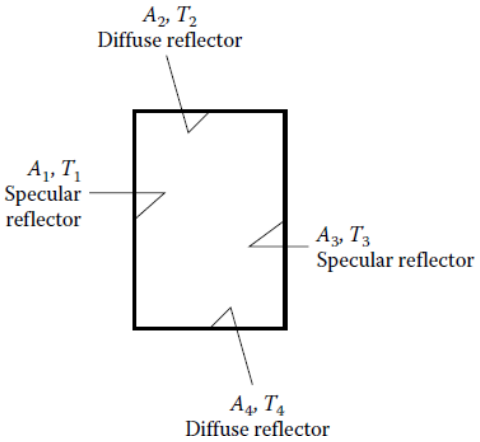

P.6.13 Two parallel plates of unequal finite width are facing each other. The lower plate is diffuse-gray, and the upper plate is a specular reflector and is gray. The geometry is long in the direction normal to the cross section shown, so the configuration is two-dimensional. The lower plate is uniformly heated from below so the energy supplied is radiated away from only its upper surface. The upper plate has its upper surface cooled so its lower surface (the specular reflector) is maintained at 600 K. The surroundings are at 400 K. For simplicity, do not subdivide the plate areas.

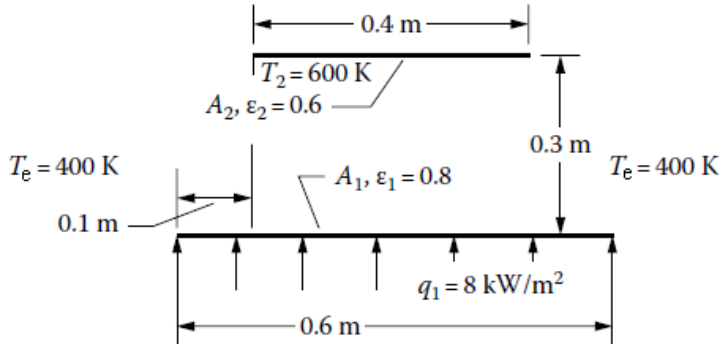

(a) Obtain the temperature of the lower plate and determine what heat flux must be extracted from the upper plate to maintain its specified temperature.

(b) The surface A_2 on the upper plate is now roughened to make it a diffuse reflector, without changing its emissivity. How much will this change the temperature of the lower plate?

Answer: (a) $T_1 = 712.8$ K, $q_2 = -939$; (b) $T_1 = 708.8$ K (4.0 K decrease), $q_2 = -810.2$ W/m^2.

P.6.14 A diffuse plate A_1 that is not heated or cooled by external means is facing a larger plate as shown. The spacing between the plates is small. The plates are long in the direction normal to the cross section shown, so the geometry is two-dimensional. The upper plate is gray and is a specular reflector. It is cooled to 300 K. The environment is at a higher temperature, 550 K, so that radiant energy is reflected into the space between the plates. For simplicity, do not subdivide the plate areas.

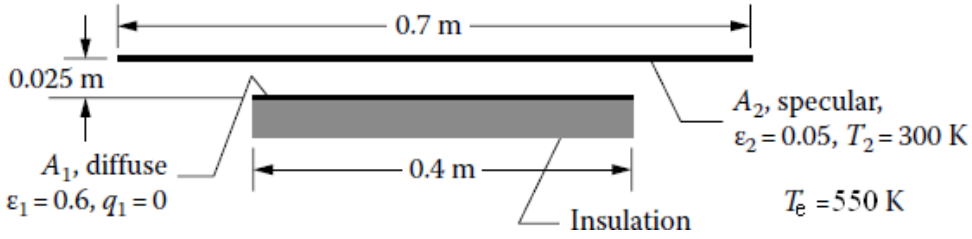

(a) What is the temperature of the lower plate A_1?

(b) If A_2 on the upper plate is made diffuse without changing its emissivity, how much is the temperature of the lower plate changed?

Answer: (a) $T_1 = 506$ K; (b) $T_1 = 537$ K (a 31 K increase).

P.6.15 Two parallel plates shown in Homework Problem P.5.20 are of finite width (infinite length normal to the cross-section). Both plates are perfectly insulated on the outside. Plate 1 is uniformly internally heated electrically with heat flux q_e. Plate 2 has no externally supplied heat input ($q_2 = 0$). The environment is at zero temperature. Plate 1 is black, while plate 2 is a diffuse-gray emitter and specular reflector with emissivity ε_2. Derive an integral equation formulation for the surface temperature distributions. Compare with the formulation in Homework Problem P.5.20.

P.6.16 A shield system of *N* large closely spaced flat-plate thin shields with all shield surfaces of emissivity ε_s is placed between an outer surface at T_1 with emissivity ε_1 and another surface at T_2 with emissivity ε_2. Derive an expression for the heat flux *q* between surfaces *1* and *2*.

Answer: $$q = \frac{\sigma\left(T_1^4 - T_2^4\right)}{\left(\frac{1}{\epsilon_1} + \frac{1}{\epsilon_2} - 1\right) + N\left(\frac{2}{\epsilon_s} - 1\right)}.$$

P.6.17 Two large plane parallel surfaces A_1 and A_2 are separated by 80 radiation shields having an $\varepsilon_s = 0.040$ coating on both sides. However, by accident, 15 of the shields were coated on only the upper side. The $\varepsilon_s = 0.85$ for the uncoated sides. What is the rate of heat transfer for the defective system, and how does it compare with the heat flow rate when none of the shields are defective (all are coated on both sides)? All surfaces are gray. Give heat flow rates in W/m^2.

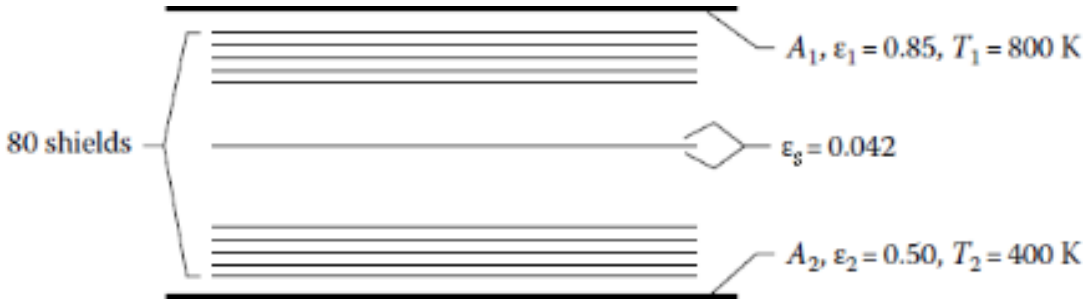

Answer: 5.55 W/m^2; 6.11 W/m^2; 10% increase.

P.6.18 A long rectangular enclosure is shown in cross-section (two-dimensional geometry). The interior surfaces 1 and 4 are diffuse-gray with specified wall temperatures. A group of N thin diffuse-gray radiation shields is placed on the diagonal. Derive an algebraic expression for the heat flow Q from the surfaces at T_1 to those at T_4 in terms of the quantities given. Evaluate the result for $\varepsilon_1 = 0.79$, $\varepsilon_4 = 0.20$, $\varepsilon_s = 0.10$, H = 1.20 m, W = 0.90 m, N = 6, $T_1 = 600$ K, $T_4 = 400$ K, and for 1 m of length in the third dimension.

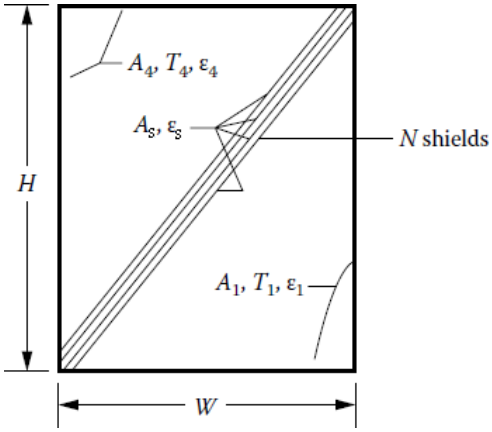

Answer: $Q = \dfrac{A_2\sigma\left(T_1^4 - T_4^4\right)}{\dfrac{A_2}{A_1}\left(\dfrac{1}{\varepsilon_1} + \dfrac{1}{\varepsilon_4} - 2\right) + 1 + N\left(\dfrac{2}{\varepsilon_s} - 1\right)}$ =74.9 W.

Chapter 7:

P.7.1 Consider the fin in Example 7.3 and in the further development in Equation 7.5 that follows the example. The environment temperature is nonzero at T_e. The diffuse fin now has more general spectral properties such that the spectral emissivity is ε_λ. However, it is assumed that ε_λ can be approximated as independent of temperature.

(a) Write the energy balance that now applies of the type in Equation 7.5.
(b) Put the equation in dimensionless form like Equation 7.3.2, using the same parameters where possible.
(c) Discuss how to best obtain the solution for T(x), and how to present the results. Discuss whether the results with $T_e \neq 0$ can be related to those for $T_e = 0$.

P.7.2 Assume the fin in Example 7.6 extends from a black plane surface at T_b that is very large compared with the fin length. How would the fin formulation be modified to account for the interaction between the fin and the base surface?

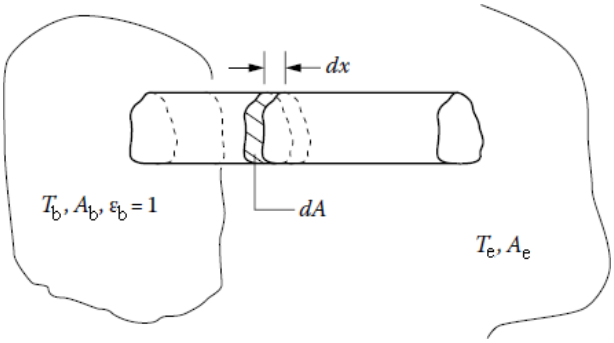

P.7.3 Two thin vertical posts stand immediately adjacent to a pool of molten material at temperature T_m and are diametrically across the pool from each other. The posts have a square cross-section of area A_x, are of length L, and have thermal conductivity k. The entire surface of the posts has emissivity ε. The pool is of radius r and is assumed to be black. A breeze blows across the posts, and the air has temperature T_a. The air motion produces a heat transfer coefficient h between the post surface and the air.

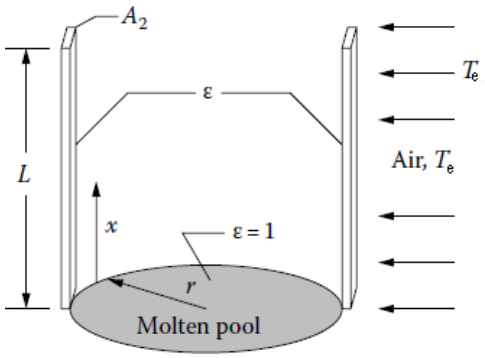

Derive an equation for the temperature distribution T(x) along the posts, including the effect of mutual radiative exchange by the posts. Assume that the temperature at the bottom of the posts is equal to the temperature of the molten pool. Also, assume that the effect of the temperature of the surroundings T_e on radiative transfer can be neglected. Show the necessary boundary conditions for the problem and relations for all of the required configuration factors. (You do not need to substitute the F's into the equation, however.)

P.7.4 How would the analysis in Homework Problem P.7.3 be modified to include the effect of a non-zero environment temperature?

P.7.5. An infinitely long enclosure is shown in cross-section below. It is separated into two compartments by a conducting plate with thermal conductivity k = 45 W/m•K. The properties and conditions on the enclosure surfaces are shown in the table. The vertical ends are at specified temperatures, and the horizontal sides are insulated on the outside.

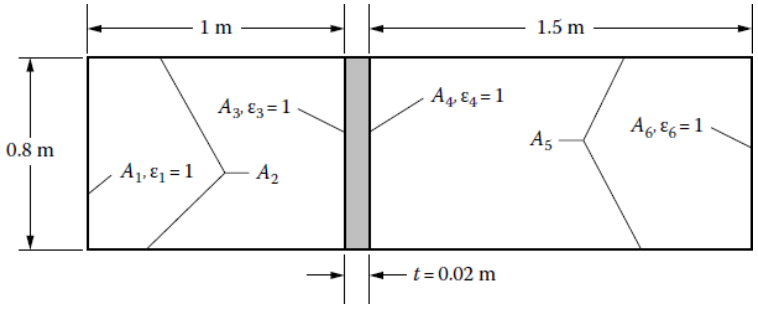

Surface	Emissivity, ϵ	Net heat flux, q (W/m^2)	Temperature, K
1	1.0		1800
2	0.1	0	
3	1.0		
4	1.0		
5	0.3	0	
6	1.0		200

Determine the values of the missing table entries. Assume for simplicity that the surfaces need not be subdivided.

Answer: $q_1 = q_4 = -q_3 = -q_6 = 87{,}667$ W/m^2, $T_2 = 1749$ K, $T_3 = 1693$ K, $T_4 = 1254$ K, and $T_5 = 1055$ K.

P.7.6 Thin wire is extruded at fixed velocity through a die at temperature T_0. The wire then passes through air at T_a until its temperature is reduced to T_L. The heat transfer coefficient to the air is h, and the wire emissivity is ε. It is desired to obtain the relation between T_L and T_0 as a function of wire velocity V and distance L. Derive a differential equation for wire temperature as a function of distance from the die and state the boundary conditions. (*Hint:* Compute the energy balance for flow in and out of a control volume fixed in space.)

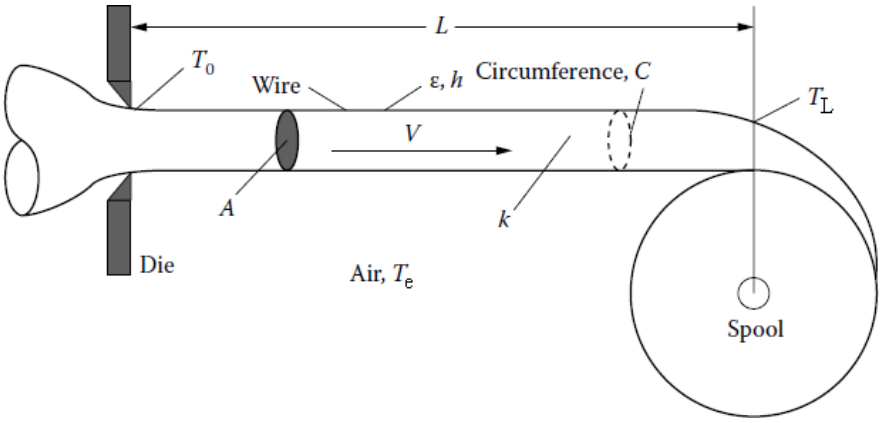

P.7.7 A single circular fin is to dissipate energy from both sides in a vacuum to surroundings at low temperature. The fin is on a tube with 2-cm outer diameter. The tube wall is maintained at 750 K by vapor condensing on the inside of the tube. The fin has 20 cm outer diameter and is 0.30 cm thick. Estimate the rate of energy loss by radiation from the fin if the fin is made from stainless steel [k = 35 W/(m•K)] with a clean surface ($\varepsilon = 0.15$). What is the effect on energy dissipation of increasing the fin thickness to 0.60 cm?

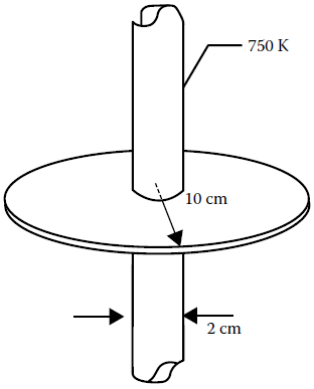

Answer: (c) 65 W; 91.2 W.

P.7.8 The billet in Homework Problem P.5.1 has air at 27°C blowing across it that provides an average convective heat transfer coefficient of $\bar{h}=24\ W/(m^2 \cdot K)$. Estimate the cooling time with both radiation and convection included.

Answer: 4.47 hours.

P.7.9 Opaque liquid at temperature T(0) and mean velocity $\bar{u}$ enters a long tube that is surrounded by a vacuum jacket and a concentric electric heater that is kept at uniform axial temperature T_e. The heater is black, and the tube exterior is diffuse-gray with emissivity ε. The convective heat transfer coefficient between the liquid and the tube wall is h, and the tube wall thermal conductivity is k_w. Derive the relations to determine the mean fluid temperature and the tube wall outer surface temperature as a function of distance x along the tube (assume that the liquid properties are constant).

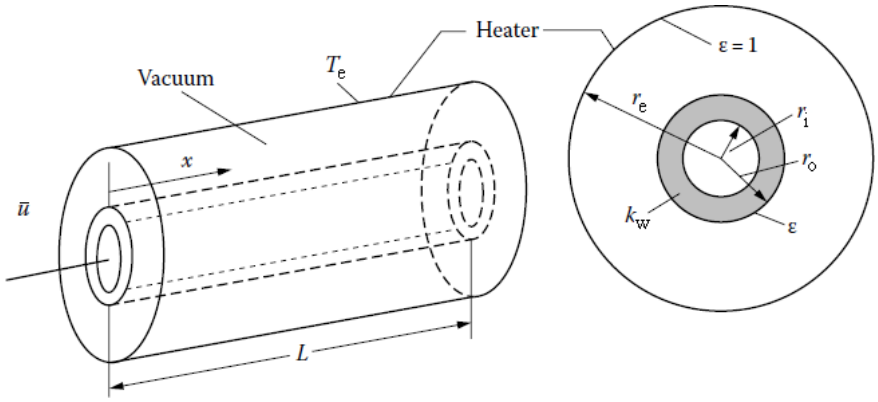

P7.10 A solar collector is designed to fit onto the horizontal section of a roof as diagrammed below. Flow is from the right to the left in the tubes of the collector. A tilted white diffuse roof section at the left side helps to reflect additional solar flux onto the collector. Set up the equations for determining the local temperature of the tubes for two cases: (a) no flow in the tubes, and (b) flow of water in each tube of 2.00 kg/min. Indicate a possible solution method. Assume that the roof and collector are very long normal to the cross section shown.

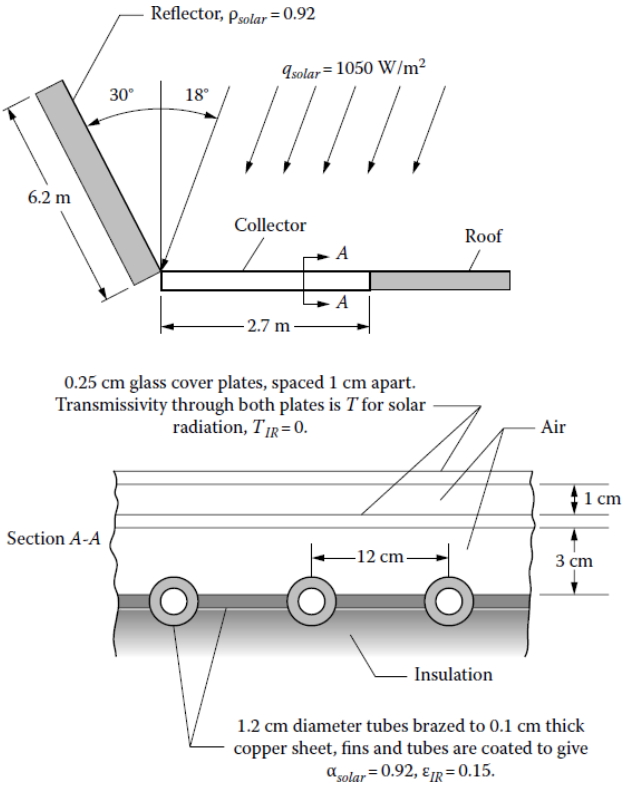

P.7.11 A radio antenna extends normal to a spacecraft surface as shown in the diagram below. The antenna has a circular cross section with diameter D=1 cm. The spacecraft itself is very large, and its surface can be considered to be black with uniform temperature T_b=500K. The environment is at T ≈ 0 K. The antenna material has emissivity =ε(gray, diffuse) and thermal conductivity k = 40W/(m·K).

(a) Derive the differential equation for the temperature distribution in the antenna, T(x). Note any assumptions. Include the effect of radiation exchange between the antenna and the spacecraft.

(b) Place the equation in a convenient nondimensional form, using the nondimensional temperature $\mathcal{G}(X)=T(X)/T_b$, and X = x/L.

(c) Provide a plot of $\mathcal{G}(X)$ vs. X for ε = 0.3, 0.5, and 1.0.

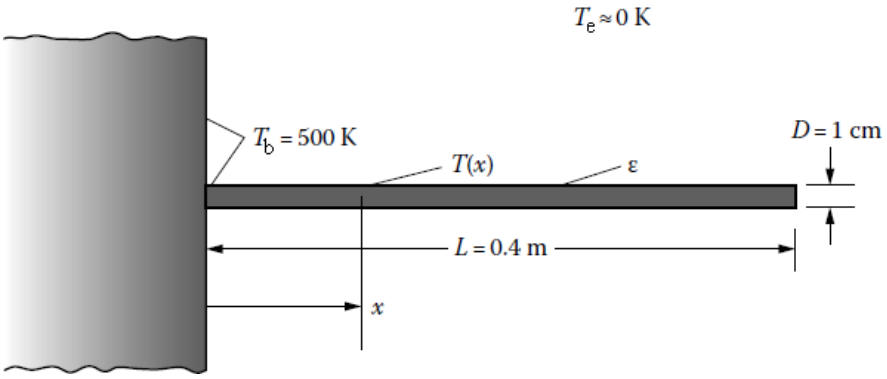

P.7.12 Evaluate numerically the configuration factor between two infinitely long parallel plates of equal finite width joined along one edge and making an angle of 45°. Use a numerical integration of the analytical integral form in Example 4.6 using the trapezoidal rule (this Appendix, Section I) to obtain the result and compare it with the exact solution.

Answer: 0.61732.

P.7.13 Evaluate numerically the configuration factor between two infinitely long parallel plates of equal finite width joined along one edge and making an angle of 45°. Use a numerical integration of the analytical integral form in

Example 4.6 using Simpson's Rule (this Appendix, Section I) to obtain the result and compare it with the exact solution.

Answer: 0.61732

P.7.14 A long gray empty circular tube is in the vacuum of outer space so that the only external heat exchange is by radiation. The metal tube is coated with a material that has a solar absorptivity α_S and an emissivity in the infrared region of ε_{IR}. The solar flux q_S is incident from a direction normal to the tube axis, and the surrounding environment is at a very low temperature T_e that can be neglected in the radiative energy balances. The geometry is as shown in cross-section. The tube is empty so there is internal radiative exchange. Energy is conducted circumferentially within the tube wall. The wall thermal conductivity is k_w.

(a) Set up the energy relations required to obtain the temperature distribution around the tube circumference assuming that radial temperature variations within the tube wall can be neglected.

(b) Place the energy relations in finite difference form and describe how a numerical solution can be obtained.

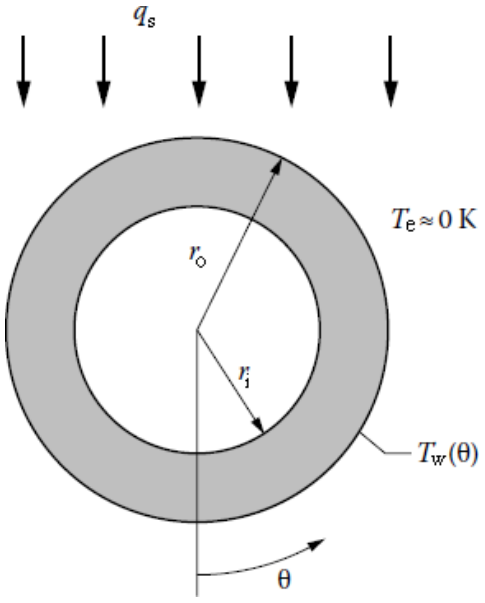

P.7.15 The tube in Homework Problem P.7.14 is shielded from solar radiation by being in the shadow of a space vehicle, so that it cools to a very low temperature. It is then suddenly exposed to the solar flux. Set up the transient energy relations required to calculate the tube circumferential temperature distribution as a function of time using the same conditions and assumptions as in Homework Problem 7.14. Place the equations in finite difference form and describe how a numerical solution can be obtained.

P.7.16 A thin sheet of copper moves through a radiative-convective oven at a velocity of 0.1 m/s. The sheet and oven are very wide. Air flows at a mass flow rate of 0.2 kg/s per meter of oven width over the sheet in counterflow, and the heat transfer coefficient between the air and sheet surface is constant along the sheet at a value of h = 100 W/(m^2•K). The back of the sheet is insulated. A black radiant heater at T_{Heater} = 1200 K covers the top of the oven as shown. The radiant heater does not interact convectively with the air stream. Louvered curtains at each end of the oven are opaque to radiation but allow air flow. The emissivities of all surfaces are shown.

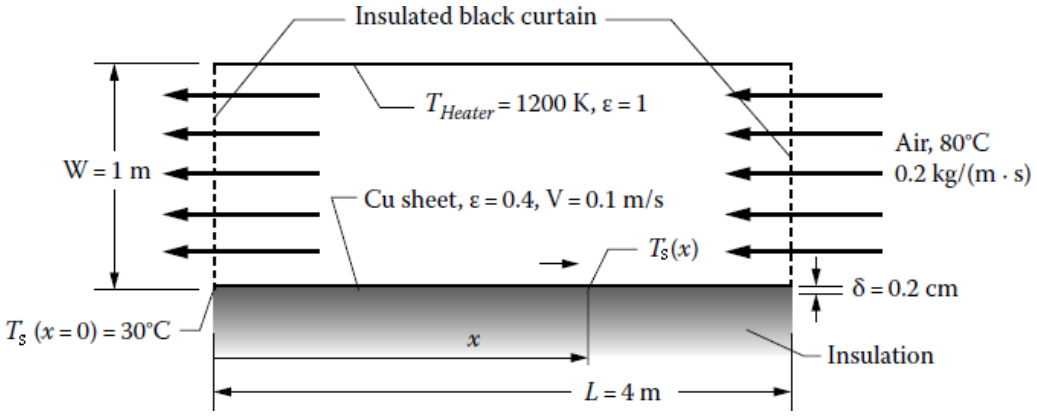

Find the temperature distribution $T_S(x)$ along the copper sheet as a function of position x within the oven and present the result graphically. Discuss all assumptions made in the solution and justify them by numerical argument where possible. Data for copper sheet: k_s = 400 W/(m•K); $c_{p,s}$ = 385 J/(kg•K); ρ_s = 9000 kg/m^3.

P.7.17 For the geometry shown below with one conducting wall:

a) Provide the final governing equations necessary for finding $T_1(x_1)$ and $q_2(x_2)$ in nondimensional form using appropriate nondimensional variables.

b): Find the temperature distribution $T_1(x_1)$ and the heat flux distribution $q_2(x_2)$ and show them on appropriate graphs.

Boundary conditions are $q_1(x_1) = \left[100x_1 - 50x_1^2\right](\text{kW/m}^2)$ where x_1 is in meters, T_2=500 K, and T_3 = T_4 = 300K. Properties for the diffuse surfaces are shown on the figure.

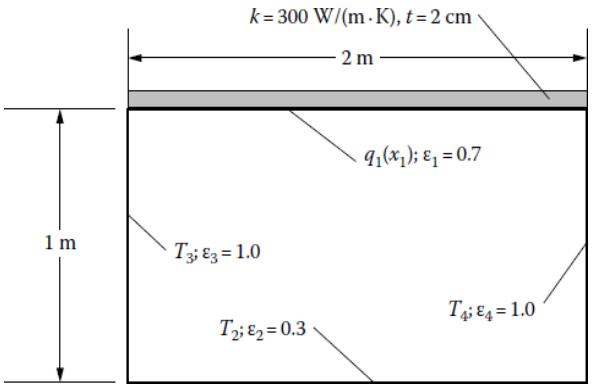

Show that your solution is grid-independent, and meets overall energy conservation. Compare your solution to the results for the nonconducting case.

Answer: T_1(max) = 1117.7 K with no conduction, T_1(max) = 1102.1 K with conduction, and q_2(max) = ~ -10,100 W/m^2 with no conduction and q_2(max) = ~ -9,700 W/m^2 with conduction.

Chapter 11:

P.11.1 A plane layer of semitransparent medium without scattering is at a uniform temperature of T_m = 950 K. The layer is 0.28 m thick. The medium has three absorption bands with constant absorption coefficients $\kappa_{\lambda 1}$ = 5.5 m^{-1}, $\kappa_{\lambda 2}$ = 4.6 m^{-1}, and $\kappa_{\lambda 3}$ = 3.8 m^{-1} in the wavelength bands from 1.3 to 3.1 μm, 3.65 to 5.05 μm, and 5.95 to 8.5 μm. For the remainder of the spectrum, the medium is perfectly transparent. One boundary of the layer is in contact with a black source at T_w = 1030 K. Calculate the intensities leaving the layer at the other boundary in the normal direction, 30° from the normal, and 60° from the normal.

Answer: I(x=0.28 m, θ=0°) = 10458 W/(m^2·sr);

I(x=0.28 m, θ=30°) = 10262 W/(m^2·sr); I(x=0.28 m, θ=60°) = 9699.1 W/(m^2·sr).

P.11.2 A large absorbing semitransparent medium without scattering has a single plane boundary. A black plate with constant temperature of T = 1250 K is suddenly placed in contact with that boundary. The plate radiates into the medium, which is cool enough that it does not radiate. Determine the radiative energy source $-\nabla \cdot \mathbf{q}_r$ at a location x = 0.82 m into the medium from the plane boundary if the absorption coefficient of the medium is κ = 0.75 m^{-1}.

.*Answer*: 55960 W/m^3.

P.11.3 A semi-infinite medium is absorbing, emitting, and isotropically scattering. It is gray, has n ≈ 1, and has absorption coefficient κ and scattering coefficient σ_s. The medium is initially at uniform temperature T_i. The transparent plane surface of the medium is suddenly subjected to radiative exchange with a large environment at a lower uniform temperature T_e. It is proposed to carry out a numerical solution to obtain the transient temperature distributions in the medium as it cools. Provide the energy and scattering equations in a convenient dimensionless form that are then to be placed in numerical form for solution. Include heat conduction and assume the medium is stationary. The density ρ, specific heat c, and thermal conductivity k of the medium are assumed constant.

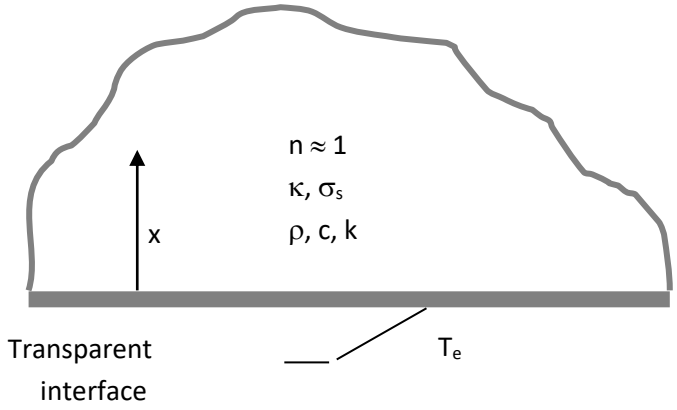

P.11.4 A furnace at atmospheric pressure with interior in the shape of a a cylinder with height equal to two times its diameter is filled with a 50:50 mixture by volume of CO_2 and N_2. The furnace volume is 0.689 m^3. The gas temperature is uniform at 1800 K and the walls are cooled. The interior surfaces are black. At what rate is energy being supplied to the gas (and removed from the walls) to maintain these conditions? For emittance values, use the Alberti et al. (2018) worksheet at ***https://doi.org/10.1016/j.jqsrt.2018.08.008.***

Answer: 295 kW.

P.11.5 Pure carbon dioxide at 1 atm and 2500 K is contained between parallel plates 0.3 m apart. What is the radiative flux received at the plates as a result of radiation by the gas For emittance values, use the Alberti et al. (2018) worksheet at ***https://doi.org/10.1016/j.jqsrt.2018.08.008.***

Answer: 163 kW/m^2.

P.11.6 A furnace being designed by a chemical company will be used to burn toxic waste composed of hydrocarbons. Complete elimination of the hydrocarbons with oxygen requires that the temperature of the combustion products in the furnace (60% CO_2, 40% H_2O by volume) be maintained at 1600 K. To prevent leakage of toxic waste or combustion products to the surroundings, the furnace interior is kept at 0.5 atm. The furnace is in the shape of a right circular

cylinder of height equal to its diameter of 4 m. What average radiative flux is incident on the interior surface of the furnace? Note any assumptions used in obtaining the result.

Answer: 124 kW/m^2.

P.11.7 Estimate the maximum radiative flux that is incident on any local area on the interior surface of the furnace described in Homework Problem P.11.6.

Answer: 137 kW/m^2.

P.11.8 Evaluate the geometric mean transmittance $\bar{\tau}_{d1-2}$ from the element dA_1 to the area A_2 in Homework Problem 5.1. The region between the areas is filled with a gray medium at uniform temperature having an absorption coefficient $\kappa = 0.035$ cm^{-1}.

Answer: 0.02341.

P.11.9 A thin black plate 1 x 1 cm is at the center of a sphere of CO_2-air mixture at a uniform temperature of 1800 K and 1 atm total pressure. The partial pressure of the CO_2 is 0.8 atm and the sphere diameter is 1 m. How much energy is absorbed by the plate? What will the plate temperature be? (Assume the boundary of the sphere is black and kept cool so that it does not enter into the radiative exchange.)

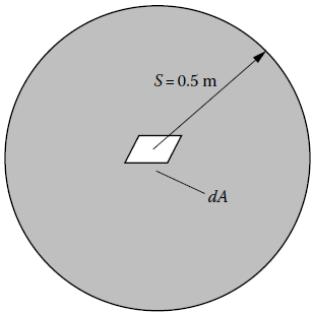

Answer: 13.0 W, 1034 K.

P.11.10 A spherical cavity is filled with an isothermal gray medium having an absorption coefficient κ. Set up the relations needed to determine the geometric mean transmittance $\bar{t}_{1-d2}$ from the cavity surface A_1 to the area element dA_2 at the center of the opening A_2.

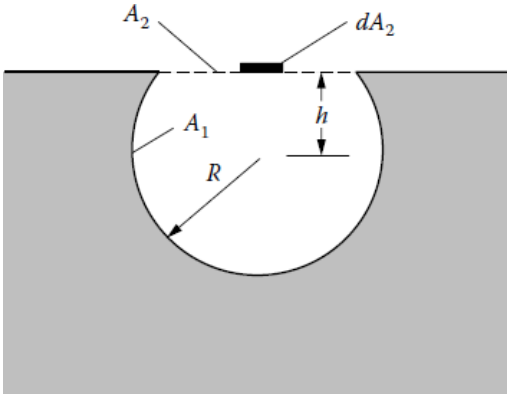

[*Note* : A similar situation is considered by Koh, J.C.Y.: *Int. J. Heat Mass Transfer*, vol. 8, no. 2, pp. 373-374, 1965.]

P.11.11 A gray isotropically scattering gas is contained between large diffuse-gray parallel plates. The plates both have emissivity ε = 0.30. Plate 1 is maintained at temperature T_1 = 1150 K, and plate 2 is at T_2 = 525 K. The medium between the plates has a uniform extinction coefficient of $\beta = 0.75$ m^{-1}. The plate geometry is shown below.

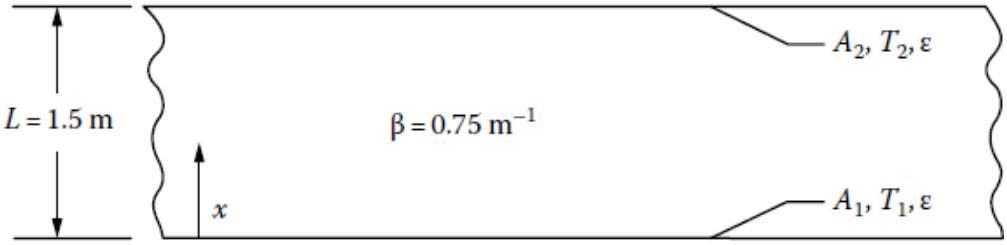

Predict the net radiative heat flux transferred between the surfaces (W/m^2) and plot the temperature distribution [$T^4(\kappa)$ - T_2^4] / (T_1^4 - T_2^4) in the gas, where $\tau = \beta x$. Heat conduction is small. Solve the problem using the nearly transparent optically thin approximation.

Answer: q = 16,740 W/m^2 : $\theta(\kappa)$ = 0.500 (constant).

P.11.12 Two gases have constant extinction coefficients β_1 and β_2 that are both much smaller than 1. The gases are separated by a thin metal barrier with low emissivity ε_s. The gases are in the form of two layers bounded by large parallel diffuse walls as shown. Radiation exchange is large compared with heat conduction that can be neglected. Using the nearly transparent approximation, obtain relations for the temperature distributions within the gases and the net radiative energy transfer from wall 1 to wall 2. Evaluate the results for ε_1 = 0.78, ε_s = 0.04, ε_2 = 0.88, T_1 = 980 K, and T_2 = 765 K. Determine the temperature jump across the thin metal barrier and determine the size of the jump as a function of ε_s.

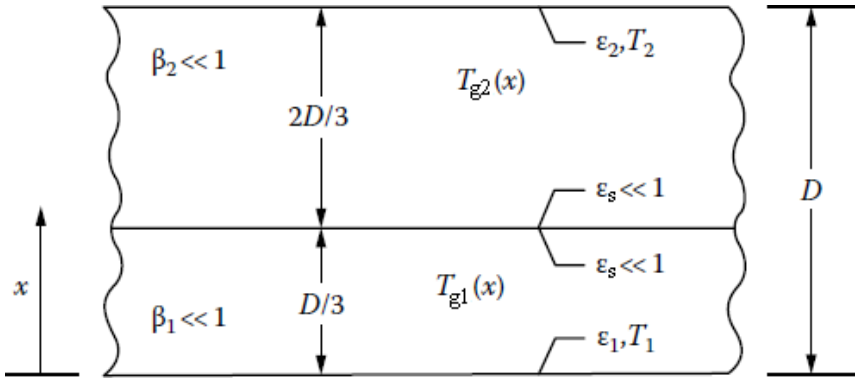

Answers: q = 652.2 W/m^2, T_{g1} = 977.6 K, T_{g2} = 769.1 K, ΔT_{jump} = 208.5 K.

P.11.13 A spherical cavity 15 cm in diameter is filled with a gray medium having an absorption coefficient of 0.1 cm^{-1}. The cavity surface is black and is at a uniform temperature of 620 K. When the medium is first placed in the cavity, the medium is cold. For this condition, use the cold medium approximation to estimate the heat flux radiated from the small opening as shown.

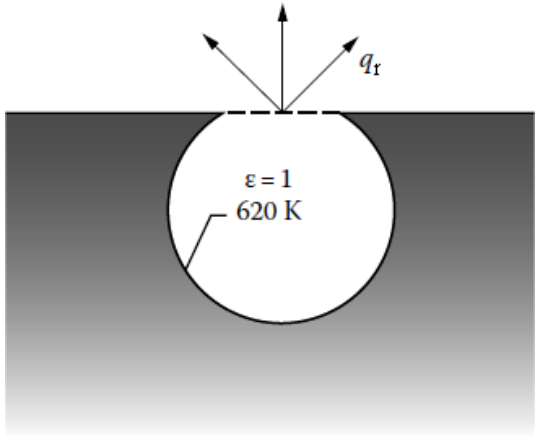

Answer: 3293 W/m^2.

P.11.14 An optically thin gray gas with constant absorption coefficient κ is contained in a long transparent cylinder of diameter D. The surrounding environment is at low temperature that can be considered zero. Initially, the cylinder is at the environment temperature. Then, an electrical discharge is passed through the gas, continuously producing in the gas a uniform energy source $\dot{q}$ per unit volume and time. Derive a relation for the transient gas temperature variation if radiation is assumed to be the only significant mode of heat transfer. What is the maximum temperature T_{max} that the gas will achieve?

Answer: $\dfrac{8\kappa\sigma T_{max}^3}{\rho c_v} t = \dfrac{1}{2}\ln\dfrac{1+\theta}{1-\theta} + \tan^{-1}\theta;\ \ T_{max} = \left(\dfrac{\dot{q}}{4\kappa\sigma}\right)^{1/4};\ \theta = \dfrac{T}{T_{max}}$.

Chapter 13:

P.13.1 Two large gray parallel plates at temperatures T_1 and T_2 and with emissivities ε_1 and ε_2 are separated by an optically thick gray medium with absorption and isotropic scattering. The medium has within it a uniform volumetric energy source of $\dot{q}$ W/m^3. Compute the temperature distribution in the medium by use of the diffusion method with jump boundary conditions for the limit of negligible heat conduction.

P.13.2 A large plate of translucent glass is laid upon a sheet of polished aluminum. The aluminum is kept at a temperature of 500 K and has an emissivity of 0.03. The glass is 2 cm thick and has a Rosseland mean absorption coefficient of $\kappa_R = 3.6$ cm^{-1}. A transparent liquid flows over the exposed face of the glass and maintains that face at a temperature of 270 K.

(a) What is the heat flux through the glass plate?

(b) What is the temperature distribution in the glass plate?

Neglect heat conduction in your calculations, and for simplicity, assume that the refractive indices of the glass and liquid are both one.

Answer: $q = 84.8$ W/m^2; $T(\tau) = 100(133.7-11.2\tau)^{1/4}$(K).

P.13.3 A long cylinder 12 cm in diameter is surrounded by another cylinder 24 cm in diameter. The surfaces are gray, the inner cylinder is at $T_1 = 910$ K with $\varepsilon_1 = 0.42$, and the outer cylinder is at $T_2 = 1075$ K with $\varepsilon_2 = 0.83$. What is the heat transfer from the outer cylinder to the inner cylinder per unit length for vacuum between the cylinders? If the space between the cylinders is filled with a gray medium having absorption and isotropic scattering with extinction coefficient $\beta = \kappa + \sigma_s = 0.41$ cm^{-1}, compute the energy transfer using the P_1 method and the diffusion method (heat conduction is neglected).

Answer: 5.59 kW/m; 3.94 kW/m; 3.89 kW/m.

P.13.4 A rectangular enclosure that is very long normal to the cross section shown has the surface conditions and properties listed in the table. The enclosure is filled with an absorbing, emitting, non-scattering gray gas in radiative equilibrium (no heat conduction, convection, or internal energy sources). Find the heat flux that must be supplied to each surface to maintain the specified temperatures. Use a finite-difference numerical solution of the energy equation including radiative transfer.

Surface	Type	Emissivity	T, K	q
1	Specular	0		0
2	Diffuse	0.713	810	
3	Specular	0		0
4	Diffuse	0.305	1300	

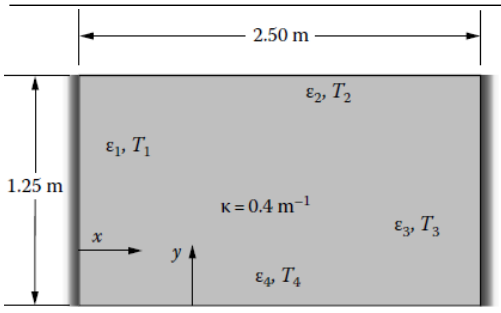

Answer: 33.5 kW/m^2.

P.13.5 The medium in the following enclosure is isotropically scattering and has attenuation coefficient $\beta = 4$ m^{-1}. The boundary conditions on the enclosure are shown. The medium is in radiative equilibrium.

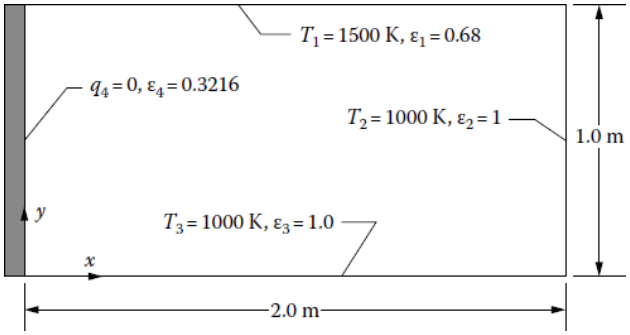

(a) Provide expressions for $E_b(x,y)$ and $q_3(x)$ using the P_1 method.

(b) Provide plots of $E_b(x,y = 0.25\text{ m})$, $E_b(x,y = 0.50\text{ m})$, and $E_b(x,y = 0.75\text{ m})$ on the same graph.

(c) Provide a plot of $q_3(x)$ on surface 3.

Do the problem numerically or analytically.

Chapter 14:

P.14.1 Construct a computer flow chart for the Monte Carlo computation of the configuration factor $F_{d1\text{-}2}$ from an area element to a perpendicular disk as shown in Example 4.4.

P.14.2 Construct a Monte Carlo computer flow diagram to obtain the specular exchange factor F^{S}_{1-2} in Homework Problem 6.11. (Assume it's an equilateral triangle.)

P.14.3 Obtain a Monte Carlo solution for the second part of Example 6.12, (i.e., that is for surface A_1 being a specular reflector.)

P.14.4 For the configuration and conditions in book Homework Problem 7.15, find $T_1(y)$ and $q(x)$ using a numerical solution, and provide plots of these quantities. Compare with the results for no conduction in the plates found in Homework Problems 5.18 and P.5.26. Show grid independence for your results.

P.14.5 Repeat Problem P.14.4 using the Monte Carlo method and compare the results with those of Problem P.14.4. Repeat for enough samples to show independence of the results to the number of samples used in the solution.

P.14.6 Obtain the solution to Homework Problem P.13.4 by using a Monte Carlo method.

P. 14.7 Two diffusely emitting and reflecting parallel plates are of finite width and infinite length normal to the cross section shown. The lower plate has uniform temperature $T_1 = 1000$ K, and the upper plate is at $T_2 = 500$ K. The plate emissivities are $\varepsilon_1 = 0.8$ and $\varepsilon_2 = 0.2$. The surroundings have a temperature of 450 K. An absorbing–emitting medium with absorption coefficient $\kappa = 0.5$ m^{-1} is between the plates. The medium is in radiative equilibrium with its surroundings (heat conduction is negligible).

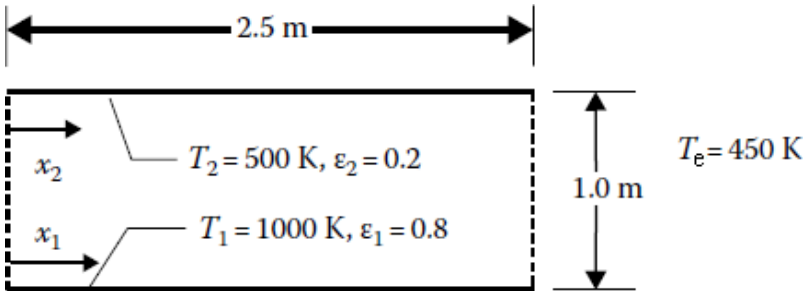

Using the Monte Carlo method, find the distribution of net radiative heat flux on each surface. Show the dependence of the results on the number of samples used in the Monte Carlo solution. Plot the results and compare them with the results of Homework Problem 5.17.

P. 14.8 Use the Monte Carlo method to determine the temperature distribution in the 2D enclosure shown below. The medium in the enclosure is nonscattering and has absorption coefficient $\kappa = 10$ m^{-1}.

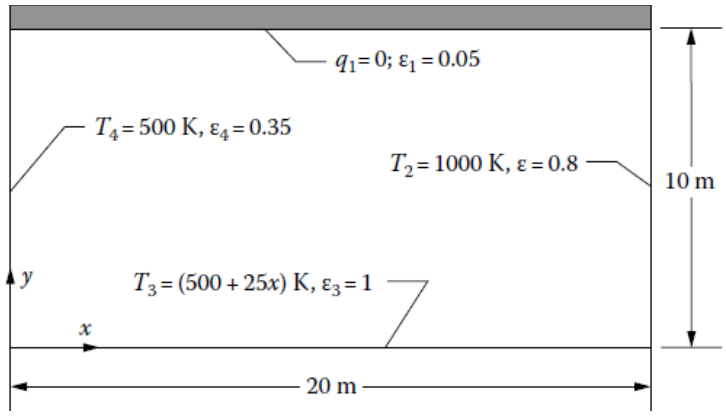

Provide plots of $q_3(x)$ on surface 3, $T_1(x)$ on surface 1, and $T_g(x = 10$ m$,y)$ and $T_g(x, y = 5$ m). Report the number of samples used in the solution.

P.14.9 The gray medium in the enclosure below is nonscattering and has an absorption coefficient of $\kappa = 4$ m^{-1} and a thermal conductivity of $k = 20$ W/m·K.

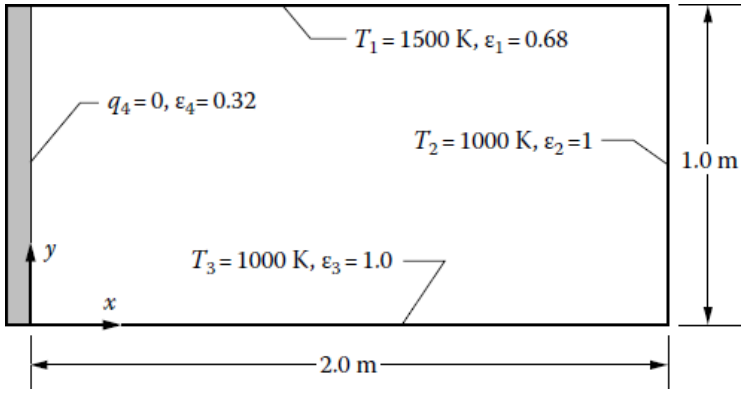

Using the Monte Carlo method for the radiative transfer,

1. Show the governing equation(s) and boundary condition for the problem in specific and dimensionless form. Indicate any simplifying assumptions that are necessary.
2. Provide a plot of $q_3(x)$ on surface 3 and profiles of the medium temperature at $T(x = 0.5, y)$ and $T(x, y = 0.25)$.
3. Show limiting solutions for the cases of $N_{CR} = 0$ and $N_{CR} = \infty$.
4. Show that the solution is grid independent.
5. Show that energy is conserved on the system boundaries.

P.14.10 Use the Monte Carlo method to determine the temperature distribution in the 2D enclosure shown below. The medium in the enclosure is nonscattering and has an absorption coefficient $\kappa = 10\ \text{m}^{-1}$ and thermal conductivity of 1.135 W/m·K.

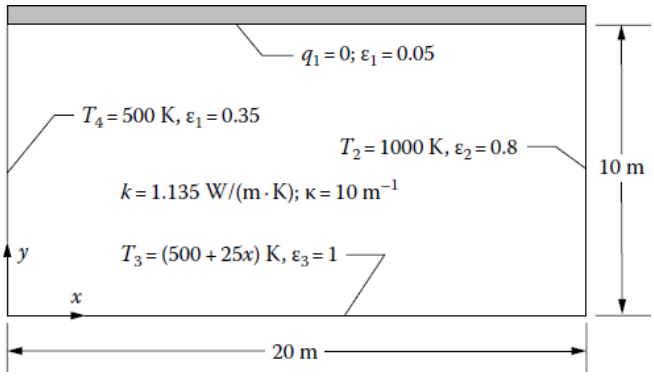

Provide plots of $q_3(x)$ on surface 3, $T_1(x)$ on surface 1, and $T_g(x = 10\ \text{m}, y)$ and $T_g(x, y = 5\ \text{m})$. Show that your solution is correct in the limit of no radiation and no conduction.

P.14.11 Use the Monte Carlo method to determine the temperature distribution in the 2D enclosure shown below. The medium in the enclosure has isotropic scattering coefficient of $\sigma_s = 5\ \text{m}^{-1}$ and absorption coefficient $\kappa = 10\ \text{m}^{-1}$ and thermal conductivity of 1.135 W/(m·K).

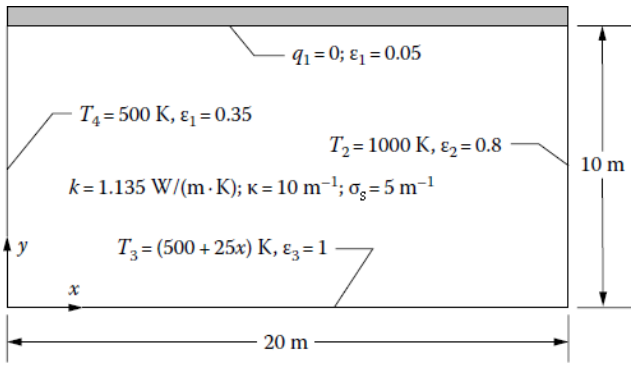

Provide plots of $T_g(x = 10\ \text{m}, y)$ and $T_g(x, y = 5\ \text{m})$. Show that your solution is correct in the limit of no radiation and no conduction.

Chapter 15:

P.15.1 In Homework Problem 12.5, for the situation of a scattering medium between gray plates, it is desired to double the amount of energy being transferred by having the scattering (nonabsorbing) particles suspended in a thermally conducting but nonabsorbing medium. What thermal conductivity of the medium is required to accomplish this?

Answer: 2.04 W/m·K.

P.15.2 A partially transparent solid absorbing sphere is placed in a black cavity at T_b. The sphere temperature is initially low. The sphere has surface transmissivity τ_0, thermal conductivity k, and absorption coefficient κ, and scattering is negligible. Transparent gas at T_g is circulating in the cavity, providing a heat transfer coefficient h at the sphere surface. Give the equations and boundary conditions to compute the transient temperature distribution in the sphere for the initial period during which emission by the sphere is small. Neglect any refraction effects and any dependence of τ_0 on angle.

P.15.3 An enclosed rectangular region is filled with an absorbing, emitting, and heat-conducting medium without scattering. The medium is gray and has absorption coefficient κ and constant thermal conductivity k. The geometry is long in the z direction normal to the cross section shown and the side dimensions in the x and y directions are d and b. The four bounding walls are black. The vertical walls are both at uniform temperature T_v, and the horizontal walls are at T_h. The medium is heated uniformly throughout its volume with a volumetric energy rate $\dot{q}(x, y)$, and the medium is not moving. Provide the energy equation and radiative transfer relations necessary to solve for the steady-state temperature distribution in the rectangular cross section. Place the equations in convenient dimensionless forms for use in a numerical solution.

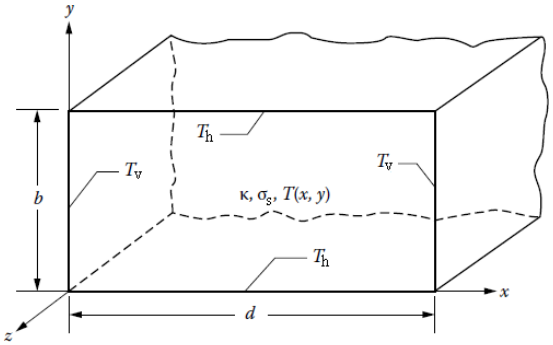

P.15.4 A plane layer of absorbing, emitting, isotropically scattering, and heat-conducting material is being heated throughout its volume with a parabolic volumetric heating rate $\dot{q}(x) = \dot{q}_{\min} + 4A\left[\frac{x}{D} - \left(\frac{x}{D}\right)^2\right]$ where A is the amplitude $\dot{q}_{\max} - \dot{q}_{\min}$. The layer is of thickness D and has constant absorption and scattering coefficients κ and σ_s and a constant thermal conductivity k. The layer is confined between surfaces that are diffuse–gray. The walls at $x = 0$ and D have emissivities ε_1 and ε_2 and temperatures T_1 and T_2.

1. By using the two-flux method, obtain a solution for the radiative heat transfer and the temperature distribution for the limit of zero heat conduction.
2. Provide the two-flux relations that can be solved for $q_r(x)$ and $T(x)$ with heat conduction included.

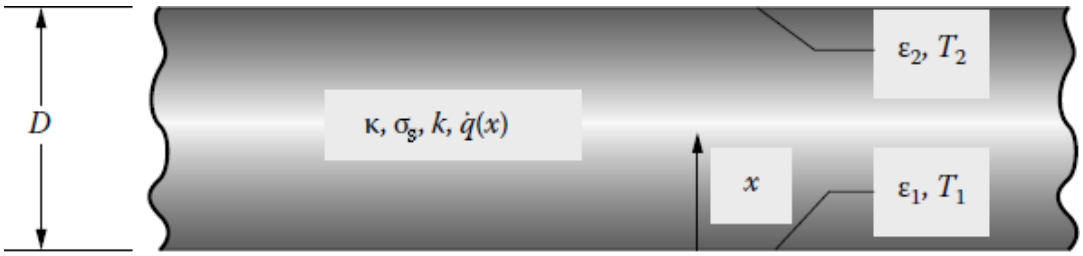

P.15.5 Using the solution ideas for the 2D analysis in Section 15.5.2 and those in the steady 1D analysis at the end of Section 13.6.3, set up the FEM for the ADI solution for the following situation with an emitting, absorbing, and conducting gray medium in a 2D rectangular enclosure that is infinitely long normal to the cross section shown. There is no scattering in the medium. The rectangular region has a uniform heating $\dot{q}$ W/m^3 throughout its volume. The steady 2D temperature distribution is to be determined. For simplicity, use a grid having the same increment size in both the x and y directions. The boundary walls are black and are at the same temperature T_w.

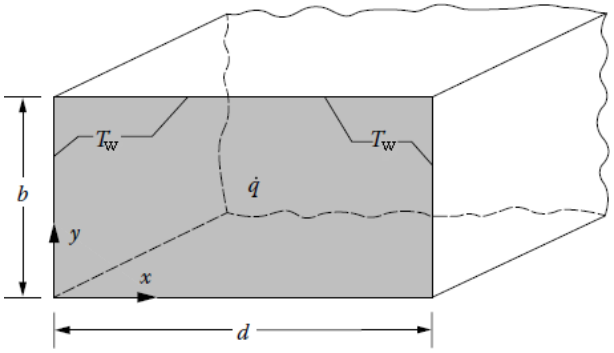

P.15.6 Modify Homework Problem P.15.5 to incorporate a variable grid size into the solution for the steady temperature distribution within a square cross section. Use the ideas in Homework Problem 15.8 extended into 2D.

P.15.7 Two large infinite parallel plates are separated by an optically thick absorbing–emitting, isotropically scattering, and conducting gas in which a chemical reaction is occurring that produces a uniform energy generation rate of $\dot{q}$ per unit volume. The plates are gray and have temperatures and emissivities T_1, ε_1 and T_2, ε_2. Determine the heat fluxes q_1 and q_2 that must be supplied to each of the plates as a result of radiation exchange combined with heat conduction between them. Use the radiative diffusion approximation, and assume that the gas is stationary and that Rosseland mean attenuation coefficient β_R and thermal conductivity k are both constant. Show how to implement the slip coefficient of Figure 15.8.

P.15.8 Two gray parallel plates with emissivities $\varepsilon_1 = 0.45$ and $\varepsilon_2 = 0.9$ are spaced 0.15 m apart. The plate temperatures are $T_1 = 515$ K and $T_2 = 297$ K. A stagnant nongray gas with spectral absorption coefficient as shown is in the space between the plates. The thermal conductivity of the gas is $k = 0.285$ W/(m·K). Using the additive method with the radiative diffusion solution, find the heat transfer between the plates. How significant is the heat conduction?

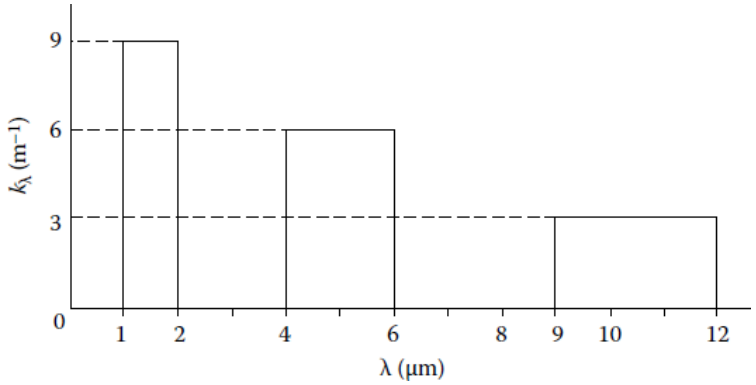

Answer: 1821 W/m^2; 23%.

P.15.9 A plane layer of semitransparent absorbing, emitting, and heat-conducting medium is between two thin metal (highly conducting) walls. The medium is not moving, and it is gray with absorption coefficient κ and thermal conductivity k. The wall surfaces are diffuse–gray with emissivities ε_1 on both sides of the wall at $x = 0$ and ε_2 on both sides of the wall at $x = D$. The large isothermal surroundings below the lower wall are filled with gas at T_{g1}, and there is a heat transfer coefficient h_1 between the gas and the outside of the lower wall. Outside the upper

wall, there is a large isothermal reservoir of gas at T_{g2} that provides a convection coefficient h_2. Set up the necessary finite-difference relations to determine the wall temperatures T_{w1} and T_{w2} and the heat flow q from T_{g1} to T_{g2}.

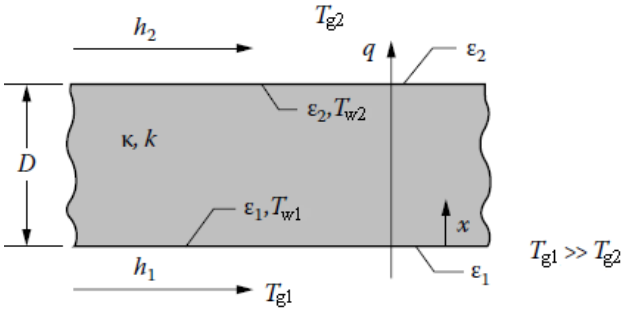

P.15.10 The gray medium in the following enclosure is nonscattering and has an absorption coefficient of $\kappa = 4\ \text{m}^{-1}$ and a thermal conductivity of $k = 20\ \text{W/m·K}$.

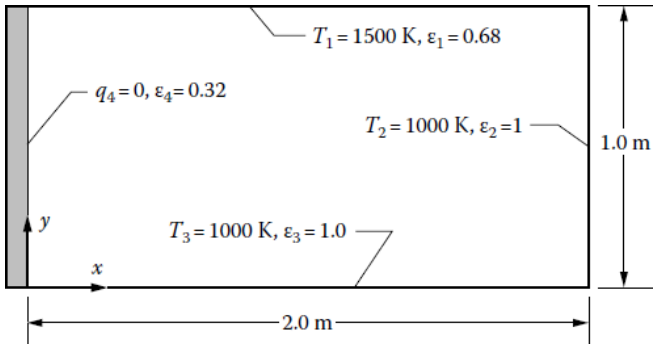

Using the diffusion method for the radiative transfer,

1. Show the governing equation(s) and boundary condition for the problem in specific and dimensionless form. Indicate any simplifying assumptions that are necessary.
2. Provide a plot of $q_3(x)$ on surface 3 and profiles of the medium temperature at $T(x = 0.5, y)$ and $T(x, y = 0.25)$.
3. Show limiting solutions for the cases of $N_{CR} = 0$ and $N_{CR} = \infty$.
4. Show that the solution is grid independent.
5. Show that energy is conserved on the system boundaries.

Chapter 17:

P.17.1 As a result of surface treatment, a partially transparent plate has a different reflectivity at each surface. For radiation incident on surface 1 in a single direction, obtain an expression for the overall reflectance and transmittance in terms of ρ_1, ρ_2, and τ.

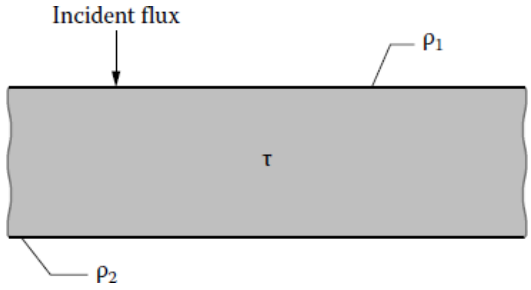

Answer: $R = \dfrac{\rho_1 + \rho_2(1-2\rho_1)\tau^2}{1-\rho_1\rho_2\tau^2}$; $T = \dfrac{(1-\rho_1)(1-\rho_2)\tau}{1-\rho_1\rho_2\tau^2}$

P.17.2 Two parallel, partially transparent plates have different τ values and a different ρ at each surface. Obtain an expression for the overall transmittance of the two-plate system for radiation incident from a single direction.

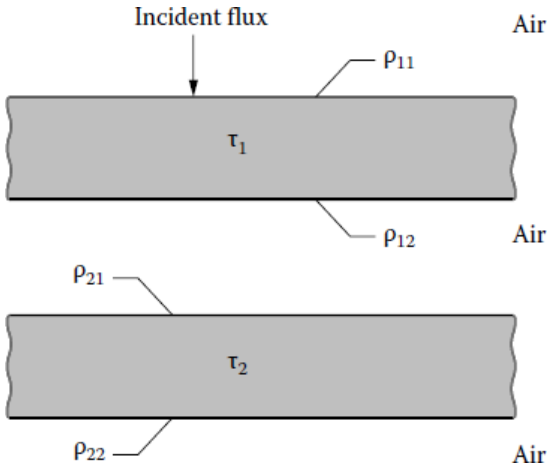

Answer:

$T = \dfrac{T_1 T_2}{1-R_{12}R_{21}}$, where $T_n = \dfrac{(1-\rho_{n1})(1-\rho_{n2})\tau_n}{1-\rho_{n1}\rho_{n2}\tau_n^2}$

and $R_{nm} = \dfrac{\rho_{nm} + \rho_{nn}(1-2\rho_{nm})\tau_n^2}{1-\rho_{nm}\rho_{nn}\tau_n^2}$

P.17.3 In a solar still, a thin layer of condensed water is flowing down a glass plate. The plate has a transmittance τ, and the water layer is assumed nonabsorbing. Obtain an expression for the overall transmittance T_L of the system for radiation incident on the glass in a single direction.

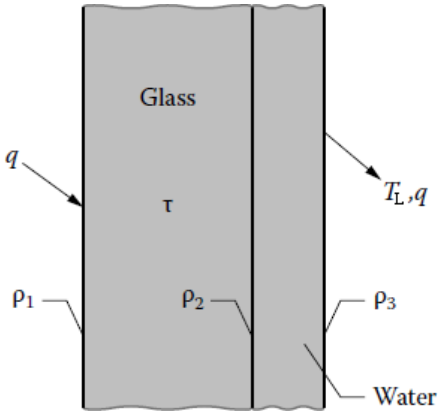

Answer: $\mathsf{T}_L = \dfrac{(1-\rho_1)(1-\rho_2)(1-\rho_3)\tau}{(1-\rho_2\rho_3)(1-\rho_1\rho_2\tau^2)-\rho_1\rho_3(1-\rho_2)^2\tau^2}$

P.17.4 Two opaque gray walls have a transparent (nonabsorbing) plate between them. The transparent plate has surface reflectivities ρ. Derive a relation for the heat transfer from wall $w1$ to wall $w2$. Neglect heat conduction in the transparent plate, and neglect the fact that ρ depends on the angle of incidence.

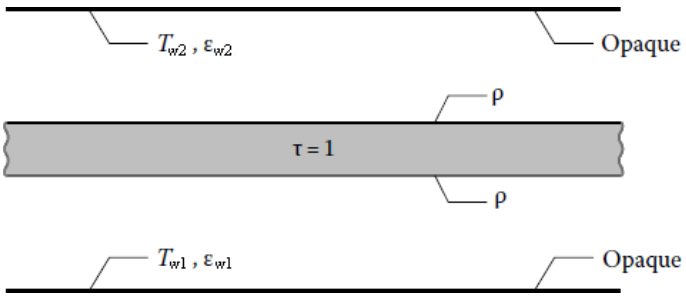

Answer: $\mathsf{q}_{w1\to w2} = \dfrac{\sigma\left(\mathsf{T}_{w1}^4 - \mathsf{T}_{w2}^4\right)}{\dfrac{1}{\varepsilon_{w1}} + \dfrac{1}{\varepsilon_{w2}} - 1 + \dfrac{2\rho}{1-\rho}}$

P.17.5 Water is flowing between two identical glass plates adjacent to an opaque wall. Derive an expression for the fraction of radiation incident from a single direction that is absorbed by the water in terms of the ρ and τ values of the interfaces and layers. (Include only radiative energy transfer.)

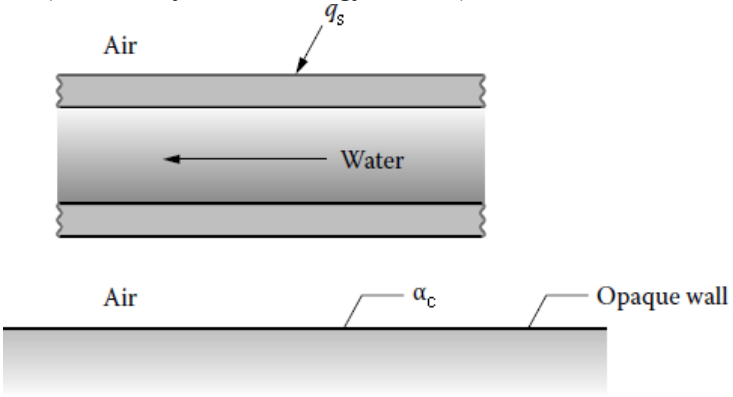

P.17.6 A diffuse radiation flux q_{air} is incident on a dielectric medium having an absorption coefficient κ and a simple index of refraction n. The air–medium interface is slightly rough so that it acts like a diffuse surface. It has a directional–hemispherical reflectivity of $\rho(\theta)$ that is assumed to be independent of θ. Derive a relation to determine the amount of incident energy directly absorbed per unit volume, dQ/dV, in the medium as a function

of depth x from the surface. For n = 1.52, obtain an estimate for the surface reflectivity for diffuse incident radiation by using Figure 3.3. Using this value and the other conditions as in Example 17.2, compute dQ/dV. How does the result compare with that in Example 17.2 and what is the reason for the difference?

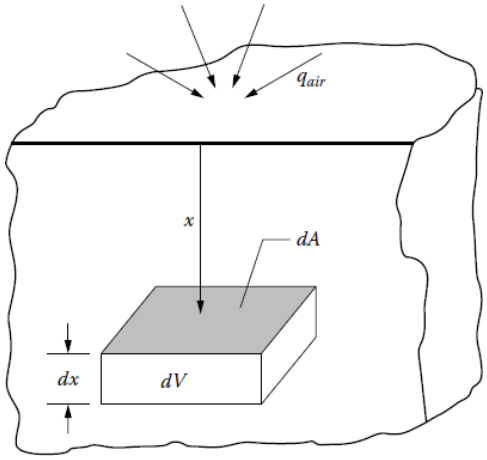

Answer: 3.08 W/cm^3.

P.17.7 A series of three parallel glass plates is being used to absorb incident infrared radiation. The incident radiation is at wavelength $\lambda = 4$ μm. The complex index of refraction of the glass at this wavelength is $n - ik = 1.40 - 5.8 \times 10^{-5}i$. The plates have optically smooth surfaces. The radiation is incident from air in a direction normal to the plates. What fraction of the incident radiation is absorbed by the center plate?

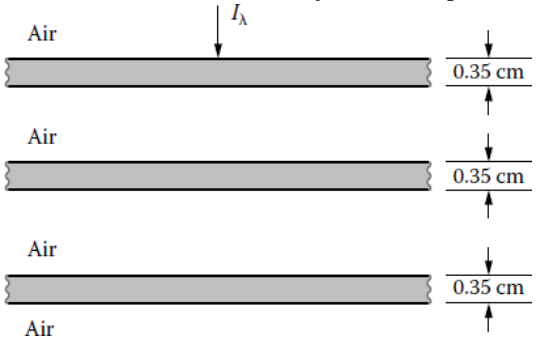

Answer: 0.237.

P.17.8 Two very thick dielectric regions with small absorption coefficients are in perfect contact at an optically smooth interface A_i. Prior to being placed in contact, region 1 was heated to a uniform temperature T_1, while region 2 was kept very cold at $T_2 \ll T_1$. The indices of refraction are such that $n_1 > n_2 > 1$. Derive an expression for the heat flux emitted across A_1 from region 1 into region 2. Evaluate the result for $n_1 = 2.35$, $n_2 = 1.54$, $T_1 = 627$ K, and $T_2 \approx 0$.

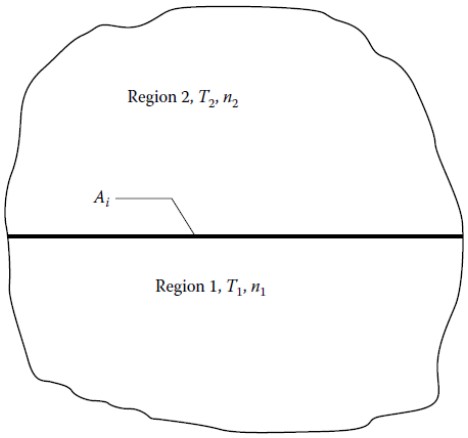

Answer: 18,800 W/m^2.

P.17.9 Two very thick dielectric regions with small absorption coefficients are separated by a plane layer of a third dielectric material that is of thickness D = 2 cm. The two interfaces are optically smooth. The plane layer between the two thick regions is perfectly transparent. This plane layer is at low temperature, having been suddenly inserted between the two dielectric regions. For the temperatures shown, calculate the net heat flux being transferred by radiation from medium 1 into medium 2. Include the effects of interface reflections. The effect of heat conduction is neglected. The indices of refraction are given in the figure.

Answer: 13.0 kW/m^2.

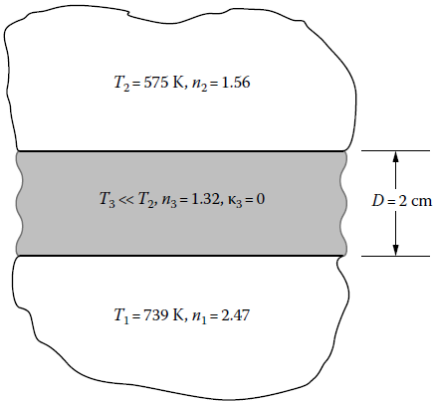

P.17.10 A layer of transmitting glass (silica) is separated from a silicon wafer by a layer of polymer. A laser provides monochromatic energy incident on the assembly of layers. The silicon wafer is opaque at the laser wavelength and has surface absorptivity α = 0.694. The silica has a refractive index that gives a surface reflectivity for the laser energy of ρ_{SiO_2} = 0.04 and has transmittance for laser energy of τ_{SiO_2} = 0.95 Similarly, the polymer layer has a surface reflectivity for the laser energy of ρ_{poly} = 0.0452 and has transmittance for laser energy of τ_{poly} = 0.90. Derive an expression for the reflectance R for the laser energy of the glass/substrate assembly, and also determine the fraction of the incident laser energy that is deposited in the silica and polymer layers.

Answer: 0.302.

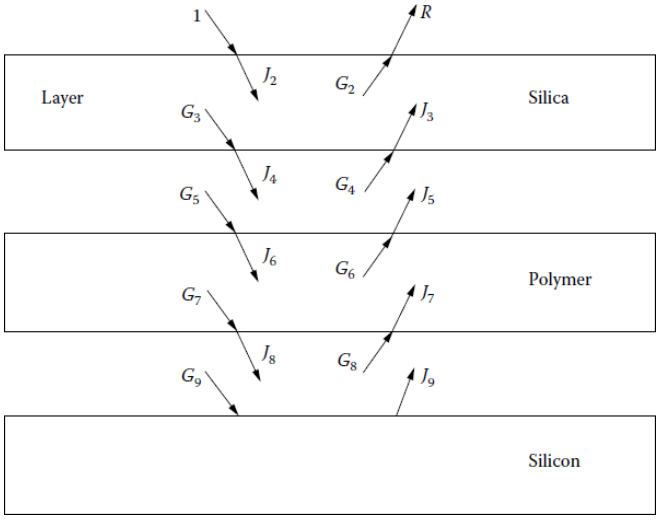

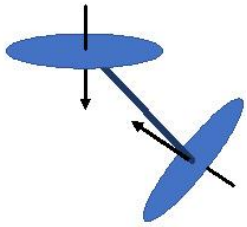

Q: PROPOSED ONE-SEMESTER SYLLABUS

Below is a syllabus for a one-semester course in radiation heat transfer. The syllabus is based on a 15-week semester with two 90-minute classes per week, with 27 lecture sessions and three session left for examinations, class evaluation, etc. It concentrates on the fundamental blackbody properties (Chapter 1), the radiative properties of surfaces (Chapters 2, 3), the definition and use of configuration factors (Chapter 4), energy transfer among gray-diffuse surfaces and in enclosures with gray-diffuse surfaces, and solution techniques for these problems (Chapter 5). The Monte Carlo section for transfer among surfaces is drawn from Chapter 14 and introduced at this point. Interactions with conduction and/or convective transfer at enclosure boundaries are then treated (Chapter 7). Chapter 8 on the electromagnetic theory fundamentals is introduced to show the fundamental basis for what has gone before. Finally, the absorption characteristics of participating media (Chapter 9) are introduced to show their important spectral characteristics, the mathematical treatment of transfer through a participating media and a simplified mean-beam-length solution technique is shown (Chapter 11), and a more exact but intuitive method (diffusion solution) is examined as one example of a more general case (Chapter 13). Finally, Chapter 19 is used to kindle interest in contemporary applications of radiation.

This proposed one-semester syllabus ignores many important basic subjects such as the emerging areas of micro-nanoscale effects, inverse problems and solution methods, and the presence of bifurcation/chaos in nonlinear problems. Many important applications are also only noted in passing, although some are discussed in Chapter 19. The course instructor may wish to spend some time on any or all these subjects.

Much material in the book is skipped, but could well be incorporated into a second course, particularly one that concentrates on radiative transfer in participating media.

Chapter 1. Introduction to Radiative Transfer (3 class sessions)

- 1.1 Thermal Radiation and the Natural World
- 1.2 Thermal Radiation in Engineering
- 1.3 Thermal Radiation and Thermodynamics
- 1.4 Nature of the Governing Equations
- 1.5 Electromagnetic Waves vs. Photons
- 1.6 Radiative Energy Exchange and Radiative Intensity
- 1.7 Solid Angle
- 1.8 Spectral Intensity
- 1.9 Characteristics of Emission
  - 1.9.1 Perfect Emitter
  - 1.9.2 Radiation Isotropy in a Black Enclosure
  - 1.9.3 Perfect Emitter in Each Direction and Wavelength
  - 1.9.4 Total Radiation into Vacuum
  - 1.9.5 Blackbody Intensity and Its Directional Independence
  - 1.9.6 Blackbody Emissive Power: Cosine-Law Dependence
  - 1.9.7 Hemispherical Spectral Emissive Power of a Blackbody
  - 1.9.8 Planck's Law: Spectral Distribution of Emissive Power
  - 1.9.9 Approximations to the Blackbody Spectral Distribution
  - 1.9.10 Wien's Displacement Law
  - 1.9.11 Total Blackbody Intensity and Emissive Power
  - 1.9.12 Blackbody Radiation within a Spectral Band
  - 1.9.13 Summary of Blackbody Properties
- 1.10 Radiative Energy Along a Line-Of-Sight
  - 1.10.1 Radiative Energy Loss due to Absorption and Scattering
  - 1.10.2 Mean Penetration Distance
  - 1.10.3 Optical Thickness

4.2.3 Configuration Factor and Reciprocity for Two Finite Areas
4.3 Methods for Determining Configuration Factors
4.3.1 Configuration-Factor Algebra
4.3.2 Configuration-Factor Relations in Enclosures
4.3.3 Techniques for Evaluating Configuration Factors
4.3.4 Unit-Sphere and Hemicube Methods
4.5 Compilation of Known Configuration Factors and their References: Appendix C and Web Catalog

Chapter 5. Radiation Exchange in Enclosures Composed of Black and/or Diffuse-Gray Surfaces (4 class sections)
5.1 Introduction
5.2 Radiative Transfer for Black Surfaces
5.2.1 Transfer between Black Surfaces Using Configuration Factors
5.2.2 Radiation Exchange in a Black Enclosure
5.3 Radiation Among Finite Diffuse-Gray Areas
5.3.1 Net-Radiation Method for Enclosures
5.3.2 Enclosure Analysis in Terms of Energy Absorbed at Surface
5.3.4 Matrix Inversion for Enclosure Equations
5.4 Radiation Analysis Using Infinitesimal Areas
5.4.1 Generalized Net-Radiation Method Using Infinitesimal Areas
5.5 Computer Programs for Enclosure Analysis

Chapter 14. The Monte Carlo Method (2 class sessions)
14.1 Introduction
14.2 Fundamentals of the Monte Carlo Method
14.3 Monte Carlo for Surface-to-Surface Radiation Exchange
14.3.1 Radiation between Black Surfaces
14.3.2 Radiation between Non-Black Surfaces
14.3.3 Wavelength-Dependent Properties
14.3.4 Ray Tracing

Chapter 7. Radiation Combined with Conduction and Convection at Boundaries (2 class sessions)
7.1 Introduction
7.2 Energy Relations and Boundary Conditions
7.2.1 General Relations
7.2.2 Uncoupled and Coupled Energy Transfer Modes
7.2.3 Control Volume Approach for One- or Two-Dimensional Conduction along Thin Walls
7.3 Radiation Transfer with Conduction Boundary Conditions
7.3.1 Thin Fins with 1D or 2D Conduction
7.4 Radiation with Convection and Conduction
7.4.1 Thin Radiating Fins with Convection
7.5 Numerical Solution Methods
7.5.3 Numerical Solution Techniques
7.5.4 Verification, Validation and Uncertainty Quantification

Chapter 8. **Electromagnetic Wave Theory** (skim**) (1 class session)**

Chapter 9: **Properties of Participating Media (1 class session)**
9.1 Introduction

9.2 Spectral Lines and Bands for Gas Absorption and Emission
- 9.2.1 Physical Mechanisms
- 9.2.2 Local Thermodynamic Equilibrium (LTE)
- 9.2.3 Spectral Line Broadening

9.4 Gas Total Emittance Correlations

Chapter 10 Absorption and Scattering by Particles and Agglomerates (1 class session)

10.1 Introduction
10.2 Absorption and Scattering: Definitions
- 10.2.1 Background
- 10.2.2 Absorption and Scattering Coefficients, Cross Sections, Efficiencies
- 10.2.3 Scattering Phase Function

10.3 Scattering by Spherical Particles
- 10.3.1 Scattering by a Large Specularly Reflecting Sphere
- 10.3.2 Reflection from a Large Diffuse Sphere
- 10.3.5 Geometric Optics Approximation

10.4 Scattering by Small Particles
- 10.4.1 Rayleigh Scattering by Small Spheres
- 10.4.2 Scattering Cross Section for Rayleigh Scattering
- 10.4.3 Phase Function for Rayleigh Scattering

Chapter 11. Fundamental Radiative Transfer Relations and Approximate Solution Methods (3 class sessions)

11.1 Introduction
11.2 Energy Equation and Boundary Conditions for a Participating Medium
11.3 Radiative Transfer and Source Function Equations
- 11.3.1 Radiative Transfer Equation
- 11.3.2 Source Function Equation

11.4 Radiative Flux and its Divergence Within a Medium
- 11.4.1 Radiative Flux Vector
- 11.4.2 Divergence of Radiative Flux Without Scattering (Absorption Alone)
- 11.4.3 Divergence of Radiative Flux Including Scattering
- 11.5.5 Relations for a Gray Medium

11.9 Mean Beam-Length Approximation for Spectral Radiation from an Entire Volume of a Medium to All or Part of its Boundary
- 11.9.1 Mean Beam Length for a Medium between Parallel Plates Radiating to Area on Plate
- 11.9.2 Mean Beam Length for Sphere of Medium Radiating to Any Area on its Boundary
- 11.9.3 Radiation from Entire Medium Volume to its Entire Boundary for Optically Thin Medium
- 11.9.4 Correction to Mean Beam Length when Medium is not Optically Thin

11.10 Exchange of Total Radiation in an Enclosure by use of Mean Beam Length
- 11.10.1 Total Radiation from Entire Medium Volume to All or Part of its Boundary
- 11.10.2 Exchange between Entire Medium Volume and Emitting Boundary

Chapter 13. Numerical Solution Methods for Radiative Transfer in Participating Media (1 class session)

13.1 Introduction
13.2 Series Expansion and Moment Methods
- 13.2.1 Optically Thick Media: Radiative Diffusion
  - 15.2.5.2 Diffusion Method for Combined Radiation and Conduction

Chapter 14. The Monte Carlo Method (Part of this class session)

14.4 Monte Carlo Technique for Radiatively Participating Media
- 14.4.1 Relations for Absorption and Scattering within the Medium
- 14.4.2 Net Radiative Energy Transfer between Volume and Surface Elements

Chapter 19. Applications of Radiation Energy Transfer (2 class sessions)

19.1 Solar Energy
- 19.1.1 Energy Harvesting
- 19.1.2 Astronomy, Astrophysics, and Atmospheric Radiation
- 19.1.3 Solar Energy, Global Warming, and Climate Change

19.2 Combustion and Flames
- 19.2.1 Radiation from Sooting and Non-Sooting Flames
- 19.2.2 Modeling of Flames, Burners and Furnaces

19.3 Radiation in Porous Media and Packed Beds
- 19.3.1 CSP Absorbers Using Porous Media
- 19.3.2 Porous Media Burners

19.4 Space Applications
- 19.4.1 Spacecraft Thermal Control
- 19.4.2 Rocket Nozzle Heat Transfer

19.5 Advanced Manufacturing and Materials Processing